Jack Rabbit III: Characterizing 2-Phase Ammonia Plume in a Controlled Static Environment Chamber

CSAC 25-007

Prepared by:

Matt Rowley
Logan Daniels
Michael Watson
Jennifer Holdridge
Steve Hanna
Sun McMasters
Helen Mearns

March 2025

Science & Technology

This page intentionally left blank

Chemical Security Analysis Center

Jack Rabbit III: Characterizing 2-Phase Ammonia Plume in a Controlled Static Environment Chamber

CSAC 25-007

Prepared by:

Matt Rowley, Logan Daniels, Michael Watson, and Jennifer Holdridge
(DHS S&T CSAC/Battelle)
Steve Hanna
(Hanna Consultants)
Sun McMasters
(DHS S&T CSAC)
Helen Mearns
(DHS S&T CSAC/Army DEVCOM CBC

Prepared for:

U.S. Department of Homeland Security
Science and Technology Directorate

March 2025

Science & Technology

ACKNOWLEDGEMENTS

This project was funded by the U.S. Department of Homeland Security (DHS) Science and Technology Directorate (S&T) to support the S&T Probabilistic Analysis of National Threats Hazards and Risks program, and the results inform the DHS Countering Weapons of Mass Destruction Office (CWMD). The S&T Chemical Security Analysis Center (CSAC) thanks S&T CWMD Portfolio Manager, Dr. Angela Ervin, S&T Chemical Biological Detection and Defense Program Manager, Dr. Andrea Wiggins, and CWMD Office, Dr. Joel Rynes, for their support.

The authors also acknowledge the technical expertise and reviews provided by the S&T Jack Rabbit III (JR III) Working Groups with special thanks to Dr. Ronald Meris, Defense Threat Reduction Agency (DTRA), for his contributions to the planning and execution of a series of these multi-phase experiments as the chair of the JR III Scientific Advisory Group. Appreciation also to Mr. Wayne Adams, Air Force Institute of Technology, Scientific Test and Analysis Techniques Center of Excellence, Homeland Security Community of Best Practices, for his expert statistical guidance and support in conducting the testing. The support of the JR III Modeling Working Group, including analysis by Dr. Simon Gant and Dr. Rory Hetherington (United Kingdom Health and Safety Executive) and Dr. Gemma Tickle (GT Science & Software), was useful in understanding the two-phase ammonia jet behavior and dry deposition. The Emergency Responders Working Group (Professor Andrew Byrnes from Utah Valley University) and the Instrumentation Working Group (Mr. Bruce Hinds from DTRA) provided valuable insights into instrumentation for the design of the testing. Furthermore, many JR III collaborators contributed to this effort: Mr. David Cotsman (Government of Canada); Dr. David Morton and Mr. Douglas Sommerville (S&T CSAC), Mr. James Odasso (Office of Science and Engineering, S&T), and Dr. Tesema Chekol and Mr. Charlie Strassle (Battelle Memorial Institute).

DISCLAIMER

REPORT DOCUMENTATION PAGE

Form Approved
OMB No. 0704-0188

1. REPORT DATE *(MM-DD-YYYY)*	2. REPORT TYPE	3. DATES COVERED *(From - To)*
03-21-2025	FINAL	August 2023-March 2025

4. TITLE AND SUBTITLE
Jack Rabbit III: Characterizing 2-Phase Ammonia Plume in a Controlled Static Environment Chamber

5a. CONTRACT NUMBER: FA807518D0016
5b. GRANT NUMBER: N/A
5c. PROGRAM ELEMENT NUMBER: N/A

6. AUTHOR(S)
Matt Rowley (DHS S&T CSAC/Battelle)
Logan Daniels (DHS S&T CSAC/Battelle)
Michael Watson (DHS S&T CSAC/Battelle)
Jennifer Holdridge (DHS S&T CSAC/Battelle)
Steve Hanna (Hanna Consultants)
Sun McMasters (DHS S&T CSAC)
Helen Mearns (DHS S&T CSAC/Army DEVCOM CBC

5d. PROJECT NUMBER: N/A
5e. TASK NUMBER: FA807522F0003
5f. WORK UNIT NUMBER: N/A

7. PERFORMING ORGANIZATION NAME(S) AND ADDRESS(ES)
Department of Homeland Security
Science and Technology Directorate
Chemical Security Analysis Center
8490 Ricketts Point Rd
Gunpowder, MD 21010

8. PERFORMING ORGANIZATION REPORT NUMBER
CSAC-25-007

9. SPONSORING/MONITORING AGENCY NAME(S) AND ADDRESS(ES)
Department of Homeland Security
Washington, D.C.

10. SPONSOR/MONITOR'S ACRONYM(S): N/A
11. SPONSOR/MONITOR'S REPORT NUMBER: N/A

12. DISTRIBUTION/AVAILABILITY STATEMENT
Approved for public release. Distribution is unlimited.

13. SUPPLEMENTARY NOTES: None.

14. ABSTRACT:
The chamber experiments were conducted with various ambient temperatures and relative humidities intended to cover naturally occurring environmental conditions across the United States in a static chamber. Ammonia concentration time series were recorded at more than 20 locations in the chamber, with half positioned 0.6 m from the surface and the other half at a height of 1.6 m. Videos were also recorded to characterize the initial momentum, impact on the surface, and subsequent transport and diffusion of ammonia released from the source. Additional experiments are being undertaken to study how rain and carbon dioxide may influence the ammonia plume. Further experiments are being planned using a dynamic test chamber that accounts for typical boundary layer airflow, allowing for ammonia deposition studies on plants and soils.

15. SUBJECT TERMS:
Ammonia, chamber dispersion studies,

16. SECURITY CLASSIFICATION OF:			17. LIMITATION OF ABSTRACT	18. NUMBER OF PAGES	19a. NAME OF RESPONSIBLE PERSON
a. REPORT	b. ABSTRACT	c. THIS PAGE			Dr. Shannon B. Fox
U	U	U	U	186	19b. TELEPHONE NUMBER (*Include area code*) 410-417-0906

This page intentionally left blank.

Table of Abbreviations, Acronyms, and Notations

ABBREVIATIONS/ ACRONYMS/ NOTATIONS	DEFINITION
AH	Absolute Humidity
°C	Degrees Celsius; Unit of temperature on the Celsius temperature scale
Cam 1,2	Camera 1,2
CO_2	Carbon Dioxide
CSAC	Chemical Security Analysis Center
CWMD	Countering Weapons of Mass Destruction Office
DAQ	Data Acquisition Module
DHS	U.S. Department of Homeland Security
DSC	Differential Scanning Calorimetry
DTRA	Defense Threat Reduction Agency
EC	Electrochemical
ES	Executive Summary
ERWG	Emergency Responders Working Group
FLIR	Forward Looking Infrared (Camera)
fps	Frames Per Second
FTIR	Fourier Transform Infrared (Spectrometry)
gpm	Gallons per Minute
HD	High Definition
HDPE	High-Density Polyethylene
ID	Internal Diameter
IR	Infrared
JR	Jack Rabbit
Lpm	Liters per Minute
m	Meter
mm	Millimeter
m/s	Meter per Second
Pa	Pascal
PCU	Portable Conditioning Unit
pH	-log [H+] for measuring the acidity and basicity of aqueous solutions
PID	Photoionization Detector

Table of Abbreviations, Acronyms, and Notations (Cont.)

ABBREVIATIONS/ ACRONYMS/ NOTATIONS	DEFINITION
ppm	Parts per Million
psig	Pounds per Square Inch Gauge
PT	Pressure Transducer
RH	Relative Humidity
RRV	Remote Release Valve
s	Second
S&T	Science and Technology Directorate
ΔT	Temperature Differential
t	Time
T	Temperature
TC	Thermocouple
TIC	Toxic Industrial Chemical
TGA	Thermogravimetric Analysis
TS	Test Scenario
WG	Working group
WSP	Water Sensitive Paper

TABLE OF CONTENTS

PAGE

LIST OF TABLES

PAGE

LIST OF FIGURES

PAGE

This page intentionally left blank.

EXECUTIVE SUMMARY

The U.S. chemical supply chain is evolving as global demand for ammonia increases, driven by the rising need for fertilizers and its potential use as an alternative energy source. With the increased transportation and storage of ammonia in various locations, understanding how ammonia plumes are influenced by environmental conditions is essential for hazard assessment. To address this, environmental controlled chamber experiments were conducted to fill these data gaps in atmospheric dispersion modeling and address chemical reactivity concerns under a range of environmental conditions. Dispersion modeling data gaps identified were ammonia rainout, reactions of ammonia with water vapor or carbon dioxide (CO_2) in a variety of environmental conditions and variations of ammonia concentration with space and time.

In this study, environmental variables such as temperature, humidity, rainfall, and excess CO_2 were explored. The test chamber was preconditioned to various temperature and relative humidity (RH) setpoints that simulated average and extreme environmental conditions to collect data within a static (i.e., with no mean motions prior to the ammonia release) environmental chamber.

This report documents a detailed description of the methodologies employed and the measurements taken in accordance with the 11 different test scenarios (TSs), covering a wide range of possible environmental conditions. With up to four replicates, this matrix resulted in a total of 30 trials. TSs included varying temperatures and RH conditions. Also included were scenarios simulating conditions of rainfall by introducing liquid water in controlled amounts and patterns to study the effects of light and heavy rain and a scenario where carbon dioxide (CO_2) is released. In all tests, the two-phase ammonia jet from the bottle was directed 45 degrees downwards. During all tests, a "catch tray" was placed at the floor, centered at the location that the ammonia jet would strike the tray. A scale measured the mass of liquid in the tray, and video cameras were pointed at the tray from different angles. **Table ES-1** provides a summary of each TS's environmental variables and number of replicates conducted, which is denoted as A, B, C, or D. (repeats of the experiment using the same environmental variables). NOTE: AH (absolute humidity in g/m^3) equals RH (expressed as a fraction) times the saturated water vapor content in g/m^3. In the atmosphere, the RH is nearly 100% while it is raining. However, in these tests, the chamber was conditioned (prior to turning on the "rain") with 50 % RH.

Table ES-1. Test Matrix

TS No.	Temp (°C)	RH (%)	AH (g H_2O per m^3 air)	Number of Replicates	Description	Ammonia Mass Released in Test Environment Volume
1	5	90	5.9	1 (A)	High humidity, varied temperature	~0.375 lb. (170 grams) (±15%) into 1,800-ft^3 (51 m^3) chamber
2	15	90	11.8	2 (A,B)		
3	-15	25	0.3	3 (A,B,C)	Extreme Environmental Conditions (Artic, Desert, Swamplands)	
4	40	10	5.8	3 (A,B,C)		
5	33	90	32.9	3 (A,B,C)		
6	22	50	8.6	3 (A,B,C)	Light Rain	
7	22	50	8.6	3 (A,B,C)	Heavy Rain	
8	30	60	18.2	4 (A,B,C,D)	Excess CO_2	
9	10	60	5.6	3 (A,B,C)	Ambient Conditions	
10	22	60	12.0	2 (A,B)		
11	35	60	24.1	3 (A,B,C)		

The mass of ammonia released, mass of liquid pooled on the catch tray, and the ammonia concentration at 18 locations within the static chamber were measured and recorded with a suite of instrumentation (i.e., liquid mass, gas concentration, temperature, RH, and pressure) and documented with high definition and infrared videos. Each release was monitored for the first 30 minutes to allow monitoring the eddies generated by the initial momentum jet after which mixing fans were activated for 10 minutes to attempt to homogenize the ammonia for calculating the mass balance. Finally, simulated rain and excess CO_2 were introduced to the test environment. Experimental results were then obtained and processed to calculate the fraction of liquid from the ammonia release, along with the ammonia mass balance. A summary of TS 1 through TS 5 and TS 9 through TS 11 experimental conditions and some results as a function of the various environment initial conditions are provided in **Table ES-2**. The simulated rain (TS 6 and TS 7) and excess CO_2 (TS 8) experimental conditions and some results are provided in **Table ES-3** and **Table ES-4**, respectively.

Table ES-2. Summary of Experimental Conditions and Selected Results, Standard Approach TSs

TS No.	Test Environment Initial Conditions				Initial Pressure in lecture bottle (psia)	Liquid Fraction [a]	Derived Ammonia Mass Balance
	Temp (°C)	RH (%)	AH (g H_2O per m^3 air)	Average Air Density of mixture of dry air, water vapor, and ammonia (kg/m^3)			
1A	5.3	85.5	5.9	1.245	76	40.8%	100.4%
2A	15.5	89.8	11.9	1.196	110	29.3%	106.9% [b]
2B	15.6	89.1	11.8	1.208	109	29.7%	106.3% [b]
3A	-17.0	25.5	0.4	1.339	41	56.3%	100.1%
3B	-15.2	29.9	0.5	1.330	38	58.4%	99.8%
3C	-18.1	11.5	0.1	1.358	37	59.8%	99.2%
4A	41.0	11.1	6.0	1.102	233	14.1%	91.7%
4B	40.5	10.9	5.7	1.100	237	13.5%	92.7%
4C	40.2	11.2	5.8	1.103	233	14.4%	93.6%
5A	33.8	89.4	33.2	1.116	191	11.2%	90.1%
5B	33.2	89.8	32.4	1.120	190	11.4%	88.7%
5C	33.7	89.8	33.2	1.110	190	11.9%	89.2%
9A	9.4	61.2	5.5	1.232	87	37.0%	99.1%
9B	9.4	60.4	5.5	1.239	91	36.8%	99.5%
9C	10.3	59.8	5.7	1.222	96	35.2%	98.9%
10A	21.9	61.2	11.8	1.193	133	29.9%	94.7%
10B	22.5	60.7	12.1	1.183	137	26.4%	94.2%
11A	34.6	59.6	23.1	1.110	200	11.8%	84.6%
11B	35.6	60.3	24.6	1.117	207	12.2%	83.8%
11C	35.2	61.2	24.5	1.124	202	11.8%	84.0%

NOTE: [a]The liquid fraction of the ammonia release was calculated from experimental measurements. It is expressed as a percentage of the liquid ammonia mass captured in the catch tray, weighted against the total ammonia mass released from the lecture bottle. This value is a direct measurement of the liquid mass on the catch tray using a scale. [b]High mass balance is attributed to the uncertainties in the photoionization detector concentration measurements at higher relative humidity.

When the calculated ammonia release fractions were compared to the environmental variables tested, lower temperature TSs 1, 3, and 9 exhibited higher liquid fractions relative to other TSs.

When the mass released from the source is compared to the mass observed within the chamber, the mass-balance yield indicates a degree of ammonia loss depending on the environmental conditions. The mass balance ranged between 84% and 100% when all trials are considered. Its reproducibility suggests that the high temperatures yield the lowest ammonia mass balance; cold temperatures (-15 to 0 °C) yielded ammonia mass balances close to 100%, while hot temperatures (30 °C to 40 °C) yielded values from about 84 to 90%. Based on the measured values [1], the environmental conditions, characterized by higher temperature and increased humidity, likely caused a shift in the mass balance, resulting in a lower yield.

The AH variable was also related to mass balance because AH is a function of temperature. Moreover, the temperature strongly affects the pressure in the ammonia lecture bottle (factor of 6 or 7 higher for 40 °C than for -15 °C). The video revealed that there may be substantial water condensation occurring within the ammonia plume cloud in the initial jet and for a minute or so after the release stopped. The video also shows the ammonia behavior and its movement as it interacts with its surroundings. At higher AH, the

dense cloud hovered over the catch tray then spilled over the tray lip, accumulated near the floor and evaporated.

The plume pH measurements that were made suggested that the ammonia gas-water vapor equilibrium within the plume shifted toward the ammonium ion at higher temperature, allowing potential chemical reactions. Solid residue, indicative of ammonium carbonate or ammonium bicarbonate, was observed on the floor and catch tray underside after high temperature (AH) tests. This was not observed during the colder tests and may be a reason for the 100% ammonia mass balance yield.

Table ES-3. Summary of Experimental Results, Simulated Rain Scenarios (TS 6 and TS 7)

22 °C / 50% RH (±1 °C and ±1.5% RH)							
TS No.	Simulated Rain					Ammonia Mass Balance	
	Rain Introduced	Rain Start (min)	Rain Stop (min)	Total Rain Volume (L)	Rain Pool pH	Total Ammonia Released (grams)	Yield After Rain
6A	During Release	-0.5	5.0	5.5	10.3	194.1	59.6%
6B	During Release	-0.5	5.0	5.5	10.0	202.7	58.7%
6C	After Release	17.0	22.0	4.8	9.1	158.6	79.0% [b]
7A	During Release	-0.5	3.5	17.1	11.0 [a]	193.3	47.8%
7B	During Release	-0.5	3.5	17.1	10.1	180.7	48.7%
7C	After Release	17.0	22.0	21.4	10.5	182.7	55.8% [b]

NOTE: [a]TS 7A: Unique pH placement closer release and with smaller rain collection beaker and funnel.
[b]Ammonia mass balance yield without the rain is 92.5% and 92.6% for TS 6C and TS 7C, respectively.

The rain scenario demonstrated the highest removal of ammonia; more ammonia was absorbed into the rainwater when the rain was active during the two-phase release event (i.e. two-phase release event with a strong momentum jet, which lasted for about 10 seconds) compared to raining during the gas phase only.

From these environment-controlled experiments, it has been observed that the headspace pressure, which is a function of temperature, is the dictating factor. Therefore, it is inherently safer for storage or transportation to occur in a cold environment. The headspace pressure primarily governs the pressure of the containment vessel, whether it is a storage tank or a tanker vessel. When the temperature varies from -18 °C to 40 °C, the pressure ranges from 37 psi to 233 psi. Being in a cold environment significantly lowers the headspace pressure, which decreases the flow rate in the event of a leak and increases the liquid fraction, reducing downwind hazards.

Table ES-4. Summary of Experimental Results, Excess CO_2 Scenario (TS 8) [a]

30 °C / 60% RH (±1 °C and ±1.5% RH)									
TS No.	Excess CO_2						Ammonia Mass Balance		
	CO_2 Introduced	CO_2 Start (min)	CO_2 Stop (min)	Total CO_2 Mass (grams)	CO_2 Yield	Solid Present?	Total Ammonia Released (grams)	Yield Before CO_2	Yield After CO_2
8A	After Release	10	12	864	98.7%	NO	177.4	92.7%	89.5%
8B	After Release	11	14	1,131	97.4%	NO	174.2	91.3%	87.4%
8C	Before Release	-4	-2	1,188	96.2%	YES	193.9	92.0% [b]	80.3%
8D	Before Release	-10	-5	1,265	95.8%	YES	184.7		79.3%

NOTE: [a]CO_2 was introduced both after and prior to the ammonia release at time zero. The mass of CO_2 released, along with the corresponding mass yield contributing to the reaction, was calculated and compared to environmental conditions without CO_2 to determine its effects on ammonia release. [b]Data was not collected; the value is the TSs 8A/B Yield Before CO_2 average.

The excess CO_2 did not result in a notable reaction with ammonia gas. Despite CO_2 not reacting directly with ammonia, this experiment was conducted to determine if any reaction might occur with moisture in the air, resulting in the formation of carbonic acid as an intermediate, which is formed when CO_2 is in aqueous solution. Carbonic acid, a weak acid, reacts readily with ammonia. [2] Under the controlled humidity and stoichiometric ratio examined in this study, no noticeable removal of ammonia was observed. However, the formation of a white solid was noted within the catch tray and liquid pool. The solid did not readily sublime at room temperature and was analyzed. The analysis suggested the solid was a mixture of ammonium carbonate and/or ammonium bicarbonate and concluded the solid was not ammonium carbamate. A different solid residue accumulated in the catch tray, as the liquid pool evaporated during very cold temperature (-15 °C) conditions. The solid sublimed at temperatures just above freezing. Based on the considerable observation differences and lack of water vapor, it was assumed that this solid was ammonium carbamate.

In summary:

- Temperature: The primary factor influencing temperature is the pressure behind the two-phase jet release.
- Humidity (water vapor content [in g/m3] of air): Humidity largely influences the formation of visible white clouds (plumes) through the condensation of ambient water vapor, which contributes to liquid-phase reactions.
- Rain: The effects of heavy and light rain on the ammonia plume were the most prominent among all environmental factors examined in the study.
- CO_2: Although ammonia does not directly react with CO_2, there is a condition where excess CO_2 in a high-humidity environment could drive a reaction with ammonia in a confined space.

These factors will aid in advancing modeling algorithms for consequence assessments and developing mitigation strategies to reduce hazards.

This page intentionally left blank.

1.0 INTRODUCTION

1.1 Introduction

The Jack Rabbit (JR) III test series is to experimentally characterize toxic inhalation hazard ammonia releases. An accidental or intentional large-scale release of anhydrous ammonia can rapidly generate a lethal vapor cloud when the pressurized liquid is released from containment. Critical knowledge and data gaps exist, requiring experimentation to inform the scientific foundation to advance modeling, emergency response, community protection, countermeasures, and mitigation technologies and strategies. To address these gaps in the understanding of anhydrous ammonia plumes, the U.S. Department of Homeland Security (DHS) Science and Technology Directorate (S&T) and the DHS Countering Weapons of Mass Destruction Office (CWMD) collaborated with the Defense Threat Reduction Agency (DTRA) to design and execute chamber tests.

The objectives of the chamber experiments are first to study and experimentally characterize the effects of environmental factors (temperature, humidity, and carbon dioxide [CO_2])/water, and rainfall) on released ammonia plume behavior, reactivity, and environmental fate; and then identify critical data targets and inform development of test plans for subsequent field release experiments. This report describes the results from the environmental controlled chamber experiments and comprehensive datasets to inform the following:

- Improved chemical hazard modeling
- Better planning and capability to withstand/recover quickly from release incidents
- More efficient and effective emergency response
- Improved mitigation measures to reduce the impact to affected populations and infrastructure

1.2 Background

Demand for anhydrous ammonia has rapidly increased due to its agricultural use and low carbon emissions when utilized as a fuel. [6] Anhydrous ammonia is readily available in bulk quantities, which introduces hazards and risks from potential accidental releases into the environment. There are minimal experimental data involving anhydrous ammonia releases in an environmental controlled chamber that identify the physical dispersion and chemical reactivity dependances on natural environmental factors like temperature, humidity, air density, rainout, and excess CO_2 conditions.

Anhydrous ammonia is most commonly stored in two different ways: 1) as a refrigerated liquid at ambient pressure (temperature must be less than the boiling point of -34 °C); and 2) as a pressurized

liquefied gas at near-ambient temperature. For the same mass of ammonia, the release from refrigerated storage is less hazardous than the release from pressurized storage. This is because the refrigerated liquid forms a pool on the ground and enters the atmosphere by evaporation, whereas the pressurized liquid is a two-phase momentum jet, with a much larger emission rate directly into the atmosphere. Thus, the current study focusses on pressurized liquefied storage.

To address first responder operational needs for responding to toxic gas release incidents, JR III Scientific Advisory Group and JR III Technical Working Groups (WGs) were formed to bring science-driven solutions to the identified capability gaps. Core WGs include Data Quality, Modeling, Surface Deposition and Reactivity, Source Term, Instrumentation, Emergency Response, and Health and Human Effects. Moreover, in the past two years, detailed laboratory studies and a small-scale outdoor ammonia release at the Technology Experimentation and Characterization Field Trials at the West Desert Test Center, U.S. Army Dugway Proving Ground, took place to address some of the knowledge gaps concerning hazardous ammonia releases. [7, 8, 9] Languirand et al. (2023) carried out experiments at the U.S. Army Combat Capabilities Development Command Chemical Biological Center where small concrete sections were exposed to liquid ammonia in a laboratory chamber, and the absorption and subsequent evaporation measured. [10]

In preparation for the anticipated large-scale JR III ammonia field trials, three experimental phases were identified, and the following three phases (with respective sponsors) were:

- Phase I – DTRA: Proof-of-concept cloud dispersion and deposition in a static chamber at a range of typical temperature and relative humidity (RH) conditions. [1]
- Phase II – S&T Chemical Security Analysis Center (CSAC): Static chamber studies on the effects of extreme environmental conditions (temperature, RH, rainfall, excess CO_2) on ammonia (liquid and vapor) releases.
- Phase III – Transport Canada: Dynamic chamber (including wind flow) studies of soil and vegetation effects on deposition and evaporation of ammonia.

This technical report focuses on observations and results for Phase II, including cloud flow and dispersion (chamber), rainout (deposition) for a range of temperature and RH, covering effects of extreme environmental conditions on ammonia release characteristics. In addition, a few tests investigated interactions between ammonia, ambient water, and CO_2. The Phase I test matrix was completed in advance of the Phase II test matrix; the test approaches for the liquid and gas measurements were likewise similar. The Phase I results were used to identify trends that were further investigated during Phase II. [1] Phase III testing is currently underway.

1.3 Overview

The objective of experimental results reported herein builds upon the Phase I test results and evaluates the effects of simulated extreme environmental conditions on pressurized liquified anhydrous ammonia releases. In addition, the physical and chemical interactions between ammonia, ambient water vapor, ambient rain, and CO_2 were also studied. Several experimental variables were considered in Phase II, including:

- Temperature (°C)
- Relative Humidity (%), which can be combined with temperature to calculate Absolute Humidity (AH) (g/m^3)
- Simulated Rainfall ($g/s \cdot m^2$)
- Excess CO_2 (ppm)

The Phase II test matrix was informed by Phase I test results and initial Phase II tests at high RH, where condensation occurred that interfered with concentration measurements. The final Phase II test matrix, analyzed in this report, consisted of 11 test scenarios (TSs) defined by unique ambient temperature and RH values.

A group of three TSs was intended to simulate temperature and humidity, naturally occurring extreme conditions, arctic winter (subzero temperature), arid desert (hot and dry), and tropical swampland (hot and humid). A pair of TSs were conducted at high RH and at hot and cold temperatures to investigate potential condensation effects after the ammonia release. A second group of three TSs included ambient temperature and RH values replicated from the Phase I average environmental conditions, maintaining RH at 60% to assess temperature dependency and collect additional data on ammonia gas, liquid, and condensed vapor. The third group of TSs consisted of excursion trials incorporating rain and CO_2 to demonstrate proof of concept, testing whether ammonia interacts with simulated raindrops and excess CO_2. The two simulated rainfall TSs presented in this report studied the effects of light and heavy rainfall on the ammonia plume and on the deposited liquid ammonia. The excess CO_2 TS investigated reactions between CO_2, water vapor and liquid, and ammonia vapor and liquid systems.

The test environment chamber was equipped with a suite of instruments to continuously monitor and record ambient thermodynamic variables (temperature, RH, and pressure) and ammonia gas concentrations. These measurements are consistent with those carried out during the JR III Phase I Chamber Studies. [1] The sensor suite was slightly altered for the unique simulated rain and excess CO_2

TSs (a pH probe was added for rain measurements, and CO_2 sensors were added for the CO_2 reaction investigation).

The pre-conditioned test environment was isolated and static for about one minute prior to the release, during the approximate 10-second release and for an additional 30 minutes after the release. After 30 minutes, mixing fans were initiated to induce ammonia gas homogenization for the mass balance calculation. Finally, the test environment was scrubbed with the chamber ventilation system. Deviations from this standard test timeline were noted in the test data and report discussions. The ammonia release, measurements, and post-test ventilation scrubbing were all operated remotely, and the accompanying data were recorded on a central data acquisition (DAQ) module. The collected datasets were imported to, and evaluated with, Microsoft Excel.

2.0 TECHNICAL APPROACH

The experimental methodology designed to meet objectives and a description of the specific measurements are provided in this section. Details on the technical approaches are provided in the following key areas:

- Test Matrix
- Test Environment
- Environmental Conditioning
- Test Equipment and Sensors
- Ammonia Source
- Measurements in the Chamber
- Calibrations
- Test Procedure
- Simulated Rain Scenarios
- Excess CO_2 Scenario
- Description of Delivered Data

2.1 Test Matrix

The Chamber Studies documented in this report evaluated pressurized liquified anhydrous ammonia release scenarios and two primary environmental variables, namely temperature in °C and RH in %. AH in units of grams of water vapor per cubic meter was then calculated from the actual temperature, RH, and test chamber pressure measurements. The environmental conditions (temperature and RH) for this test series were selected to simulate extreme and average environmental conditions. In addition, engineered systems were designed to simulate rain and CO_2 effects on the ammonia plume and deposited liquid.

The 11 TSs are summarized in the test matrix provided in **Table 1**. The environmental temperature and RH values simulated in the test matrix are indicated on the psychrometric chart provided in **Figure 1**. TSs that fall on the same dashed, horizontal red lines have the same AH and vapor pressure. Temperature and RH combinations were selected to mimic average as well as extreme environments. The wide range of test conditions shown on the psychrometric chart (**Figure 1**) was chosen to simulate an ammonia release at a variety of locations and environments, such as deserts, humid swamps, and artic winter conditions. The "Number of Replicates" indicates the number of times that a test was run for those temperature and RH conditions. In all cases, the ammonia release mass was 0.375 lb. (170 grams) (±10%), and the chamber volume was 1,800 ft^3 (51 m^3).

Table 1. Test Matrix for Extreme and Average Conditions (as determined by Temperature and RH), with Some Taking Place During Artificial Rain, and Some Having CO_2 Introduced.

TS No.	Temp (°C)	RH (%)	AH (g H_2O per m^3 air)	Number of Replicates	Description	Ammonia Mass Released in Test Environment Volume
1	5	90	5.9	1 (A)	High humidity, varied temperature	~0.375 lb. (170 grams) (±10%) into 1,800 ft^3 (51 m^3) chamber
2	15	90	11.8	2 (A,B)		
3	-15	25	0.3	3 (A,B,C)	Extreme Conditions (Artic, Desert, Swamplands)	
4	40	10	5.8	3 (A,B,C)		
5	33	90	32.9	3 (A,B,C)		
6	22	50	8.6	3 (A,B,C)	Light Rain	
7	22	50	8.6	3 (A,B,C)	Heavy Rain	
8	30	60	18.2	4 (A,B,C,D)	Excess CO_2	
9	10	60	5.6	3 (A,B,C)	Ambient Conditions (varied temperature and average RH repeats of Phase I TSs; included pH paper data collection)	
10	22	60	12.0	2 (A,B)		
11	35	60	24.1	3 (A,B,C)		

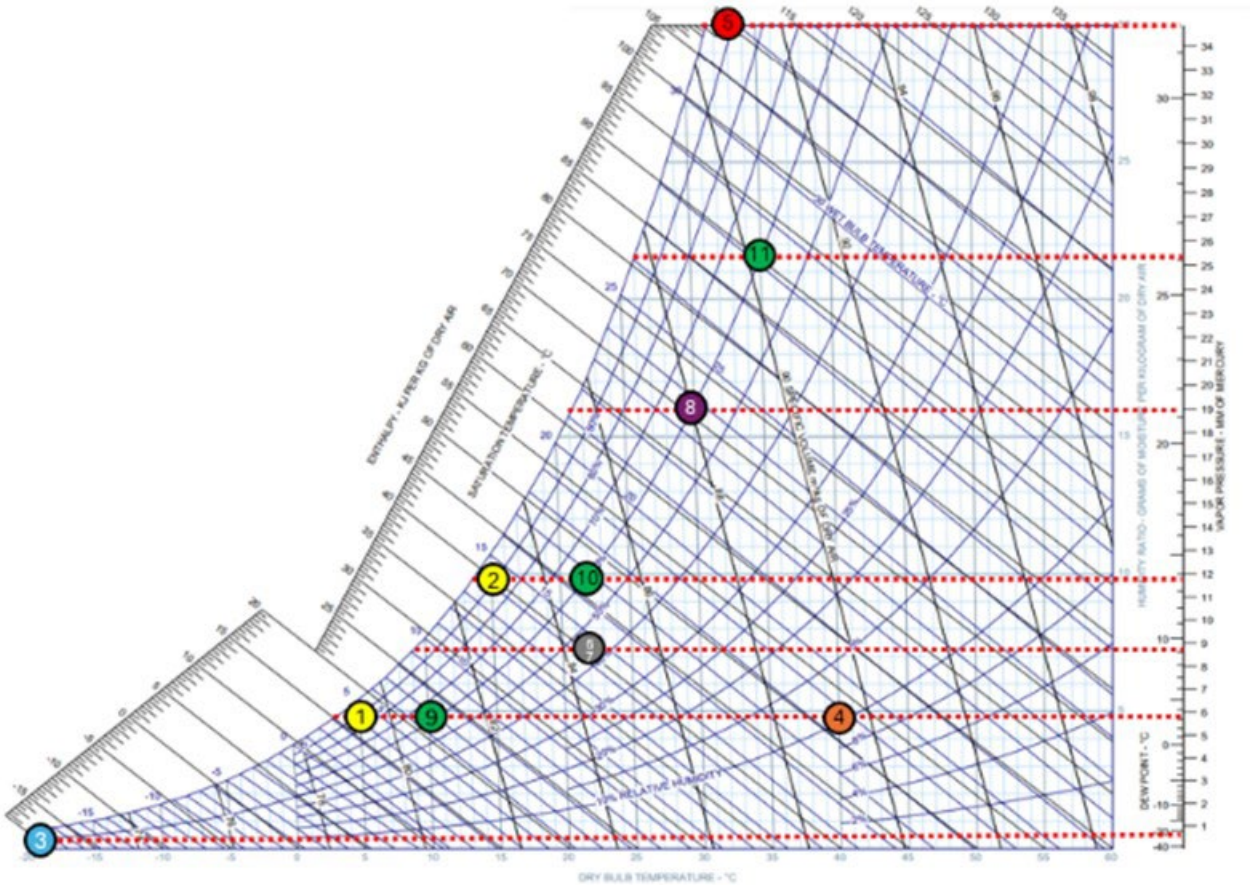

Figure 1. Test matrix test scenarios denoted on a psychrometric chart. The horizontal axis is dry bulb air temperature, and the vertical axis is vapor pressure (proportional to AH).

2.2 Test Environment

All tests were conducted within the static chamber, which is a carbon steel cuboid with internal dimensions 9.50 feet (2.90 m) tall, 9.50 feet (2.90 m) wide, 40.0 feet (12.2 m) long, and an internal volume of 3,610 ft^3 (102 m^3). Conditioning the full volume of the chamber was deemed excessively time-consuming. To accelerate the test matrix completion rate by reducing conditioning time, the final test environment volume was reduced by a factor of two by constructing a rigid, insulated false wall within the chamber. The wall was positioned on the 20.0 feet (6.10 m) centerline, giving an actual test environment volume of ~1,800 ft^3 (51 m^3).

Throughout this report, mentions of chamber connection locations, ancillary equipment locations, and viewing perspectives are identified using cardinal directions. For reference, the chamber door is located on the south end, and the south half of the chamber was referred to as the "anteroom." The test environment was constructed inside the north half of the chamber, per **Figure 2**.

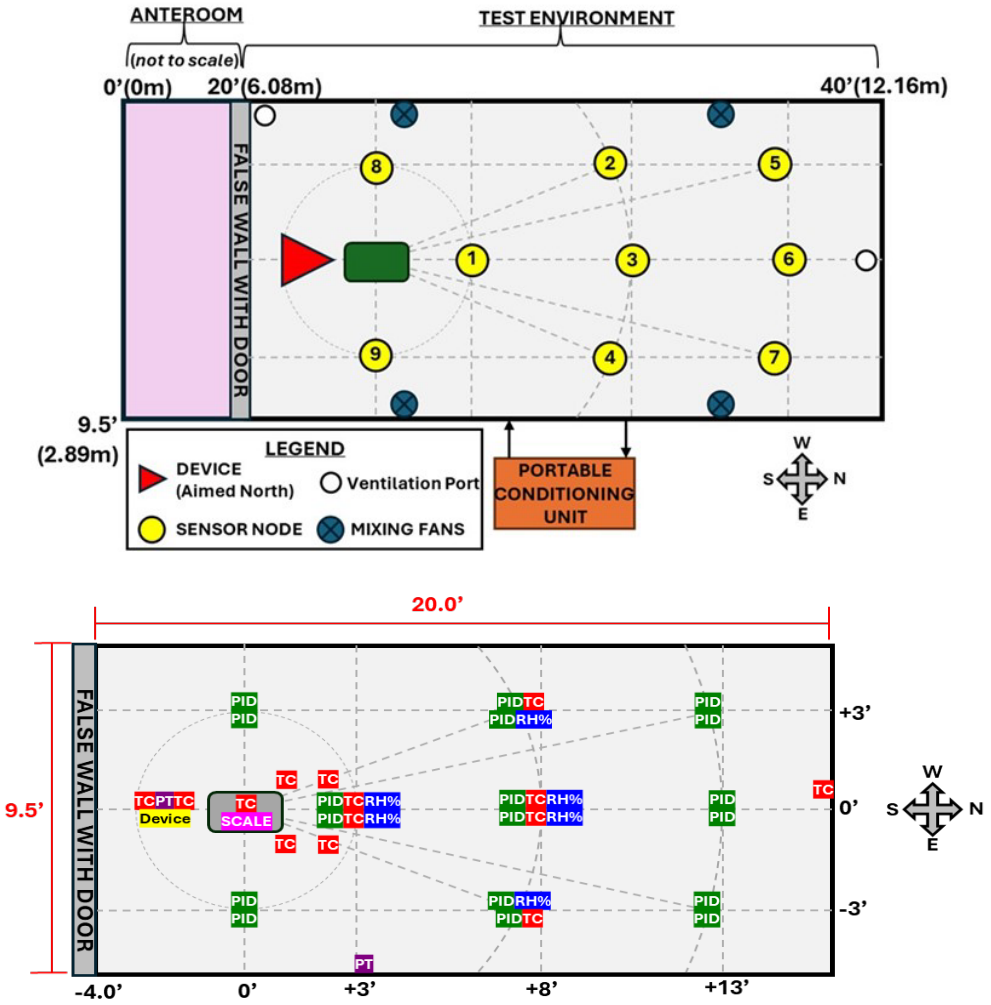

NOTE: (Top) The "Device" is the pressurized ammonia lecture bottle from which pressurized liquefied ammonia was released. (Bottom) Instrumentation Layouts. PID-Photoionization Detector, TC-Thermocouple, RH%-Relative Humidity, and PT-Pressure Transducer.

Figure 2. Test environment configuration.

Within the test environment, various types of gas sensors were placed on 6.0 feet (1.8 m) vertical poles (referenced in this report as sampling "nodes") constructed of aluminum strut channel affixed to aluminum mounting bases. A total of four 16" (41 cm) oscillating mixing fans were mounted on the walls (two each on the west and east wall) at two heights. Each mixing fan was capable of moving 1,700 ft^3 (48 m^3) of air per minute, providing a mixing rate of 6,800 ft^3 (~190 m^3) per minute. LED lights lined the walls to provide adequate lighting with minimal heat generation into the test environment. All support equipment was mounted with magnets. Photographs of the inside of the test environment are provided in **Figure 3**.

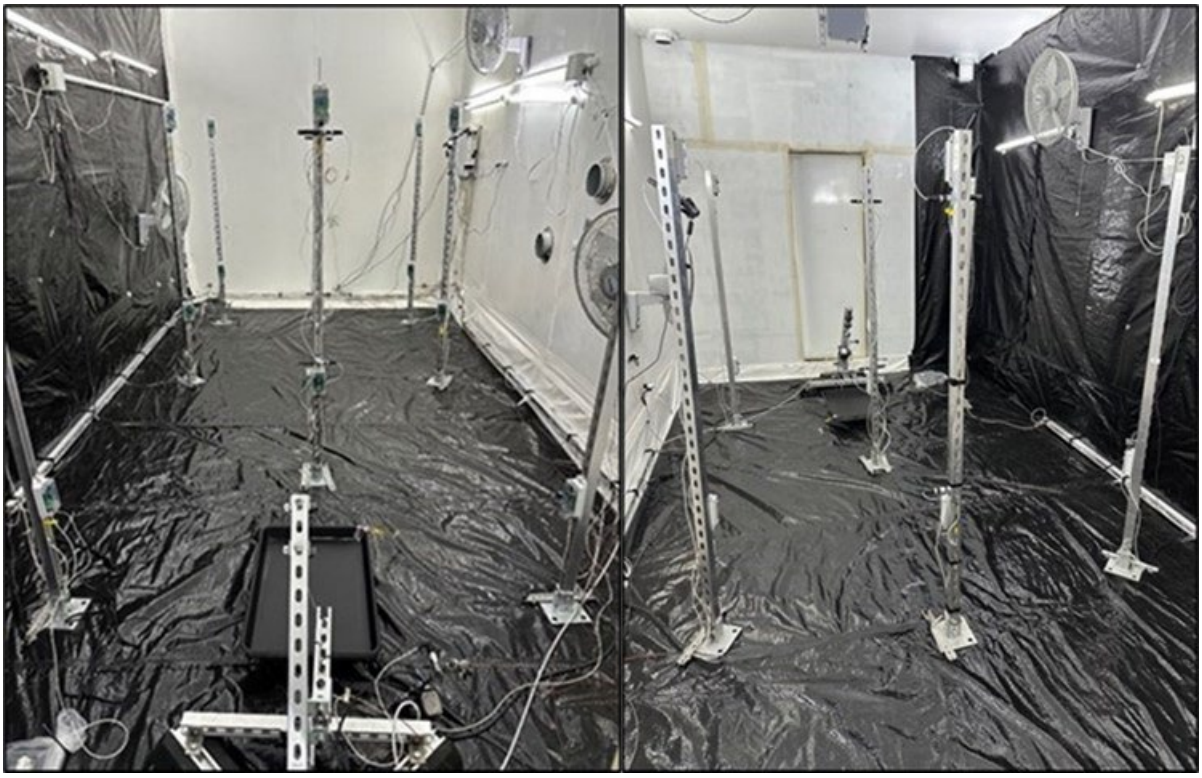

NOTE: The “catch tray” is seen in the left photo.

Figure 3. Test environment setup view to north (left) and south (right).

The walls of the test environment were painted with Rust-Oleum CV740 alkyd enamel white paint to protect the carbon steel walls from corrosion. Wall seams were sealed with silicone caulking and taped over with polypropylene film tape for further leak protection. The floor and walls were lined with a high-density polyethylene (HDPE) tarp.

The exterior of the test environment was coated with a 3.00” (7.62 cm) layer of closed-cell spray foam insulation to minimize thermal conduction from the ambient conditions though the chamber walls. The closed-cell spray foam had an insulation R-value of 7.00 per inch (2.76 per cm) and the 3.00” (7.62 cm) layer is rated to reduce thermal conduction through the walls by 96%.

Post-test ventilation (initiated about 40 minutes after the release ended) for the test environment was driven by a blower connected to a ceiling port on the north end. Ambient air was also provided from a second ceiling port in the southwest corner. The blower pulled air from the test environment and directed it through two packed bed scrubber drums arranged in parallel.

The scrubber drums were packed with impregnated activated carbon, designed specifically for scrubbing of ammonia gas. The scrubbed test environment air was processed in accordance with the test site’s

physical hazard analysis site control program. All ceiling ventilation ports were equipped with remotely controlled blast gates to control test chamber flows. All ventilation plumbing was comprised of 4.00" (10.2 cm) diameter polyvinyl chloride piping, which has excellent compatibility with liquid ammonia and anhydrous ammonia up to 48 °C.

2.3 Environmental Conditioning

The test environment temperature and humidity were controlled with the industrial portable conditioning unit (PCU) shown in **Figure 4**.

Figure 4. Portable conditioning unit (Russell Technical Products).

The PCU (Russell Technical Products, 810-3-3-AC) was positioned outside of the chamber with the inlet/outlet ports ducted directly to respective flanges on the east wall of the test environment. The ducting was insulated and equipped with a gate valve at the respective wall ports to isolate the test

environment from the PCU during testing. The PCU recirculated the pre-test environment air at 650 ft^3/minute (18.41 m^3/minute) and could condition the test environment air down to approximately -20 °C.

Before every test, the PCU conditioned the test environment with the ventilation isolation valves closed and the mixing fans turned on. The test environment sensor suite was monitored until the average temperature and RH reached the desired test conditions, and the lecture bottle temperature equilibrated to the air temperature for several minutes. The conditioning equipment and mixing fans were turned off and the PCU input/output duct valves were closed no less than one minute before release. The resulting configuration was an isolated and static test environment conditioned to the desired TS temperature and RH for the start of all Phase II tests. The PCU was used to precondition the test environment for all TSs and was not used during the test timeline (i.e., turned off and isolated from t = -1 minute through test completion).

2.4 Test Equipment and Sensors Specifications

This section defines the specifications of the suite of gas sensors, video, and ancillary equipment that were utilized within the test environment.

2.4.1 Photoionization Detectors

Photoionization detectors (PID) were the primary measurement instrument for the space and time-variable ammonia gas concentration within the test environment. IonScience MiniPID 2 sensors, shown in **Figure 5**, were utilized at all nodes and sensor height locations. There are nine locations in the chamber where measurements were taken (**Figure 2**). At each location, sensors were placed at two heights: one at 2 feet (0.61 m) designated as Low or L and the other at 6 feet (1.83 m) designated as High or H. Three arcs of sensors are used at 3 feet (0.915 m), 8 feet (2.44 m), and 13 feet (3.96 m) distances from the center of the release source. Each arc had three sensors—one at the center of the chamber and one at either side of the chamber at 1 foot (0.31m) from the wall. The layout for all sensors is included later in **Section 2.6**.

The PIDs featured a fast response time of less than 8 seconds and had an operational temperature range from -40 °C to 65 °C and an RH range from 0% to 90% (non-condensing). The PIDs could not be poisoned by extreme concentrations but could be compromised if residue permeated the protective filter and deposited on the lamp window. PID accuracy deterioration could be indicated by the baseline voltage signal drifting from the average established during calibration. The PID body diameter was 0.79” (2.0 cm), and it was 0.65” (1.7 cm) tall.

The PIDs were equipped with a 10.60 eV lamp, sufficiently above the 10.18 eV ionization energy of ammonia. The difference in ionization potential between a volatile compound and the lamp determined the response factor that was used to translate the PID response signal (millivolts) to concentration. The response factor for ammonia with a 10.60 eV lamp was 8.5 (i.e., 10 millivolt signal = 85 ppm). The PIDs had a linear detection range at concentrations below approximately 1,000 ppm, and a non-linear range at higher concentrations. Since concentrations in excess of 1,000 ppm were expected and the simple correction factor relationship would not be sufficient, manual calibrations were performed to derive the concentration measurements from the PID response, as described in **Section 2.7.3**. The PIDs were kept consistent with their respective nodes, i.e., PIDs stayed on the same node and height for every test.

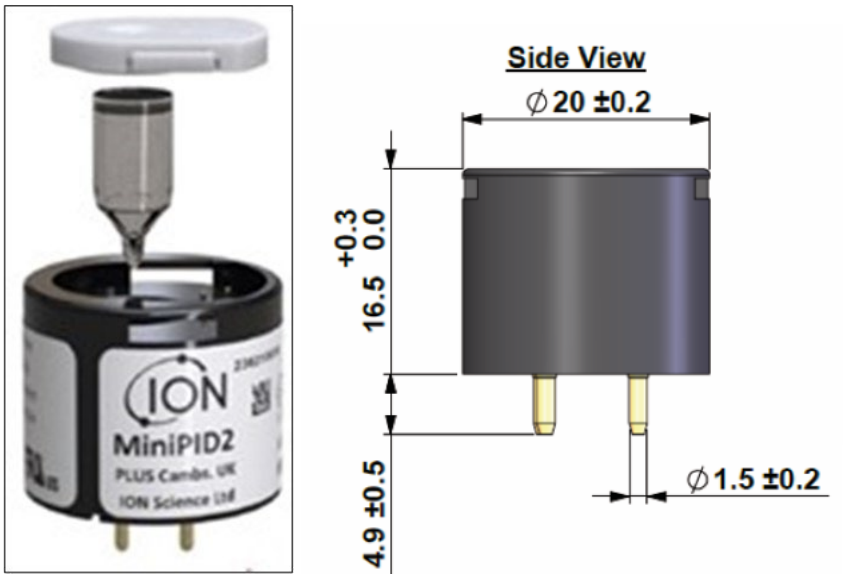

Figure 5. Photoionization detector (IonScience) with dimensions in mm.

2.4.2 Relative Humidity (RH) Probes

Six RH probes were used to measure the test environment RH. The Rotronic PC52 RH probes (**Figure 6**) featured a detection range of 0%-100% RH with a response time of less than 10 seconds. The rated accuracy was ±2.0% between 10% and 90% RH. The RH probes were rated for temperatures between -20 °C to 80 °C.

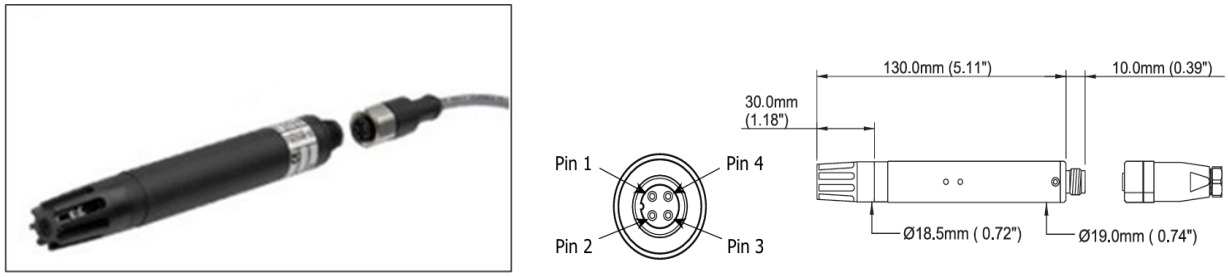

Figure 6. Relative humidity probe (Rotronic).

2.4.3 Thermocouples

Two (2) styles of K-type thermocouples (TC), which measure temperature, were utilized depending on the measurement application approach. The TCs that were used featured a temperature range of -200 °C to 925 °C with a response time of 0.5 seconds and an accuracy rating of ±0.75 C. However, due to the chemical compatibility with ammonia, special precautions had to be taken to ensure accurate measurements.

The TCs used to measure the chamber air, ammonia release stream, and liquid pooling temperatures were sheathed and grounded in 316 stainless steel (**Figure 7**, top). The other style of TCs used to measure wall and lecture bottle surface temperatures had an exposed sensor tip (**Figure 7**, bottom), which had poor chemical compatibility with ammonia. The exposed tip TCs were compressed to the surface of interest and sealed with adhesive insulation to accurately measure the temperature of the surfaces and to protect them from ammonia exposure.

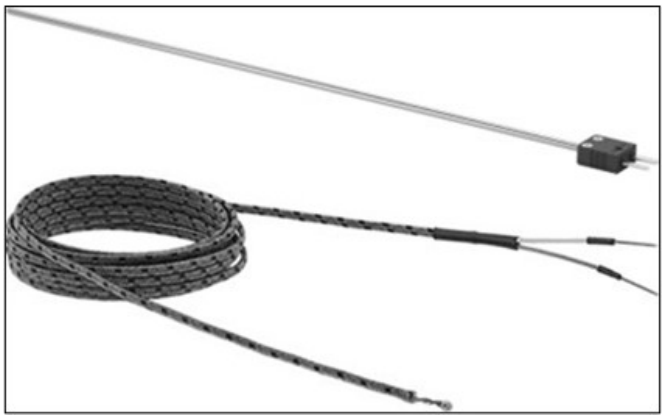

NOTE: Sheathed TC (top); Exposed sensor tip TC (bottom).

Figure 7. Thermocouple, type K 1/8 in (3.2 mm) x 24 in (612 mm) probe size.

2.4.4 Pressure Transducers

Pressure transducers (PT) measured the test environment ambient pressure and release manifold pressure. The OMEGA Engineering PX119 PTs (**Figure 8**) featured a piezoresistive ceramic sensor with a measurement range of 0-300 psia with ±0.5% accuracy, and a 1 millisecond response time. Their operating temperature range was -40 °C to 135 °C. The wetted parts were constructed of stainless steel. In this test series, three PTs were used. One PT was used to record test chamber pressure (chamber PT, remained constant), one was used to record lecture bottle pressure as shown in **Figure 2** (manifold PT, which was initially at the vapor pressure of ammonia at that temperature, and then rapidly decreased to ambient pressure in the approximate 10-second duration of the release), and one was used for the rain system pressure (rain PT).

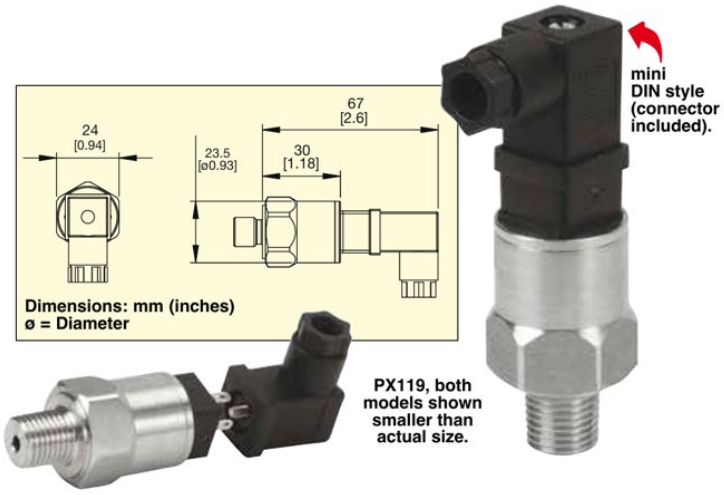

Figure 8. Pressure transducer (OMEGA Engineering).

2.4.5 Catch Tray and Scale

An aluminum pan was used as a catch tray for the ammonia release impact point. The lips around the edge of the tray helped contain as much as of the rained-out liquid as possible. The catch tray was placed on top of a bench scale as shown in **Figure 9** to measure the mass of liquid ammonia and possible water vapor and ammonia gas condensation within the catch tray. The catch tray was positioned such that the south edge was directly underneath the manifold outlet port (the release point) and aligned for the ammonia jet to impact the centerline of the tray.

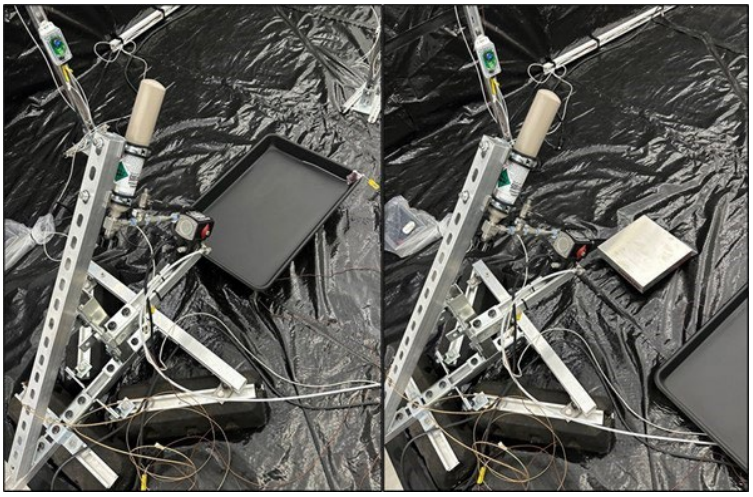

Figure 9. Release configuration with catch tray (left) and scale underneath (right).

The catch tray was constructed of 12-gauge aluminum (0.080”, 2.0-millimeter (mm) thickness), weighed 2.20 kg, and measured 25.8” (65.4 cm) long by 17.8” (45.1 cm) wide by 2.25” (5.72 cm) deep (i.e., the lip around the edge). The catch tray was primed with self-etching primer (Rust-Oleum 249322 Automotive) and painted with matte black enamel (Rust-Oleum 7776830). The self-etching primer was used to increase the durability of the paint coating. The flat black enamel was chosen to provide a chemically compatible, durable coating with low reflectance and high emissivity backdrop for the Forward Looking Infrared (FLIR) camera. These properties ensured the catch tray would not reflect infrared (IR) light from objects around the test environment back to the IR camera.

The scale (Ohaus Defender 6000) was designed to withstand the high-pressure jet without compromising its weighing accuracy. The scale was 10.0” (25.4 cm) long by 10.0” (25.4 cm) wide by 3.00” (7.62 cm) high. The scale capacity was 4.5 kg with 0.2 grams resolution; the mass analog output signal from the digital transmitter was wired to the DAQ for continuous recording. The catch tray mass was monitored over time to evaluate: first, the rainout mass during the 10-second duration of the momentum jet; second, the evaporation mass; and lastly, the completion time. Spot calibrations were performed on the catch tray with calibrated weight sets before each test.

2.4.6 Safety During and After the Ammonia Release

Several electrochemical sensors were positioned outside of the test environment to identify ammonia leaks for personnel safety. The AlphaSense NH3-AF electrochemical sensors (**Figure 10**) had a much lower detection range (0–100 ppm) and slower response time (<150 seconds) compared to the PIDs used inside the chamber. Electrochemical sensors were susceptible to being poisoned after being exposed to concentrations much higher than their detection range. Therefore, the electrochemical sensors were only

utilized for leak detection outside of the test environment and were not integral to the test environment sensor suite. The test environment ventilation system delivered the post-test ammonia through two packed-bed scrubbers arranged in parallel. The scrubbers had an impregnated activated carbon design specifically for scrubbing of ammonia gas. The scrubber outlets were monitored with the electrochemical sensors to determine if ammonia gas penetration occurred.

Figure 10. Electrochemical sensors (AlphaSense with a diameter of 16 mm).

2.4.7 Videos

A FLIR A325sc camera was used to record IR videos of the ammonia release stream and the catch tray contents. Also, high definition (HD) cameras were deployed at four locations within the test environment to capture the ammonia release event and visible cloud behavior. The IR videos, which feature a color-contoured temperature display, were recorded at 320 x 240 resolution at 60 frames per second (fps). It is important to note that the FLIR camera minimum temperature detection limit was -20 °C (about 13 °C above the boiling point of ammonia). The FLIR camera was mounted on the ceiling of the test environment (chamber) to provide an unobstructed top-down view of the release event and liquid pooling within the catch tray. This orientation also provided the best perspective of the release event due to the FLIR camera's limited field of view. The FLIR camera was co-located with one of the HD cameras, as shown in **Figure 11**, to provide a visible reference perspective.

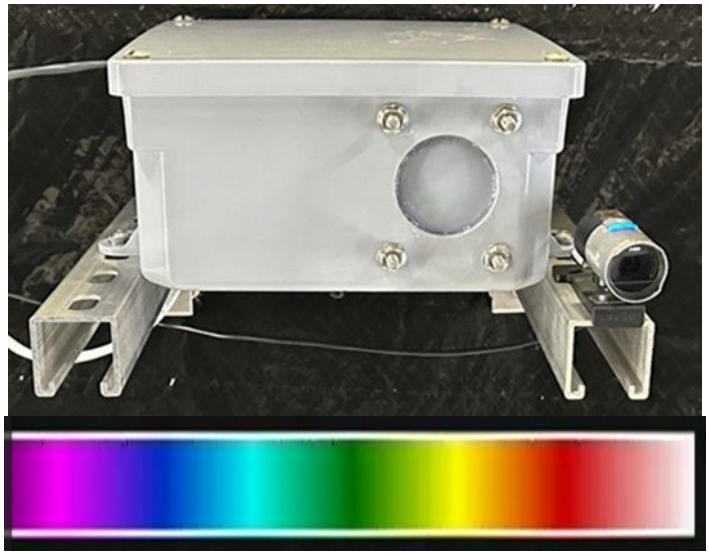

NOTE: Shown from catch tray point-of-view (looking upward). The color representation of FLIR thermal imaging the coldest temperature being the purple end, and the hottest temperatures represented by red on the bar shown above.

Figure 11. FLIR camera with dimensions of 170 × 70 × 70 mm next to HD camera.

The FLIR camera was mounted inside an enclosure to withstand the corrosive environment. It was fitted with an IR transmissive, ammonia-compatible, polymer window (Edmund Optics, #32-806). This enclosure was necessary to protect the FLIR camera from being attacked by ammonia during testing. The HD cameras did not require this protection. By co-locating both the HD camera and the IR camera, the images complement each other to show thermal changes in the plume and the visual plume.

While steps were taken to ensure the temperatures reported from the FLIR IR video were as quantitative as possible, a combination of factors limited the effectiveness of the FLIR camera. The need for a protective optical window, a wide variety of surfaces and substances in the frame with different emissivity factors, and the dependence of the temperature on a material's emissivity resulted in compounding error. This compounding error along with a temperature effect on the variables limited the effectiveness of the IR calibration. Additionally, the emissivity values for all substances of interest (e.g., pooled liquid ammonia, ammonia clouds, catch tray surface) needed to be experimentally determined to use the FLIR camera to determine surface temperature. Therefore, this report is limited to the color representation, with the coldest temperatures depicted as the purple end of the spectrum, followed by blue, green, yellow, and the hottest temperatures represented by red on the bar. More details on calibration can be found in **Section 2.7.2**.

Four (4) HD cameras were deployed inside the test environment to capture the ammonia release event. Camera 1 (Cam 1) was used to capture a top-down view of the ammonia outlet (co-located with the FLIR

IR camera). Camera 2 (Cam 2) was positioned on the east wall to capture a side view of the ammonia release, catch tray, and subsequent vapor cloud. Cameras 3 and 4 (Cam 3 and Cam 4) were used at various locations throughout the chamber depending on points of interest. These cameras were mainly positioned in the north end to capture the wide-angle perspective of the ammonia vapor cloud progression. The HD cameras recorded at 1080p resolution at 30 fps.

2.5 Ammonia Source

The ammonia source was a 12.0” (30.5 cm) long by 2.0” (5.1 cm) diameter lecture bottle filled with ~0.375 lb. (170 grams) of pressurized liquefied anhydrous ammonia (actual values measured ranged from 0.337 lb. to 0.439 lb. (153 grams to 199 grams)). The lecture bottle was mounted to a rigid aluminum frame with pipe clamp hangers and oriented for a 45° release angle with respect to the ground, as shown in **Figure 12** and **Figure 13**. The release manifold outlet port was positioned 12.0” (30.5 cm) above the catch tray.

A customized release manifold constructed out of stainless-steel pipe and fittings was attached to the lecture bottle regulator valve, and included a PT, backup safety valve, and remote release valve (RRV). The regulator valve attached to the lecture bottle served as the initial control valve to prime (i.e., fill the release manifold with ammonia, up to the RRV) the ammonia source for test execution. The release event (i.e., t = 0, test initiation) was controlled with the electronically activated pneumatic RRV. The RRV was rated for liquid and gaseous ammonia handling and a maximum pressure of 720 psi and minimum temperature of -46 °C. A backup valve was installed between the regulator valve and RRV in case the RRV failed to open while the manifold was primed. This backup safety valve was rated for 1,000 psi and -37 °C and included a lockable handle for safety.

Stainless steel was chosen for the ancillary piping and fittings to ensure compatibility with liquid and gaseous ammonia at a wide range of temperatures with a pressure rating greater than the expected manifold pressures. The threaded connections were sealed with polytetrafluoroethylene tape to ensure a complete seal and compatibility with ammonia.

Care was taken to ensure the lecture bottle regulator valve outlet was the manifold’s flow-restricting orifice at 0.125” (0.318 cm). To achieve this value, 0.250” (0.635 cm) National Pipe Thread piping and fittings (0.364” (0.925 cm) internal diameter [ID]) were used to build the release manifold; the RRV was a full-bore ball valve with equivalent ID. A 3.0” (7.6 cm) straight length of pipe was the manifold outlet

attached downstream of the RRV. The release manifold total length (regulator valve to outlet) was 12.0” (30.5 cm).

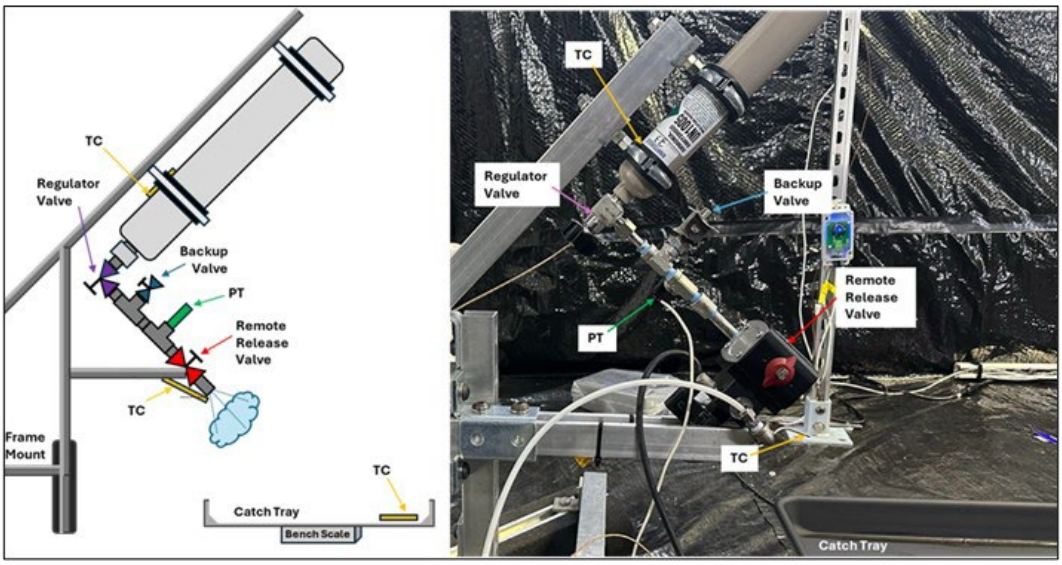

NOTE: Not to Scale. TC = Thermocouple (**Section 2.4.3**). PT = Pressure Transducer (**Section 2.4.4**)

Figure 12. Ammonia source configuration; schematic (left) and actual (right).

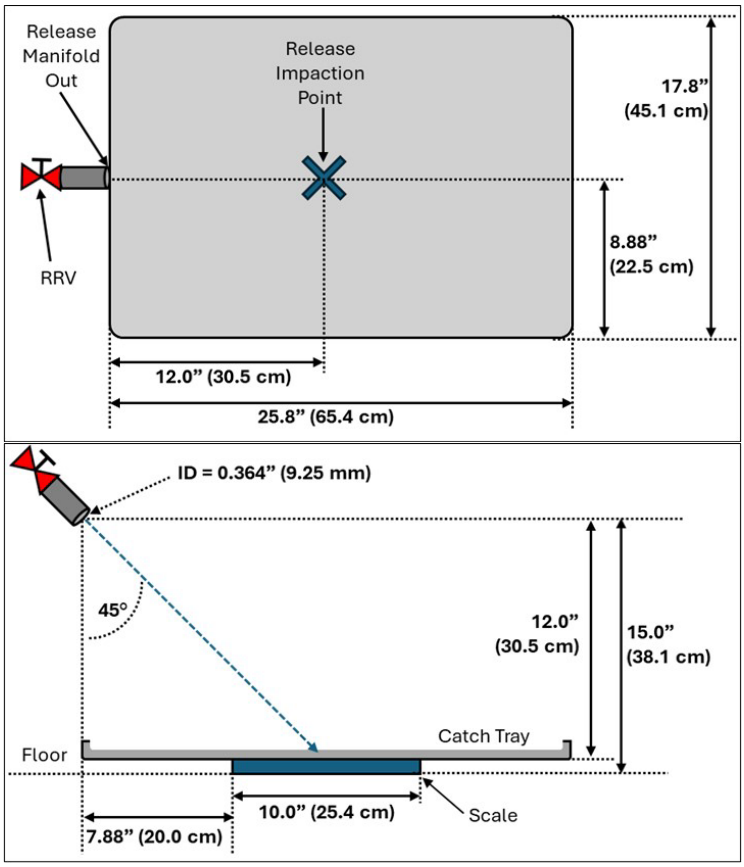

Figure 13. Ammonia source dimensions; X-Y (top) and X-Z (bottom).

The ammonia source and release manifold were equipped with several sensors to characterize the temperature and pressure during the release event. All ammonia source measurements were recorded on the same DAQ as the sensor suite used for the test environment.

2.5.1 Ammonia Release Temperature

The lecture bottle temperature was equilibrated to the test environment temperature before test execution. Three (3) K-type TCs were used to measure the temperature of the ammonia source as shown in **Figure 12**. An exposed tip style TC was installed between the lecture bottle body and pipe clamp hangers. This lecture bottle TC was used to determine the surface temperature of the lecture bottle body, which was assumed to be the temperature of the ammonia inside. The lecture bottle temperature measurement was evaluated against the theoretical temperature (i.e., the pressure associated with the ammonia vapor pressure at a certain temperature) calculated from the manifold PT as described in the next section (**Section 2.5.2**.). This TC also captured the temperature reduction due to expansion and pressure drop of the ammonia during the release, but the measurements may have been limited due to the rapid spread of ammonia. The two-phase jet lasted 5 to 10 seconds in all TSs. A second stainless steel-clad TC was used

to determine the temperature of the ammonia stream at the outlet of the release manifold. The release point TC was placed with care to limit the interference on the outlet stream. A third stainless clad TC was used to measure the temperature of the liquid pool in the catch tray. In the photograph, that TC is several centimeters above the tray, but it was lowered into the tray during the tests.

2.5.2 Ammonia Release Pressure

A PT, as described in **Section 2.4.4**, was installed in-line with the release manifold between the lecture bottle regulator valve and the RRV. This manifold PT was used to measure the manifold pressure when it was primed, and to monitor for potential manifold leaks.

Furthermore, this manifold PT was used to calculate the theoretical temperature of the ammonia within the lecture bottle. Note that the ammonia vapor pressure above the ammonia liquid in the lecture bottle was being dictated by the temperature set within the chamber. **Figure 14** provides the theoretical vapor pressure of anhydrous ammonia as a function of temperature [11].

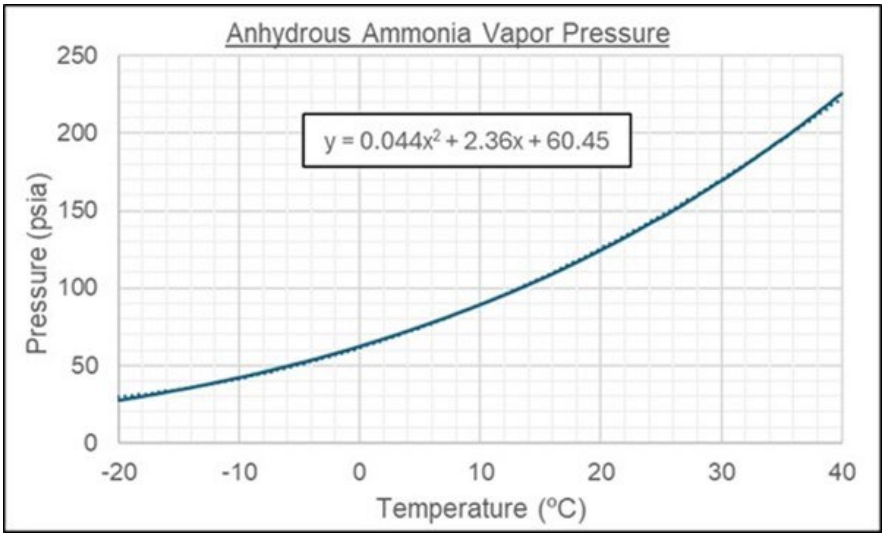

NOTE: The equation embedded in the graph [11] showing "y" which is the vertical axis (pressure) and "x" which is the horizontal axis (temperature). The equation is valid only for pressure expressed in psia and temperature expressed in °C.

Figure 14. Anhydrous ammonia vapor pressure vs. temperature.

The second order trendline represents the equation used to calculate the "theoretical" temperature of the lecture bottle contents, from the measured pressure when the manifold was primed. These calculations are provided in the test data files. The results showed that the theoretical lecture bottle temperature agreed within ±2 °C of the actual lecture bottle temperature measurement.

Attempts were made to use the manifold pressure measurement to calculate the theoretical flow rate during release but were not successful due to the large variations in pressure due to turbulence in the flow, and two-phase release dynamics.

2.5.3 Ammonia Release Mass Balance

The ammonia mass balance for each release test and replicate, expressed as ammonia gas yield, in percent, was calculated from experimental measurements. The mass of the anhydrous ammonia lecture bottle was quantified pre-test (full) and post-test (empty) for each individual test. The mass difference is the denominator in **Equation 1**.

$$Ammonia\ Gas\ Yield\ (\%) = \frac{Ammonia\ mass\ from\ PIDs\ during\ mixing}{(Lecture\ bottle\ pretest\ mass\ -\ post\ test\ mass)} * 100 \qquad (1)$$

Equation 1

The total mass of ammonia gas during mixing was calculated from the average concentration, as measured by all 18 PIDs, multiplied by the chamber volume during the homogenization time step. Homogenization occurred when the four mixing fans were activated well after observations of liquid evaporation were complete (typically at 30 minutes for 10 minutes). The average concentration value was calculated after 5 minutes of mixing. The locations of the 18 concentration measurements used to calculate the average are described later in **Section 2.6**. This approach was verified to produce a 100% mass yield, despite the unaccounted uncertainties associated with point measurements.

2.5.4 Ammonia Release Liquid Fraction

The liquid fraction of the ammonia release was calculated using the catch tray mass as determined from the scale measurements and the lecture bottle tare mass, per **Equation 2:**

$$Liquid\ Ammonia\ Fraction\ (\%) = \frac{Liquid\ Ammonia\ mass\ in\ catch\ tray}{(Lecture\ bottle\ pre\ test\ mass\ -\ post\ test\ mass)} * 100 \qquad (2)$$

Equation 2

The analog output of the scale was utilized to record the ammonia release liquid fraction and evaporation rate. More detail on the catch tray and scale can be found in **Section 2.4.5**. A possible issue was identified whereby the liquid in the catch tray could include condensed ambient water vapor (due to the very cold momentum jet and the cooling of the catch tray). This issue was addressed by subtracting mass (the plateau region after evaporation was completed) as part of the data analysis. It should be noted that the

videos showed liquid splashing off the tray onto the surrounding floor. Since the release occurred in two phases, much of the liquid ammonia could have been in aerosols, which are small enough to be carried by the momentum jet. Thus, there remains uncertainty in the estimated liquid ammonia fraction, as it is not accounted for in the mass on the catch tray. **Section 3.2.3** discusses the detailed context regarding the magnitude of drops in relation to the overall liquid pool mass on the catch tray for measuring the pooled liquid fraction.

2.6 Measurements in the Chamber

Measurements in the chamber consisted of ammonia concentration, RH, temperature, and pressure. Winds (flow) were not measured. All measurements were synchronized, time stamped and recorded on a single DAQ. Other time-dependent ancillary measurements recorded on the DAQ included catch tray mass, outputs of leak detection sensors, and chamber ventilation variables. DAQ recording of measurements was initiated at least 5 minutes before the release event, continued through the entire test timeline, and was completed after post-test scrubbing (usually about 40–60 minutes). Data collection occurred at 1.0 Hz intervals. Raw data were exported into the test data template, as described in **Section 2.11**.

The test environment contained nine PID sensor nodes as previously depicted in **Figure 2**. A more detailed version that specifies individual sensor locations within the test environment is provided as **Figure 15**. Both polar and Cartesian coordinates for each node, including the device and source can be found in **Table 2**.

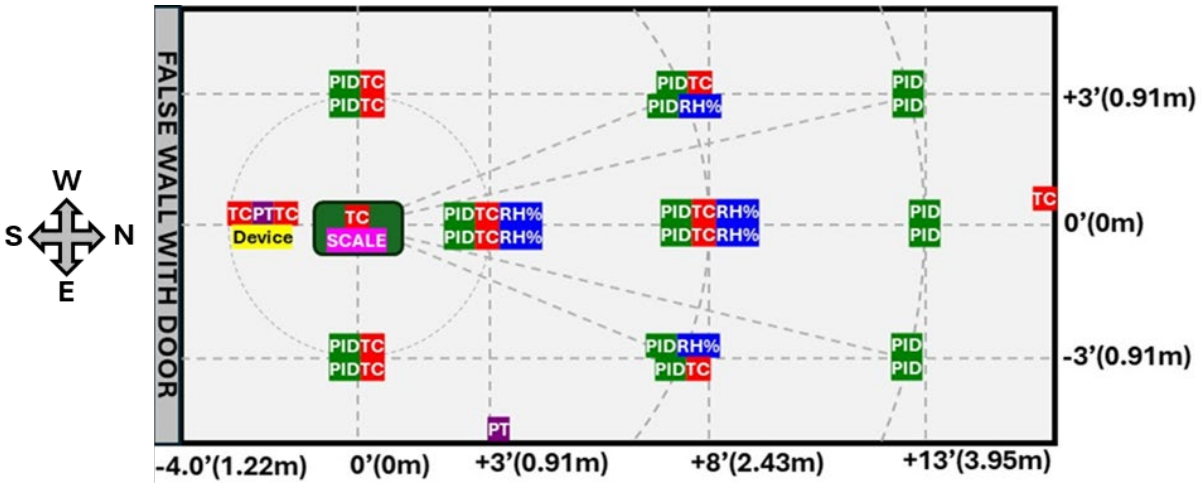

NOTE: PID measures ammonia concentration, TC temperature, PT pressure, and RH relative humidity.

Figure 15. Test environment individual sensor locations.

Each node contained sensors at two heights:2.0 feet (0.61 m) ("L", low) and 6.0 feet (1.83 m) ("H", high). The two heights are assumed to be representative of a layer at each node. The L measurements represent the layer from 0 (floor) to 4.25 ft (1.30 m), and the H measurements represent the layer from 4 ft (1.22 m) to 9.5 ft (2.90 m) (ceiling). There are three arcs of three samplers, at radial distances of 3 ft (0.91 m), 8 ft (2.43 m), and 13 ft (3.95 m). The outermost sensors are always 3 ft (0.91 m) from the axis (center) of the chamber and 1.75 ft (0.53 m) from sides. The "0" distance is at the center of the scale under the catch tray, which is 4 ft (1.22 m) from the "false wall with door." The end wall on the right is 3 ft (0.91 m) from the closest sampler.

This configuration was used to capture ammonia time and spatial patterns at standing respirable heights and to estimate a vertical difference between the L and H samplers. A photograph of a typical configuration of a group of sensors at node 1H is in **Figure 16**. Note that the sensors are a few cm separated horizontally and vertically.

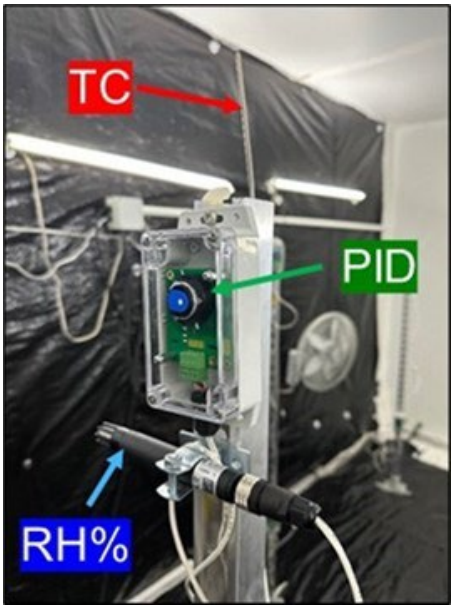

NOTE: For a sense of scale, the PID is about 6 inches (15 cm) higher than the RH%).

Figure 16. Setup of individual sensors at node 1H.

The coordinates for each node are provided in **Table 2**. The ammonia release was directed along the center of the grid due north, which was considered 0° for the polar coordinates. The north direction is to the right in **Figure 15**. The center of the catch tray was located at (0',0°). The table also includes the coordinates for the FLIR, HD Cam #1 and HD Cam #2 for every test replicate. Cam #3 and Cam #4 were placed at various locations throughout the test matrix and are defined in the individual data files.

Table 2. Sensor Node Coordinates, Relative to Center of Catch Tray

Node No.	Polar Coordinates (distance, angle, height)	Cartesian Coordinates (x, y, z)
Device	(1', 180°,1'3") (0.305m, 180°,0.381m)	(-1', 0',1'3") (-0.305m,0m,0.381m)
Catch Tray	(0', 0°,3") (0m, 0°,0.076m)	(0', 0',3") (0m,0m,0.076m)
FLIR	(0', 0°, 9'6") (0m, 0°, 2.90m)	(0', 0', 9'6") (0m, 0m, 2.90m)
Cam1	(0', 0°, 9'6") (0m, 0°, 2.90m)	(0', 0', 9'6") (0m, 0m, 2.90m)
Cam2	(5'2", 292°,1') (1.57m, 292°, 0.305m)	(2', 4'9",1') (0.610m, 1.45m, 0.305m)
1	(3', 0°) (0.914m, 0°)	(3', 0') (0.914m,0m)
2	(8', 22°) (2.44m, 22°)	(7'5", 3') (2.26m,0.910m)
3	(8', 0°) (2.44m, 0°)	(8', 0') (2.44m,0m)
4	(8', 338°) (2.44m, 338°)	(7'5", -3') (2.26m,-0.914m)
5	(13', 13°) (3.96m, 13°)	(12'6", 3') (3.81m,0.914m)
6	(13', 0°) (3.96m, 0°)	(13', 0') (3.96m,0m)
7	(13', 347°) (3.96m, 347°)	(12'6", -3') (3.81m,-0.914m)
8	(3', 90°) (0.914m, 90°)	(0', 3') (0m,0.914m)
9	(3', 270°) (0.914m, 270°)	(0', -3') (0m,-0.914m)

The majority of sensor nodes, and all of the PIDs, were placed downwind of the release to capture as much as possible of the plume during and after the release. Node 1 was located 3.00 feet (0.914 m) away from the center of the catch tray and was centered along the expected release path. Nodes 2, 3, and 4 were positioned along an 8.00-foot (2.44 m) arc or radius, and nodes 5, 6, and 7 were placed along a 13.0-foot (3.96 m) arc or radius. Nodes 8 and 9 were placed 3.00 feet (0.91m) to the west and east of the center of the catch tray, respectively, and therefore are on the same arc or radius as node 1.

2.7 Calibrations

Several background characterization pre-tests and ammonia calibrations were performed.

First, the ability of the test environment to maintain consistent temperature throughout the 30-minute static chamber timeline (i.e., how well the chamber was insulated from the outside environment) was characterized.

Second, the FLIR camera was corrected to account for the use of an IR transmissive window, which was needed to shield the camera from the corrosive test environment.

Third, the PIDs had a small linear range that did not fully encapsulate the expected range of ammonia concentrations. To solve this issue, a calibration at a wide range of concentrations was performed.

2.7.1 Test Environment Background Temperature

Several background calibrations were performed to characterize the temperature response inside the static test environment to the ambient conditions outside of the chamber with no ammonia present. These calibrations facilitated the ability to distinguish the thermal response related to the ammonia release, from the ambient background temperature variations during the static test timeline. However, the resulting correlation was only applicable during the static test environment.

The test environment was conditioned with the PCU and mixing fans to pre-determined temperatures dependent on the ambient temperature (ΔT) outside the test chamber. This study allowed the definition of a range of temperatures (test environment temperature – ΔT [outside of test chamber]). After a steady state ΔT was achieved (test environment air and wall temperatures were equilibrated within a few tenths of a degree °C), the PCU and the mixing fans were turned off (this is assumed to be t = 0) and the test environment was isolated for 30 minutes. The temperature inside the test environment was recorded, and the average air temperature at t = 30 minutes was documented. The results for the background calibrations are provided in **Figure 17**.

The background temperature tests in **Figure 17** were performed over a ΔT range of ±25ºC. The temperature rate on the y-axis is expressed in units of °C/minute. The linear trendline was fitted to the results with the condition that the line passes through (0,0). The calibration curve was applied to the observed test data.

For example, if TS 1 (10 °C) were carried out with ambient conditions at 20 °C, the background temperature rate (from the calibration curve in **Figure 17**) would be -0.056 °C/minute, resulting in a final test environment temperature of 11.68 °C at t = 30 minutes.

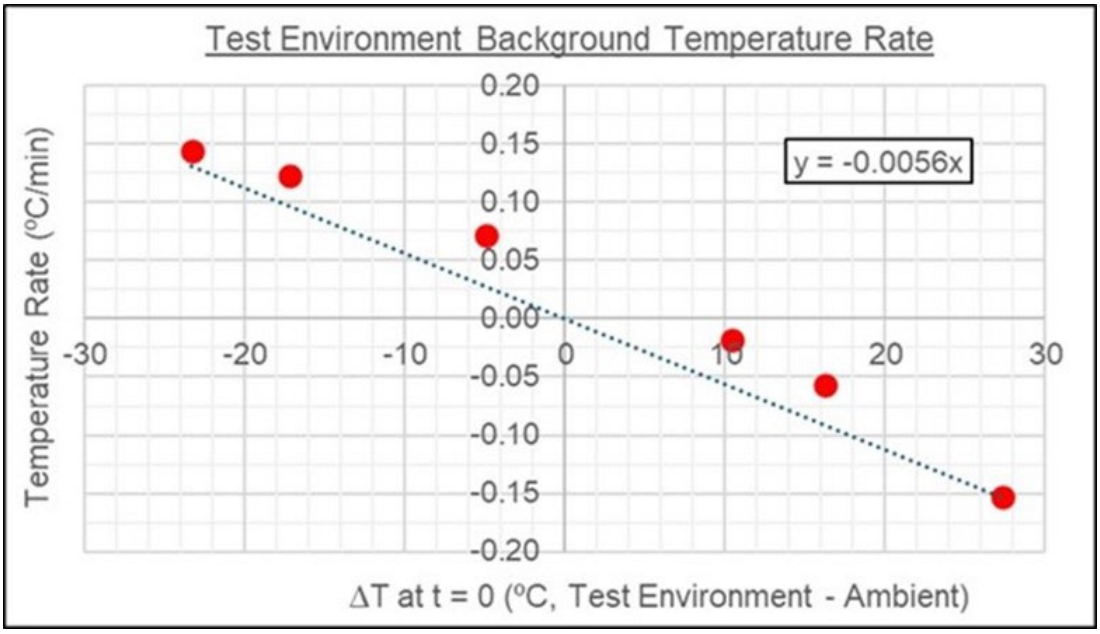

Figure 17. Test environment background temperature rate.

2.7.2 Forward Looking Infrared (FLIR) Camera Calibration

The FLIR camera was calibrated to account for the spectral response of the protective IR transmissive window. A Fourier Transform Infrared (FTIR) Spectrometer was used to determine the spectral response for the 7.5–14 µm range utilized by the FLIR camera. The calibration data are displayed in **Figure 18**.

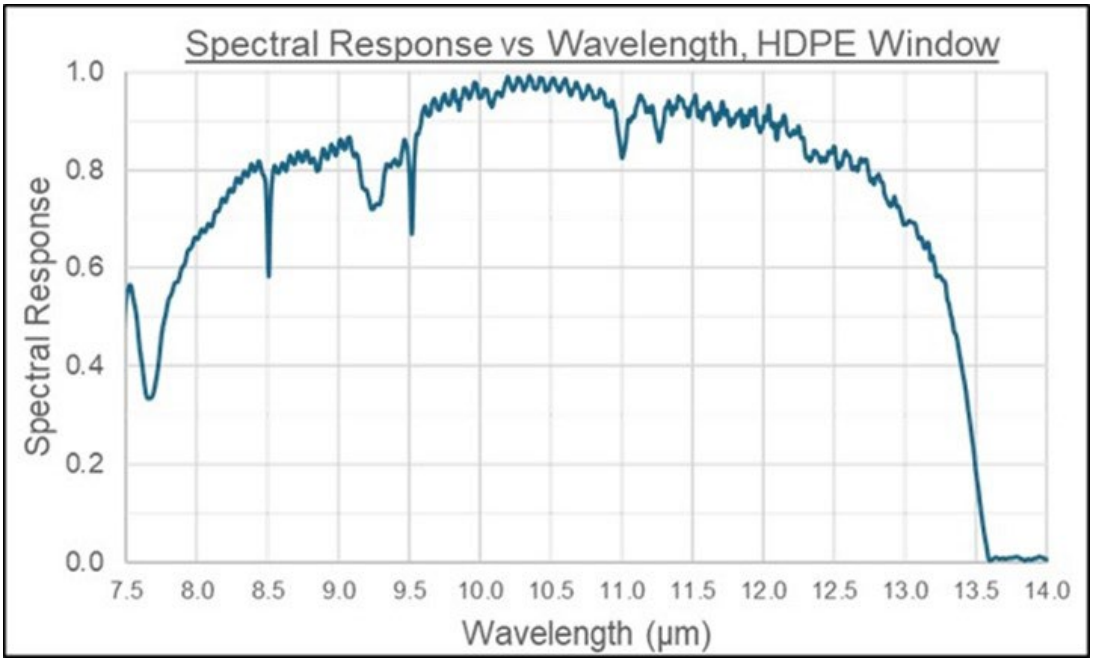

Figure 18. Spectral response of HDPE polymeric IR window.

The spectral response data were imported into the FLIR Research Studio recording software, which used the data to correct for the reduced transmission. However, in addition to the minimum detection limit of -20 °C, due to the relationship between a substance's emissivity and temperature, the FLIR camera was unable to quantitatively determine the temperature of the initial two-phase ammonia momentum jet, the liquid ammonia in the tray, or the ammonia drifting around the chamber. The qualitative FLIR observations can be found in **Section 3.2.3**.

2.7.3 PID Calibration

Assuming that the net weight of the ammonia in the lecture bottle was 0.375 lb. (170 grams), the average concentration, after complete mixing in the test chamber, was expected to be close to 4,882 ppm (converting from mass per unit volume units to ppm using average room temperature and pressure). Since the ammonia release was likely to have localized concentration maxima of 20,000 ppm, it was decided to calibrate the PIDs up to 20,000 ppm. The PIDs were manually calibrated using ammonia calibration gas concentrations of 10 ppm, 100 ppm, 1,000 ppm, 10,000 ppm, and 20,000 ppm. Unique calibration curves were developed for each individual PID. The configuration of the calibration apparatus with 18 PIDs is shown in **Figure 19**.

The calibration setup seen in **Figure 19** was constructed as a manifold of PIDs with two separate inlet/outlet flow configurations. In the top part of **Figure 19**, the red path was used to challenge the PIDs with calibration gas and the green path was used to pump ambient air through the manifold to clear out ammonia between challenges. The two flow paths were always isolated. During the gas challenge, the red valves were open, and the green valves were closed and vice versa for the pump down. The gas challenge flow was driven by pressure from the gas cylinder and maintained at 4.0 liters per minute with a flow regulator. The pressure increases above ambient were minimized by using several parallel flow paths within the manifold.

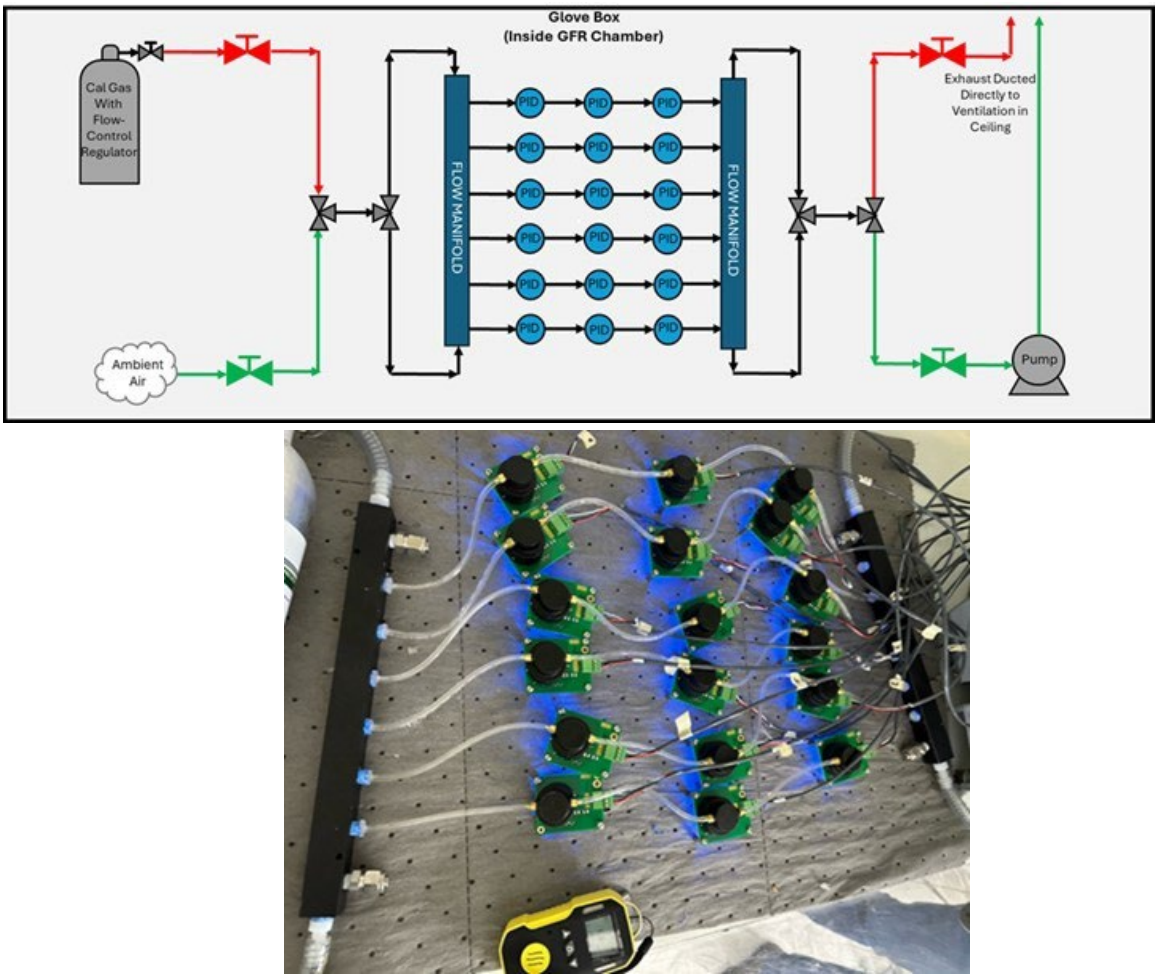

Figure 19. Calibration flow diagram (top) and photo of actual calibration configuration (bottom).

One (1) calibration cycle consisted of a 5-minute gas challenge, followed by a 5-minute pump down period. Three (3) consecutive calibration cycles were executed to create a triplicate calibration dataset for each calibration gas concentration. Results were monitored in real time to ensure that a steady state concentration was achieved during the gas challenge and concentrations returned to zero during the pump down time. The documented concentration for each gas challenge cycle was recorded as a 30-second average during the steady state concentration time period. Each calibration started with a 5-minute static period to ensure proper baseline signals before the first cycle was initiated.

The calibration curves were developed by plotting the measured analog signal response (in volts) with the baseline removed versus the calibration gas concentration (in ppm) for each calibration gas concentration. For example, the plot for PID_1L calibration results is provided as **Figure 20**.

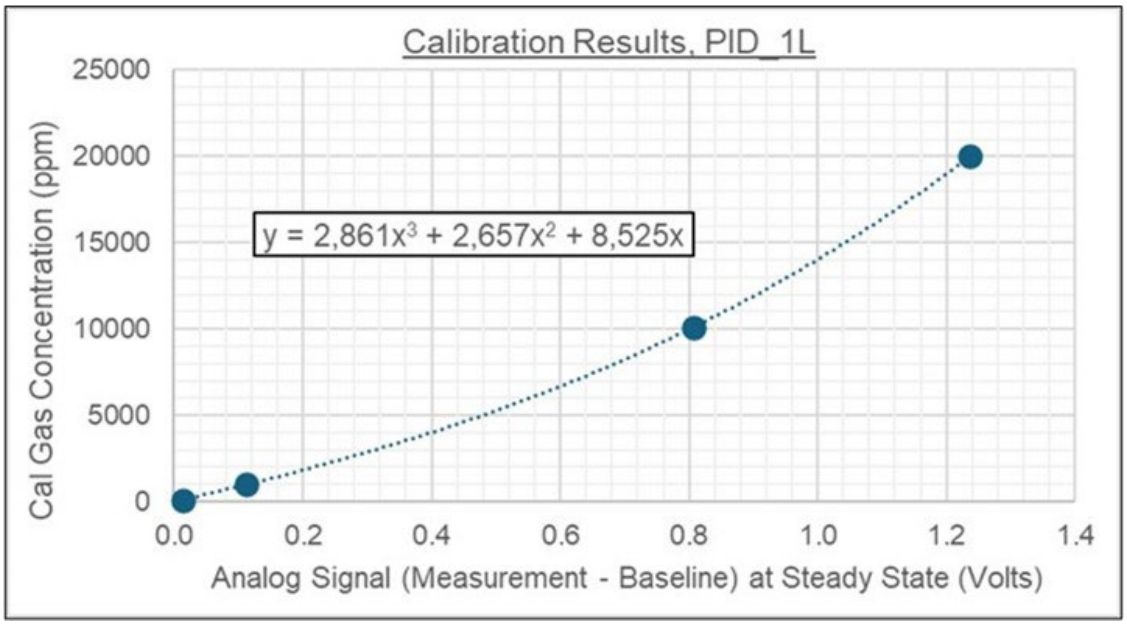

NOTE: The calibration curve constants are valid only for concentration (y) in units of ppm and signal (x) in units of volts.

Figure 20. Calibration curve for PID_1H.

The calibration curve that was used was established by fitting a third-order polynomial trendline to the measurement results. The third-order polynomial (listed in the small box in **Figure 20** for PID 1L) was best suited to capture the linear range at low concentrations and non-linear range at much higher concentrations. This trendline fitting was repeated for each individual PID dataset to develop unique calibration curves. Each PID's calibration curve polynomial formula was documented in the test data Microsoft Excel spreadsheet delivered for each test.

The calibration concentration time series were analyzed after applying the unique calibration formulas to each PID's raw dataset. For example, **Figure 21, Figure 22**, and **Figure 23** demonstrate the calibration concentration series for PID_1H for the five calibration concentrations (10, 100, 1000, 10,000, and 20,000 ppm). Each calibration concentration challenge was repeated in triplicate, ensuring sufficient time (about 4 minutes) to return to baseline before being challenged again. Each calibration lasted 35 minutes and included three successive applications of standard calibration gas for 4 minutes at 5, 15, 25-minute time intervals. These three calibration concentrations were followed by 6 minutes of zero concentration.

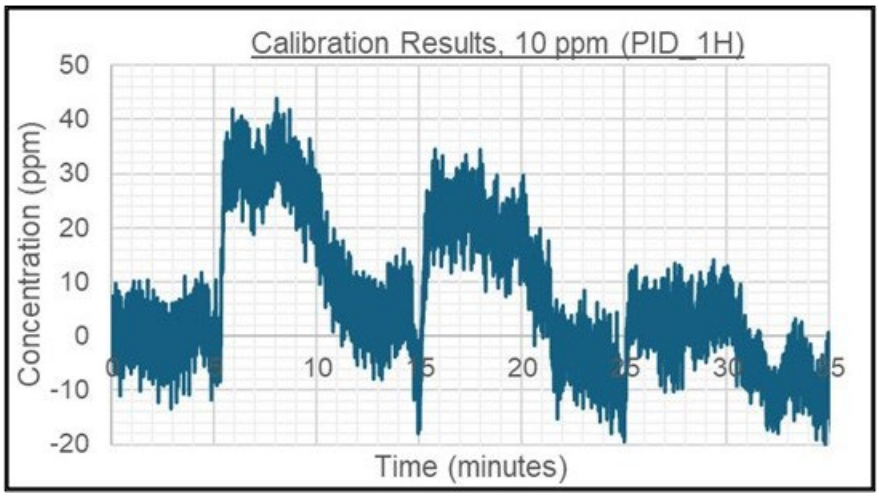

Figure 21. Calibration concentrations time series for PID_1H (10 ppm).

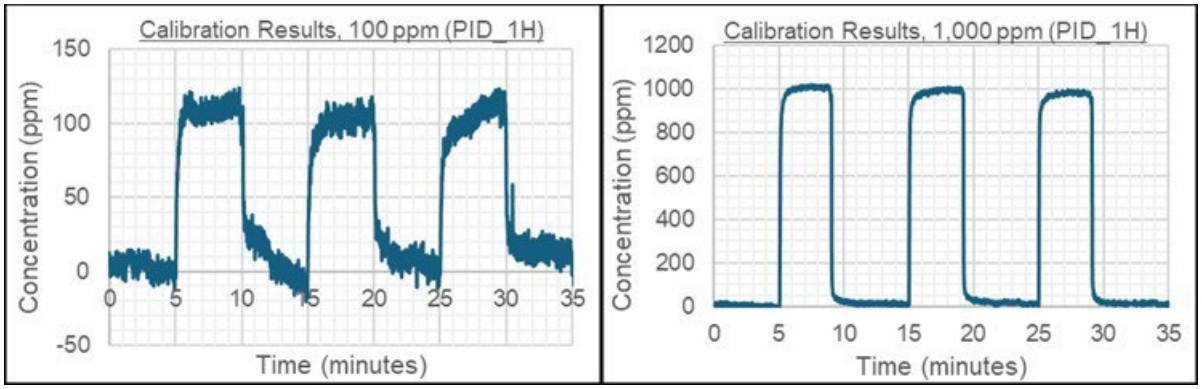

Figure 22. Calibration concentration time series for PID_1H; 100 ppm (left) and 1,000 ppm (right).

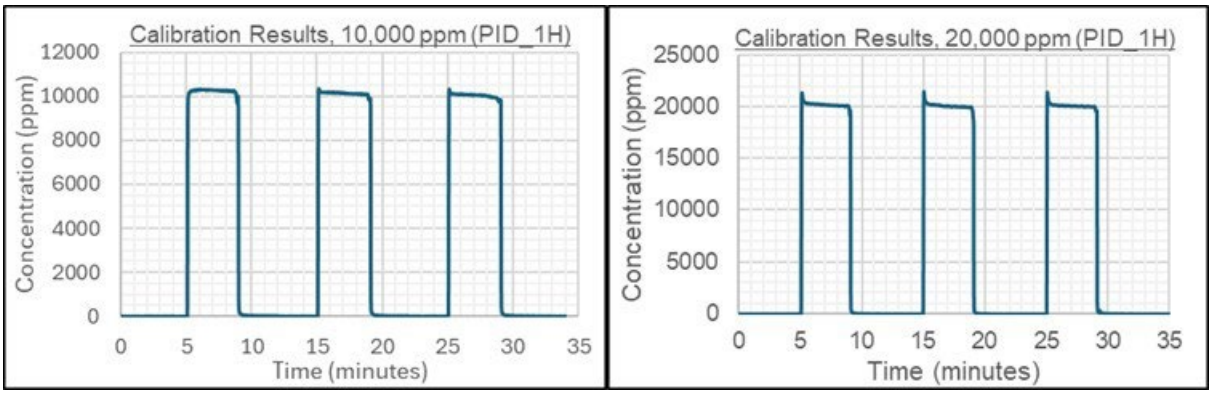

Figure 23. Calibration concentration time series for PID_1H; 10,000 ppm (left) and 20,000 ppm (right).

It is important to note from **Figure 21**, for the 10-ppm calibration gas, the baseline noise and the accuracy of detection were as large as the 10-ppm signal. The natural sensor baseline noise without any gas challenge (i.e., t = 0 to t = 5 minutes) was about ±10 ppm. This noise had the same magnitude during the

calibration gas challenge, and the measured concentrations were highly variable. A consistent, steady-state concentration could not be distinguished at the 10-ppm calibration concentration. According to **Figure 22** and **Figure 23**, for challenge gases with concentrations of 100, 1000, 10,000, and 20,000 ppm, the PID accuracy and repeatability were much improved and the relative error ([concentration variability]/[mean concentration magnitude]) decreases as the calibration concentration increases. The concentration uncertainty range is seen to be ± 10 ppm for the 100-ppm calibration gas. Based on the above results, it was decided that the minimum detection limit should be 100 ppm. This was found to be adequate for most of the concentrations observed during the tests.

Example plots of overlayed PID results with the time series for both pre- and post-calibration ammonia concentrations are provided as **Figure 24** for 1,000 ppm and **Figure 25** for 10,000 ppm. A detailed summary of this process and more time series plots are provided in **Appendix A**.

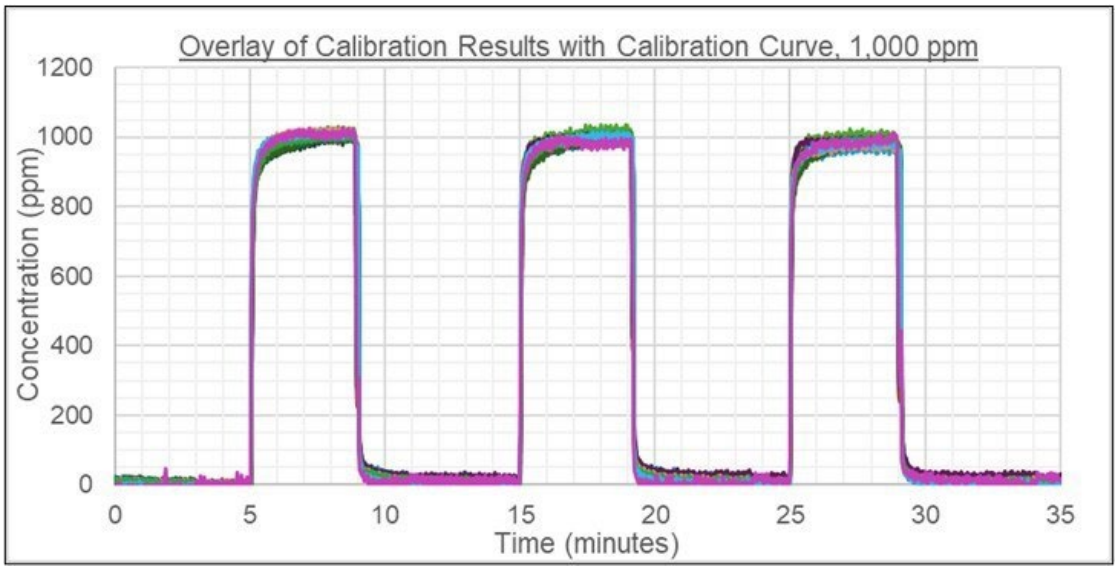

Figure 24. Overlay of ammonia concentration time series for 1,000 ppm.

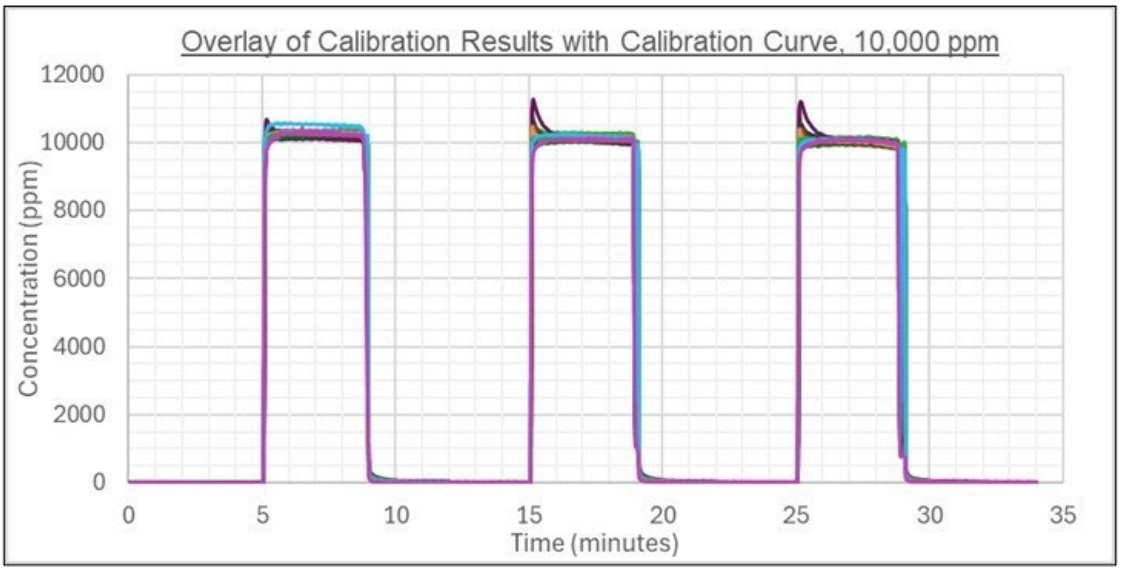

Figure 25. Overlay of ammonia concentration time series for 10,000 ppm.

The overlay results re-affirm the increase in accuracy and repeatability at the concentrations expected during the test timeline (> 1000 ppm). Additionally, these figures depict a consistent return to zero baseline.

The initial baseline at 0 ppm was monitored and recorded before and after every test and compared to the baselines recorded between t = 0 and 5 minutes during calibration. Deviations from the calibration baseline, called baseline drift, would indicate there was an issue with the PID. No baseline drifts greater than about 10 ppm were observed during the test matrix; therefore, it was determined that the PIDs were still operating as calibrated.

2.8 Test Procedure

A standard test procedure and accompanying checklist was followed to ensure every test was conducted consistently (the checklist is provided in **Appendix B**).

First, the electronic equipment including cameras, DAQ, lights, and sensors were powered on and ensured to be functioning correctly. Then, the cameras were aligned and focused and the mixing fans, and blowers were tested to ensure proper function. The ammonia lecture bottle was then weighed and installed in the frame; the exhaust system blast gates (air duct valves) were closed; and the PCU blast gates were opened. The mixing fans and PCU were powered on, and then the chamber was conditioned within ±1 °C and ±1% RH of the desired TS temperature and RH. The chamber walls and air temperatures were monitored to ensure they reached the set environmental conditions.

After the chamber and lecture bottle were conditioned, the RRV was tested for functionality. Then, the DAQ, HD cameras, and FLIR camera were set to record. Next, the lecture bottle was armed by opening the regulator valve to prime the release manifold. The door to the chamber was sealed, and final checks on the conditioning setpoints were monitored. The test execution was deemed imminent at t = -1 minute, at which point the PCU and fans were turned off to create a static, closed chamber. The general standard approach test timeline is provided in **Table 3**.

Table 3. Standard Approach Scenario Test Procedure Timeline

Test Timeline (t = XX minutes)	Procedure Event
-5.0	Pre-conditioning setup achieved. Manually open regulator valve. Close test environment door. Start collecting background measurements from all sensors.
-1.0	Turn OFF PCU and close isolation valves. Turn OFF mixing fans.
0	Initiate test by opening RRV.
30.0	Turn mixing fans ON.
40.0	Test Complete. Open ventilation valves and start scrubbing.

Once the chamber had settled for 1 minute, the RRV was opened. The opening of the RRV designated test initiation, t = 0, began the 30-minute period when the ammonia was emitted and spread around the test chamber. During this time, the test environment was left undisturbed by fans or external air changers, and the sensors and videos were operating. One major use of the videos was to determine when liquid ammonia evaporation from the catch tray was complete.

At t = 30 minutes, the mixing fans were turned on and left on for 10 minutes to ensure the chamber was as homogenized as possible.

After about 40 minutes, the fans were turned off for 1 minute to allow for a final spot check measurement of liquid left in the catch tray, since the mixing fans introduced noise in the catch tray measurement.

Finally, the mixing fans were powered back on, and the exhaust system blast gates and blower were powered on to begin the scrubbing cycle. The scrubbing cycle was run until the PID measured concentrations returned to near baseline. Once it was safe to enter the test chamber (below Occupational Safety and Health Administration permissible exposure limit of 50 ppm), the RRV was closed, and the lecture bottle was removed from the stand and weighed. The chamber was inspected for any liquid

pooling, solid deposits, or anomalies, and observations were recorded. The DAQ and camera recordings were stopped, and the recordings were saved and processed.

2.9 Simulated Rain Scenarios Approach

TSs 6 and 7 were designed to evaluate the potential effects of rain on the released ammonia plume, and to investigate the potential effects of rain during future large-scale ammonia releases and aid in planning emergency response.

Several changes were made to the test environment to facilitate the rain TSs. Changes included alterations to the sensor layout, installation of water spray nozzles, and addition of a PT and a pH sensor.

2.9.1 Simulated Rain Test Environment

To simulate rain falling through the ammonia plume as accurately as possible in the test chamber, two full cone rain nozzles were utilized. Because there were concerns that the raindrops would contact the instrumentation and potentially cause electrical shorts and interferences, nodes 1–4, 8, and 9 were moved outside of the expected rain area. The rain pattern and the updated test environment layout are shown in **Figure 26**. The configuration was the same in TS 6 and TS 7.

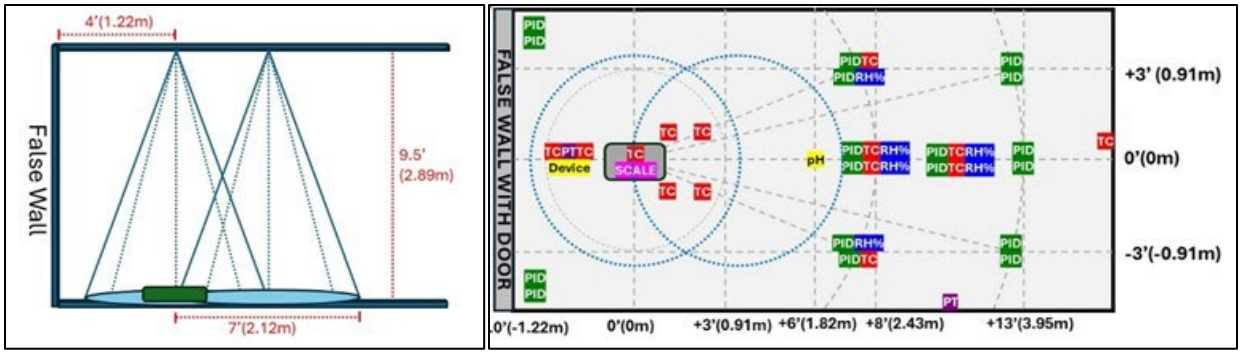

NOTE: Left: Rain circular spray patterns where the vertical axis is up (east and west) and the horizontal axis is distance south and north, and the pale green rectangle near the left end is the catch tray. Right: Revised Test Environment Layout, using the same variables as in **Figure 15**, except that the pH sampler and the PT are now included

Figure 26. Rain pattern and updated test environment layout for TS 6 and TS 7.

The rain nozzles on the ceiling were spaced to best balance a uniform, circular rain distribution and overlap without greatly reducing the floor-level surface area exposed to rain. The overlap ensured that the ammonia plume would not pass through any void spaces between the two rain circular areas. The nozzles mounted to the ceiling (9.5 feet (2.9 m) high) with a magnet and produced an approximately 7.0-foot (2.1 m) diameter rain surface area on the test environment floor.

2.9.2 Simulated Rain Equipment and Instrumentation

Two pairs of rain nozzles were used; each pair was designed and calibrated to achieve the two specific rainfall rates. Photos of the integrated water supply manifold on the ceiling and the rain nozzle are in **Figure 27**. NOTE: there is black plastic covering the surface of the ceiling as was done on all surfaces of the test chamber.

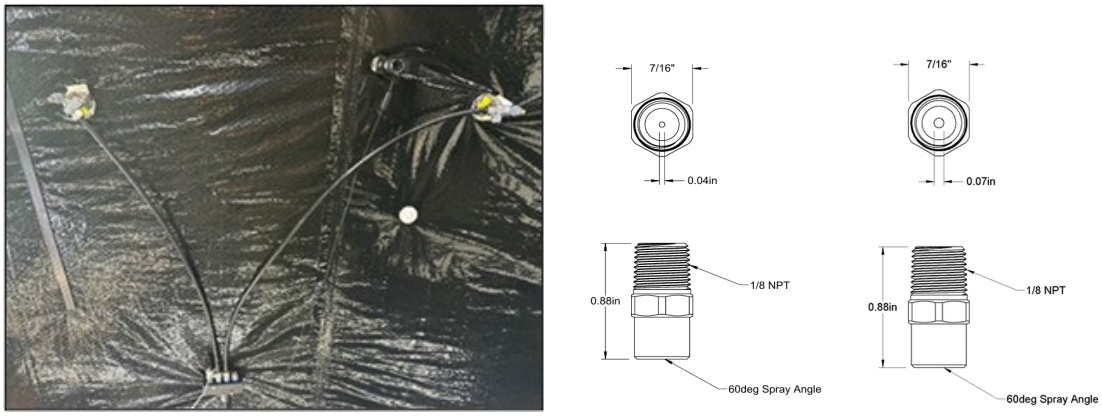

Figure 27. Water supply manifold on ceiling (left); a full-cone spray nozzle for TS 6 (center) and TS 7 (right).

For TS 6, the "light rain" or "low-flow" scenario, the pair of nozzles (McMaster 32885K811) had a 0.040" (1.02 mm) orifice and were rated for a 0.10 gallons per minute (gpm) (0.38 liters per minute (Lpm)) flow rate at 20 pounds per square inch gauge (psig) (137.095 kPa) supply pressure. For TS 7, the "heavy rain" or "high-flow" scenario, the pair of nozzles (McMaster 32885K831) had a 0.070" (1.78 mm) orifice and were rated for a 0.50 gpm (1.9 Lpm) flow rate at 20 psig (137.095 kPa) supply pressure. Both sets of nozzles were rated up to 400 psi, made of 303 stainless steel, and had a spray angle of 60°. It should be noted that the downward rain velocity was not measured in this study, nor was it matched to real raindrop conditions, as this is a static chamber without wind speed. Based on the flow rate, applied pressure, and measured drop sizes, the estimated rain velocity was between 2 and 10 meters/second.

Additional instrumentation was installed to monitor and record the mass of rain released for a specific time period and the pH of the pooled rainwater. A PT, as specified in **Section 2.4.4**, was installed in-line with the water supply to determine the water supply pressure to the water nozzles and was manually calibrated to ensure the desired flow rate through the nozzle's orifice. The water flow was optimized by adjusting the pressure supply regulators, and the settings were verified by collecting water from the nozzle. These parameters were then applied during the test.

A gel-filled pH probe (OMEGA PHE-1311) was utilized during the rain TSs to assist in the determination of the concentration of ammonia in the rainwater. This rugged, general purpose pH probe was rated for a pH range of 0-14 and temperatures of 0 °C to 100 °C. The pH probe measurement signal was transmitted to the DAQ with a pH transmitter (Hanna Instruments HI8711). The pH system was calibrated at 7.00 and 10.01 using a typical procedure for laboratory pH probes as specified by the pH controller.

At the start of each test, the pH probe was placed in a beaker with a known quantity of water from the same source supplied to the nozzles. An example setup from light/heavy rain TSs is shown in **Figure 28**. A glass graduate cylinder or a plastic graduated cylinder was used to collect light and heavy rain respectively. The collected liquid (ammonia/water) weight was determined by calculating the difference between the pre-test and post-test weights.

The sampling locations were adjusted one time. First the glass cylinder was positioned close to the catch tray during TS 7A, per **Figure 28** shown below. The larger capacity plastic cylinder was positioned further away for the remaining tests. With this adjustment, each simulated rain test was replicated to ensure the repeatability of rain collection over the ammonia plume for pH measurements, along with the rain itself (i.e., TSs 6A/B/C and TSs 7B/C). The water reservoir without the funnel was weighed before and after each test, so a dilution calculation could be performed. A known dilution factor and a measure of the pH allowed for estimation of the quantity of ammonia dissolved into the collected rainwater. However, the uncertainties associated with this estimation, including the pH relation with ammonia concentration and the homogeneity of the rain spray dimensions were not accounted for. The real-time data collected from the pH probe, in conjunction with the measured temperature, will be further investigated but is not part of this data report.

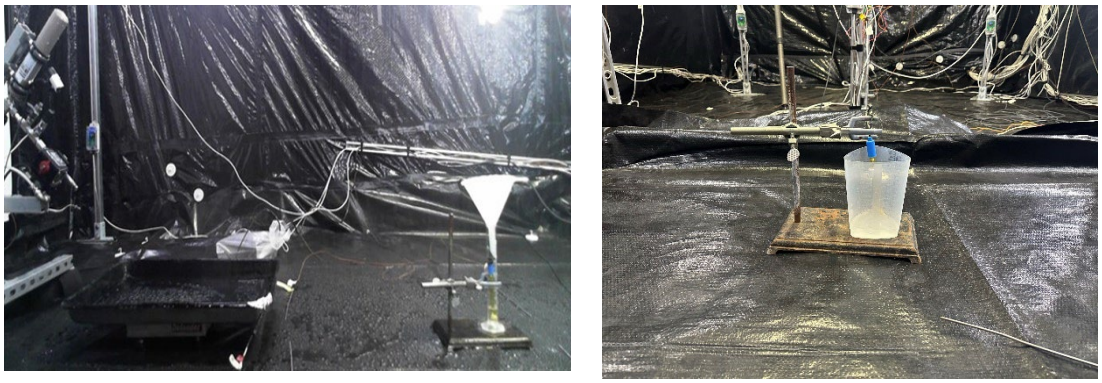

Figure 28. Rainwater sample collection for pH measurement for light rain TS (left) and heavy rain TS (right).

2.9.3 Simulated Rain Test Procedure and Timeline

The simulated rain TS replicates were split between two approaches:

1. For the A/B replicates, the procedure approached was to initiate the simulated rain before the release event.
2. For the C replicate, the approach was to initiate the simulated rain after the release event and after all liquid ammonia had evaporated. This was estimated when no measurable weight changes occurred from the catch tray during the trial period.

The pre-conditioned test environment setpoints were reduced to 20 °C and 50% RH due to the rapid RH increase when the rain was activated. The rain durations were established to maintain the test environment below 90% RH to ensure that high RH would not affect the PID ammonia concentration measurements.

During TSs 6A/B (light rain), the rain was begun 30 seconds before the ammonia release was initiated (at t=0) to ensure that the rain was at a steady state during the 5 to 10 seconds of release. The rain stopped when the test environment (chamber) RH reached 90%, which was observed to occur at about 5.0 minutes. The test environment was then kept as static as possible until the mixing fans were activated at t = 20.0 minutes. During this period (from 5.0 to 20.0 minutes), ammonia evaporated back into the air from the rainwater/ammonia pools mixture. The ventilation system was activated at t = 50.0 minutes, at which time the tests were considered complete.

A similar procedure was followed for TSs 7A/B (heavy rain), but the rain was stopped at t = 3.5 minutes, rather than the 5.0 minutes used in TSs 6A/B. The heavy rain during TSs 7A/B accelerated the time to reach 90% RH in the test environment (chamber).

The testing procedure and timeline were the same for TS 6C and TS 7C, when the rain was initiated after the release and after all the liquid ammonia in the tray evaporated. The ammonia release occurred at t = 0. Then, the mixing fans were turned on at t = 5.0 minutes to expedite liquid ammonia evaporation and ensure as homogenized as possible gas-phase ammonia concentration. The mixing fans were turned off at t = 16.5 minutes, and the rain was started under near static test environment conditions at t = 17.0 minutes. The rain continued for 5 minutes and was stopped at t = 22.0 minutes. Mixing fans were initiated at t = 25.0 minutes to ensure the chamber was as well-mixed as possible, and to encourage evaporation from the pooled rain-ammonia mixture. The ventilation system was turned on at t = 55.0 minutes when the tests were considered complete.

2.9.4 Simulated Rainfall Rate Calibration

The rain nozzles were calibrated by plotting the known water supply rate (in gpm) versus the water supply pressure (in psig). The water supply pressure was measured with the PT, and the mass of water collected per unit time was measured with the scale. This process was repeated over a range of water supply pressures for both nozzles. The pressure versus flow rate observations were plotted to develop a calibration curve, as shown in **Figure 29**.

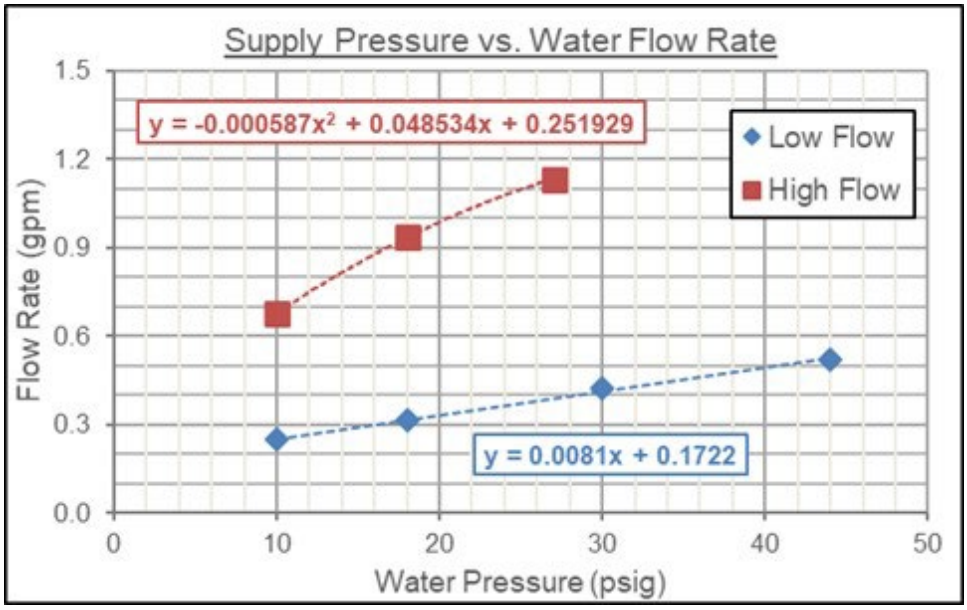

NOTE: It is important to note that the "constants" have dimensions due to the plotting of gpm vs psig.

Figure 29. Supply water pressure vs. water flow rates for two nozzles (TS 6–low flow for light rain and TS 7–high flow for heavy rain).

The required water pressures to achieve the target rainfall rates were calculated using the calibration equations and the rain envelope geometries. It is assumed that the rain rate is the same over the entire envelope. The target rainfall rates were based on metrics established by the American Meteorological Society. Light, moderate. and heavy rainfall rates were categorized as <0.10" (<2.5 mm) per hour, 0.10" (2.5 mm) to 0.30" (7.6 mm) per hour, and >0.30" (>7.6 mm) per hour, respectively [12].

Using the calibration curve, the flow rates for light and heavy rainfall rates were determined to be 0.24 gpm (0.91 Lpm) at 10 psig (68.547 kPa) and 1.12 gpm (4.24 Lpm) at 27 psig (185.078 kPa), respectively. The rainfall rates are calculated by multiplying the nozzle coverage area (3.5-foot (1.07 m) radius) by the desired rainfall rate. An example calculation is shown in **Equation 3**:

$$\left[0.3\frac{in}{hr}\right] * [\pi * (3.5\ ft)^2] * \frac{144\ in^2}{ft^2} * \frac{gal}{231\ in^3} * \frac{hr}{60\ min} = 0.24\ gpm \quad (3)$$

Equation 3

For TS 6, the lowest rainfall rate achievable was 0.30” (7.6 mm) per hour due to the low-flow nozzle minimum pressure specification. For TS 7, the rainfall rate of 1.4” (3.6 cm) per hour was chosen, because it qualifies as heavy rainfall and was 4.7 times larger than the light rainfall rate. It was decided not to exceed this heavy rainfall rate because larger volumes of rainfall would have increased the amount of standing water during a test. This would impact the location of sensors, sensor signal wire, the scale, and power circuits.

2.9.5 Simulated Rain Drop Size Measurement

The rain drop size was a key experimental parameter that influenced the ammonia-water interaction. The experimental rain drop size was desired to simulate average rain drops and ranged from 0.039” to 0.079” (1.0 to 2.0 mm) diameter. Light rain drops average ~0.020” (0.50 mm). Heavy rain drops average ~0.20” (5.0 mm).

The drop size was measured using water sensitive paper (WSP) cards. The bright yellow WSP cards permanently changed to blue when exposed to water. The diameter of the color change allowed for calculation of estimating the volume of the airborne water drop. The spread factor is also known as the wicking coefficient. This value represents the relationship between the amount a drop wicks and spreads on WSP and the volume of the original airborne drop. For example, a drop with an actual volumetric diameter of 0.023” (0.59 mm) would result in a measured 0.039” (1.0 mm) diameter on the WSP. The actual volumetric diameter, however, is only an estimation since the spread factor depends on the volume of the water drop, its velocity, and the assumption of a spherical drop.

Figure 30 shows the WSP card images for the low-flow (top) and high-flow (bottom) nozzles at the calibrated flow rates. Each WSP was exposed to rainfall for 5 seconds. There was no ammonia release during this time.

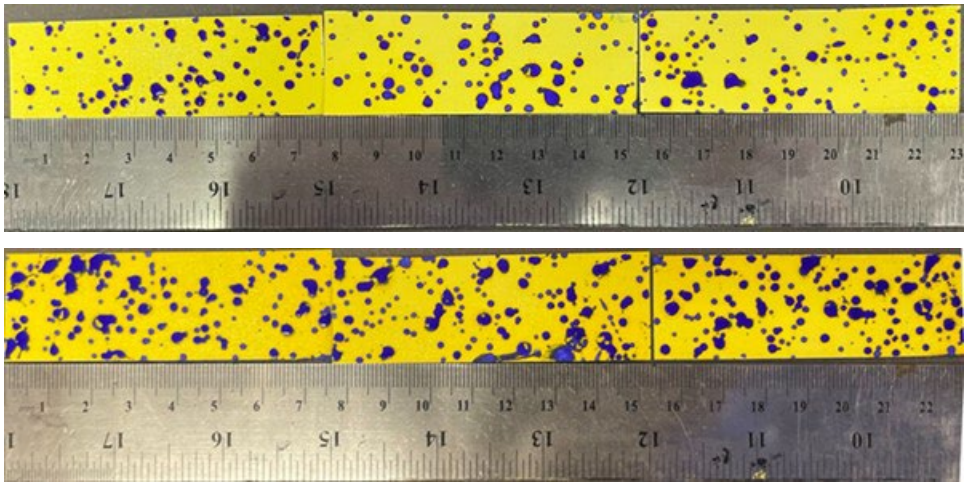

Figure 30. WSP cards drop size, TS 6 (low-flow, top) and TS 7 (high-flow, bottom).

Analysis of the patterns above suggests that both nozzles produced similar-sized drops. The results for the low-flow nozzle suggest drop diameters ranging from 0.014” to 0.067” (0.35 mm to 1.7 mm) and averaging 0.039” (1.0 mm). For the high-flow nozzle drop diameters range from 0.026” to 0.071” (0.66 mm to 1.8 mm) and average 0.051” (1.3 mm). The low-flow nozzles produced about 32 drops per square inch (5 drops per square centimeter), and the high-flow nozzles produced about 71 drops per square inch (11 drops per square centimeter). The spread factor was applied to these diameters to calculate a 0.067” (1.7 mm) average drop diameter (while falling through the air) for the low-flow nozzle, and a 0.083” (2.1 mm) average drop diameter (while falling through the air) for the high-flow nozzle. The ranges agree with known rain drop diameter ranges of 0.023” to 0.11” (0.59 mm to 2.9 mm) for the low-flow nozzles and 0.043” to 0.12” (1.1 mm to 3.1 mm) for the high-flow nozzles.

2.10 Excess CO_2 Scenario

The reaction between ammonia and excess CO_2 has been studied. TS 8 was implemented to investigate the feasibility of a mitigation method for accidental ammonia release within indoor storage/transport or refrigeration areas. The test environment temperature and RH were chosen to mimic a pump room in an industrial setting, which was recommended by the emergency responders working group (ERWG). The findings from these experiments could aid in first responders’ responses to an ammonia release or support the feasibility of a CO_2-based ammonia suppression system.

2.10.1 Test Environment for CO_2

All excess CO_2 TS replicates were conducted in the same test environment configuration as other non-rainwater Phase II tests (see **Figure 15**) with two instrumentation exceptions. The instrumentation grid and source injection point for CO_2 are shown in **Figure 31**.

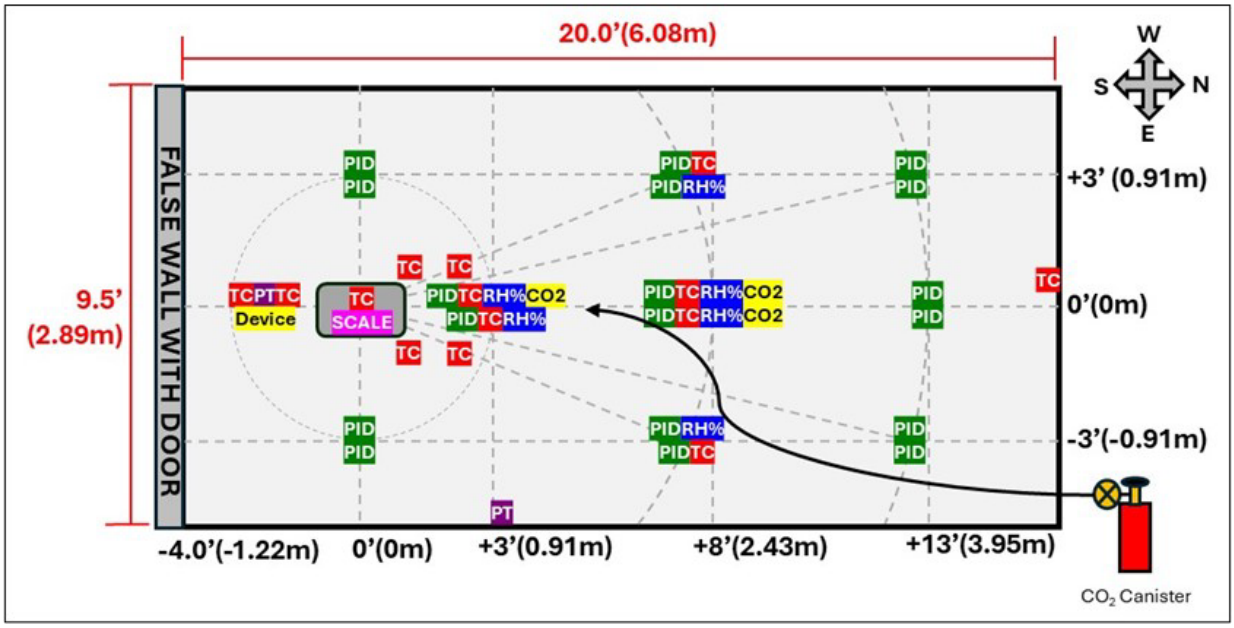

Figure 31. Test environment layout for TS 8 (CO_2).

The four TCs from sensor Nodes 8 and 9 were placed on the floor just north of the catch tray. The CO_2 canister was positioned outside the north end of the test environment.

2.10.2 CO_2 Measurements

The three CO_2 concentration sensors were implemented at Nodes 1 and 3. The Alphasense IRC-A1-CO_2-A-NDIR (**Figure 32**) had a detection range of 0 to 50,000 ppm with a response time of 40 seconds. The sensors had a full-scale resolution (accuracy) of 100 ppm. The sensors had an operating temperature range of -20 °C to 55 °C. Consequently, the test conditions to which the sensors were subjected were well within the operating temperature range. The linear operating range of the sensor is between 10 ℃ and 40 ℃.

Figure 32. CO_2 sensor for TS 8 (AlphaSense) with dimensions in millimeters.

2.10.3 CO_2 Source

The CO_2 was in a 2.5-pound canister with a CGA 320 valve from Kegco (ZXB2.5-R) (**Figure 33**). The canister, acquired from local vendors, had a working pressure of 1,800 psig (12,338.55 kPa). The canister was connected to a Victor Equipment Company regulator (SR450D-346). The regulator's outlet pressure was set to 20 psig (137.095 kPa) to ensure constant pressure and minimize freezing of the regulator. The valve on the regulator was manually manipulated on the outside of the test environment during the CO_2 injection period. Care was taken to maintain the test chamber pressure during the introduction of carbon dioxide.

Figure 33. CO_2 cylinder (left) and regulator (right).

Black polyethylene tubing (0.375" [9.53 mm] ID), connected to the regulator, was inserted through a cord grip on the north end of the chamber and was mounted to sensor node 1L pointed vertically toward the

top of the chamber as depicted in **Figure 2**. The vertical release configuration promoted better CO_2 distribution facilitating the gas to disperse within the chamber.

2.10.4 CO_2 Test Timeline

During the CO_2 tests, two sets of duplicates were performed and were differentiated when the CO_2 was injected.

The first set of duplicates (A/B) was a "CO_2 injection post-release event" after complete evaporation of ammonia. The test preparation was the same as previous tests in Phase II. The test environment was conditioned to 30 °C and 60% RH. The anhydrous ammonia was released as a two-phase jet from the pressurized bottle and was allowed to evaporate completely. The mixing fans were turned on to aid in the evaporation of the ammonia aerosol and liquid pool. Once a steady state ammonia concentration was achieved, the CO_2 was released into the chamber with the mixing fans still on. The concentrations of CO_2 and ammonia were monitored for 50 minutes before initiating the ventilation system to scrub the test environment.

The second set of duplicates (C/D) involved a CO_2 injection before the release event. The test environment was conditioned to the same setpoints as the A/B replicates (30 °C/60% RH). Once the test environment was conditioned and the release manifold was primed for release, the CO_2 was injected into the chamber with the mixing fans on. The CO_2 injection time range was from t = -3 minutes to -1 minute. The mixing fans were turned off 1 minute before the ammonia release. The goal was to have the CO_2 mixed uniformly throughout the chamber before the ammonia was introduced. The ammonia was released into the test environment under static conditions at t=0. The mixing fans were turned on after 30 minutes. After 10 minutes of mixing, the ventilation system was initiated to scrub the test environment.

2.10.5 CO_2 Sensor Calibration

The CO_2 sensors were originally calibrated by the manufacturer before shipment. To validate the CO_2 sensor accuracy, two background tests were performed in the test environment. Each background test consisted of two challenges of CO_2 via the technical approach previously discussed in this section. The test environment temperature and RH were set to the pre-determined TS conditions (30 °C/60% RH).

During the injection of CO_2, the mixing fans were powered on to ensure a homogeneous mixture of gas. Once the CO_2 concentration reached a steady state after the first injection, the chamber was held for an extended period. A second injection was added to establish two data points for the linear calibration

curve. The mass of CO_2 added per injection was determined from the pre-injection and post-injection mass of the CO_2 canister.

Using the data obtained from the background tests, the theoretical concentrations of CO_2 after each injection were calculated from the mass of CO_2, assuming complete mixing. These concentrations were plotted as a function of the individual CO_2 sensor signal response (voltage). The baseline voltage at ambient conditions was the average atmospheric concentration of CO_2. A linear regression was created to accurately calculate the CO_2 concentration in the chamber. The linear regression calibration curves are shown in **Figure 34**.

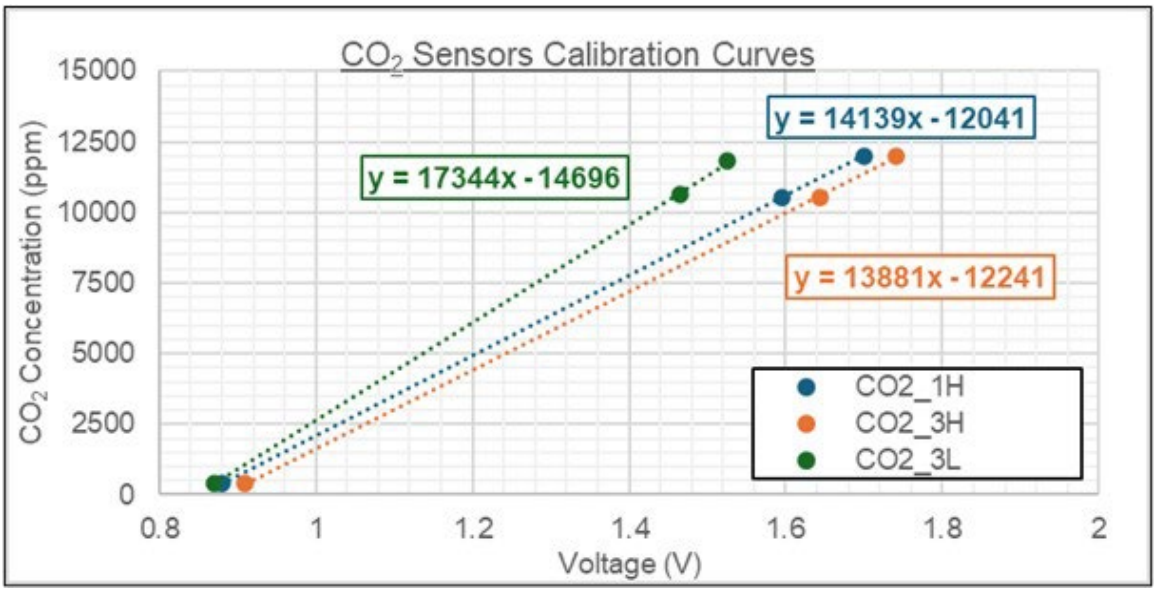

NOTE: The voltage, V, is observed by the sensor. The CO_2 concentration is calculated as the mass of CO_2 released divided by the volume of the test chamber.

Figure 34. CO_2 sensor calibration curves.

2.11 Description of Delivered Data

The recorded and analyzed data for each test were delivered in Microsoft Excel format. Each test data file has a worksheet detailing the following:

- **Notes:** Overall summary of important data points, including starting environmental conditions, pre- and post-test mass of the lecture bottle, homogenized concentration measured by the PIDs, catch tray mass measurements, test timeline, and notes and observations.
- **Sensor Specifications:** Overview of the placement of sensors within the test chamber and the range and response times for each sensor type. HD video camera locations were also specified.

- **Raw Data:** The raw voltage data for all sensors that were exported from the DAQ. The test timeline is also specified, with t = 0 for test initiation.
- **Baselines:** Recorded PID and scale baseline voltage, and the calibration coefficients used for each PID.
- **Photoionization Detectors (PID):** Applies the calibration curves and baselines to the raw signal data, reporting concentration (ppm) data for each PID for each timepoint. Additional datasets include average overall concentration, average high concentration, average low concentration, and concentration difference.
- **Temperature:** Temperature measurements from each TC and an average temperature for various locations in the chamber.
- **Percent Relative Humidity (RH):** RH measurements from each RH probe and an average RH for various locations in the chamber.
- **Absolute Humidity (AH):** Calculations for the AH at each timepoint at high and low sensor heights using the average RH and TC data for each height.
- **Air Density:** Calculations of air density (accounting for all gasses present – dry air, water vapor, ammonia, and CO_2) at high and low sensor heights at each timepoint.
- **Devices:** Data for the manifold PT, ambient PT, scale output, tray TC, manifold out TC, and lecture bottle body TC; also includes the calculated theoretical ammonia temperature within the lecture bottle based on the manifold PT measurements.

Other data delivered include HD and IR videos of each test. These videos were edited to focus on the initial release, ammonia cloud, and catch tray liquid pooling to keep the file size and video length manageable.

3.0 RESULTS

A summary of Phase II experimental results for the standard approach TSs set is provided in **Table 4**, and the experimental results for the simulated rainfall and excess CO_2 TSs are provided in **Table 5** (TS 6 and TS 7) and **Table 6** (TS 8), respectively.

Table 4. Summary of Experimental Conditions and Selected Results, Standard Approach TSs

TS No.	Test Environment Initial Conditions				Ammonia Release		Derived Ammonia Mass Balance
	Temp (ºC)	RH (%)	AH (g H_2O per m^3 air)	Average Air Density of mixture of dry air, water vapor, and ammonia (kg/m^3)	Initial Pressure in lecture bottle (psia)	Liquid Fraction [a]	
1A	5.3	85.5	5.9	1.245	76	40.8%	100.4%
2A	15.5	89.8	11.9	1.196	110	29.3%	106.9% [b]
2B	15.6	89.1	11.8	1.208	109	29.7%	106.3% [b]
3A	-17.0	25.5	0.4	1.339	41	56.3%	100.1%
3B	-15.2	29.9	0.5	1.330	38	58.4%	99.8%
3C	-18.1	11.5	0.1	1.358	37	59.8%	99.2%
4A	41.0	11.1	6.0	1.102	233	14.1%	91.7%
4B	40.5	10.9	5.7	1.100	237	13.5%	92.7%
4C	40.2	11.2	5.8	1.103	233	14.4%	93.6%
5A	33.8	89.4	33.2	1.116	191	11.2%	90.1%
5B	33.2	89.8	32.4	1.120	190	11.4%	88.7%
5C	33.7	89.8	33.2	1.110	190	11.9%	89.2%
9A	9.4	61.2	5.5	1.232	87	37.0%	99.1%
9B	9.4	60.4	5.5	1.239	91	36.8%	99.5%
9C	10.3	59.8	5.7	1.222	96	35.2%	98.9%
10A	21.9	61.2	11.8	1.193	133	29.9%	94.7%
10B	22.5	60.7	12.1	1.183	137	26.4%	94.2%
11A	34.6	59.6	23.1	1.110	200	11.8%	84.6%
11B	35.6	60.3	24.6	1.117	207	12.2%	83.8%
11C	35.2	61.2	24.5	1.124	202	11.8%	84.0%

NOTE: [a]The liquid fraction of the ammonia release was calculated from experimental measurements. It is expressed as a percentage of the liquid ammonia mass captured in the catch tray, weighted against the total ammonia mass released from the lecture bottle. This value is a direct measurement of the liquid mass on the catch tray using a scale. [b]High mass balance is attributed to the uncertainties in the PID concentration measurements at higher relative humidity.

Table 5. Summary of Experimental Results, Simulated Rain Scenarios (TS 6 and TS 7)

TS No.	22 °C / 50% RH (±1 °C and ±1.5% RH)						
	Simulated Rain					Ammonia Mass Balance	
	Rain Introduced	Rain Start (min)	Rain Stop (min)	Total Rain Volume (L)	Rain Pool pH	Total Ammonia Released (grams)	Yield After Rain
6A	During Release	-0.5	5.0	5.5	10.3	194.1	59.6%
6B	During Release	-0.5	5.0	5.5	10.0	202.7	58.7%
6C	After Release	17.0	22.0	4.8	9.1	158.6	79.0% [b]
7A	During Release	-0.5	3.5	17.1	11.0 [a]	193.3	47.8%
7B	During Release	-0.5	3.5	17.1	10.1	180.7	48.7%
7C	After Release	17.0	22.0	21.4	10.5	182.7	55.8% [b]

NOTE: [a]TS 7A: Unique pH placement closer release and with smaller rain collection beaker and funnel. [b]Ammonia mass balance yield without the rain is 92.5% and 92.6% for TS 6C and TS 7C, respectively.

Table 6. Summary of Experimental Results, Excess CO_2 Scenario (TS 8) [a]

30°C / 60% RH (±1°C and ±1.5% RH)									
TS No.	Excess CO_2						Ammonia Mass Balance		
	CO_2 Introduced	CO_2 Start (min)	CO_2 Stop (min)	Total CO_2 Mass (grams)	CO_2 Yield	Solid Present?	Total Ammonia Released (grams)	Yield Before CO_2	Yield After CO_2
8A	After Release	10	12	864	98.7%	NO	177.4	92.7%	89.5%
8B	After Release	11	14	1,131	97.4%	NO	174.2	91.3%	87.4%
8C	Before Release	-4	-2	1,188	96.2%	YES	193.9	92.0% [b]	80.3%
8D	Before Release	-10	-5	1,265	95.8%	YES	184.7		79.3%

NOTE: [a] CO_2 was introduced both after and prior to the ammonia release at time zero. The mass of CO_2 released, along with the corresponding mass yield contributing to the reaction, was calculated and compared to environmental conditions without CO_2 to determine its effects on ammonia release. [b] Data was not collected, the value is the TS 8A/B Yield Before CO_2 average.

Eleven (11) different TSs were investigated during Phase II to evaluate the ammonia release event and subsequent time and space variations in ammonia concentrations within a static test environment chamber at various environmental conditions and conditions. Each TS consisted of pre-conditioning the test environment to unique temperature and RH setpoints that simulated a broad range of environmental conditions, including some extremely hot and cold conditions.

Three (3) TSs (TSs 1, 2, and 5) investigated high RH conditions in which the release event would likely trigger water vapor condensation within the test environment. Two (2) TSs targeted extreme cold (TS 3) and hot (TS 4) test environments, both with low RH conditions. Three (3) TSs (TSs 9, 10, and 11) explored equilibriums between the ammonia plume and water vapor at average environmental conditions typical of those previously studied in Phase I [1]. TS 8 was designed to study the interaction between ammonia and CO_2 gas by injecting CO_2 gas into the test environment before and after the release event. TSs 6 and 7 focused on mass transfer between ammonia and rainwater drops for typical low and high rain rates before and after the release event. Two other scenarios were planned in the original test matrix to study additional high humidity and fog test conditions but produced no useful data due to measurement errors caused by condensation on the instruments.

The Phase II data were grouped and reported as two separate sets:

1. Results and discussions for Phase II TSs of high RH (TSs 1/2/5), extreme cold and dry (TS 3), extreme hot and dry (TS 4), and average conditions (TSs 9/10/11). These TS approaches were considered to be closely equivalent to the Phase I tests [1], where there was a wide range of RH and temperature values, referred to as the "standard approach" TS set.

2. Results and discussions for Phase II tests in the presence of simulated rain (TSs 6/7) and excess CO_2 (TS 8). These three TSs involved unique approaches that deviated from the standard test approach.

Test environment temperature and RH conditions at initiation (t = 0) were typically within ±1 ºC or ±1% RH of the target setpoint. Calculations of parameters such as AH, air density, and space-averaged temperature, RH, and ammonia concentration were derived from experimental measurements. The air density (i.e., density of mixture of dry air, water vapor and ammonia gas) calculation formulas can be found in **Appendix C**. These parameters are discussed in greater detail in the following subsections.

It was important to note the release event during the extreme RH TSs triggered water vapor condensation within the test environment. In those cases, the test environment RH persisted above 95% for the majority of the test timeline, which was the PIDs operational limit defined by the manufacturer. Additionally, the PID manufacturer specified the measurement sensitivity could be affected at RH above 75%. Therefore, TSs 1, 2, and 5 results specifically derived from PID concentration measurements should be considered to have larger uncertainites than those provided in **Appendix A**.

3.1 Experimental Observations

The following section defines the ammonia observed from the release event with descriptions specific to this test approach and measurements, summarizes the typical ammonia plume and liquid pool characteristics after the release, and documents the post-test solid residue observed.

3.1.1 Liquid Ammonia Release Fraction

Textbooks and journal review articles (e.g., Britter et al., 2011) [13] describe the release of ammonia from pressurized liquefied gas storage as a two-phase jet. For a given release aperture, the velocity of the jet, the mass release rate, the fractions of the mass that are gas and liquid, and the aerosol size diameter of the liquid phase, depend on the storage tank pressure. Larger pressure produces a larger mass release rate and smaller aerosol diameter.

Liquid anhydrous ammonia is present in the high-velocity jet as tiny aerosol drops, some of which accumulates a liquid “rained out” pool within the catch tray during the release. Some of the rain-out was not captured by the tray but hit the floor off the sides of the tray. Other ammonia aerosol drops were reflected off the tray and subsequently quickly evaporated. The total liquid pool mass (ammonia and water vapor condensation) in the tray was measured immediately after release, and the liquid phase anhydrous ammonia mass released was back calculated from the total liquid pool mass, which remained unchanged for the duration of each trial. Although the liquid pool was not analyzed to determine whether it was ammonia or water, if it persisted (non-evaporative for longer than 25 minutes), it is anticipated that the pool consists of a mixture of ammonia and water. The pooled liquid release fraction was quantified

with respect to the total ammonia released for all Phase I [1] and Phase II tests. The liquid ammonia evaporated from the pool before the measurements for the overall mass balance were obtained from the real-time measurements of the catch tray weight throughout the entire duration of each trial. The liquid-phase release fraction results are presented in **Section 3.2.1**.

The gas-phase anhydrous ammonia was immediately flashed out of the release stream during the release event. It was assumed that this phase had minimal interaction with ambient water vapor. However, any entrained water vapor into the expanding momentum jet could result in condensation due to the very cold temperature of the jet.

3.1.2 Visible Ammonia Cloud Observations

The visible ammonia plume was due to the two-phase momentum jet resulting from the pressurized release. This jet, with initial velocity about 10–20 m/s, and directed downwards at 45 degrees, entrained ambient air as it travelled from the release point to the tray. The catch tray and lip deflected the ammonia plume back upwards at an angle of about 45 degrees toward the ceiling near the far end of the chamber. The visibility of the cloud after reflection depended on the RH in the test environment. It is now known whether the aerosol drops in the visible cloud after reflection were all ammonia, all condensed ambient water, or a combination. **Figure 35** provides HD video screenshots of the visible ammonia plume during release from three of the TSs with interrelated humidity conditions (TSs 4B, 9C, and 11B). TS 4 and TS 9 had equal AH, but significantly different RH; TS 9 and TS 11 had equal RH, but notably different AH.

Cam 1, TS 4B (40 °C) RH = 10% AH = 5.7 g H_2O / m^3 Air	Cam 1, TS 9C (10 °C) RH = 60% AH = 5.7 g H_2O / m^3 Air	Cam 1, TS 11B (35 °C) RH = 60% AH = 24.6 g H_2O / m^3 Air
		
Cam 2, TS 4B (40 °C) RH = 10% AH = 5.7 g H_2O / m^3 Air	**Cam 2, TS 9C (10 °C) RH = 60% AH = 5.7 g H_2O / m^3 Air**	**Cam 2, TS 11B (35 °C) RH = 60% AH = 24.6 g H_2O / m^3 Air**
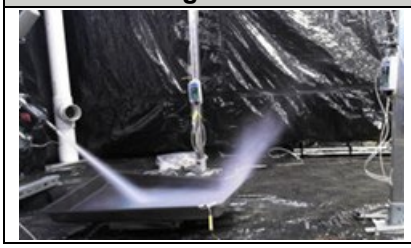		

Figure 35. HD video screenshots, initial cloud opacity during release versus RH/AH for TS 4B, TS 9C, and TS 11B.

To interpret these figures, comparing the water content in a high RH environment, it is clear that the visible cloud in the photos is more prominent under high AH conditions. Considering the ammonia boiling point of -34 °C is far below the three environment-controlled temperatures tested (10, 35, and 40 °C), while the liquid pool directly on the catch tray is -60 °C, the visible cloud reflected off the catch tray likely contains tiny drops of condensed water and/or ammonium. Whether the ambient water will condense depends on the saturation deficit = AH (100% - RH)/100%. Note that this depends on both AH and RH. The saturation deficit is 51.3 g/m3 for TS 4B, 2.3 g/m^3 for TS 9C, and 9.8 for TS 11B. The visible ammonia plume cloud persisted the longest during the 90% RH TSs (TSs 1/2/5). In all these trials, the saturation deficit was less than 10 g/m^3. Example screenshots from Cam 4, located 8.0 feet (2.4 m) high on the north wall, during TS 2A and TS 5A are displayed in **Figure 36**.

Cam 4, TS 2A, t = 3 seconds	Cam 4, TS 5A, t = 3 seconds
	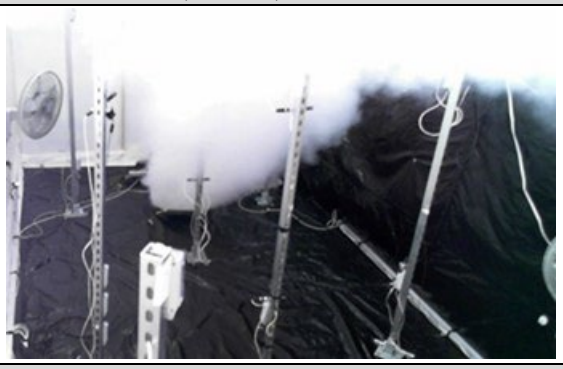
Cam 4, TS 2A, t = 13 seconds	**Cam 1, TS 5A, t = 6 seconds**
	

Figure 36. HD video screenshots, at t=3 and 13 seconds time for TS 2A and at t=3 and 6 seconds for TS 5A.

The persistent cloud was observed under 90% RH conditions, indicating potential condensation of water vapor upon the release of a cold jet of ammonia. The visible plume traversed the ceiling and reached the north wall before obstructing the camera view. The observed plume was estimated to reach the north wall at t = 13 seconds during TS 2 and t = 6 seconds during TS 5. These extreme saturation deficit conditions resulted in a visible cloud throughout the test environment. The visible cloud was faint but noticeable shortly after release and typically disappeared after a few minutes.

During the several minutes that the cloud generated by the momentum jet was visible, it was observed to circulate around the chamber, with eddy sizes approximately equal to the chamber width and with speeds of a few 10s of cm/s. The speeds slowly decreased and approached zero after several minutes. The various eddies that were generated are likely responsible for the periodicity in the observed wisps rising from the catch tray. Typically, they might head towards the South for a minute and then towards the North during the next minute.

The simulated rain TS 6 and TS 7 experiments produced visible effects on the cloud when the rain system was activated during the release event. Screenshots of the narrow release jet and the visible cloud during this time for TS 6 (20 °C, 75% RH, and light rain) and TS 7 (22 °C, 60% RH, and heavy rain) are provided in **Figure 37**. Screenshots from TS 10 are included for reference to a release at similar conditions but without rain. Although the top figures captured by Camera 1 positioned directly above the release source do not show clear distinctions, the bottom figures, from Camera 3, suggest that the rain clearly "knocked down" the visible cloud; the magnitude was dependent on the rain rate.

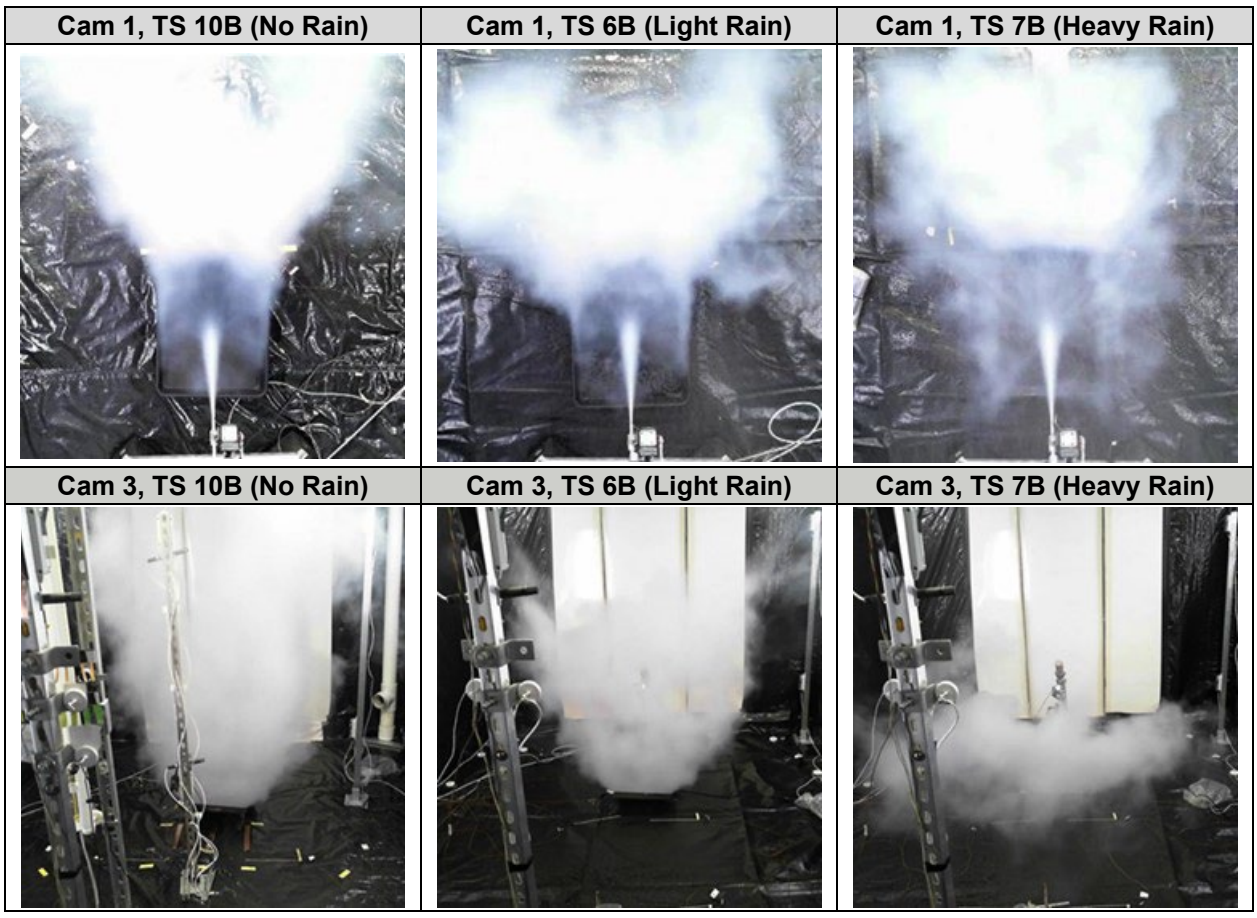

Figure 37. HD video screenshots, ammonia release and cloud during rain for TSs 6B, 7B, and no rain for TS 10B.

3.1.3 Evaporation of Liquid Pool in the Catch Tray

After the release, a visible faint cloud was observed over the liquid pool in the catch tray. The cloud from the catch tray travelled various directions during the initial minute after release, likely due to the previously mentioned eddies generated in the chamber by the momentum jet. Example screenshots of the visible cloud from the liquid pool captured at t = 1 minute for various TSs are provided in **Figure 38**.

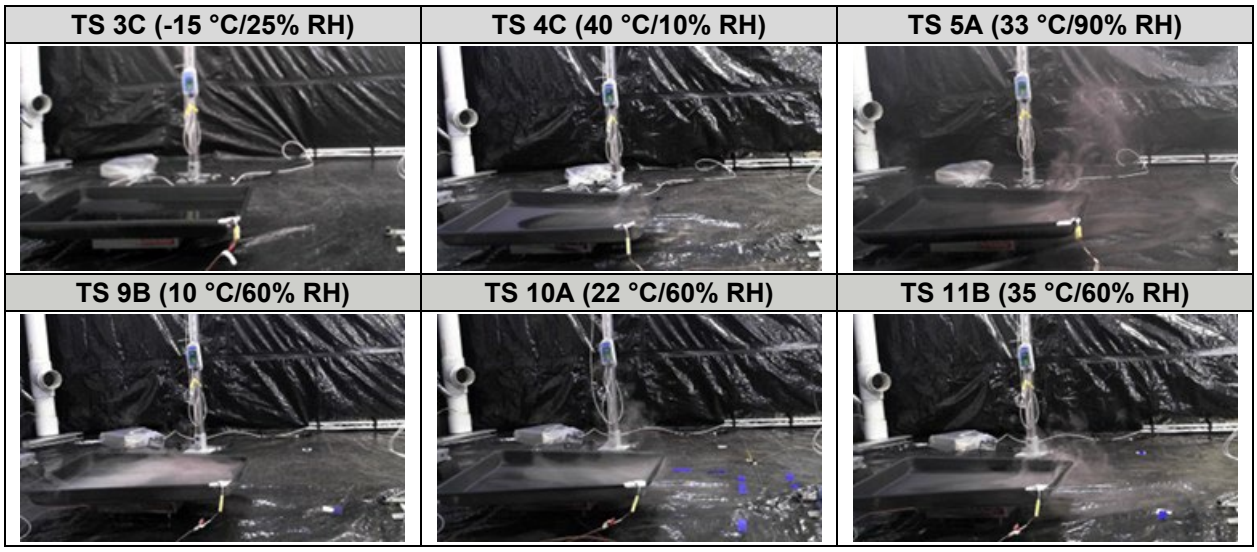

Figure 38. HD video screenshots, Cam 2 visible plume above catch tray, t = 1 minute for TSs 3C, 4C, 5A, 9B, 10A, and 11B.

In most cases after t = 1 minute, the liquid pool visible cloud could be observed travelling northwest along the floor surface. The liquid pool in the catch tray consistently reached temperatures around -60 °C, which indicates subcooled boiling, since the boiling temperature is -34 °C. The subcooled boiling state likely induced ammonia evaporation and water vapor condensation in parallel. The ammonia would be in gas phase and not visible. The visible cloud was therefore likely composed of condensed water vapor.

3.1.4 Solid Residue (TS 3 at -10 °C and 30% RH and TS 8 at 20 °C and 50% RH with CO_2)

Post-test observations were documented during safe entry conditions after the test and scrubbing timelines were complete. Post-test observations were limited to trace residue. It was not possible to document other surface condensation or solid residue due to the long wait time and inability to control the test environment conditions before test operators could safely enter.

The Phase I report documented several instances where a white solid was observed post-test on the floor and underneath the catch tray [1]. The solid pH was measured with a wetted pH indicator strip to be ~8.0 on average. A similar white solid residue was observed during Phase II; example photos are provided in **Figure 39**.

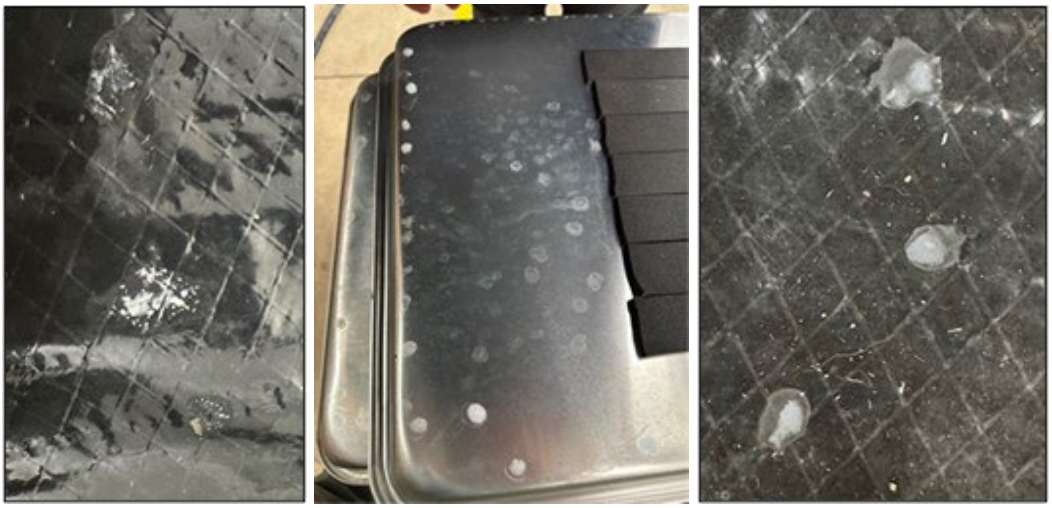

NOTE: The catch tray is 65.4 cm length x 45.1 cm width x 5.72 cm deep (which is the lip around the edge).

Figure 39. Post-test solid residue: TS 4B (left), TS 5A (center), and TS 11A (right).

The Phase II post-test solid residue on the floor and catch tray was observed to be similar to the Phase I post-test solid, and equivalent pHs were found [1]. This solid residue was not analyzed beyond the pH measurements.

There were two Phase II TSs where significant formation of a white solid residue was directly observed within the catch tray. During TS 3 (T = -15 °C and RH = 30%), the white solid was not immediately observed after the release, but it appeared along the liquid pool boundaries as the liquid evaporated over time. TSs 8A/B (T = 30 °C, RH = 50%, CO_2 applied after ammonia evaporation) replicates did not generate any solid, but TSs 8C/D (CO_2 applied just prior to release) replicates immediately formed the white solid on the catch tray, and the observed solid mass increased as the liquid pool evaporated over time. Time-lapse screenshots of the solid formation during TS 3C and TS 8C are provided in **Figure 40**. Results from TS 8 are discussed in more detail in **Section 3.5**.

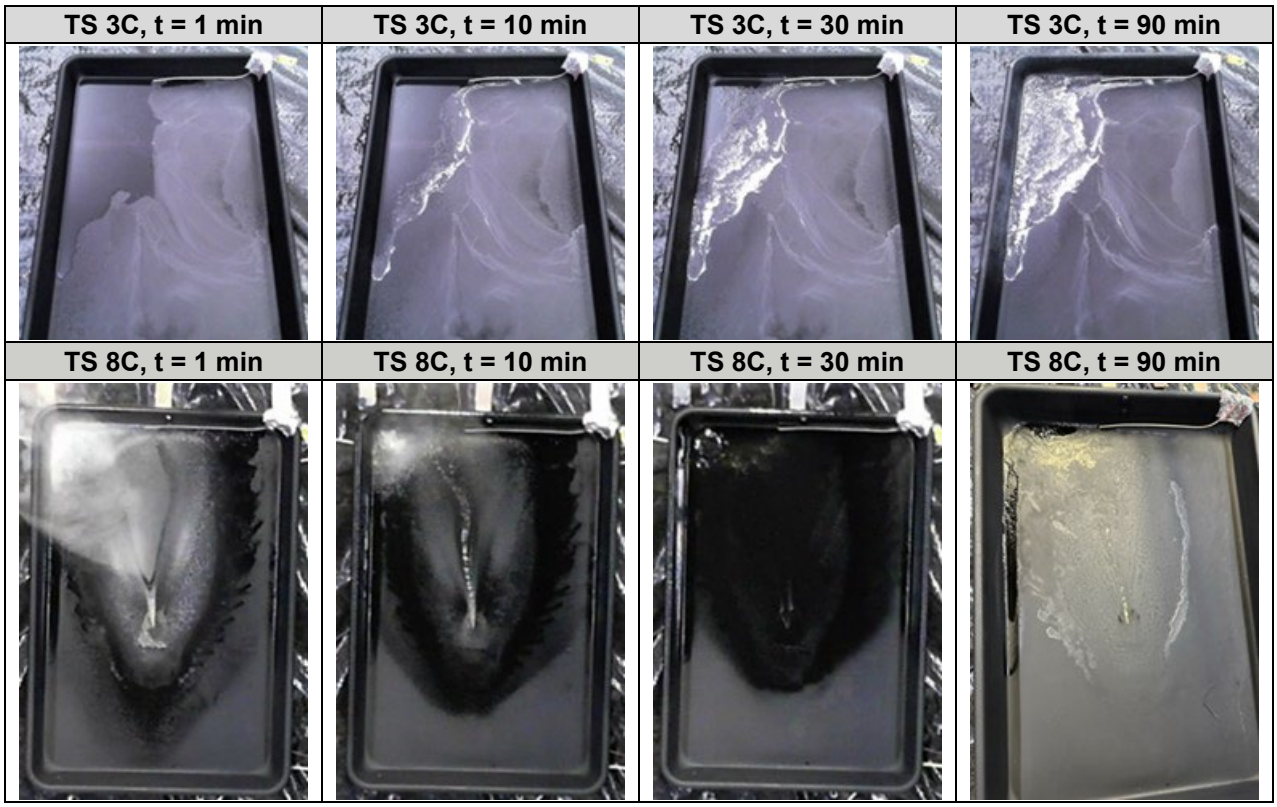

Figure 40. HD video screenshots, solid residue formation for TS 3C (-15 °C/25%) and TS 8C (20 °C/50% + CO_2).

The liquid pool evaporation during TS 3, for chamber temperature of -10 °C, left behind the white crystalline solid that covered the original surface area of the liquid pool. However, for TS 8, for chamber temperature of 20 °C and CO_2, most of the solid accumulated within the liquid pool as it evaporated, and the bulk mass of the solid residue, remained in the northwest corner of the catch tray.

Upon safe entry conditions, the test engineers were able to enter the test environment to obtain up-close photographs of the residual solid. The TS 3B photographs are provided in **Figure 41**, and the TS 8C photographs are provided in **Figure 42**.

Figure 41. Post-test solid residue for TS 3B (-15 °C/25% RH). Left-The catch tray is 65.4 cm length x 45.1 cm width x 5.72 cm deep. Right- Human finger.

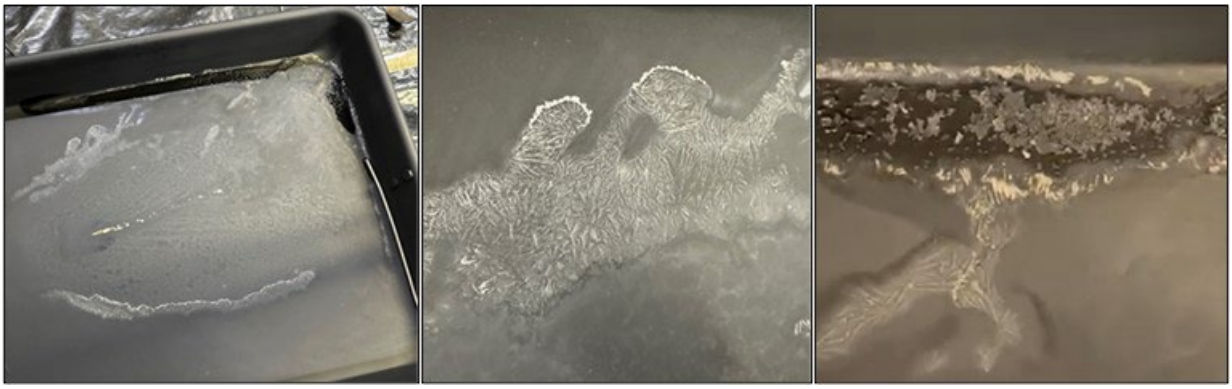

Figure 42. Post-test solid residue for TS 8C (CO_2).

The post-test solid residue was similar-looking between TS 3 and TS 8, but there were some interesting anomalies. The white crystalline structures formed along the edges of the original liquid pool during both TSs. The TS 3 solid appeared uniform throughout the catch tray, while the majority of the TS 8 solid collected as larger chunks that were still wet from the trace liquid remaining. The TS 8 dried solid did not sublime when exposed to ambient conditions (23 °C/62% RH) and persisted much longer than the TS 3 solid. A solid sample of the TS 8 residue was obtained for both C and D replicates after all of the liquid evaporated from the catch tray.

The TS 3 solid was difficult to maintain long enough to obtain a sample for analysis; it readily sublimed at extremely cold conditions. For reference, the picture of the TS 3B solid in **Figure 41** was captured inside the test environment at -3°C, while the ambient temperature was 5 °C. The solid sublimed within a few minutes after the tray was removed from the test environment and subjected to the ambient

conditions. The solid sublimation was evaluated during TS 3C and screenshots of the solid sublimation at t = 90, 120, and 150 minutes are provided in **Figure 43**.

TS 3C, t = 90 min	TS 3C, t = 120 min	TS 3C, t = 150 min
		

Figure 43. HD video screenshots, solid residue sublimation for TS 3C (-15 °C/25%).

The photographs demonstrate that most of the solid sublimed within the 60-minute observation time period, between 90 and 150 minutes. The sublimation was evaluated *in situ* by placing one low range (0 to 100 ppm) electrochemical sensor on the catch tray ("EC_TRAY," pictured in the right photograph of **Figure 43**) and another electrochemical sensor ("EC_CHAMBER") near Node 1L around t = 145 minutes. The time series of concentration measurements are presented in **Figure 44**. The test environment was static from t = 147 to 152 minutes and from t = 156 to 162 minutes. The mixing fans were on, and the test environment was ventilated outside of these time ranges. The test environment temperature was 4 °C.

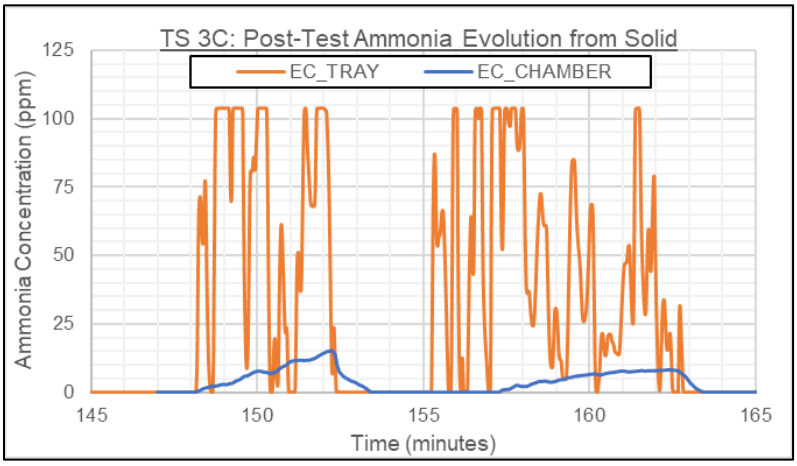

Figure 44. Concentration time series during post-test solid sublimation for TS 3C (-15 °C/25% RH).

The EC_TRAY concentration profile demonstrates time variability of gas-phase ammonia resulting from the sublimation. The EC_CHAMBER concentration time series are much smoother because the measurement was made much farther from the source. These concentration observations confirm the

presence of ammonia gas due to sublimation from the solid but cannot provide any further characterization. The solids from TS 3 and TS 8 were also analyzed with wetted pH strips with a pH range of 0–13. The pH strip color changes are displayed in **Figure 45**.

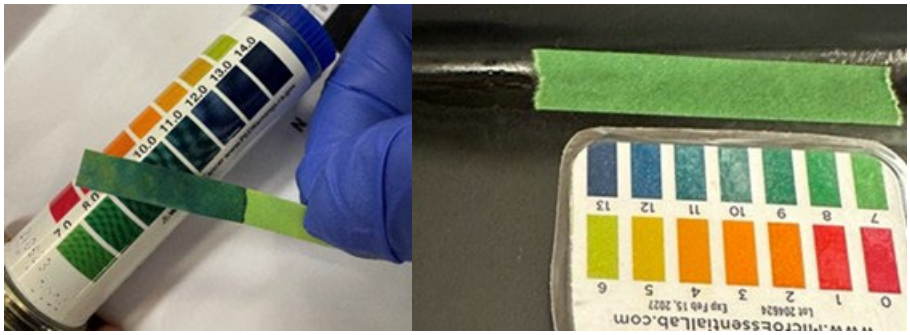

Figure 45. pH of post-test solid residue for TS 3 (left) and TS 8 (right).

The pH of the TS 3 solid was observed to be 9–10, which aligns with the pH of ammonium carbamate. No further analysis of the samples was conducted, except for pH measurements and confirmation that they were formed under low-humidity conditions.

The measured pH of the TS 8 solid was observed to be 7–8, which aligns with the pH of either ammonium carbonate or ammonium bicarbonate. It is confirmed in **Section 3.5.3** that, for TS 8, there was a mixture of ammonium carbonate and ammonium bicarbonate.

3.2 Liquid Ammonia Observations, Standard Approach (i.e., not rain or CO_2) TS

The pressurized liquefied anhydrous ammonia was released from the lecture bottle as a two-phase mixture (gas and liquid). The momentum jet leaving the release aperture contained both ammonia gas (a result of flashing) and liquid tiny aerosol drops, which are generated as a result of the flashing. The mass median diameter of the aerosols is about 50 µm (see Britter et al., 2011 [13]) for the higher pressures (occurring with higher temperature) and is larger for the lower pressures (occurring with lower temperature). The Phase I and II pressures varied by a factor of about 7 for the temperature range from about -15 °C to 40 °C.

The Phase I report details the analysis approach for the time variation of liquid mass within the catch tray from 10 °C to 35 °C [1]. The same measurement and analysis approach was utilized during Phase II to validate Phase I results and extend the temperature range. An attempt is made in this Phase II analysis to characterize the fraction of the liquid, and the catch tray is always the standard orientation (i.e., the tray was not inverted for any of the Phase II tests). The observed liquid mass pooled within the catch tray is

listed in **Table 7**. The collected liquid in catch tray does not represent the ammonia liquid drops deposited on the floor around the catch tray and dispersed through the test environment.

Table 7. Experimental Results, Liquid Pooling, Standard Approach TSs

TS No.	Test Environment Initial Conditions			Total Ammonia Released (grams)	Liquid mass in Catch Tray	
	Temp (ºC)	RH (%)	AH (g H_2O per m^3 Air)		Liquid Ammonia Mass (grams)	Liquid Ammonia Release Fraction
1A	5.3	85.5	5.9	189.2	77.1	40.8%
2A	15.5	89.8	11.9	187.1	54.8	29.3%
2B	15.6	89.1	11.8	189.8	56.4	29.7%
3A	-17.0	25.5	0.4	174.2	98.1	56.3%
3B	-15.2	29.9	0.5	163.7	95.6	58.4%
3C	-18.1	11.5	0.1	168.1	100.5	59.8%
4A	41.0	11.1	6.0	182.8	25.8	14.1%
4B	40.5	10.9	5.7	178.0	24.1	13.5%
4C	40.2	11.2	5.8	172.5	24.9	14.4%
5A	33.8	89.4	33.2	180.1	20.1	11.2%
5B	33.2	89.8	32.4	181.9	20.8	11.4%
5C	33.7	89.8	33.2	187.5	22.4	11.9%
9A	9.4	61.2	5.5	186.0	68.8	37.0%
9B	9.4	60.4	5.5	187.1	68.9	36.8%
9C	10.3	59.8	5.7	150.2	52.8	35.2%
10A	21.9	61.2	11.8	193.4	57.9	29.9%
10B	22.5	60.7	12.1	151.1	39.9	26.4%
11A	34.6	59.6	23.1	169.8	20.1	11.8%
11B	35.6	60.3	24.6	181.6	22.2	12.2%
11C	35.2	61.2	24.5	177.2	20.9	11.8%

The time variation of the measured liquid pool mass within the catch tray throughout the static test environment duration is displayed for all standard approach TSs in **Figure 46**, **Figure 47**, and **Figure 48**.

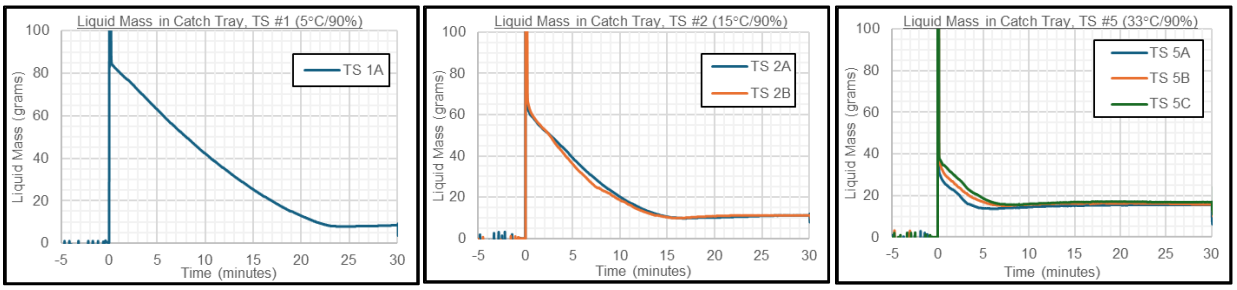

Figure 46. Liquid mass in catch tray time series; high humidity: TS 1 (left), TS 2 (center), TS 5 (right).

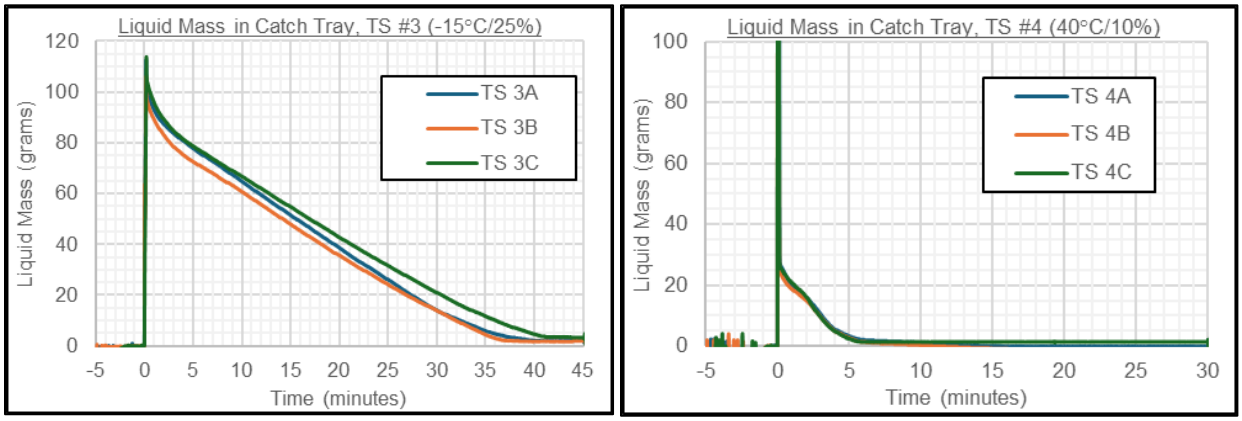

NOTE: TS 3 x-axis and y-axis extended ranges

Figure 47. Liquid mass in catch tray time series; extreme cold TS 3 (left) and extreme hot TS 4 (right).

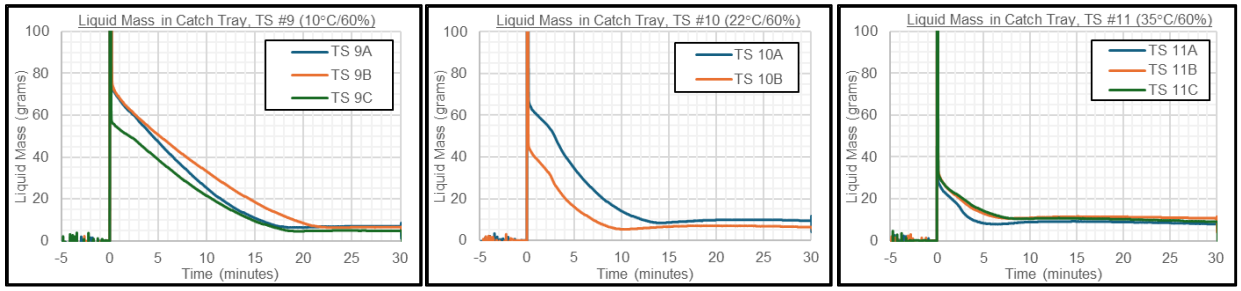

Figure 48. Liquid mass in catch tray time series; average condition: TS 9 (left), TS 10 (center), TS 11 (right).

The liquid mass time series demonstrated excellent repeatability between replicates (i.e., A, B, and C), and TSs 9, 10, and 11 aligned with their nearly-equivalent Phase I tests (Phase I TSs 1, 2, and 3 not shown here) [1]. In all cases, the initial liquid mass is influenced by the environmental temperature, with larger liquid pools observed at lower temperatures within 1 minute. The evaporation of the pool results in faster decreases in mass at higher temperatures. The mass plateau region indicates a larger mass at higher temperatures, which may be attributed to liquid water condensing from the entrained ambient water vapor. Since the water content in the liquid pool was not independently analyzed, further assessment is required to fully understand this observation.

3.2.1 Liquid Ammonia Release Fraction

The liquid mass measured within the catch tray was used to calculate the fraction of the released liquid that is in the liquid pool. This is determined by measuring the liquid pool at the initial release, the weight of the non-evaporating liquid pool after 10 minutes, and the weight of the non-evaporating liquid pool once the time series indicated at the evaporation was complete (that is time series plateau), which

remained for the rest of trials duration of at least 30 minutes. The pooled liquid phase ammonia release fractions are plotted as a function of test environment temperature in **Figure 49**.

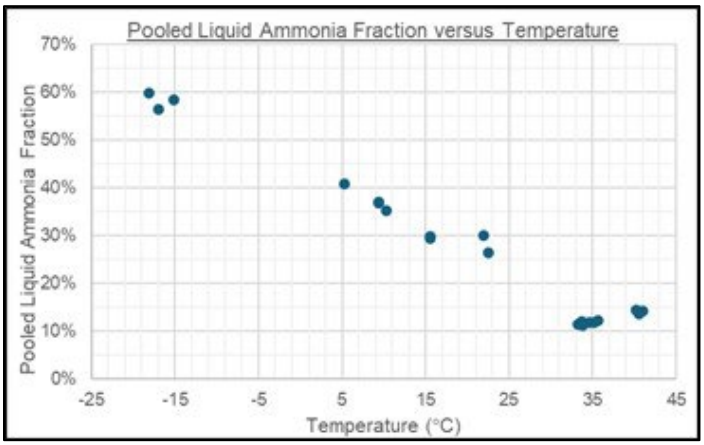

Figure 49. Ammonia release fraction as a pooled liquid vs. temperature.

The experiment temperatures ranged from -18.1 °C to 41.0 °C, which encompassed the practical range of temperature conditions nationwide. These results depicted a strong linear relationship between temperature and the release fraction of pooled liquid ammonia. Each TS replicate had repeatable results, and the linear trendline aligned with the Phase I results [1]. As the temperature increased, the release pressure increased and aerosolized a larger fraction of the total ammonia released, therefore the pooled liquid phase-ammonia mass captured within the catch tray decreased. This finding clearly demonstrates that the environmental temperature governs the headspace pressure in a pressurized lecture bottle. The lowest environmental temperature tested (-15 °C) resulted in a reduced vapor pressure of -15 psi compared to the hottest temperature tested (40 °C at 240 psi), leading to the significant formation of a liquid pool in all trials tested. Further modeling of this phenomenon will be required to understand the flash fraction and the median aerosol drop diameters under different temperatures.

3.2.2 Possible Water Vapor Condensation Liquid Pool

The temperature and RH variations near the liquid pool were observed during Phase I. These measurements indicated that 100% RH was achieved above the liquid pool in the catch tray (this is expected because the air is very cold just above the liquid ammonia pool [1]). Additionally, the liquid mass time series plateaued at levels above zero when ammonia evaporation was expected to be complete. Phase II HD videos confirmed that minor amounts of liquid were still present in the catch tray after t = 30 minutes, as seen in example screenshots acquired at this timepoint from Cam 1 in **Figure 50**.

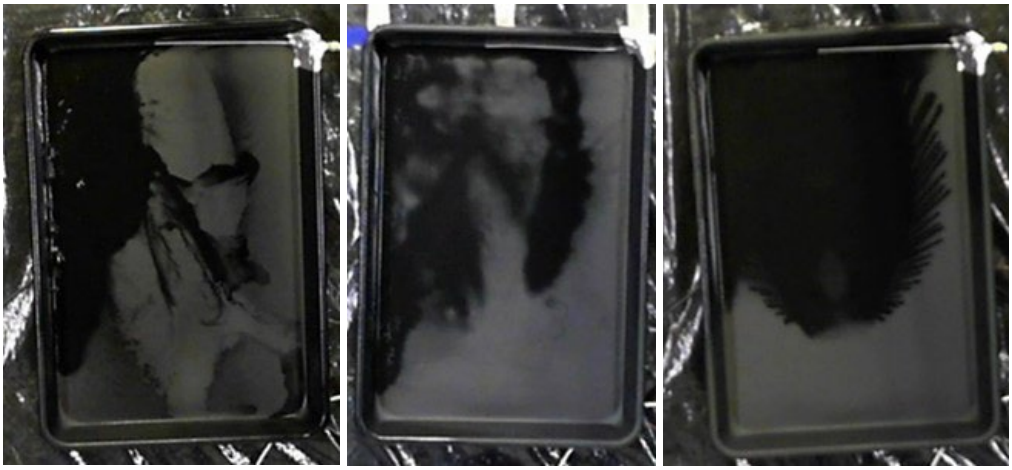

Figure 50. Trace liquid visible in the dark section of the catch tray, t = 30 minutes for TS 9A (left), TS 10B (center), TS 11A (right).

The remaining liquid was assumed to be mostly water vapor condensation that condensed into the subcooled liquid pool with a small amount of ammonia due to the high ammonia vapor pressure above the liquid during this time. The reported water condensate mass was documented as the mass value when the plateau occurred after ammonia evaporation stopped. The water condensate mass was translated to a mass fraction of the total liquid pool, which was plotted as a function of AH in **Figure 51**.

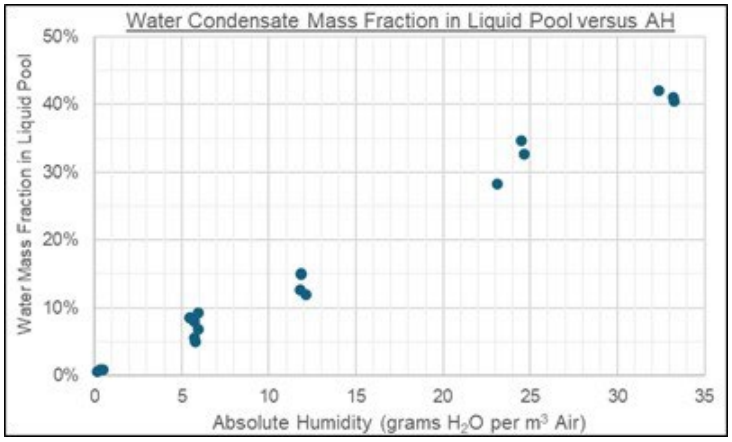

Figure 51. Mass fraction of water condensate in pooled liquid vs. AH.

The results indicated a linear relationship between the AH and the mass fraction of water vapor condensate within the liquid pool when exposed to the ammonia environment. Although the purity of the liquid (water) has not been analyzed, given the closed environment conditions and the hydrophilicity of ammonia, it is believed to be aqua ammonia. From the various TSs studied, the tests conditions with the largest water condensate mass fraction were TS 5 and TS 11. Further analysis is required to better understand this observation.

3.2.3 Liquid Ammonia Drops

The IR videos are used to assess the presence of liquid drops. Example FLIR screenshots from several Phase II TS combinations at t = 20 seconds are provided below. The perspective was from the ceiling view down to the catch tray. **Figure 52** displays screenshots of the extreme humidity TSs for different temperatures. **Figure 53** provides similar plots for the extreme cold and hot TSs, and **Figure 54** provides plots for average cold and hot condition TSs. It is important to note that the FLIR camera was not able to be calibrated to this unique application (see **Section 2.7.2)**. Therefore, the color contours of each FLIR screenshot should not be considered to be associated with specific temperatures. However, relative differences can be seen. The color contours from coldest to hottest are: black, purple, dark blue, light blue, green, yellow, red, and white.

TS 1A (5 °C/90% RH)	TS 2B (15 °C/90% RH)	TS 5A (33 °C/90% RH)
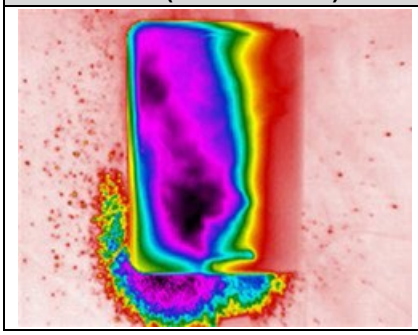	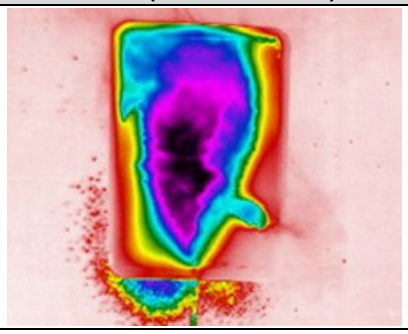	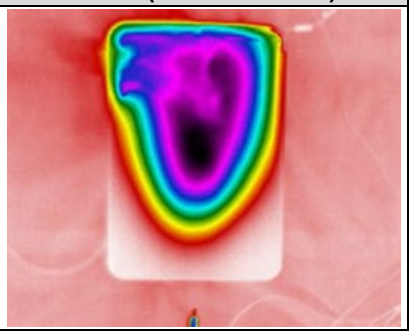

NOTE: The dots to the side are individual large drops.

Figure 52. FLIR screenshots, relative liquid temperatures at t = 20 seconds, high RH (90%).

TS 3A (-15 °C/25% RH)	TS 3B (-15 °C/25% RH)
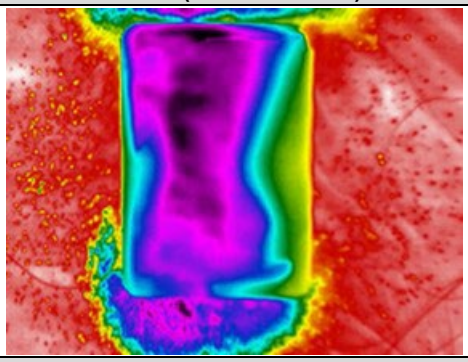	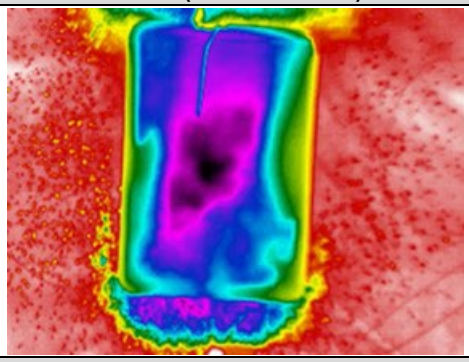
TS 4A (40 °C/10% RH)	**TS 4B (40 °C/10% RH)**
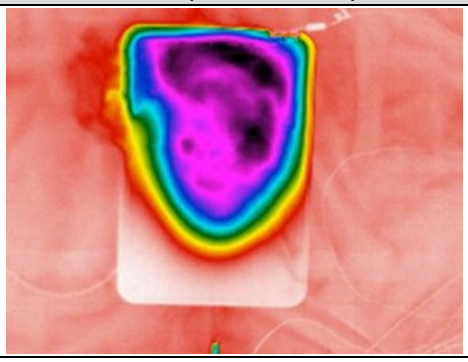	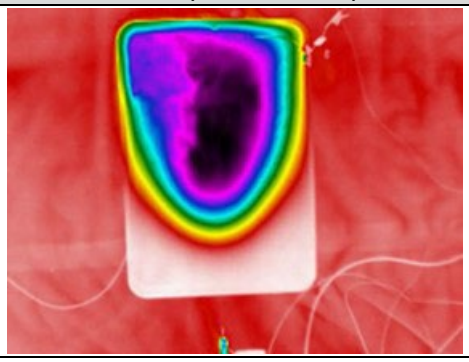

NOTE: The dots to the side are individual large drops.

Figure 53. FLIR screenshots, relative liquid temperatures at t = 20 seconds, extreme hot (40 °C) and cold (-15 °C), low RH.

TS 9A (10 °C/60% RH)	TS 9B (10 °C/60% RH)
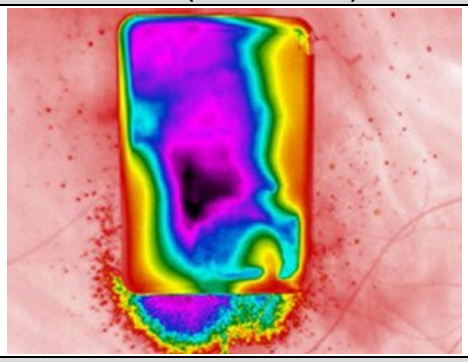	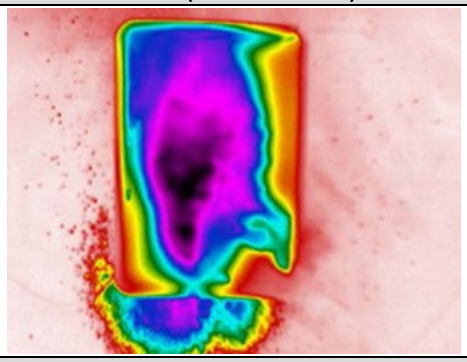
TS 11A (35 °C/60% RH)	**TS 11B (35 °C/60% RH)**
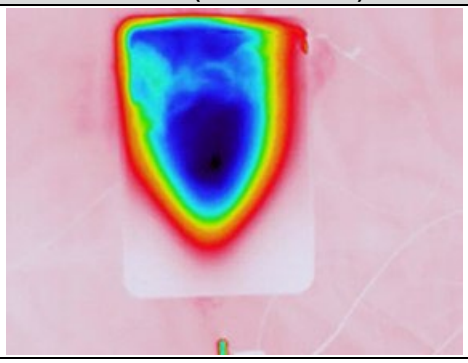	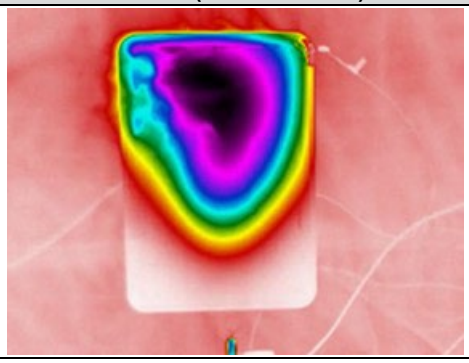

NOTE: The dots to the side are individual large drops.

Figure 54. FLIR screenshots, relative liquid temperatures at t = 20 seconds, average hot (35 °C) and cold (10 °C), 60% RH.

The FLIR photographs suggested the drop formation was dependent on the test temperature, but not humidity. This is because the low temperature cases had low pressure in the ammonia lecture bottle, and hence larger water drops after flashing (Britter et al., 2011 [13]). The drop accumulation was the greatest in the south edge, followed by the west edge and east edge. It was assumed that many of the drops around the south edge dripped from the release manifold outlet during release. The west edge had more accumulation than the east likely due to bouncing off the slightly warped catch tray during release. The drops around the west and east edges disappeared by t = 1 minute, and the south edge drops disappeared by t = 2 minutes.

3.3 Ammonia Plume Observations, Standard Approach (i.e., not rain or CO_2) TSs

This section discusses the ammonia plume observations for the standard approach TSs. These tests did not involve the use of rain or CO_2. The ammonia plume after impact on the catch tray was assumed to be composed of anhydrous ammonia gas, some ammonia aerosols, some entrained ambient dry air, some ambient water vapor (gas), and some condensed ambient water vapor. It is known that the PIDs measure concentrations of ammonia gas. However, it is not known whether the PID can also include the liquid ammonia aerosols in its measurement.

The time (2-second resolution) and space (18 locations in chamber) variations of the ammonia concentrations were characterized by the measurements from the PIDs. At a few of the PIDs locations, RH was measured, temperature was measured by TCs, and pressure was measured by PTs. There were two heights of measurement (2 ft or 0.6 m and 6 ft or 1.9 m) within the test environment, which allowed the analysis of vertical differences of ammonia concentration and air density. Additional discrete measurements of the ammonia plume were carried out with pH-based approaches. The Phase II experimental results specific to the ammonia plume are provided in **Table 8**.

Table 8. Experimental Results, Ammonia Plume, Standard Approach (i.e., no rain or CO_2)

TS No.	Test Environment Initial Conditions				Initial Pressure in lecture bottle (psia)	Liquid Fraction [a]	Derived Ammonia Mass Balance
	Temp (°C)	RH (%)	AH (g H_2O per m^3 air)	Average Air Density of mixture of dry air, water vapor, and ammonia (kg/m^3)			
9A	9.4	61.2	5.5	1.232	87	37.0%	99.1%
9B	9.4	60.4	5.5	1.239	91	36.8%	99.5%
9C	10.3	59.8	5.7	1.222	96	35.2%	98.9%
10A	21.9	61.2	11.8	1.193	133	29.9%	94.7%
10B	22.5	60.7	12.1	1.183	137	26.4%	94.2%
11A	34.6	59.6	23.1	1.110	200	11.8%	84.6%
11B	35.6	60.3	24.6	1.117	207	12.2%	83.8%
11C	35.2	61.2	24.5	1.124	202	11.8%	84.0%

NOTE: [a]The liquid fraction of the ammonia release calculated here is expressed as a percentage of the ammonia mass, weighted against the total ammonia mass released from the lecture bottle. This value is a direct measurement of the liquid mass on the catch tray using a scale.

3.3.1 Ammonia Concentration Differences between Low (2 ft or 0.61 m) and High (6 ft or 1.82 m) Sampling Levels

In one analysis approach, the datasets containing individual PID concentration observations were analyzed after separating the sensors into two vertical levels. The PIDs at the 2.0-foot (0.61 m) height were averaged to report a single average concentration at the 2.0 ft (0.61 m) level of the test environment ("PID_LOW), and the PIDs at the 6.0-foot (1.8 m) height were averaged to a report single average

concentration in the 6.0 ft (1.8 m) level of the test environment ("PID_HIGH,"). These plots are documented in **Appendix D**.

The videos and the PIDs C observations at individual locations showed much time and space variability in the first minute or two after release. The videos showed the strong momentum jet, which lasted only about 10 seconds, hitting the catch tray and reflecting upwards towards the ceiling near the back of the chamber. Thus, the middle of the jet might "hit" only a few specific PID locations, and the max C could be at a location at the far and upper part of the chamber. This powerful initial jet led to eddies of ammonia swirling around the chamber for at least 2 minutes but decreasing in intensity. It resulted in some "sloshing" back and forth, from one end of the chamber to the other, that is seen in the C time series at some locations. Also, during the first few minutes, the liquid ammonia pool in the catch tray (and some off the side) evaporated as shown in the videos, and the visible cloud rising from the pool moved in varying speeds and directions. As a result of these effects, one PID might be in the ammonia plume for a minute, while its neighbor was at the edge or off the ammonia plume. Then the situation would be reversed. After about 10 minutes, the ammonia concentration throughout the chamber slowly tended towards homogenization. Then, at about 30 minutes, the fans were turned on, resulting in further homogenization. The average concentration difference at any time was assumed to equal the PID_LOW averaged concentration minus the PID_HIGH averaged concentration. The time series of these observed concentration differences for the Phase II standard set (i.e., not the rain or CO_2 tests) TSs are shown in **Figure 55**, **Figure 56**, and **Figure 57**. TSs are grouped according to RH.

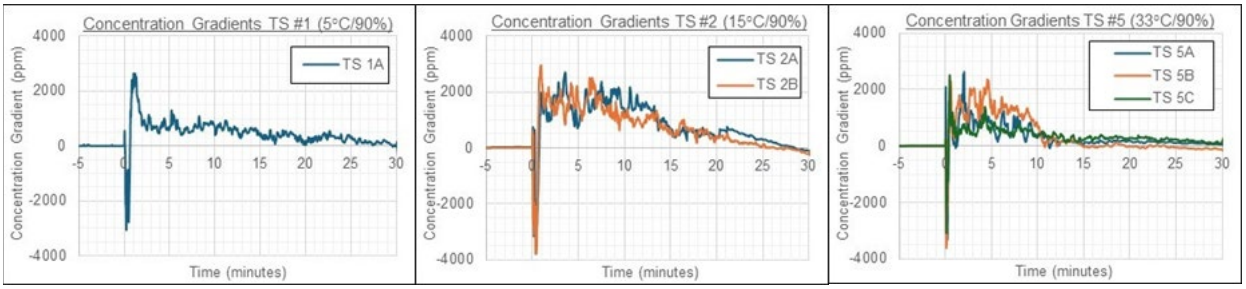

Figure 55. Ammonia concentration differences (C LOW – C HIGH) time series high RH (all 90%): TS 1 (T = 5 °C, left), TS 2 (T = 15 °C, center), TS 5 (T = 33 °C) right).

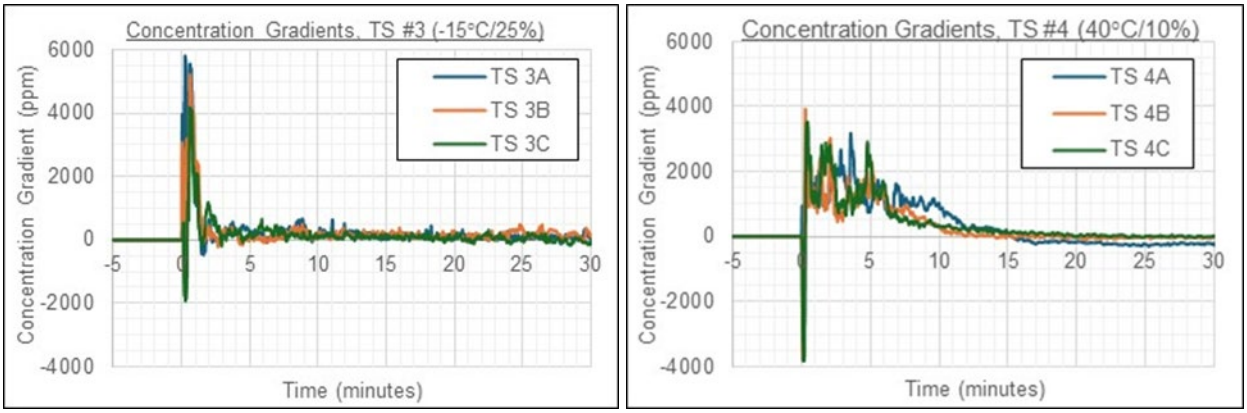

Figure 56. Ammonia concentration differences (C LOW – C HIGH) time series low RH; extreme cold TS 3 (T = -15 °C, left) and hot TS 4 (T = 400 °C, right).

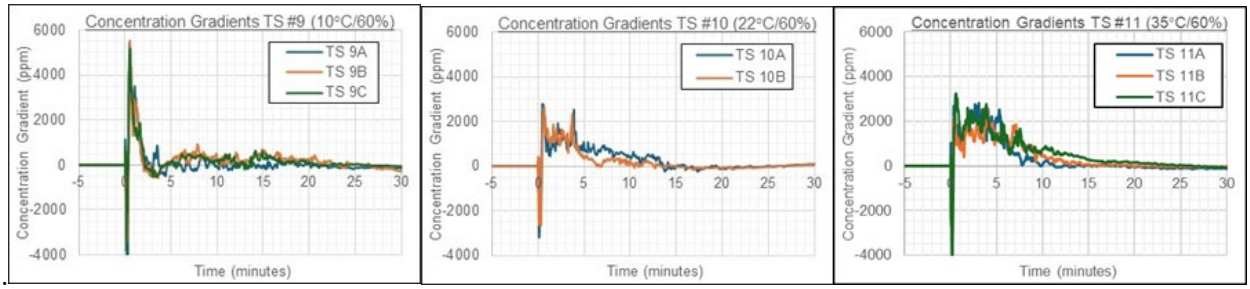

Figure 57. Ammonia concentration differences (C LOW – C HIGH) time series with all RH = 60%; TS 9 (T = 10 °C, left), TS 10 (T = 22 °C, center), TS 11 (T = 35 °C, right).

The concentration difference time series plots look similar to those reported for the Phase I tests [1]. The concentration differences are initially (in the first few seconds) strongly negative, which can be attributed to the two-phase jet reflecting off the tray and moving towards the upper part of the chamber (thus the L - H concentration differences are -4000 to -2000 ppm). After about 10 or 20 seconds, this quickly reverses in all TSs, and a positive spike with a difference of 2000 to 6000 ppm is observed between average L and average H PIDs. This spike decreases markedly during the next minute and then slowly decreases (with fluctuations) over the next few minutes. During this period, ammonia gas is evaporating from the liquid pool and causing the average gas concentration in the lower half of the chamber to increase more than in the upper part, except for TS 9. Concentrations differences do not decrease as quickly in the hotter TSs. Eventually, all TS concentration differences converged to a nearly zero difference before t = 30 minutes.

The individual L and H concentration time series from TS 3B (-15 °C/25%) and TS 11C (35 °C/60%) are provided in **Figure 58**. Note that all concentrations eventually (at 40 minutes) converge to a concentration of about 4300 to 4700 ppm, as expected, the final concentrations are lower for the hotter TSs on the right.

Some of the slow increase in concentrations seen in the left-hand figure (-15 °C) can be attributed to evaporation from the liquid pool, which was larger for the colder releases. For the right-hand figure (35 °C), sinusoidal fluctuations with a period of about 2 minutes indicate sloshing in the lower part of the chamber, resulting in a higher concentration at located at L PIDs (TS 4)

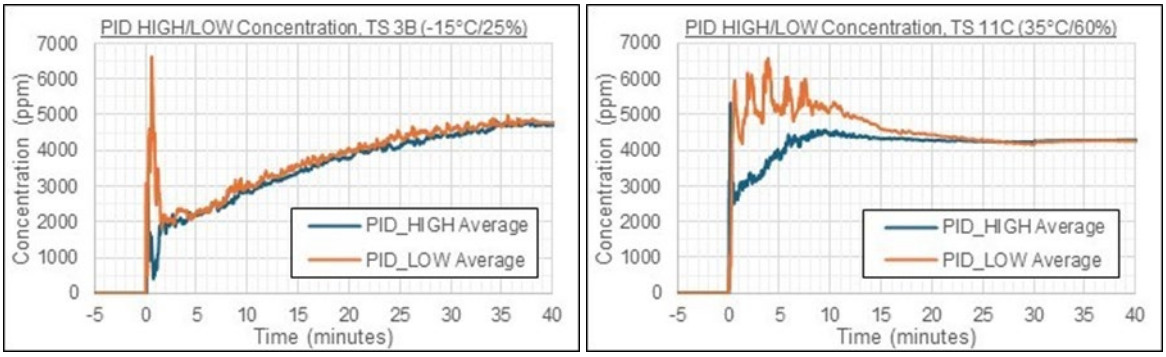

Figure 58. Example PID_ HIGH average /LOW average concentration time series for TS 3B (-15 °C/25%, left), and TS 11 °C (25 °C/60 %, right).

3.3.2 Air Density Differences

The thermodynamic effects of the ammonia release and plume within the test environment were also assessed using air density calculations. The term "air density" refers to the density of the dry air/water-vapor/ammonia gas mixture. "Vapor" is synonymous with "gas." As done for the concentration difference methodology described in the previous section, the RH/TC measurements and the ammonia measurements at the 2.0-foot (0.61 m) height were used to calculate the air density at that level (AirDensity_LOW), and the RH/TC measurements and the PIDs at the 6.0-foot (1.8 m) height were used to calculate the air density at that level (AirDensity_HIGH,). The temperature measurements from the co-located ammonia sensors at both low and high were used to determine the temperature difference. A common PT measurement was also used for both calculations. These plots are documented in **Appendix E**.

The air density differences were calculated by subtracting the AirDensity High values from the AirDensity_Low values for each time. The time series for all Phase II standard set TSs are provided in **Figure 59**, **Figure 60**, and **Figure 61**. Background air density differences, due to the ambient and test environment temperature difference, plus the effect of decreasing density with height in an adiabatic atmosphere, are provided as the grey dotted lines and are considered the baseline reference.

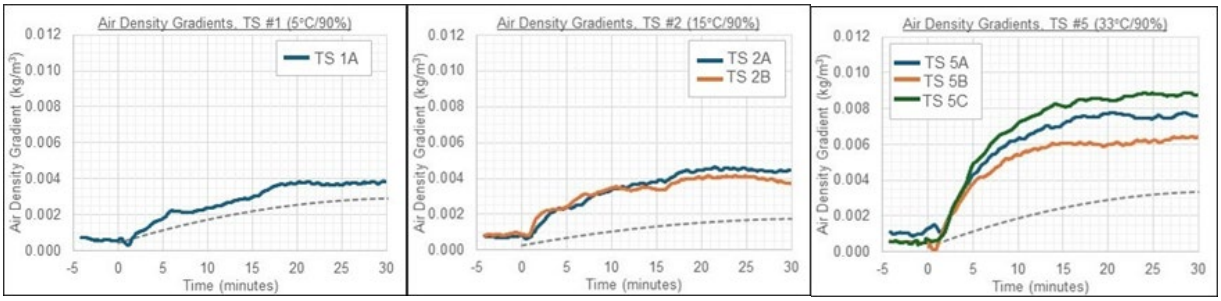

Figure 59. Air density difference time series; high RH for TS 1 (5 °C/90%, left), TS 2 (15 °C, 90%, center), TS 5 (33 °C/90%, right).

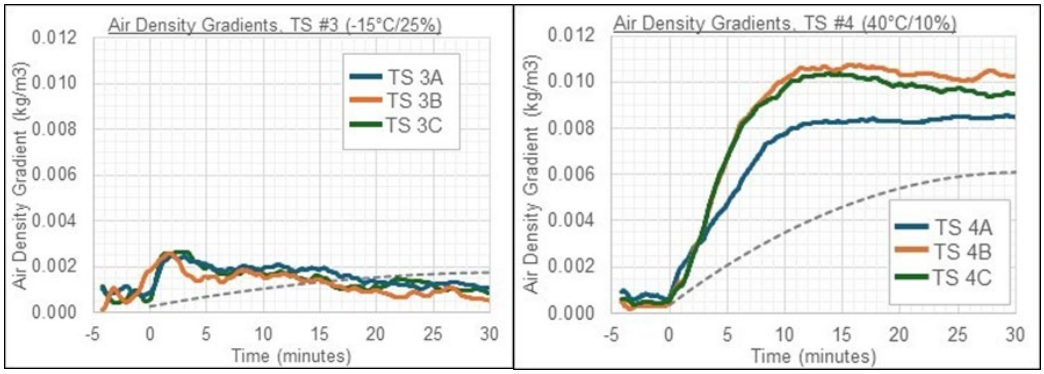

Figure 60. Air density difference time series; extreme cold TS 3 (-15 °C/25%, left) and hot TS 4 (40 °C/10%, right).

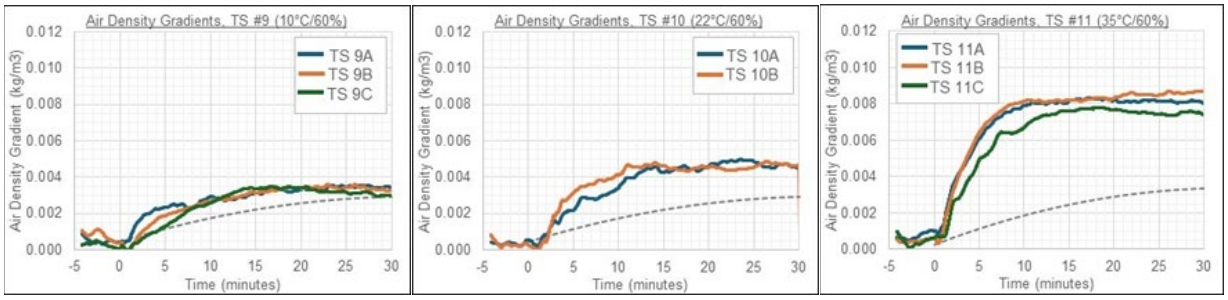

Figure 61. Air density difference time series for TS 9 (10 °C/60%, left), TS 10 (22 °C/60%, center), TS 11 (35 °C/60%, right).

The air density difference time series aligned with the noted trends previously identified in Phase I [1]. The hot TSs air density differences drastically increased beyond the background differences during the initial 10 minutes due to the LOW air density increasing faster than the respective HIGH air. The time range of observable air density difference observation aligned with the time when the concentration difference time series shifted from negative stratification to neutral. Both dataset trends implied that the thermodynamic effects of the residue/particulate phase interactions with water vapor and evaporation

were complete, and the aerosolize vapor phase ceased to exist. After this time, the air density difference plateaued as the HIGH and LOW air density time series returned to trending at the same rates and could suggest that the test environment system was at thermodynamic equilibrium and the remaining detected ammonia existed in the gas phase.

3.3.3 Uncertainties at High Relative Humidity (RH)

The high (90%) RH tests (TSs 1/2/5) proved troublesome for accurate concentration measurements. The release event triggered ambient water vapor condensation within the test environment, as previously discussed in **Section 3.1.2**. The RH probes were designed for accurate measurement, even near and at 100% RH; therefore, the RH observations were used to estimate the condensation magnitude and duration. The observed RH time series at Nodes 1 and 3 during TS 2A (15 °C/90%) and TS 5A (33 °C/90%) are provided in **Figure 62**.

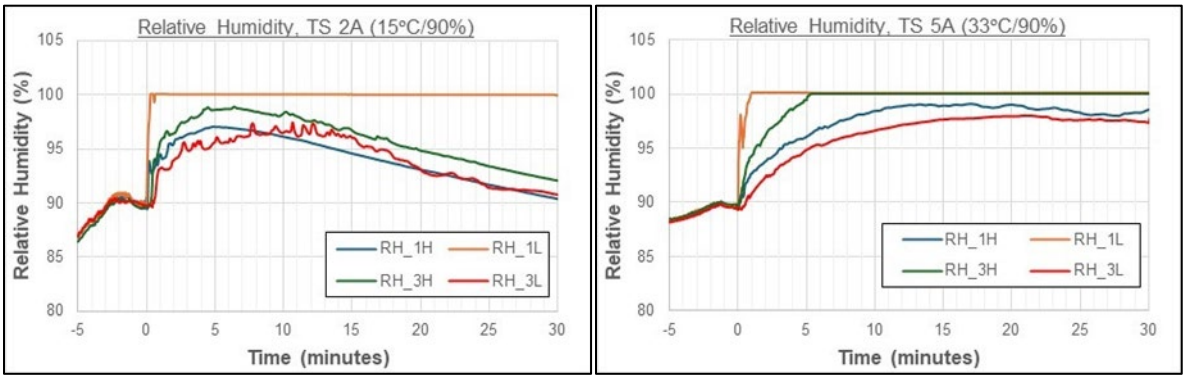

Figure 62. RH time series; 90% RH for TS 2A (15 °C, left) and TS 5A (33 °C, right).

The RH time series confirmed that 100% RH and localized condensation was achieved almost immediately at Node 1L for both TSs 2A and 5A and additionally at Node 3H for TS 5A. The TS 2A RH time series peaked between 96% and 98% at about t = 5 minutes and then decreased slowly towards 90 %, but the TS 5A RH profiles continued to increase and, after 10 or 15 minutes, plateau at about 98% to 99% RH.

These results suggest that TS 5 generated a more persistent condensation fog than TS 2. However, it is important to note that the ambient temperature and RH conditions impacted the observed RH time series. Another factor is that, at 90 % RH, the water vapor content (and the saturation deficit) is about twice as large at 33 °C than at 22 °C.

3.3.4 Ammonium/Ammonia pH Observation from TSs 9, 10, and 11

The mass balance results from TSs 9, 10, 11 aligned with those from Phase I [1] yielding a lower ammonia mass balance (84%) under 35 °C/60%RH conditions. The mass balance (ratio of mass estimated from concentration observations to known mass released) decreased as the test environment temperature increased from 10 °C, 22, to 33 °C, while humidity is set at 60%RH. This also led to higher AH levels from 6 to 24 g/m^3 as shown in **Table 1**. The observation made from the Phase I data analysis is that there were several post-test occurrences of a white residue on the chamber floor and catch tray. As part of an excursion assessment, pH paper and a pH probe were utilized to observe their corresponding changes in hydronium concentrations in the Phase II experiments. **Figure 63** shows the location of how two separate measurements were taken at the Node 3 location in **Figure 2**; one using a pH probe and the other using pH paper. This is because pH is a measurement of hydronium concentration and can be used as an indirect measurement of hydroxide ion concentrations as shown in **Equation 4**. Since the chamber is closed configuration, the released ammonia must have reacted with ambient humidity in the test environment to generate an ammonium salt byproduct. The hotter temperatures (i.e., higher release pressures) would decrease the sizes (but increase the number) of the unflashed liquid ammonia drops (aerosol). The hydrophilic nature of ammonia suggests that an increase in the number of aerosol drops and an increase in the test environment AH facilitated a greater number of ammonia-water interactions. These interactions stemmed from entrained ambient water vapor condensing or in the momentum jet generated from the release. The resultant ammonia-water equilibrium with the ammonium ($NH_4{}^+$) and hydroxide (OH^-) ions is shown in **Equation 4:**

$$NH_3 + H_2O \leftrightarrow NH_4{}^+ + OH^- \quad (4)$$

Equation 4

The ammonia in equilibrium had the ability to evaporate out of solution, but any aqueous ammonia solution or ammonium could not be measured by the PIDs, therefore the ammonia mass balance yielded less than 100%. The formation of the ammonium ion opened the possibility of side reactions.

Recommendations from Phase I dictated the implementation of Phase II TSs 9/10/11. These three TSs were executed at Phase I conditions (Phase I TSs 1/2/3), and pH measurements were integrated into the test environment [1]. The goal of the pH measurements was to determine the ammonia plume pH at varying temperatures and AH. The ammonia plume pH correlated to where the equilibrium position existed between ammonia and ammonium. The theoretical ammonia-water equilibrium position as a function of pH is provided in **Figure 63**. The pH results from TSs 9, 10, and 11 are overlayed.

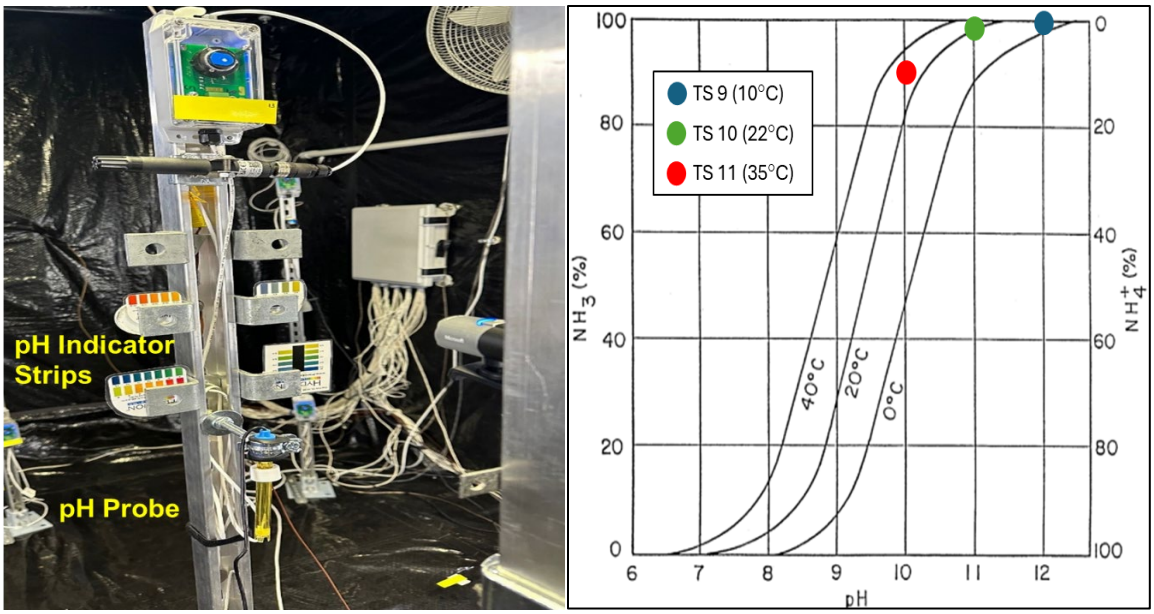

Figure 63. pH measurements (left) and ammonia-water equilibrium versus pH and temperature [14] (right).

The equilibrium plot in **Figure 63** indicates how much ammonium ion could be present at a given pH. For example, a pH = 10 suggested that the equilibrium existed as 85% ammonia and 15% ammonium at 35 °C. Since the measurements are not intended for atmospheric conditions, further studies are required to investigate how they relate to the principles defined for aqueous solutions according to Le Chatelier's principle. Increasing the concentration of ammonia would cause the equilibrium position to shift away from ammonia and toward ammonium. If the AH in the test environment increased, the potential water condensation or absorption into the residue/particulate fraction would increase the water content within the ammonia-water equilibrium. The equilibrium position would shift away from water and more ammonium ions would exist. Nonetheless this principle can be applied to the AH as well but has not been fully investigated in this experiment. The pH observations reported herein support the advancement of this notion.

From the data collected from pH indicator strips and a pH electrode are to detect any variations in the pH of ambient air. The primary pH measurement was captured with various ranges of pH indicator strips that were installed at Node 3H (**Table 2**), as pictured in **Figure 64**. A dedicated HD camera recorded the pH strip color-change response to the ammonia plume.

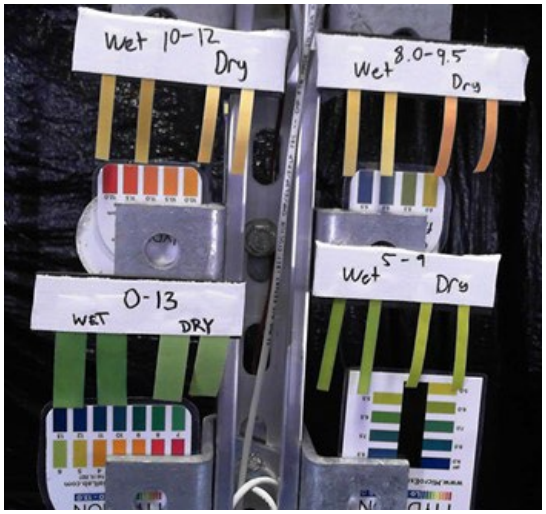

Figure 64. Pre-test pH indicator strips, node 3H for TSs 9/10/11.

The pH strips ranges were 10–12 (top left), 8.0–9.5 (top right), 0–13 (bottom left), and 5–9 (bottom right). These pH strips are intended to cover the full range of pH 10 through 13 with options for improved resolution in the higher pH ranges. Laminated indicator cards for each respective range were placed behind each set for immediate color-to-pH reference. Each range contained four strips, one pair was pre-wetted with deionized water per the standard approach for pH strip measurement, and the second pair was left dry per the request of the ERWG. The pH was found to be best observed with the pre-wetted 0–13 and 10–12 range pH strip sets. The reference color indicator as shown in the photo was used to estimate the pH concentration. Measurements out of range were excluded and determined visually after each trial. Screenshots from the HD video capturing the color change response are provided in **Figure 65**. for TS 9 and TS 11. The screenshots were cropped to only display the 0–13 and 10–12 range sets.

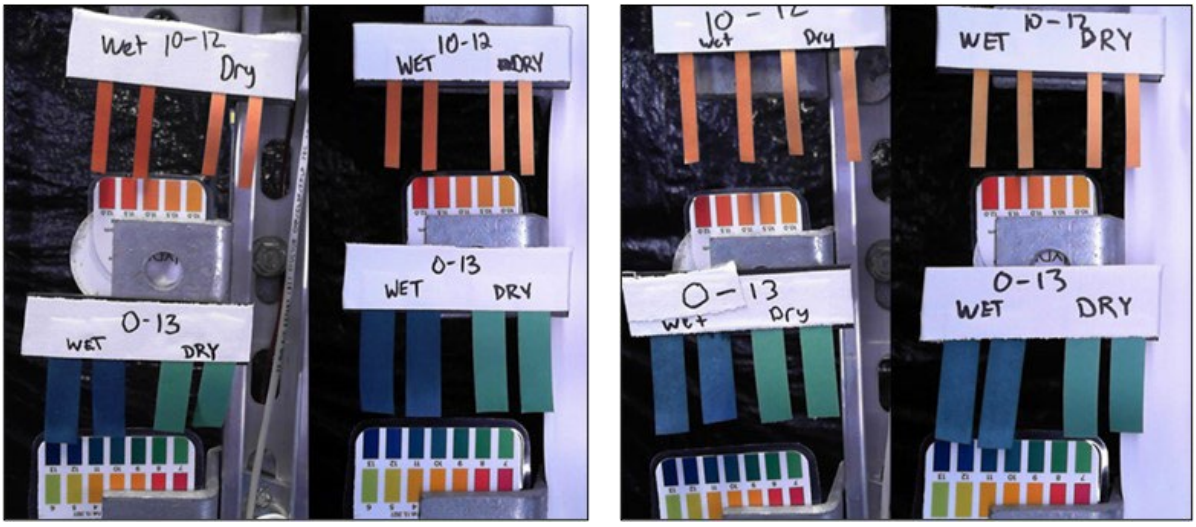

Figure 65. pH strip response to ammonia plume for TSs 9A/B (left) and TSs 11A/B (right).

The wetted pair of pH strips had a definitive response to the ammonia plume, while the dry pair response was not as dramatic. The wetted pH strip pairs clearly indicated a higher pH was measured during TS 9 compared to TS 11. Visual analysis of the wetted pairs by naked eye suggests that the measured pH during TS 9 was 11.5–12.0, and TS 11 was 10–10.5. The TS 10 pH strips (not pictured) measured ~11.0.

The secondary pH measurement was an investigative approach with a general-purpose pH electrode, as described in **Section 2.9.2**, installed at Node 3H. Although the electrode is designed to be submerged in liquid and lacks an air reference, the measurement made in air within the chamber still showed responses corresponding to changes in temperature. Therefore, the results obtained from the pH electrode are shown in **Figure 66**.

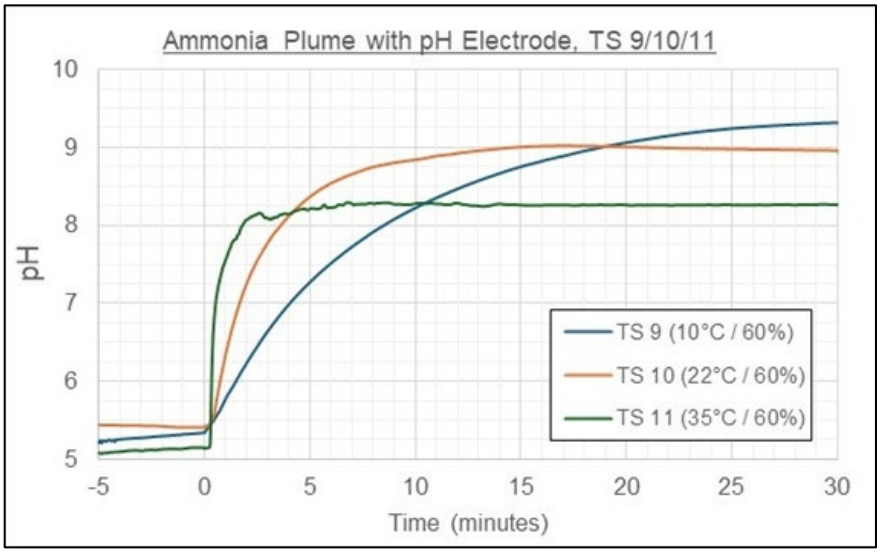

Figure 66. Time series of pH electrode response to ammonia plume for TSs 9/10/11.

The pH electrode results validated the pH trend identified with the pH indicator strips. After about 20 minutes had elapsed, the cold conditions (TS 9) resulted in the highest pH (about 9.3), and the hot conditions (TS 11) had the lowest pH (about 8.3). WSP cards were used in TSs 9, 10, and 11 to measure the drop sizes. However, the test results were inconclusive. Additional details on the WSP cards can be found in **Appendix F**.

3.4 Simulated Rain Scenario Observations (TS 6 and TS 7)

Simulated rain was used to evaluate its effects on the ammonia plume and measure the mass transfer potential of rain during TS 6 and TS 7. These tests were performed with the focus to aid in the response and evaluation of an accidental ammonia release by measuring the mass of ammonia aerosol and/or gas

scrubbed by rain during the release event and determining the quantity of gaseous ammonia scrubbed by the rain occurring several minutes after the release.

Rain was delivered at two rates based on American Meteorological Society-documented light and heavy rain rates. The light rain (TS 6) rate was 0.3" (7.6 mm) per hour. The heavy rain (TS 7) rate was 1.4" (3.6 cm) per hour. The rain was active during the 10-second ammonia release event during the A/B replicates, while the rain was activated several minutes after the 10-second ammonia release, trying to assure that liquid evaporation was complete.

All replicates were carried out at 22 °C and 50% RH. These temperature and RH conditions were similar to the Phase I TS 2 conditions [1]. The test instrumentation was re-configured to integrate the rain system, maintain accurate measurements, and prevent electrical complications in a wet environment. Additional details on the rain delivery system and approach were provided in **Section 2.9**. The ammonia concentration, rain rates, and rainwater pool pH were measured over time during each TS. The observed ammonia yields were calculated using the same process applied to the other trials without rain or CO_2. Ammonia concentration measurements continued after the rain was stopped to quantify potential ammonia evaporation from the rain pool on the test environment floor. The experimental results are provided in **Table 9**.

Table 9. Experimental Results, Simulated Rain Scenarios (TS 6 and TS 7)

TS No. [a]	Simulated Rain					Ammonia Mass Balance	
	Rain Method	Rain Start (min)	Rain Stop (min)	Rain Volume (L)	Rain Pool pH	Total Ammonia Released (grams)	Yield After Rain
6A	During Release	-0.5	5.0	5.5	10.3	194.1	59.6%
6B	During Release	-0.5	5.0	5.5	10.0	202.7	58.7%
6C	After Release	17.0	22.0	4.8	9.1	158.6	79.0%
7A	During Release	-0.5	3.5	17.1	11.0	193.3	47.8%
7B	During Release	-0.5	3.5	17.1	10.1	180.7	48.7%
7C	After Release	17.0	22.0	21.4	10.5	182.7	55.8%

NOTE: [a]TSs 6/7 replicates at 22 °C / 50% RH (±1 °C and ±1.5% RH). pH probes were located 6 feet (1.8 m) away from the center of the catch tray on the ground.

During the 6 A/B replicates, the rain system was active during the ammonia release event. It should be noted that the strong momentum jet occurred only for 5 to 10 seconds. The light rain (TSs 6A/B) continued until t = 5.0 minutes, and the heavy rain (TSs 7A/B) continued until t = 3.5 minutes. After the rain ended, the test environment was left static (still) until mixing fans were turned on at t = 20 minutes during TSs 6A/B and t = 30 minutes during TSs 7A/B. This timing information can be applied to the average observed ammonia concentrations, calculated as an average of all PIDs in the test environment. The rainwater pH is also considered (**Figure 67**).

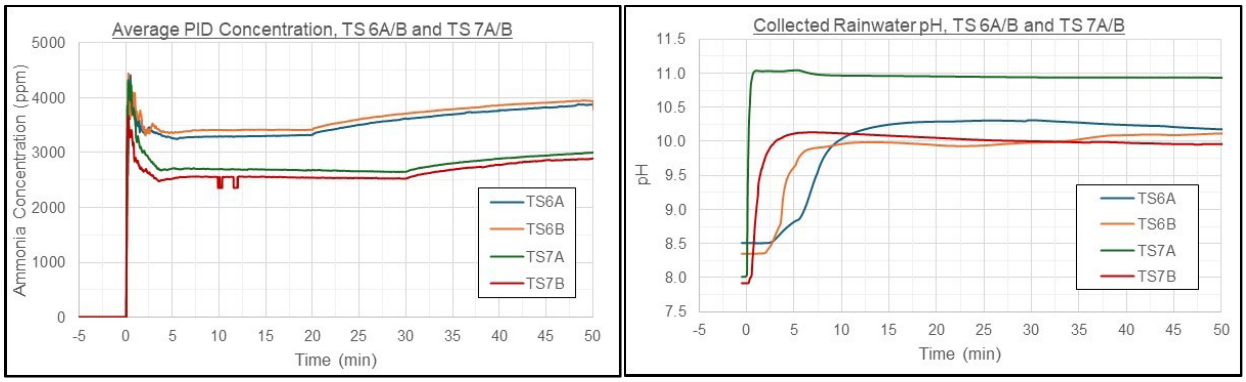

Figure 67. Average ammonia concentration, which is noted as PID concentration (left) and rainwater pH (right) for TSs 6A/B and 7A/B.

Both plots from **Figure 67** showed a significant decrease in ammonia concentration and changes in pH conditions after 5 minutes. After the initial 5 minutes of exponential decrease, the plateaued region corresponds to when the simulated rain was discontinued. The left plot (20 minutes after for TS 6 with light rain and 30 minutes after for TS7 with heavy rain) shows an increase in ammonia concentration, indicating off-gassing of ammonia from the rainwater pools.

For TS 7A, the pH probe was placed just south of Node 1. A funnel was placed on top of the graduated cylinder to further increase the sampled surface area. Screenshots from the HD videos display this configuration during the release with respect to the ammonia cloud are provided in **Figure 68**. A larger collection reservoir was used, and the pH probe sample location was moved back to Node 3 for all TS 6A, 6B, and TS 7B replicates. For reference, the top of the collection reservoir could barely be distinguished at the bottom of the TS 6B and TS 7B screenshots provided in **Figure 37**.

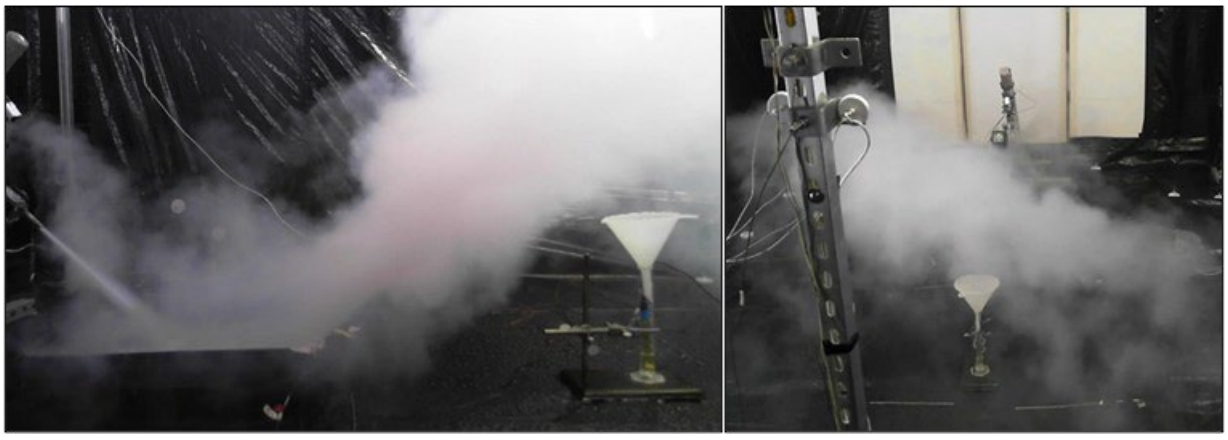

Figure 68. Ammonia vapor cloud and pH probe during rain, Cam 1 (left) and Cam 3 (right) for TS 7A.

The screenshots show why the TS 7A pH response was more immediate and sharper compared to TS 7B and TSs 6A/B. The combination of the funnel and sample location, with respect to the ammonia cloud, collected a larger surface area of rainwater that interacted with the ammonia cloud.

The pH of the collected rainfall solution did not change noticeably after the rain was complete, which could indicate that the collected solution was at equilibrium with the gaseous phase of ammonia in the chamber, and likely the collected rainfall was significantly less concentrated than the rain that had fallen closer to the device as demonstrated in TS 7A.

3.4.1 Simulated Rain After Ammonia Release (TS 6C and TS 7C)

For the TS 6C and TS 7C tests, the rain was initiated 17 minutes after the release. The mixing fans were turned on at t = 5.0 minutes to expedite evaporation from the liquid pool in the catch tray and to ensure a relatively steady state of ammonia gas concentration just prior to the rain. The fans were turned off before the rain system was activated at t = 17.0 minutes. The rain stopped at t = 22.0 minutes, and the mixing fans were turned on again. These timepoints can be considered in analyzing the average ammonia concentration observations, calculated as an average of all PIDs in the test environment. In addition, the rain pH was observed. These observations are plotted in the time series in **Figure 69**.

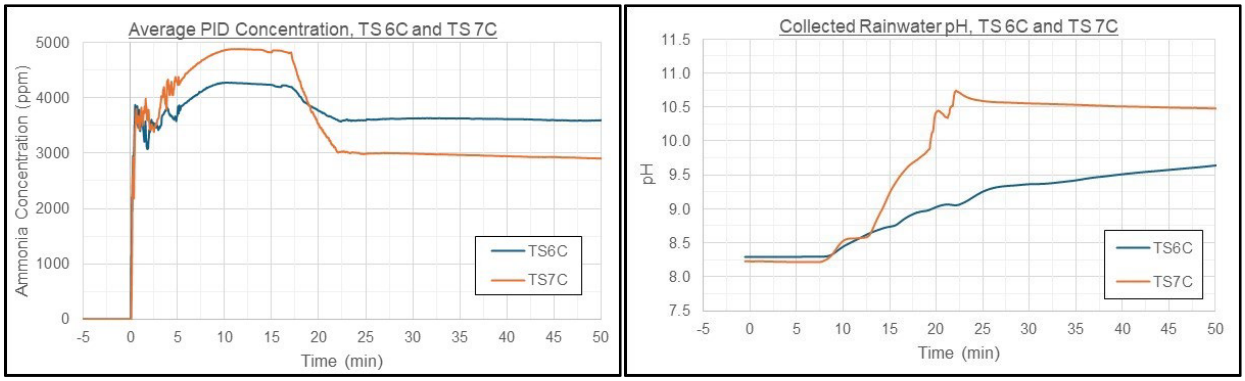

Figure 69. Time series of average PID concentration (left) and rainwater pH (right) for TS 6C and TS 7C, where rain fell between about minutes 17 and 22.

The concentration time series confirmed that a nearly steady state concentration was achieved between about 10 and 17 minutes. During the raining period, the concentrations monotonically decreased until they abruptly plateaued at 22 minutes when the rain was turned off. The light and heavy rain during TS 6C and TS 7C decreased the ammonia concentration by about 14% and 37%, respectively. TS 7C delivered approximately 4.5 times more rain but only scrubbed about 3x more ammonia gas than TS 6C.

After the rain was complete, the mixing fans were turned on, but the concentration time series did not indicate ammonia evolution from the rainwater pools that were previously observed during the A/B counterparts; this is still under evaluation.

3.5 Observations during TS 8, with Added (Excess) CO_2

The interactions of gas and liquid ammonia phases with added (excess) gas-phase CO_2 in the test environment were explored during TS 8. This TS was intended to simulate a CO_2 suppression system, which could possibly mitigate an indoor accidental release of anhydrous ammonia. The CO_2 introduction was designed to exploit three potential reactions of interest between ammonia and CO_2, two of which require water (gas or liquid). The products of these reactions were ammonium salts: ammonium carbonate, ammonium bicarbonate, and ammonium carbamate. The reaction equations are shown in **Equation 5** through **Equation 7:**

$$2\,NH_3 + H_2O + CO_2 \rightarrow [NH_4]_2CO_3 \quad (5)$$

Equation 5. Chemical Reaction for Ammonium Carbonate Product

$$NH_3 + H_2O + CO_2 \rightarrow [NH_4]HCO_3 \quad (6)$$

Equation 6. Chemical Reaction for Ammonium Bicarbonate Product

$$2\,NH_3 + CO_2 \rightarrow [NH_4][H_2NCO_2] \quad (7)$$

Equation 7. Chemical Reaction for Ammonium Carbamate Product

NOTE: CO_2 in this case, is a gas phase, while ammonia (NH_3) and water (H_2O) can be both a liquid and gas. The final resultant product of ammonium salts listed from **Equations 5**, **6**, and **7** is solid.

CO_2 is not expected to react with ammonia in the gas phase, but, in ammonia's aqueous phase, CO_2 can form an intermediate product – carbonic acid, which is a weak acid that can further react with ammonia to form ammonium carbonate and/or ammonium bicarbonate. If the test environment was extremely cold with low AH, the CO_2 could react directly with the liquid ammonia to form ammonium carbamate, which is solid.

The concentration of gas-phase ammonia and CO_2 were measured throughout the duration of the tests. The catch tray mass was measured continually until post-ventilation to ensure complete evaporation of the liquid pool, isolating the solid mass. The ammonia and CO_2 mass balance results for TS 8 are provided in **Table 10**.

Table 10. Experimental Results, Excess CO_2 Scenario (TS 8)

TS No. [a]	Excess CO_2						Ammonia Mass Balance		
	CO_2 Method	CO_2 Start (min)	CO_2 Stop (min)	CO_2 Mass (grams) Released	CO_2 Yield	Solid Present in Catch Tray?	Total Ammonia Released (grams)	Yield Before CO_2	Yield After CO_2
8A	After Release	10	12	864	98.7%	NO	177.4	92.7%	89.5%
8B	After Release	11	14	1,131	97.4%	NO	174.2	91.3%	87.4%
8C	Before Release	-4	-2	1,188	96.2%	YES	193.9	92.0% [b]	80.3%
8D	Before Release	-10	-5	1,265	95.8%	YES	184.7	92.0% [b]	79.3%

NOTE: [a]TS 8 replicates conditioned to 30 °C / 60% RH (±1 °C and ±1.5% RH). [b]Theoretical yield based on TSs 8A/B average.

The results and observations from TSs 8A/B indicated that, within the uncertainty ranges due to instruments and representativeness, there was no indication that a reaction occurred when the CO_2 was introduced after the release event and all liquid ammonia was evaporated (i.e., when there is no liquid ammonia present on surfaces). It was then decided to initiate the ammonia release event many minutes after the CO_2 was injected into the test environment. The resulting TSs 8C/D replicates were analyzed. One finding was that there had been a reaction within the liquid on the catch tray that formed a white solid as previously described in **Section 3.1.4**. The following sections detail the findings from the TS 8 replicates and the solid analysis.

3.5.1 CO_2 Gas Reaction with Gas-Phase Ammonia

A CO_2 gas reaction with ammonia gas was not observed in the HD videos and the analysis of observations during TSs 8A/B. There were no post-test indications of a solid formation in the catch tray, deposited on the floor, or aerosolized. The observed ammonia concentration time series is provided in **Appendix D**. Note that the deviation of ammonia concentration during the first 5 minutes is attributed to the CO_2 injection time. It may be that a small percentage of ammonia gas (less than 2%) leaked out of the test environment through the injection bulkhead seal due to the temporary pressure increase attributed to the additional CO_2 gas volume. The CO_2 and ammonia reaction was also considered using the CO_2 concentration measurements. The observed CO_2 concentration time series for TSs 8A/B are provided in **Figure 70**.

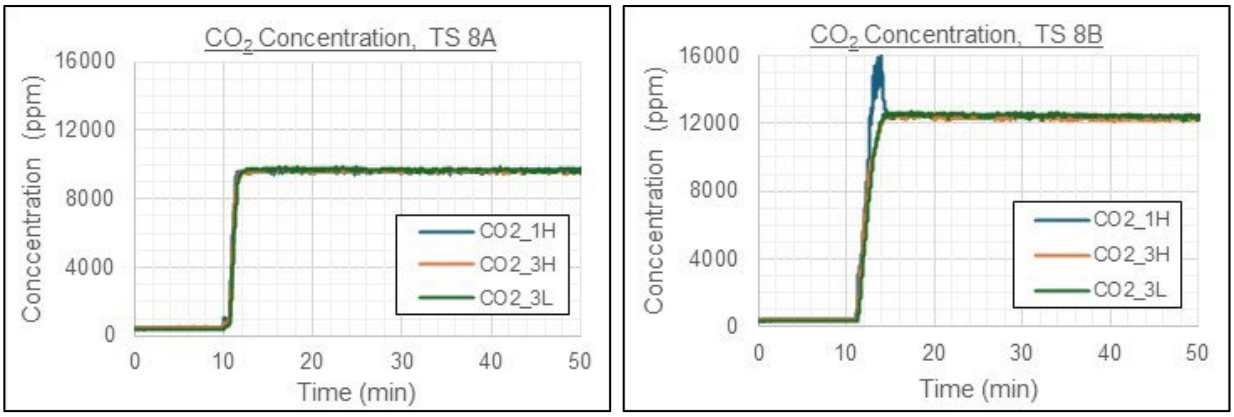

Figure 70. CO_2 concentration time series for TS 8A (left) and TS 8B (right).

The CO_2 concentration time series showed that the magnitude of the concentration remained constant after CO_2 injection into the chamber at time t = 10 minutes. The CO_2 yields revealed that roughly 98% of the CO_2 mass remained 30 minutes after the injection time. This difference (2%) in concentration drop was calculated to be associated with the consumption of 20 grams of CO_2, equivalent to 220 ppm. This magnitude of observed decrease in CO_2 concentration could not be distinguished with any certainty shortly after the CO_2 was injected because the CO_2 sensor resolution was 100 ppm. The signal noise at steady state CO_2 concentrations is attributed to the average concentration's standard deviation of ±160 ppm. The TSs 8A/B test results suggested that if a reaction occurred, the effect was small enough (ammonia yield reduced by 1.5% or less) that it could not be distinguished with visual observations or measurements.

It is assumed that ammonium carbamate was not generated because, at the time of the introduction of CO_2 gas, the test environment was not cold enough, and/or liquid anhydrous ammonia was not present. Also, ammonium carbonate and ammonium bicarbonate were not formed because the ammonia existed in the gas phase and aqueous ammonia was not present.

3.5.2 CO_2 Reaction with Liquid Phase Ammonia

Since there was no distinguishable reaction in the TSs 8A/B replicates, the order of ammonia release and CO_2 injection was reversed. The CO_2 gas was introduced into the chamber before the ammonia release to allow measurement of any reaction with liquid phase and gas-phase ammonia. During the two-phase jet release, of duration about 5 to 10 seconds, a white solid formed on the catch tray during both replicates. Additional wet solid was observed floating in the liquid pool and accumulated as the liquid evaporated as previously described in **Section 3.1.4**. It should be noted that the surface of the liquid ammonia pool was subcooled (about -50 or -60 °C). The observed catch tray mass time series from TSs 8C/D are provided in

Figure 71. The initial liquid pool mass could not be calculated due to the solid formation (the fraction of liquid and solid mass is not known).

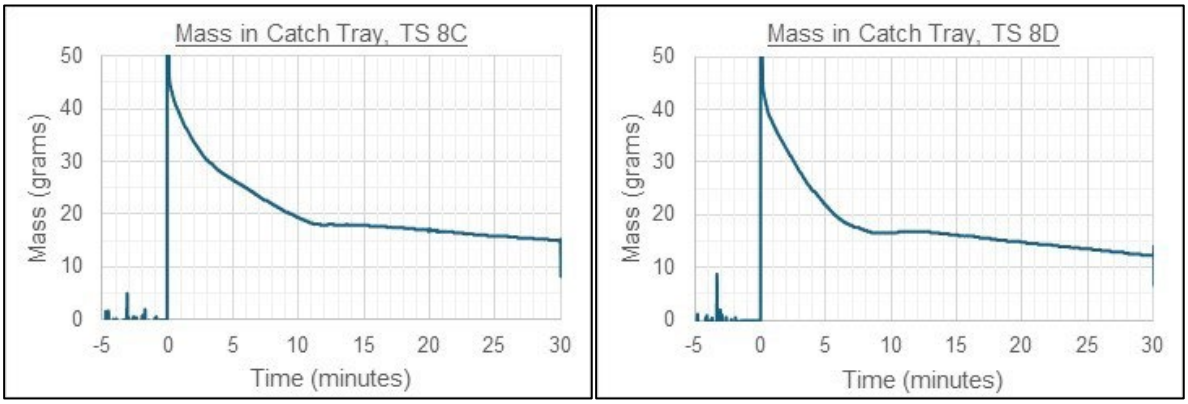

Figure 71. Time series of mass in catch tray for TS 8C (left) and TS 8D (right), when CO_2 was introduced just before the two-phase ammonia release.

The time series in **Figure 62** shows that much of the liquid pool evaporated within 10 minutes after t = 0, but a small fraction of liquid remained well after the tests were complete. This prevented solid mass quantification.

Since the CO_2 injection ended shortly before the ammonia release event, it was expected that the ammonia did not leak out of the test environment as it did during TSs 8A/B. The test engineers did not detect any ammonia odors during TSs 8C/D. The CO_2 concentration results for TSs 8C/D at three locations (1H or catch tray, 3L, 3H) are provided in **Appendix D**.

According to the CO_2 mass injected and yield during the homogenization time, roughly twice as much CO_2 mass reacted during TSs 8C/D compared to TSs 8A/B. The CO_2 concentration time series for TSs 8C/D are provided in **Figure 72**.

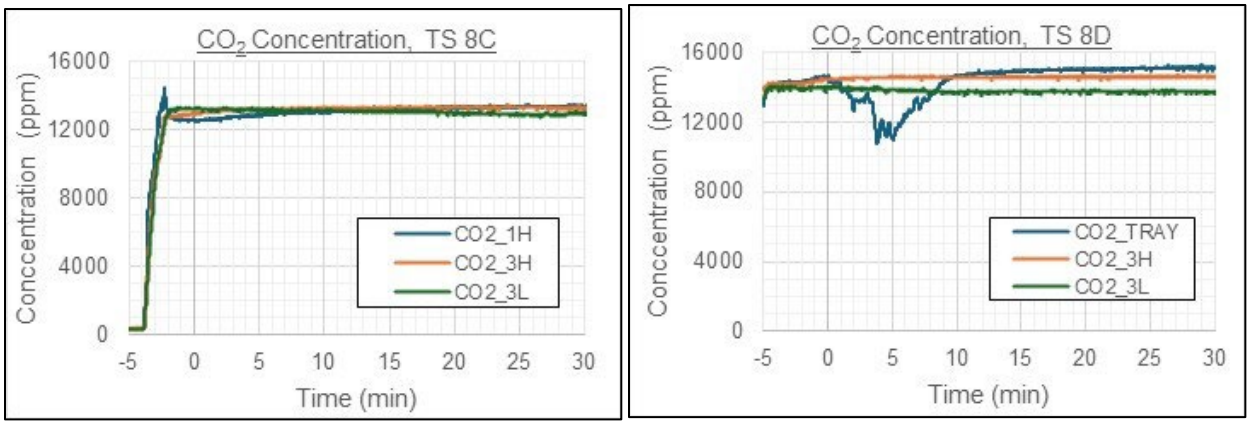

NOTE: TS 8D: CO2_TRAY is monitored at the catch tray location.

Figure 72. CO_2 concentration time series for TS 8C (left) and TS 8D (right) for 1H or tray, 3L, and 3H.

The TSs 8C/D test observations confirmed that a solid byproduct was formed during and after the release event. It was expected that the liquid-phase ammonia fraction interacted with condensed water vapor to form an aqueous ammonia solution. The CO_2 then reacted with the aqueous ammonia solution to form a carbonic acid intermediate product. The carbonic acid reacted with ammonia to produce ammonium carbonate and/or ammonium bicarbonate. Ammonium carbamate was not expected because of the warm and high AH conditions in the test environment.

3.5.3 Ammonium Salt Solid Analysis

The mass of the solid residue in the catch tray could not be quantified due to the presence of trace liquid remaining in the catch tray. Also based on previous observations from TS 3 in **Section 3.1.4**, there were concerns that the solid would sublime before a sample could be acquired. Therefore, the catch tray was removed from the test environment after ventilation was complete while there was still liquid present on the catch tray. Example photographs of the different solid forms observed at this time are provided in **Figure 73**.

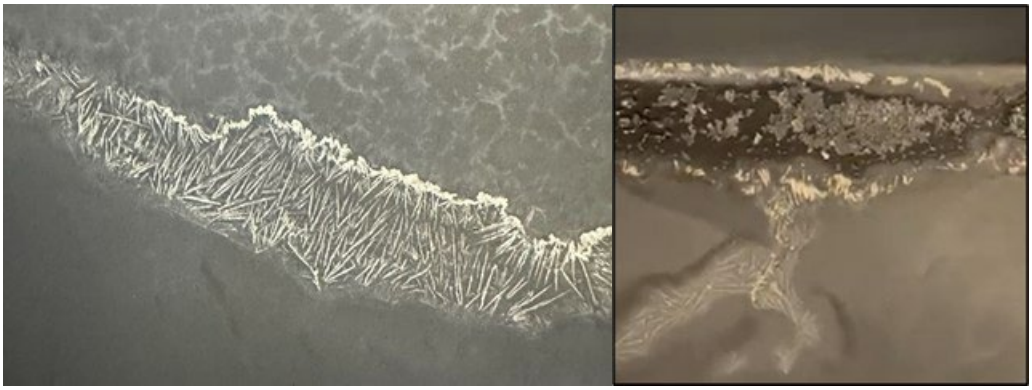

NOTE: Dry crystalline needle-like solid that initially formed at the liquid pool edges as it evaporated (left) and the larger wet solid chunks that formed within the liquid pool over time (right).

Figure 73. Solid formed in catch tray for TS 8C Post-Test.

The solid samples were submitted for compositional analysis. Details on the analysis methods, equipment, and procedures are provided in **Appendix G**. The initial analysis was conducted via FTIR spectroscopy, and the results are provided in **Figure 74**. The reference spectra for ammonium carbamate, ammonium carbonate, and ammonium bicarbonate are labelled A, B, C, respectively. The spectra for the TS 8C and TS 8D samples are labelled D and E, respectively.

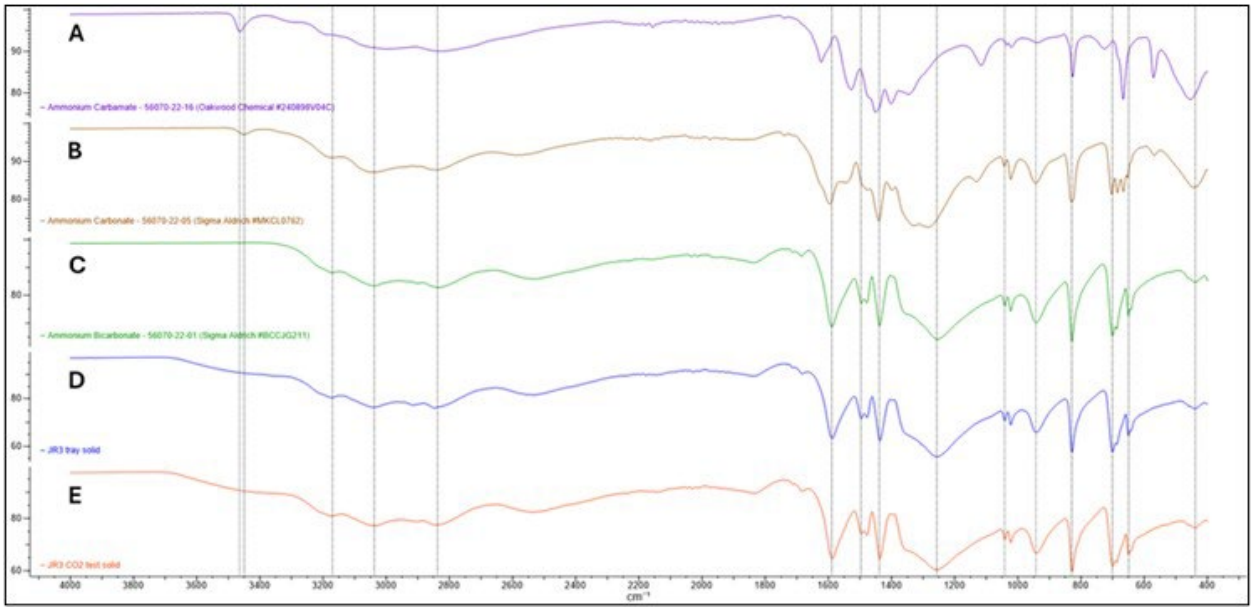

Figure 74. FTIR spectra of references and solid samples.

The FTIR results indicated that the measured spectra of both experimental samples (D and E) were equivalent to each other and overlaps with the spectra of the ammonium bicarbonate reference (C) in terms of the peak position, intensity, and shape. The spectra for the ammonium carbonate reference and

carbamate reference lacked distinct features that are not seen in the spectra for ammonium bicarbonate and the two experimental samples. The distinct spectral features were prominent peaks at ~3,450 cm^{-1}, ~1,600 cm^{-1}, ~1,400 cm^{-1}, ~1,100 cm^{-1}, 700 cm^{-1}, and ~570 cm^{-1}. The FTIR results suggested the two solid samples from TSs 8C/D could be ammonium bicarbonate.

After FTIR analysis, the solid samples were subjected to thermogravimetric analysis (TGA) and differential scanning calorimetry (DSC) analysis with the intent to quantify the purity. During the TGA analysis, all salts underwent decomposition with less than 0.2% of the starting material present at 193 °C. The results were established using the extrapolated onset temperature method. The results from the TGA analysis are shown in **Table 11**, and DSC endothermic time series is shown in **Figure 75**.

Table 11. TGA Analysis Results

Sample ID	Temperature (°C)
Ammonium Carbamate Reference	55
Ammonium Carbonate Reference	78
Ammonium Bicarbonate Reference	124
TS 8C Solid	83
TS 8D Solid	80

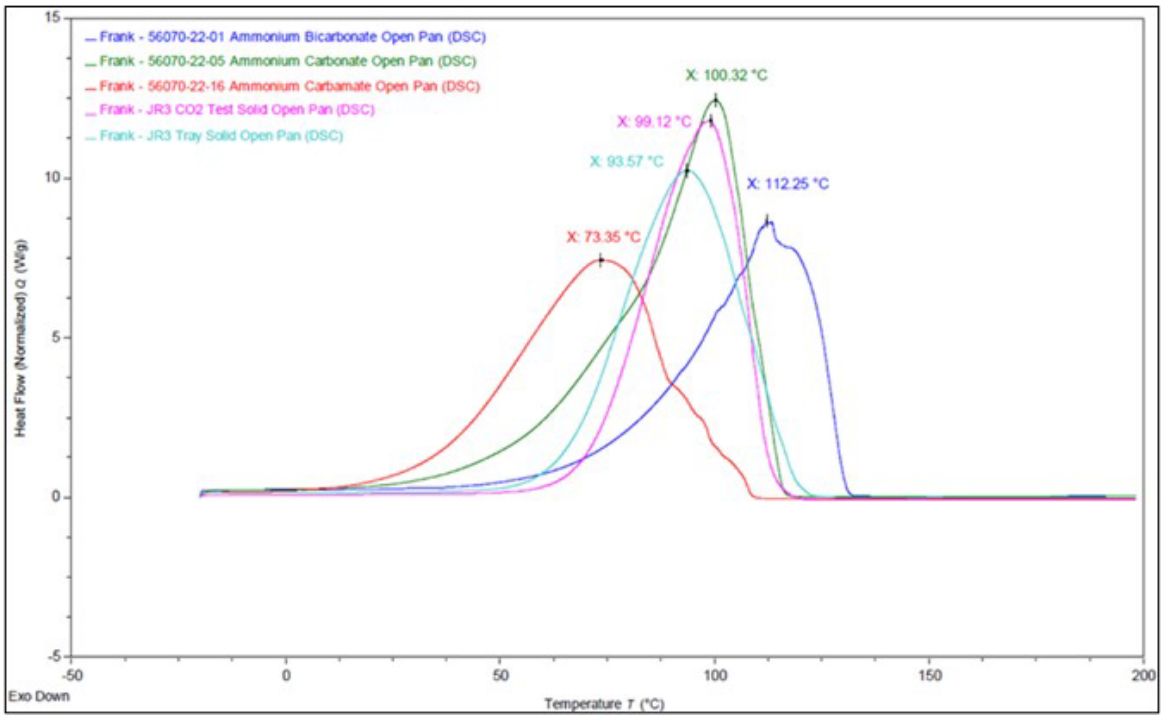

Figure 75. DSC results of references and solid samples.

The thermogram time series for the two experimental samples were similar, smooth, and continuous, however, the reference time series were slightly irregular. The DSC results indicated that the profile shape and maximum temperature for both experimental samples and ammonium carbonate were similar, which means that there is ammonium carbonate in the solid mixture that was not detected in the FTIR analysis.

3.6 Ammonia Mass Balance

The ammonia mass balance, or ammonia yield, was calculated as the ratio of 1) the ammonia gas in the Test Chamber measured by the PIDs during the homogenization time step (i.e., in the time range 20 minutes < t < 40 minutes) to 2) the mass of ammonia released. The ratio is multiplied by 100 to obtain the % yield. The approach was justified by the observation that the concentration averaged over the 18 PIDs showing minimal (plus or minus a few %) variation with time after about t = 20 minutes. By that time liquid evaporation was complete. The ammonia mass balance was calculated for every TS replicate and is provided in **Table 12**.

Table 12. Experimental Results, Mass Balance

TS No.	Ammonia Mass Balance		
	Total Ammonia Release (grams)	Homogenized averaged Ammonia Mass via PIDs during 20 min < t < 40 min (grams)	Ammonia Mass Yield
1A	189.2	189.9	100.4%
2A	187.1	200.1	106.9%
2B	189.8	201.8	106.3%
3A	174.2	174.4	100.1%
3B	163.7	163.3	99.8%
3C	168.1	166.8	99.2%
4A	182.8	167.6	91.7%
4B	178.0	165.0	92.7%
4C	172.5	161.4	93.6%
5A	180.1	162.3	90.1%
5B	181.9	161.3	88.7%
5C	187.5	167.2	89.2%
6A	194.1	115.7	59.6%
6B	202.7	119.0	58.7%
6C	158.6	125.3	79.0%
7A	193.3	92.4	47.8%
7B	180.7	88.0	48.7%
7C	182.7	101.9	55.8%
8A	177.4	158.8	89.5%
8B	174.2	152.3	87.4%
8C	193.9	155.7	80.3%
8D	184.7	146.5	79.3%
9A	186.0	184.4	99.1%
9B	187.1	186.2	99.5%
9C	150.2	148.5	98.9%
10A	193.4	183.2	94.7%
10B	151.1	142.4	94.2%
11A	169.8	143.7	84.6%
11B	181.6	152.1	83.8%
11C	177.2	148.9	84.0%

Except for TS 6, TS 7, and TS 8, the mass balance results correlate with temperature, AH, and air density to the ammonia yield. However, the primary variable driving the correlation is temperature, which determines the pressure in the lecture bottle (storage container for the pressurized liquefied ammonia), and hence determines the flashing intensity and the two-phase release rate. Further characterization of these ammonia mass balance was much more complicated. These test scenarios were designed to observe the unobstructed, natural progression of the ammonia release and ammonia plume under typical environmental conditions. There was no single variable or measurement that could easily explain ammonia yields less than 100%. A series of evidence was brought to light during the Phase II progression to describe how this could be possible. It is important to note that there are several contributions to uncertainties in the estimates of mass yield in **Table 12**. TS 1, TS 2, and TS 5 were noticeable outliers in the mass balance trends due to the falsely high ammonia concentration readings under RH conditions near the condensation point. Thus, we estimate a ± 6% uncertainty in each mass yield number. Moreover, solid residue formed in the catch tray as the liquid pool evaporated during the extreme cold and dry conditions in TS 3. Additional solid residue was observed under the catch tray and on the floor around the catch tray after numerous tests at average conditions that mimicked ammonium salts.

The simulated rain TSs (TS 6 and TS 7) demonstrated lower ammonia yields that were attributed to absorption of ammonia by the rain, exploiting the hydrophilic properties of ammonia. The rain drops readily scrubbed the ammonia. The mass transfer efficiency was dependent on the ammonia phases, rain drop size, rainfall rates, rain duration, and cloud density (but there were insufficient observations to isolate these dependencies).

The simulated rain and excess CO_2 (TS 8) results were somewhat uncertain due to issues regarding some of the variables. For example, part of the reduced ammonia yield during the excess CO_2 TS (TS 8) could be attributed to the excess atmospheric CO_2 concentration. The liquid phases of ammonia likely interacted with water vapor to form aqueous ammonia solutions. The excess CO_2 reacted with the aqueous solution to form the intermediate product carbonic acid. The carbonic acid reacted with ammonia to generate a solid ammonium salt, which was analyzed to be a mixture of ammonium carbonate and ammonium bicarbonate, but not ammonium carbamate.

4.0 SUMMARY AND CONCLUSIONS

In this study, environmental variables such as temperature, humidity, rainfall, and excess CO_2 were explored following the experimental test matrix provided in **Table ES-1**. The test environment was pre-conditioned to the TS temperature and RH setpoints, and the pressurized liquefied anhydrous ammonia, stored in a lecture bottle at its vapor pressure, was equilibrated to the test environment temperature before release. The anhydrous ammonia lecture bottle was positioned upside down at a 45° angle. The 5- to 10-second release, a 45-degree downward two-phase jet, impacted a catch tray on a scale to capture and quantify the liquid pooling dynamics. A suite of 18 PIDs, 12 TCs, 6 RH probes, and 2 PTs located throughout the test environment measured the space and time variable temperature and ammonia gas concentrations. Test videos were recorded with HD and FLIR cameras. The test environment was held static (i.e., still, with no mean wind flow or turbulence) for 30 minutes after the release to allow for complete evaporation of liquid ammonia in the catch tray and on other surfaces. Next, ammonia gas homogenization was induced with mixing fans for 10 minutes. Then, the test was considered complete after the 10-minute mixing period, at which time the test environment was scrubbed with the chamber ventilation system.

Although the test environment temperature and RH were held static, and there were no fans or other devices causing a significant flow and turbulence, during and for a few minutes after the two-phase jet release, a strong momentum jet reflected off the catch tray, headed toward the back ceiling, and subsequently caused eddies to move around the chamber. These eddies could be "seen" in the videos as wisps of white cloud moving around the chamber, with speeds of a few tens of cm/s and dimensions roughly equal to the chamber width. These eddies slowly decreased in magnitude over the 5 to 10 minutes after release. The simulated rain and excess CO_2 TSs in Phase II followed a similar approach. Tests were carried out for conditions when 1) the rain or CO_2 was introduced into the test environment just before the 5- to 10-second release event (two-phase momentum jet); and 2) rain or CO_2 was introduced into the test environment about 10 minutes after the release. **Table 13** summarizes the Phase II experiments for the standard approach TSs, including the test environment conditions, and some specific measurements. The experiments for the simulated rain and excess CO_2 TSs are provided in **Table 14** and **Table 15**.

Table 13. Summary of Experimental Conditions and Selected Results, Standard Approach TSs

TS No.	Test Environment Initial Conditions				Initial Pressure in lecture bottle (psia)	Liquid Fraction [a]	Derived Ammonia Mass Balance
	Temp (°C)	RH (%)	AH (g H_2O per m^3 air)	Average Air Density of mixture of dry air, water vapor, and ammonia (kg/m^3)			
1A	5.3	85.5	5.9	1.245	76	40.8%	100.4%
2A	15.5	89.8	11.9	1.196	110	29.3%	106.9% [b]
2B	15.6	89.1	11.8	1.208	109	29.7%	106.3% [b]
3A	-17.0	25.5	0.4	1.339	41	56.3%	100.1%
3B	-15.2	29.9	0.5	1.330	38	58.4%	99.8%
3C	-18.1	11.5	0.1	1.358	37	59.8%	99.2%
4A	41.0	11.1	6.0	1.102	233	14.1%	91.7%
4B	40.5	10.9	5.7	1.100	237	13.5%	92.7%
4C	40.2	11.2	5.8	1.103	233	14.4%	93.6%
5A	33.8	89.4	33.2	1.116	191	11.2%	90.1%
5B	33.2	89.8	32.4	1.120	190	11.4%	88.7%
5C	33.7	89.8	33.2	1.110	190	11.9%	89.2%
9A	9.4	61.2	5.5	1.232	87	37.0%	99.1%
9B	9.4	60.4	5.5	1.239	91	36.8%	99.5%
9C	10.3	59.8	5.7	1.222	96	35.2%	98.9%
10A	21.9	61.2	11.8	1.193	133	29.9%	94.7%
10B	22.5	60.7	12.1	1.183	137	26.4%	94.2%
11A	34.6	59.6	23.1	1.110	200	11.8%	84.6%
11B	35.6	60.3	24.6	1.117	207	12.2%	83.8%
11C	35.2	61.2	24.5	1.124	202	11.8%	84.0%

NOTE: [a]The liquid fraction of the ammonia release was calculated from experimental measurements. It is expressed as a percentage of the liquid ammonia mass captured in the catch tray, weighted against the total ammonia mass released from the lecture bottle. This value is a direct measurement of the liquid mass on the catch tray using a scale. [b]High mass balance is attributed to the uncertainties in the PID concentration measurements at higher relative humidity.

Table 14. Summary of Experimental Results, Simulated Rain Scenarios (TS 6 and TS 7)

TS No.	22 °C / 50% RH (±1 °C and ±1.5% RH)						
	Simulated Rain					Ammonia Mass Balance	
	Rain Introduced	Rain Start (min)	Rain Stop (min)	Total Rain Volume (L)	Rain Pool pH	Total Ammonia Released (grams)	Yield After Rain
6A	During Release	-0.5	5.0	5.5	10.3	194.1	59.6%
6B	During Release	-0.5	5.0	5.5	10.0	202.7	58.7%
6C	After Release	17.0	22.0	4.8	9.1	158.6	79.0% [b]
7A	During Release	-0.5	3.5	17.1	11.0 [a]	193.3	47.8%
7B	During Release	-0.5	3.5	17.1	10.1	180.7	48.7%
7C	After Release	17.0	22.0	21.4	10.5	182.7	55.8% [b]

NOTE: [a]TS 7A: Unique pH placement closer release and with smaller rain collection beaker and funnel. [b]Ammonia mass balance yield without the rain is 92.5% and 92.6% for TS 6C and TS 7C, respectively.

Table 15. Summary of Experimental Results, Excess CO_2 Scenario (TS 8) [a]

30 °C / 60% RH (±1 °C and ±1.5% RH)									
TS No.	Excess CO_2						Ammonia Mass Balance		
	CO_2 Introduced	CO_2 Start (min)	CO_2 Stop (min)	Total CO_2 Mass (grams)	CO_2 Yield	Solid Present?	Total Ammonia Released (grams)	Yield Before CO_2	Yield After CO_2
8A	After Release	10	12	864	98.7%	NO	177.4	92.7%	89.5%
8B	After Release	11	14	1,131	97.4%	NO	174.2	91.3%	87.4%
8C	Before Release	-4	-2	1,188	96.2%	YES	193.9	92.0% [b]	80.3%
8D	Before Release	-10	-5	1,265	95.8%	YES	184.7		79.3%

NOTE: [a] CO_2 was introduced both after and prior to the ammonia release at time zero. The mass of CO_2 released, along with the corresponding mass yield contributing to the reaction, was calculated and compared to environmental conditions without CO_2 to determine its effects on ammonia release. [b] Data was not collected; the value is the TS 8A/B Yield Before CO_2 average.

Since the pressurized liquefied anhydrous ammonia (~0.375 lb. [170 grams]) lecture bottle temperature was equilibrated with the pre-conditioned test environment temperature before the release, the lecture bottle release pressure was directly related to the temperature. The associated vapor pressure was measured for each trial and is aligned with the saturation vapor pressure at the prescribed temperature. Thus, the pressure was higher at the high temperature (40 °C) than at the low temperature (-15 °C). The release event was initiated inside the static test environment, and the duration time of the two-phase jet ranged from 5 seconds (at 41 °C) to 12 seconds (at 18 °C). As seen in the IR videos and verified by the temperature sensors near the catch tray, the release stream consistently reached subcooled temperatures below -60 °C. This measurement was critical to understanding the larger liquid fraction and the ammonia that remained as liquid on the catch tray.

This was supported by the measurements made of liquid ammonia fraction. It was directly measured by recording the mass of the liquid pool within the catch tray over time. The liquid pool consisted of ammonia and water vapor condensate, which could eventually be differentiated by the evaporation curve (i.e., the liquid remaining after 2 or 30 minutes must be water). However, there are many sources of uncertainty, such as the aerosol that reflected off the catch tray during the momentum jet period and the liquid that spilled onto the floor. The experimental results confirmed a direct, linear relationship between liquid-phase ammonia fraction and temperature from -18 °C to 41 °C which is discussed in **Section 3.2.1** (**Figure 57**). This will be further evaluated; nonetheless, it is important to state that the dependence on temperature is mainly due to the fact that the ammonia lecture bottle pressure increases with temperature.

- When the mass released from the source is compared to the mass observed within the chamber, the mass-balance yield indicates a degree of ammonia loss depending on the environmental conditions. Even with the consideration of the uncertainty in the measurements, the greater than 10% loss in mass yield is repeatedly observed under hot and humid conditions (TS 5 & TS 11) and during rain (TS 6 & TS 7), and during excess CO_2 conditions (TSs 8 C/D). Hot/Humid conditions are directly associated with the highest AH (24–33 kg/m^3).

- TS 5/TS 11 – HD camera video recordings showed the most prominent visible plume filling the chamber. The modeling studies underway to reveal real-time plume visualization/concentration in each ammonia sensor location using the data collected.
- TS 6/TS 7 – The rain scenario demonstrated the highest removal of ammonia; more ammonia was absorbed into the rainwater when the rain was active during the two-phase release event (i.e. strong momentum jet, which lasted for about 10 seconds) compared to raining during the gas phase only.
- TS 8 C/D – A reaction was observed within the ammonia two-phase jet when the excess CO_2 formed the carbonic acid, which proceeded to react with ammonia, which formed white solid within the catch tray and liquid pool. The solid residue accumulated within the liquid pool as larger chunks, which significantly prolonged the liquid evaporation. The TS 8 white solid did not readily sublime at room temperatures, and the pH was 7–8. The composition of the solid was analyzed via FTIR, TGA, and DSC. The analysis suggested that the TS 8 solid was a mixture of ammonium carbonate and/or ammonium bicarbonate. The analysis results confirmed that the TS 8 solid was not ammonium carbamate. It should be noted that the excess CO_2 tested did not react with gaseous ammonia when it was released after ammonia was released (TSs 8 A/B). This is a notable finding, highlighting the need for a quantitative stoichiometric ratio of water, ammonia, and CO_2 to establish conditions where the formation of carbonic acid is optimal, requiring further research.

From this study, the following conclusions were drawn based primarily on the experimental measurements and these conclusions will aid in advancing modeling algorithms for consequence assessments and developing mitigation strategies to reduce hazards:

- Temperature Dependency: the primary factor influencing temperature dependence is the pressure behind the two-phase jet release. At lower environmental temperatures, the reduced headspace vapor pressure results in a narrower, more constricted flow and a larger rainout (accumulation of liquid) in the catch tray. Measuring the temperature of the liquid pool tray clearly indicates that the ammonia remains in liquid form due to the subcooled temperatures under atmospheric pressure. However, an area of uncertainty is the diameter of the liquid aerosol within the two-phase jet. Moreover, the data from these temperature-controlled experiments align with findings from ammonia field trials [15], which measured the rainout of the two-phase jet. That is a higher liquid fraction under refrigerated conditions, which is also reflected by the cold environmental conditions in this study. The best approximation, calculated by Britter et al. (2011) [13] suggests a mass median diameter of 50 microns for superheated ammonia when pressurized ammonia is released to ambient pressure. Further research and data analysis are underway in collaboration with the JR III Modelers Working Group.
- Humidity Dependency: Humidity largely influences the process through the condensation of ambient water vapor, which contributes to liquid-phase reactions. The visible white cloud was prominently observed under high-humidity conditions, suggesting that the white plume reflecting off the catch tray consists of liquid ammonia and ammonium at the source, while the drifting

white plume seen under high-humidity conditions is likely due to condensed ambient water vapor near the source. However, the visible white cloud filling the chamber showed ammonium content. Therefore, ammonia concentration measurements are being further modeled for 3D visualization to better understand ammonia hazards at the source and how it diffuses within the chamber under various environmental conditions. Although real-time data was collected during the ammonia release, the uncertainty of data requires further analysis, which is not included in this report. The dataset from the 18 PIDs will be evaluated using computational modeling tools. This modeling effort in complementing with the video footage will contribute to characterizing and simulating the movement of a two-phase jet by combining video recordings of controlled releases under various environmental conditions with ammonia concentration observations to contour the cloud and track its progression within the chamber. It should be noted that the observations are very specific for the unique orientation, with the jet directed 45 degrees downwards towards the middle of the catch tray. Also, the amount of captured liquid ammonia depends on the geometry of the catch tray lip.

- Rain Dependency: The effects of heavy and light rain on the ammonia plume were most prominent among all environmental factors examined in this study. Controlled rain, applied from a 9.5-foot (2.9 m) ceiling in the chamber over the two-phase jet release source, demonstrated notable impacts. Although coagulation efficiency was not calculated from this study, the decrease in mass balance yield indicates the effectiveness of rain in removing ammonia, resulting in a reduced ammonia concentration in the mid-field (8 feet (2.4 m) from the source). Further analysis of chemical reactions in rainfall, including real-time pH measurements from the collected liquid pool is underway to understand the influence of pH and temperature during rainfall, using aqueous ammonia equilibrium calculations [16].
- CO_2 Dependency: Although ammonia does not directly react with carbon dioxide, there is a condition where excess CO_2 in a high-humidity environment could drive a reaction with ammonia in a confined space. For this reaction to occur, carbonic acid must first be formed by dissolving CO_2 in water. Carbonic acid then reacts to ammonia. The by-products of this reaction will be further evaluated to understand the environmental conditions driving the reaction kinetics to form solid ammonium salts.

This page intentionally left blank.

5.0 REFERENCES

1. Rowley et al. 2024. *Technical Report for Jack Rabbit III Support, Phase I: Small Scale Cloud Dispersion Studies*. Internal report to Defence Threat Reduction Agency.

2. Olson, R.; Youle, P.V. The Strength of Carbonic Acid. The Rate of Reaction of Carbon Dioxide with Water and Hydroxyl Ion *J. Am. Chem. Soc.* **1940,** *62* (5), 999–1310.

3. Fox, S.; Storwold, D. *Project Jack Rabbit: Field Tests* CSAC-11-005; U.S. Department of Homeland Security, Science and Technology Directorate, Chemical Analysis Security Center, Aberdeen Proving Ground, MD, 2011 (cleared for public release 2018). https://www.dhs.gov/sites/default/files/publications/csac-11-006_r1_project_jack_rabbit_field_tests_pr-508c.pdf

4. Nicholson, D. et al. Final Test Report for Jack Rabbit (JR) II West Desert Test Center U.S. Army Dugway Proving Ground, UT, 2017. https://www.dhs.gov/sites/default/files/publications/CSAC_Jack%20Rabbit%20II%20Final%20Report.pdf

5. Fox, S. et al. Overview of Jack Rabbit II (JR II) field experiments and summary of the methods used in the dispersion model comparisons. *Atmos. Environ.* **2021,** *269,* JR II Model Comparison Special Issue.

6. Preparing our Ports for the Future of Alternative Maritime Fuels. https://www.dhs.gov/science-and-technology/news/2024/11/14/feature-article-preparing-our-ports-future-alternative-maritime-fuels

7. Hanna, S. et al. Gaps in toxic industrial chemical model systems: Improvements and changes over past 10 years. *Process Saf. Prog.* **2022,** *41* (1), 151–166.

8. Chemical Security Seminars 2021. Agenda. Cybersecurity & Infrastructure Security Agency. https://www.cisa.gov/sites/default/files/publications/css-agenda-20211208-detail-508.pdf. (accessed February 24, 2025)

9. TECFT 2025 Dugway, Technology Experimentation & Characterization Field Trials. https://www.atec.army.mil/dpg/TECFT/index.html (accessed February 24, 2025)

10. Languirand, E.R. et al. Evaporation of anhydrous ammonia from small concrete coupons and implications regarding evaporation from a large accidental spill on concrete. *Process Saf. Prog.* **2023,** *43* (2), 364–373.

11. The EngineeringToolBox. Ammonia - Vapour Pressure at Gas-Liquid Equilibrium. Available at www.engineeringtoolbox.com/ammonia-pressure-temperature-d_361.html. (accessed July 2024).

12. American Meteorological Society (AMS). “Rain”. Glossary of Meteorology, Available at: https://glossarytest.ametsoc.net/wiki/Rain. (accessed August 2024).

13. Britter, R. et al. Toxic industrial chemical (TIC) source emissions modeling for pressurized liquefied gases. *Atmos. Environ.* **2011,** *45* (1), 1–25.

14. Huang, Ju-Chang, and Chii Shang. “Air Stripping.” Scientific Figure on ResearchGate. Available at https://www.researchgate.net/figure/Effects-of-pH-and-temperature-on-the-distribution-of-ammonia-and-ammonium-ion-in-water_fig3_227135665. (accessed October 2024).

15. Dharamavaram, S. et al. Red Squirrel Tests: Air Products' ammonia field experiments. *Process Saf. Prog.* **2023,** *42* (3) 481–498.

https://www.researchgate.net/publication/369953221_Red_Squirrel_Tests_Air_Products'_ammonia_field_experiments

16. Emerson, K. et al. Aqueous Ammonia Equilibrium Calculations: Effect of pH and Temperature. *J. Fish. Res. Board Can.* **1975,** *32* (12), 2379–2383.

17. Czernia, Dominik, and Bogna Szyk. Air Density Calculator. Omni Calculator. Available at www.omnicalculator.com/physics/air-density. (accessed March 2024).

APPENDIX A: PID CALIBRATION

This page intentionally left blank.

A summary of the calibration results for all PIDs at 100 ppm and 1,000 ppm calibration gas concentrations is provided in **Table A-1** and the results for 10,000 ppm and 20,000 ppm calibration gas concentration is provided in **Table A-2**.

Table A-1. Summary of Calibration Results: 100 PPM and 1,000 PPM

PID No.	100 PPM Calibration					1,000 PPM Calibration				
	Cycle 1	Cycle 2	Cycle 3	Average	StDev	Cycle 1	Cycle 2	Cycle 3	Average	StDev
PID_1H	113	105	112	110	4	1,007	996	981	995	13
PID_1L	106	103	116	108	7	1,005	998	981	995	12
PID_2H	96	95	105	98	5	993	1,002	994	996	5
PID_2L	125	118	125	123	4	999	986	963	983	19
PID_3H	107	116	129	117	11	997	1,002	982	994	11
PID_3L	66	62	74	67	6	1,016	1,019	1,005	1,013	7
PID_4H	123	123	133	126	6	993	998	984	992	7
PID_4L	113	105	115	111	5	996	993	977	989	10
PID_5H	93	88	99	93	5	1,006	1,000	983	997	12
PID_5L	110	131	112	118	12	1,009	980	991	993	15
PID_6H	107	106	113	109	4	1,010	996	979	995	15
PID_6L	92	87	97	92	5	999	1,002	989	997	7
PID_7H	71	120	80	90	26	1,044	975	1,039	1,019	38
PID_7L	94	91	102	96	5	995	998	981	991	9
PID_8H	117	114	125	119	6	1,000	1,001	988	996	7
PID_8L	106	99	107	104	4	1,016	998	973	996	22
PID_9H	94	86	92	91	4	1,000	1,002	988	997	7
PID_9L	114	109	120	114	5	1,008	1,005	980	997	16

Table A-2. Summary of Calibration Results: 10,000 PPM and 20,000 PPM

PID No.	10,000 PPM Calibration					20,000 PPM Calibration				
	Cycle 1	Cycle 2	Cycle 3	Average	StDev	Cycle 1	Cycle 2	Cycle 3	Average	StDev
PID_1H	10,238	10,098	9,978	10,105	130	20,066	19,965	19,998	20,010	52
PID_1L	10,269	10,116	9,983	10,122	143	20,109	19,986	19,932	20,009	91
PID_2H	10,205	10,123	10,038	10,122	83	20,051	19,967	20,011	20,010	42
PID_2L	10,192	10,053	9,896	10,047	148	20,147	19,923	19,858	19,976	152
PID_3H	10,168	10,137	10,043	10,116	65	19,963	20,009	20,053	20,008	45
PID_3L	10,369	10,278	10,130	10,259	121	20,163	20,008	20,012	20,061	88
PID_4H	10,152	10,124	10,072	10,116	41	20,003	19,987	20,039	20,010	26
PID_4L	10,182	10,000	9,889	10,024	148	20,052	19,986	19,996	20,011	36
PID_5H	10,206	10,097	9,972	10,092	117	20,024	19,974	20,030	20,010	31
PID_5L	10,240	10,086	10,037	10,121	106	20,062	20,106	19,862	20,010	130
PID_6H	10,239	10,104	9,968	10,104	135	20,140	19,969	19,918	20,009	117
PID_6L	10,082	9,981	9,927	9,997	78	19,906	19,809	19,828	19,848	51
PID_7H	10,165	10,012	9,919	10,032	124	19,440	19,378	19,144	19,320	156
PID_7L	10,158	10,032	9,936	10,042	111	20,020	19,971	20,038	20,010	35
PID_8H	10,324	10,159	10,053	10,178	137	20,138	20,003	20,018	20,053	74
PID_8L	10,283	10,079	9,960	10,108	163	20,119	19,989	19,925	20,011	98
PID_9H	10,228	10,075	10,029	10,111	104	20,070	19,968	19,992	20,010	53
PID_9L	10,198	10,178	10,018	10,131	99	20,326	20,043	19,977	20,115	185

This page intentionally left blank.

APPENDIX B: TEST CHECKLIST

This page intentionally left blank.

Jack Rabbit 3 Phase I Test Checklist Test#:_____ Temperature and RH:___°C and ____%

Checkmark (✓)	Task
	Turn On Electronic Equipment: o NI DAQ o FLIR o Cameras o Lights
	Ensure Fans and Exhaust blower are functioning properly, and spot check the ceiling blast gates to ensure they are closed.
	Ensure Sensors are reading correctly: o PIDs o RH o EC o TC o PT o Scale
	Verify the scale is functioning properly and record readings. 2kg: _____ 2.5kg:_____ 3kg:_____
	Ensure the cameras are orientated for the correct shot. o Align Cameras o Focus Cameras o Deselect auto focus
	Condition Chamber to Specified Temp and RH o Temp:_____ o RH:_____
	Weigh the LB with the plug and Teflon gasket assembly attached to the LB. Pre-Test Weigh t:_____(g) LB#:_____
	Inspect manifold and ensure the safety valve is locked out and the relief valve is closed. o Safety Valve o Relief Valve
	Install the Lecture bottle in the stand: o Ensure the regulator valve is closed. o Attach thermocouple to LB body
	Connect the release manifold to the Lecture bottle. Verify the following: o New PFTE gasket is used for CGA adapter. o Manifold Exhaust TC is in line with the exhaust stream. o Position catch tray and respective TC with respect to the exhaust stream
	Allow LB and Chamber to reach the desired temperature and RH. o LB Temp:_____ o Chamber Temp:_____ o Chamber RH:_____
	Close the blast gates on the chamber to seal for testing.

Work Performed by:_____Date:_____

Figure B-1. Test checklist template, page 1.

Jack Rabbit 3 Phase I Test Checklist Test#:_____ Temperature and RH:___°C and ____%

	○ East and West wall Blast gate ○ North wall blast gate ○ Manual and Automatic PCU inlet and outlet Blast gate
	Confirm RSO's approval, turn on warning lights, and announce Test over HERLA intercom. RSO on Call:_____ ○ Amber Lights ○ Red Lights ○ Announce test
	Hit record on the DAQ, FLIR, and Cameras and record time for DAQ start. ○ DAQ Time:_____ ○ FLIR Time:_____ ○ Cameras Time: _____
	Enter Chamber and open regulator valve on lecture bottle
	Exit test Chamber, seal test wall door and GFR door
	Allow LB and manifold to equilibrate
	Turn off Mixing Fans
	Ensure all things are recording and all steps above are checked off. ○ DAQ ○ HD Cameras ○ FLIR
	Arm release switch with key and ensure light is on
	Flip switch to trigger the relief valve and allow the entire contents of the LB to empty. Record t=0: t=0:_____
	Wait 30 seconds after the LB is emptied completely
	Turn on mixing fans to generate a homogenized mixture in the chamber after 15 minutes
	Allow the homogenized mixture to read on the sensors for 15 minutes
	Open the automatic blast gates on the chamber ceiling (North/East/West).
	Turn on the exhaust blower and allow the chamber to scrub for 1 hour or until the concentration has reached a safe level
	Don proper PPE to enter the chamber
	Wave personal detector in the anteroom to ensure it is safe to enter
	Wave personal detector in test room to ensure it is safe to enter
	Once it is safe to enter the test room, close the regulator valve before removing the LB from manifold from the stand
	Reattach Washer and plug and weigh the LB. Post test Weight:_____(g)
	Inspect chamber for visual observations and record in notes section below: (pooling, condensation, anomalies, etc.) Make note if it can be seen on the camera as well.
	Clean up the chamber if necessary, following the cleanup procedure.
	Stop recording on the DAQ and Save the excel file to the proper location

Additional Notes / Changes in Procedure:

Work Performed by:_____ Date:_____

Figure B-2. Test checklist template, page 2.

APPENDIX C: AIR DENSITY CALCULATION

This page intentionally left blank.

Water Vapor Pressure:

$$P_{vapor}[Pa] = \left(6.1078 * \left[10^{\frac{7.5*T(^{\circ}C)}{T(^{\circ}C)+237.3}}\right]\right) * RH \quad \text{(C-1)}$$

[17]

Dry Air Pressure:

$$P_{dry}[Pa] = \left(PT_{Chamber}[psi] * 6894.76\left[\frac{Pa}{psi}\right]\right) - P_{vapor}[Pa] \quad \text{(C-2)}$$

[17]

Ammonia Vapor Pressure:

$$P_{NH3}[Pa] = \left(\frac{C_{NH3}[ppm]}{0.08206\left[\frac{L \cdot atm}{mol \cdot K}\right] * T_{air}[K] * 1000\left[\frac{mg}{g}\right]}\right) * \left(8.314\left[\frac{m^3 \cdot Pa}{K \cdot mol}\right] * T_{air}[K]\right) \quad \text{(C-3)}$$

Air Density:

$$\rho_{air}\left[\frac{kg}{m^3}\right] = \left(\frac{P_{vapor}[Pa]}{461.495\left[\frac{J}{kg * K}\right] * T[K]}\right) + \left(\frac{P_{dry}[Pa]}{287.058\left[\frac{J}{kg * K}\right] * T[K]}\right) + \left(\frac{P_{NH3}[Pa]}{488.21\left[\frac{J}{kg * K}\right] * T[K]}\right) + \quad \text{(C-4)}$$

[17]

This page intentionally left blank.

APPENDIX D: PID CONCENTRATION PLOTS

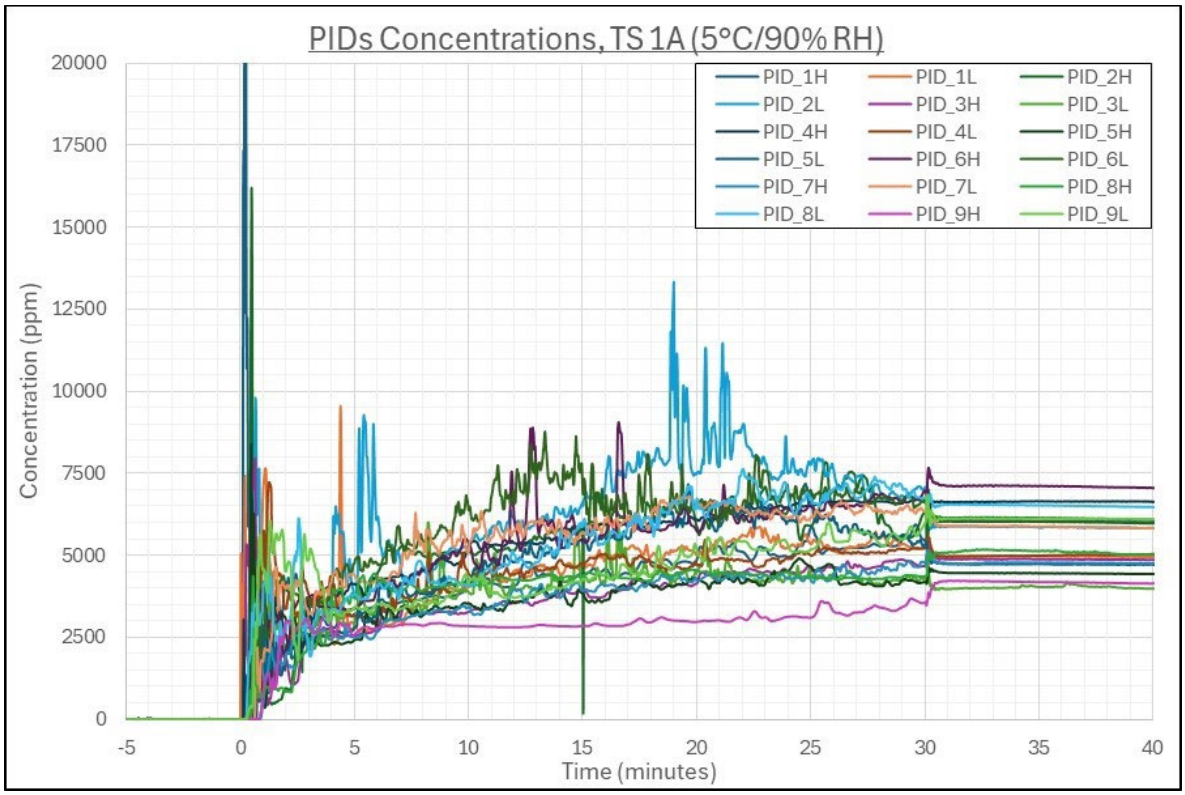

Figure D-1. Overlay of individual PID concentration time series, TS 1A.

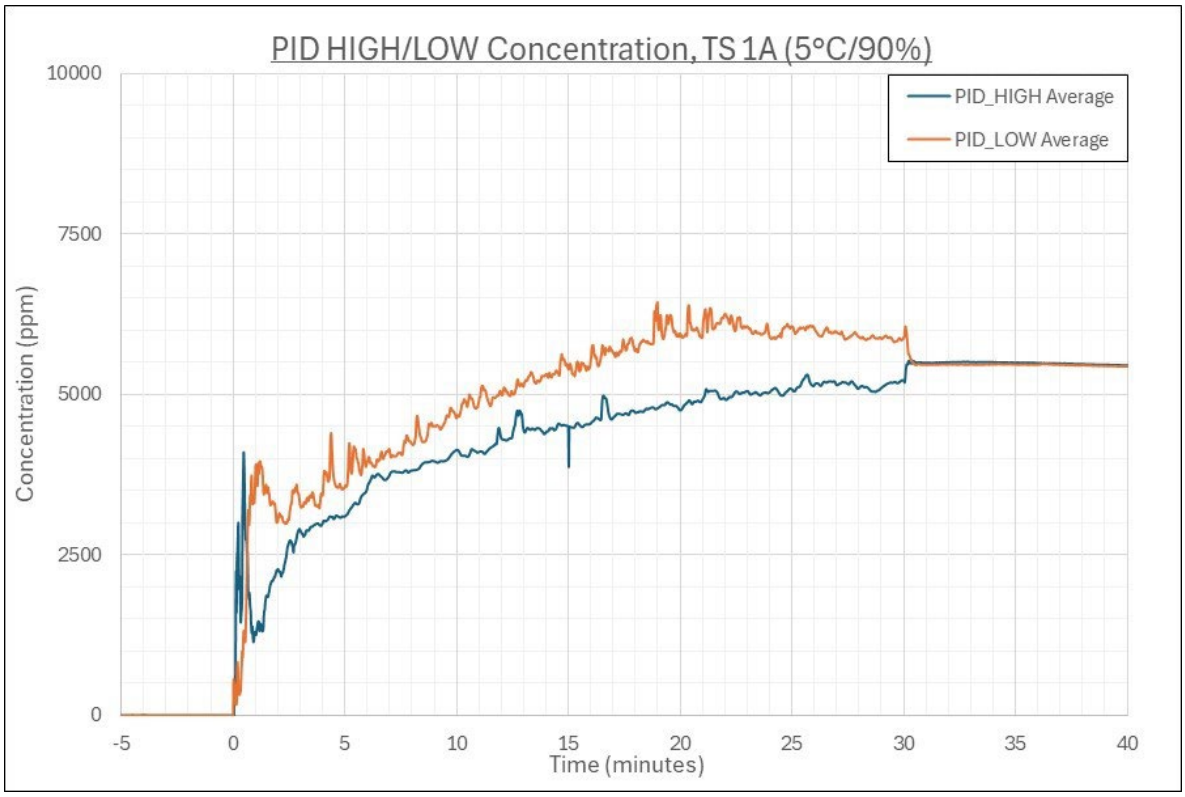

Figure D-2. Average concentration time series for HIGH PIDs and LOW PIDs, TS 1A.

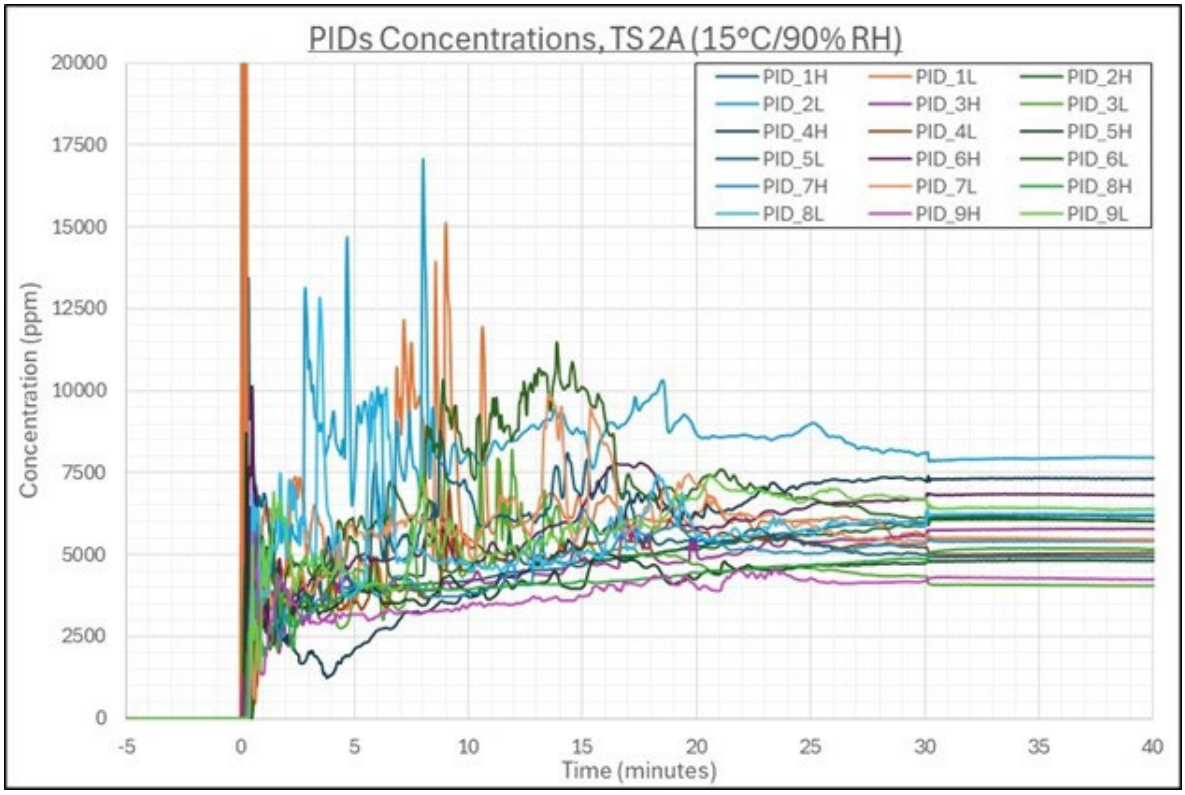

Figure D-3. Overlay of individual PID concentration time series, TS 2A.

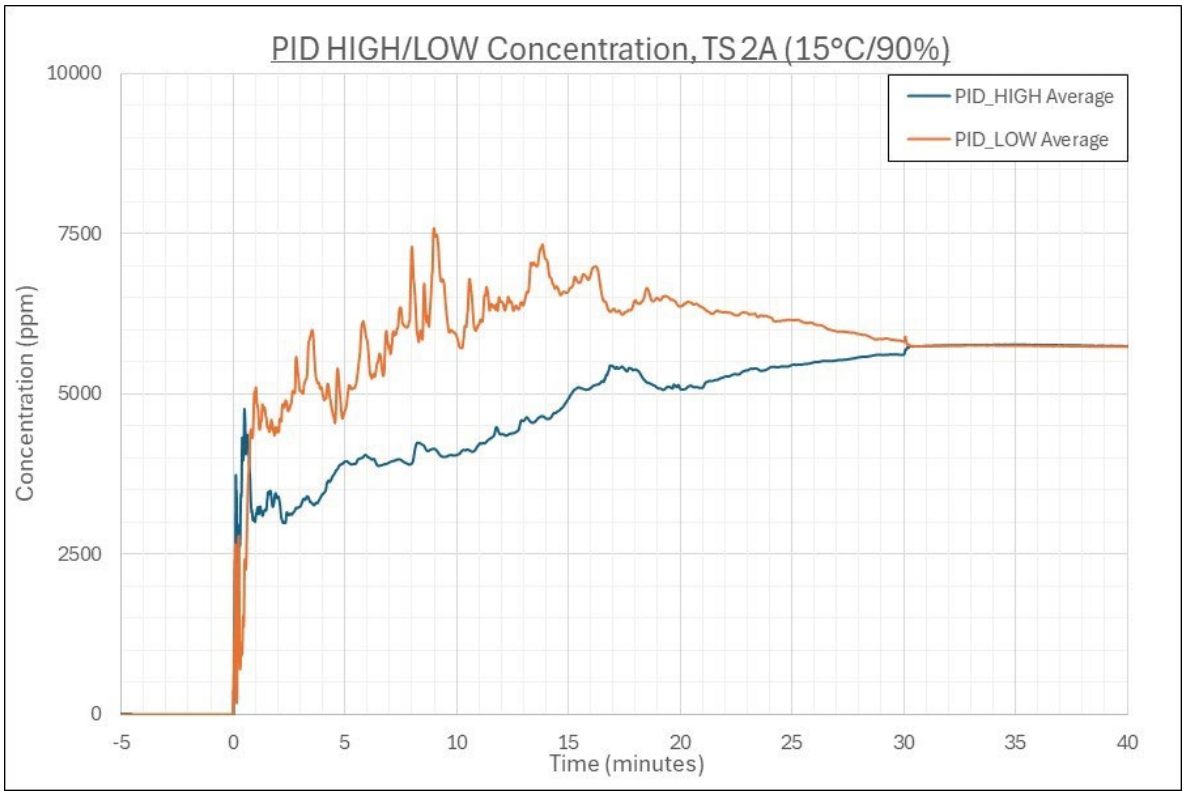

Figure D-4. Average concentration time series for HIGH PIDs and LOW PIDs, TS 2A.

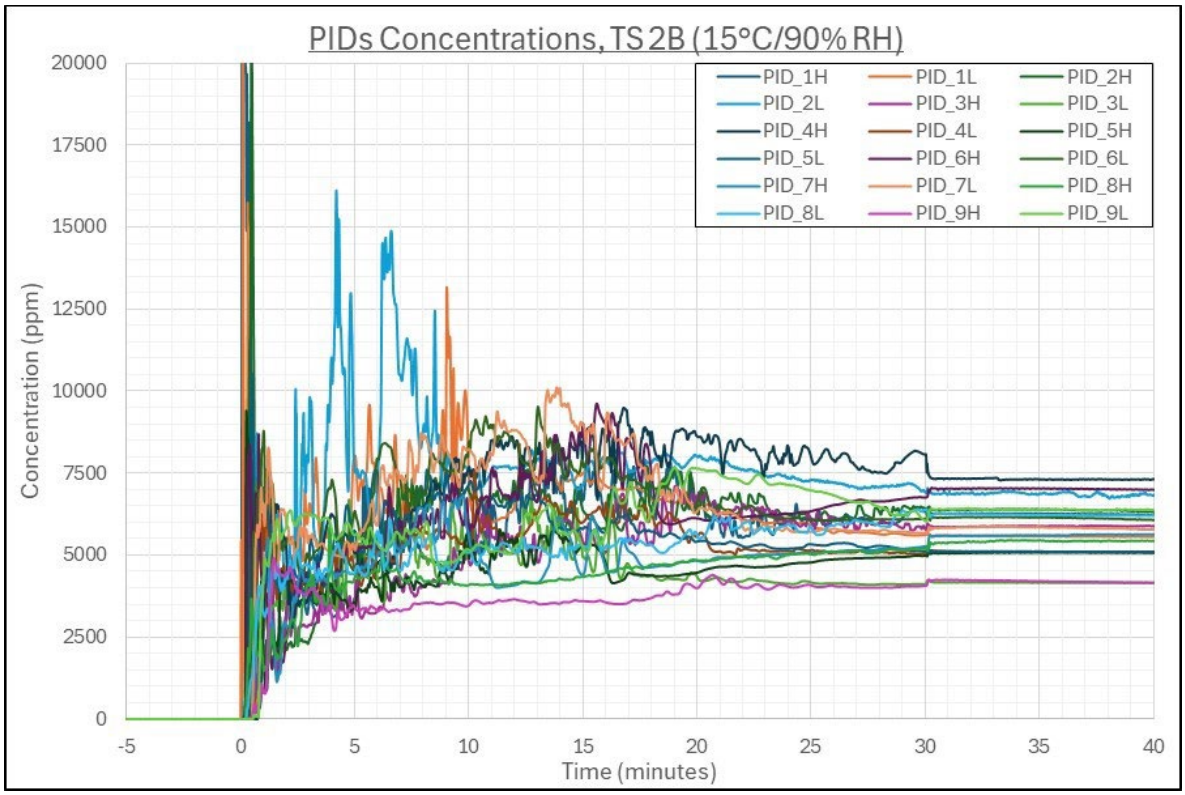

Figure D-5. Overlay of individual PID concentration time series, TS 2B.

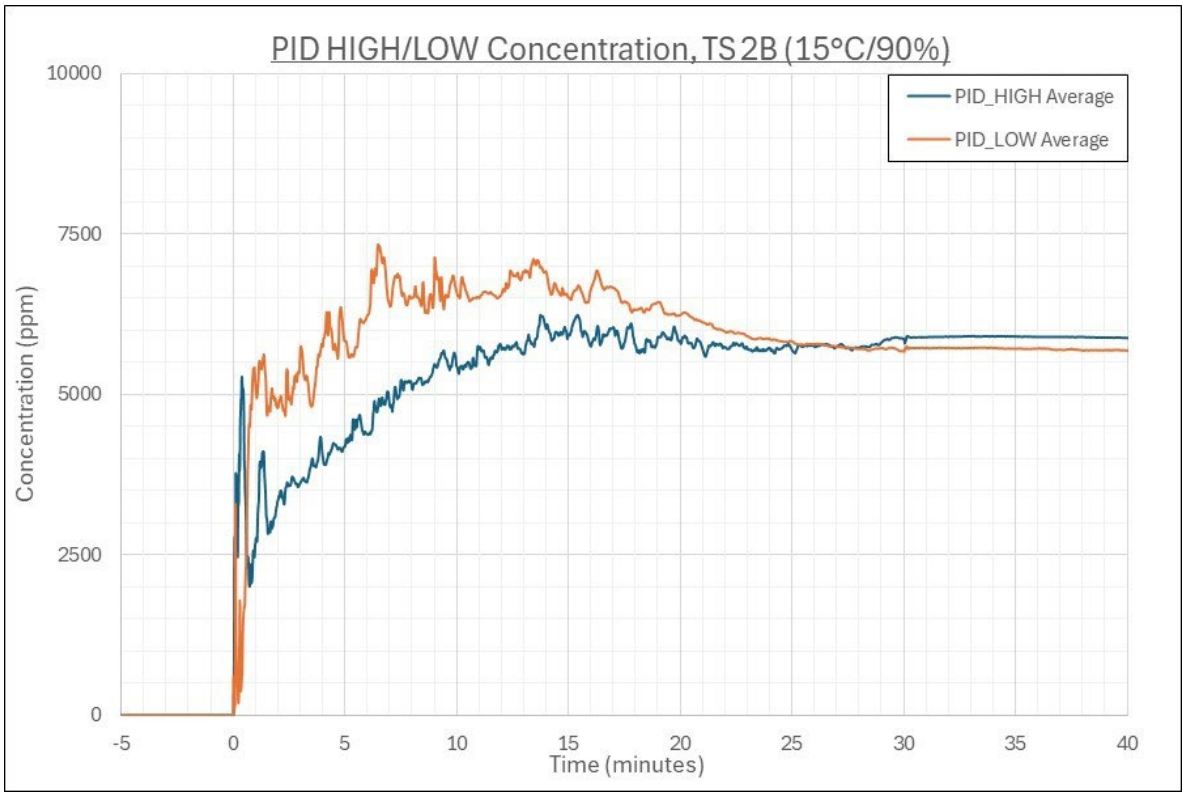

Figure D-6. Average concentration time series for HIGH PIDs and LOW PIDs, TS 2B.

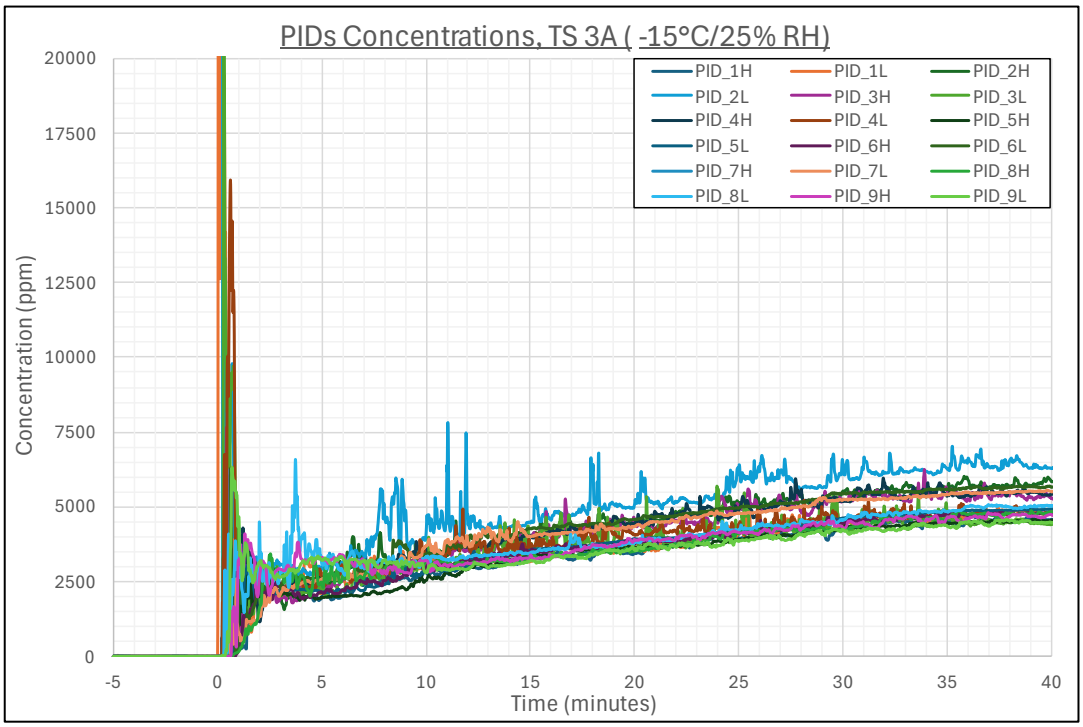

Figure D-7. Overlay of individual PID concentration time series, TS 3A.

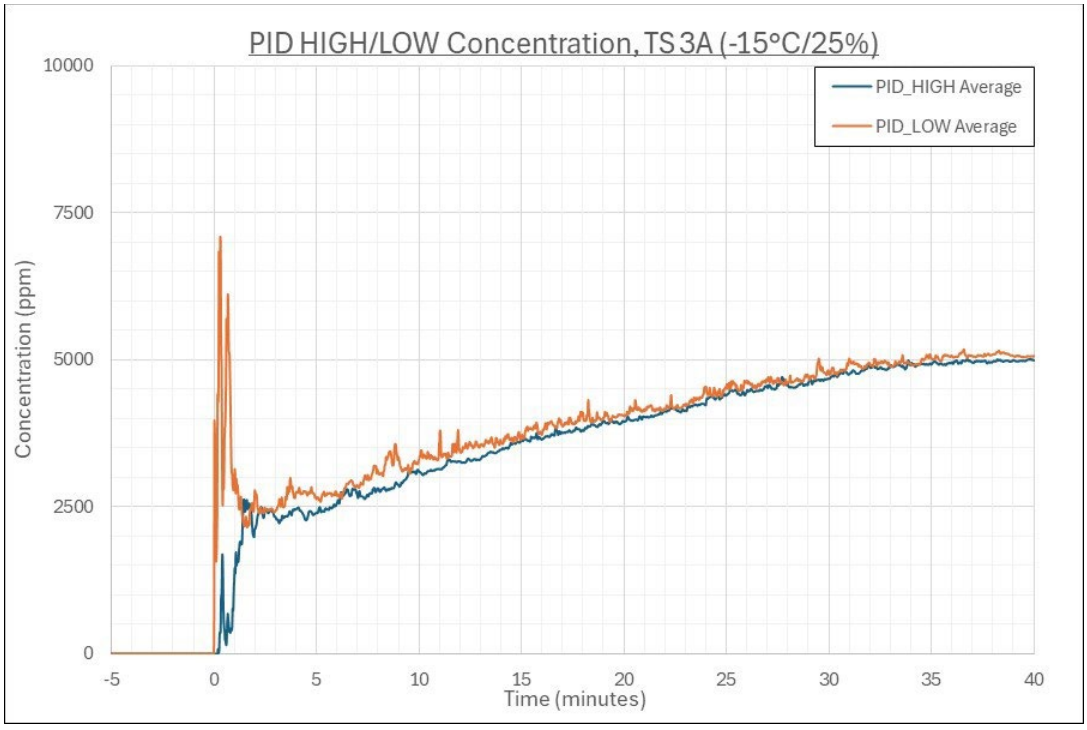

Figure D-8. Average concentration time series for HIGH PIDs and LOW PIDs, TS 3A.

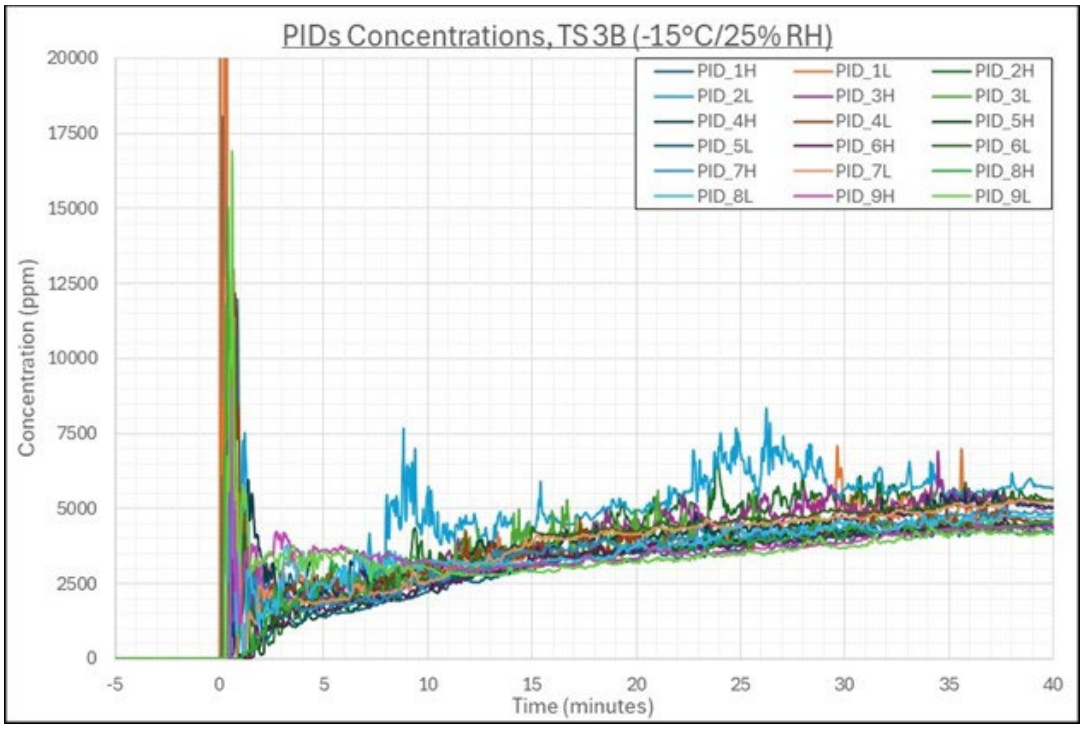

Figure D-9. Overlay of individual PID concentration time series, TS 3B.

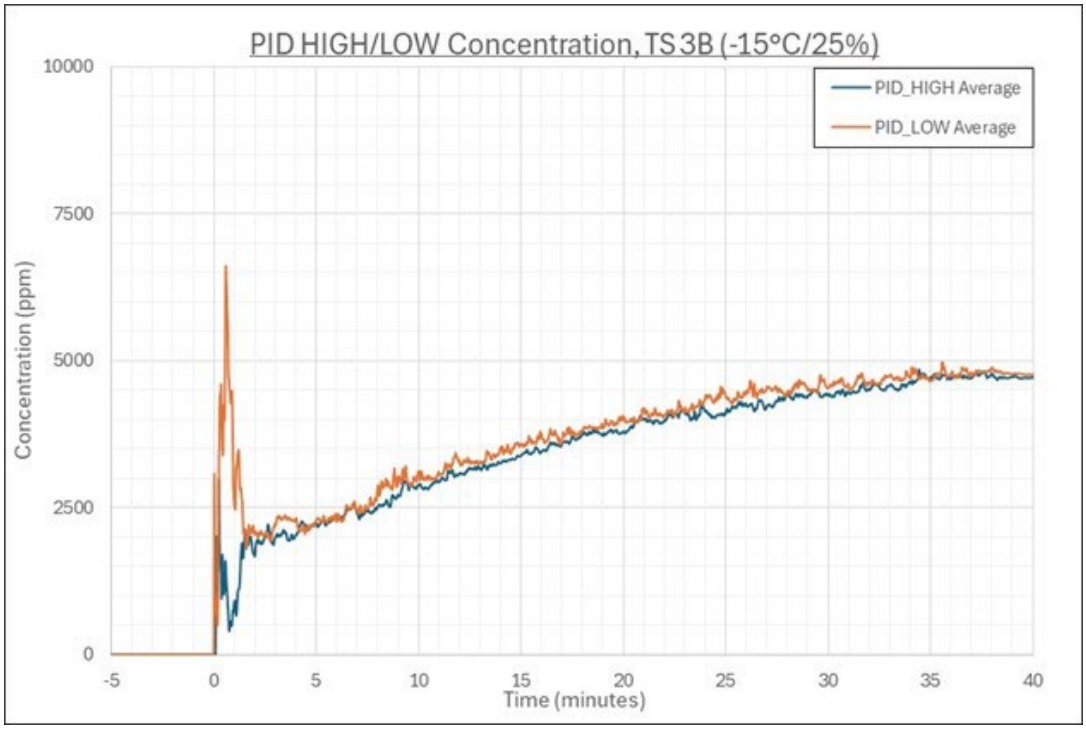

Figure D-10. Average concentration time series for HIGH PIDs and LOW PIDs, TS 3B.

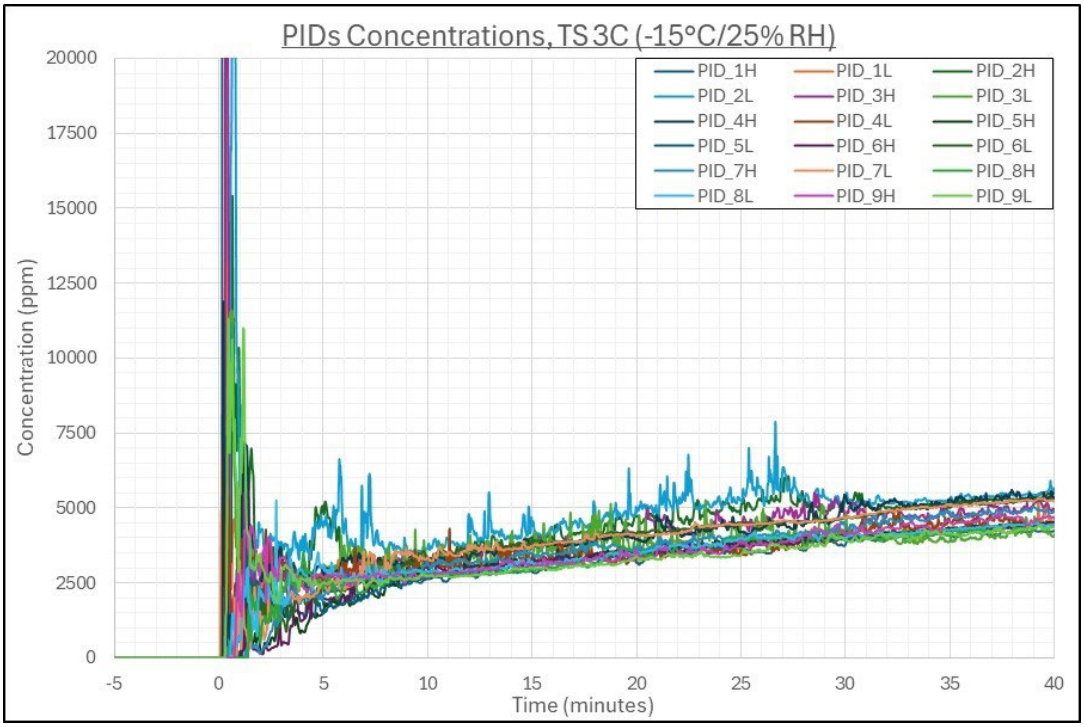

Figure D-11. Overlay of individual PID concentration time series, TS 3C.

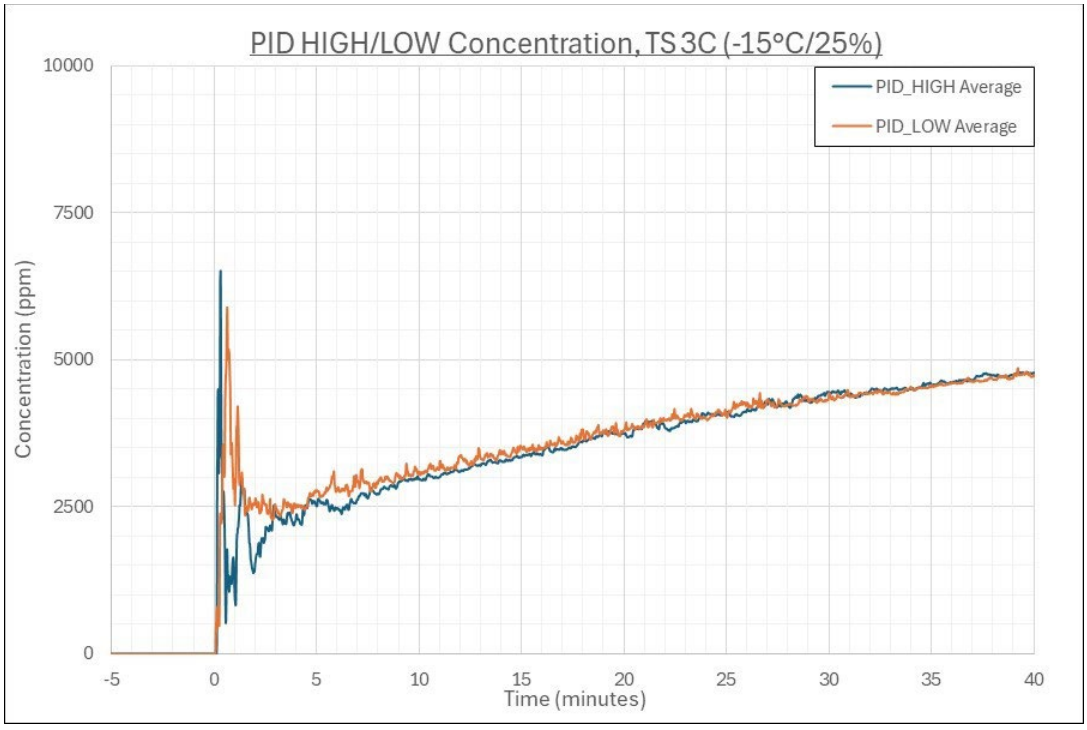

Figure D-12. Average concentration time series for HIGH PIDs and LOW PIDs, TS 3C.

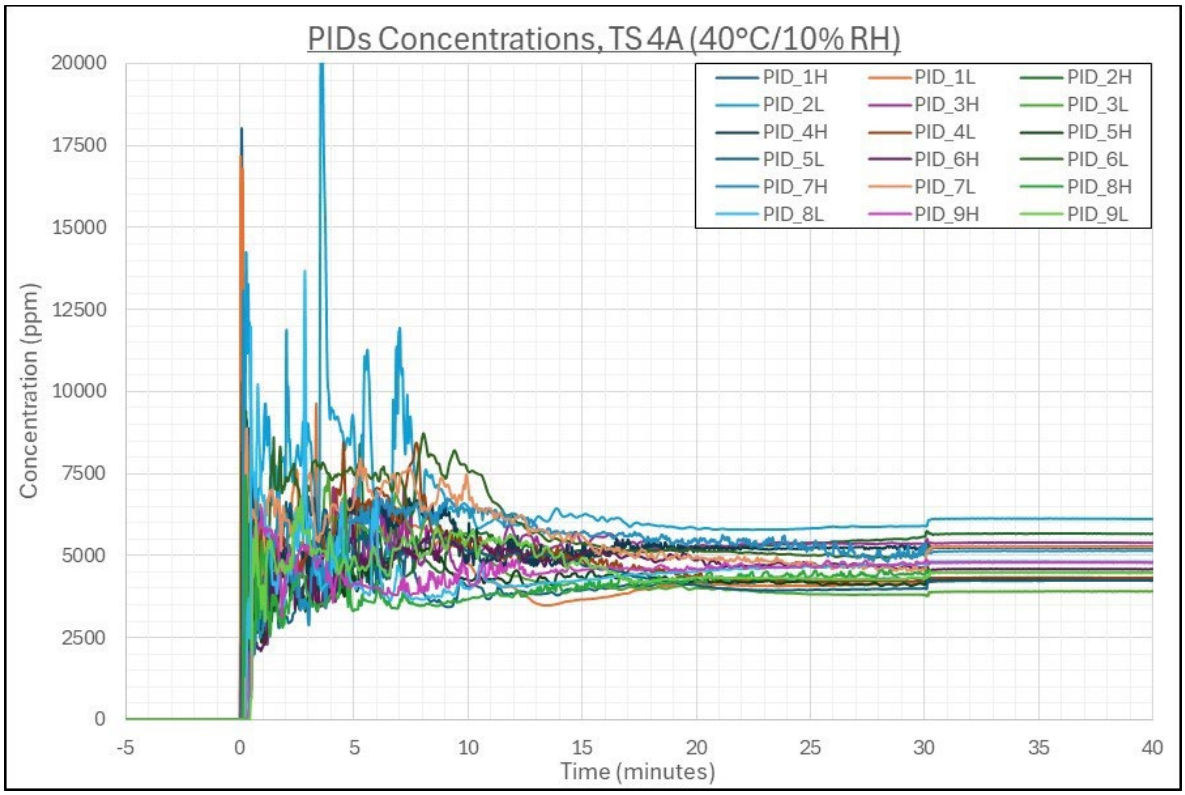

Figure D-13. Overlay of individual PID concentration time series, TS 4A.

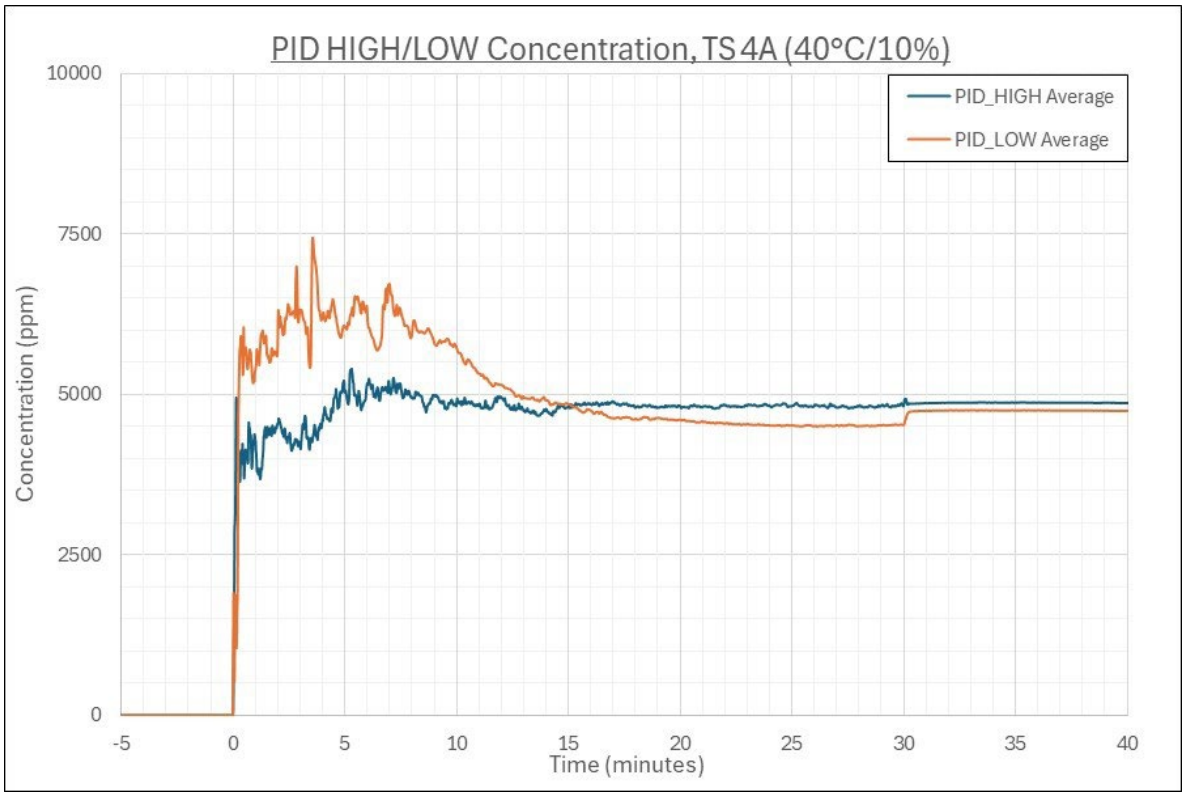

Figure D-14. Average concentration time series for HIGH PIDs and LOW PIDs, TS 4A.

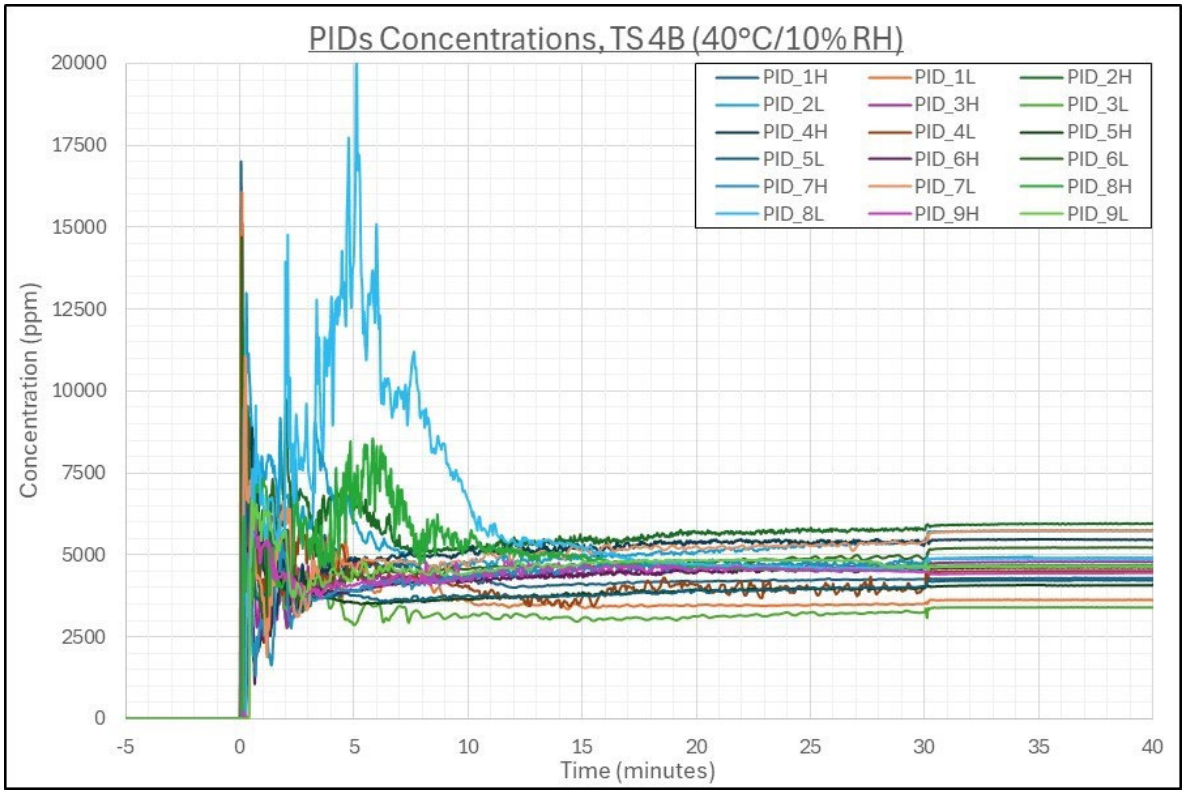

Figure D-15. Overlay of individual PID concentration time series, TS 4B.

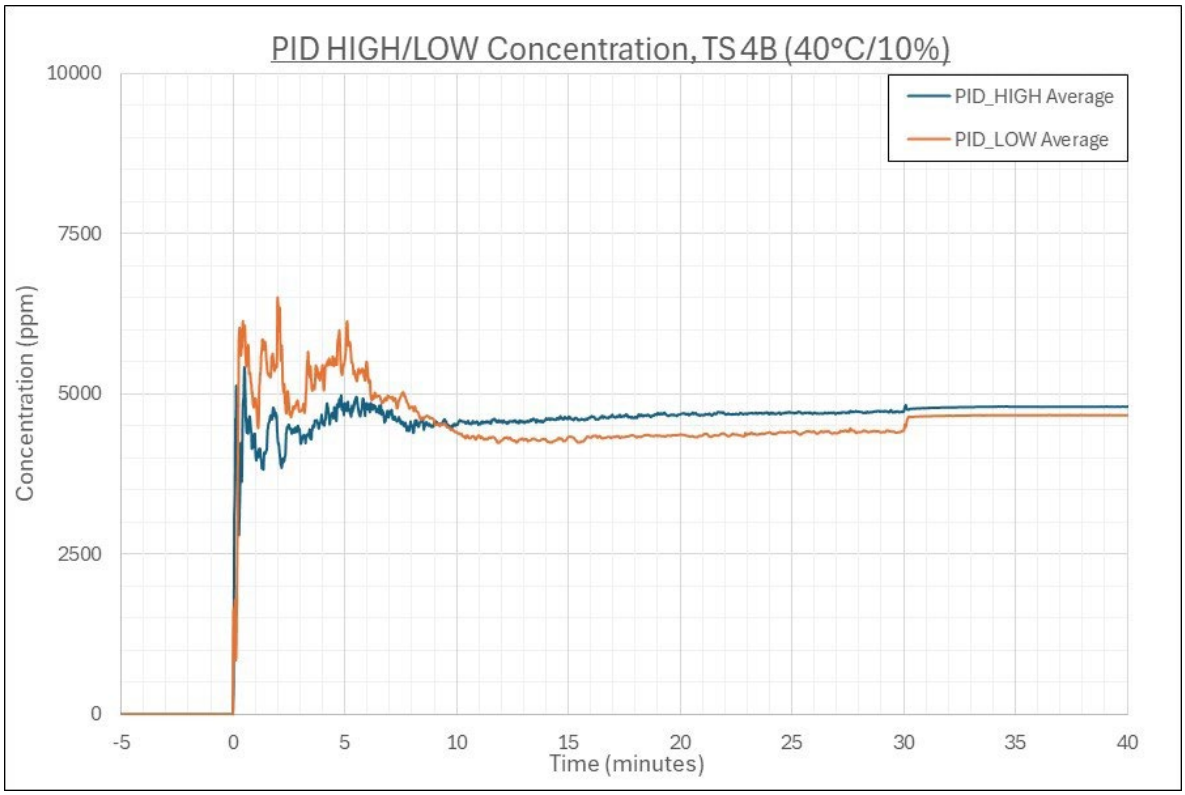

Figure D-16. Average concentration time series for HIGH PIDs and LOW PIDs, TS 4B.

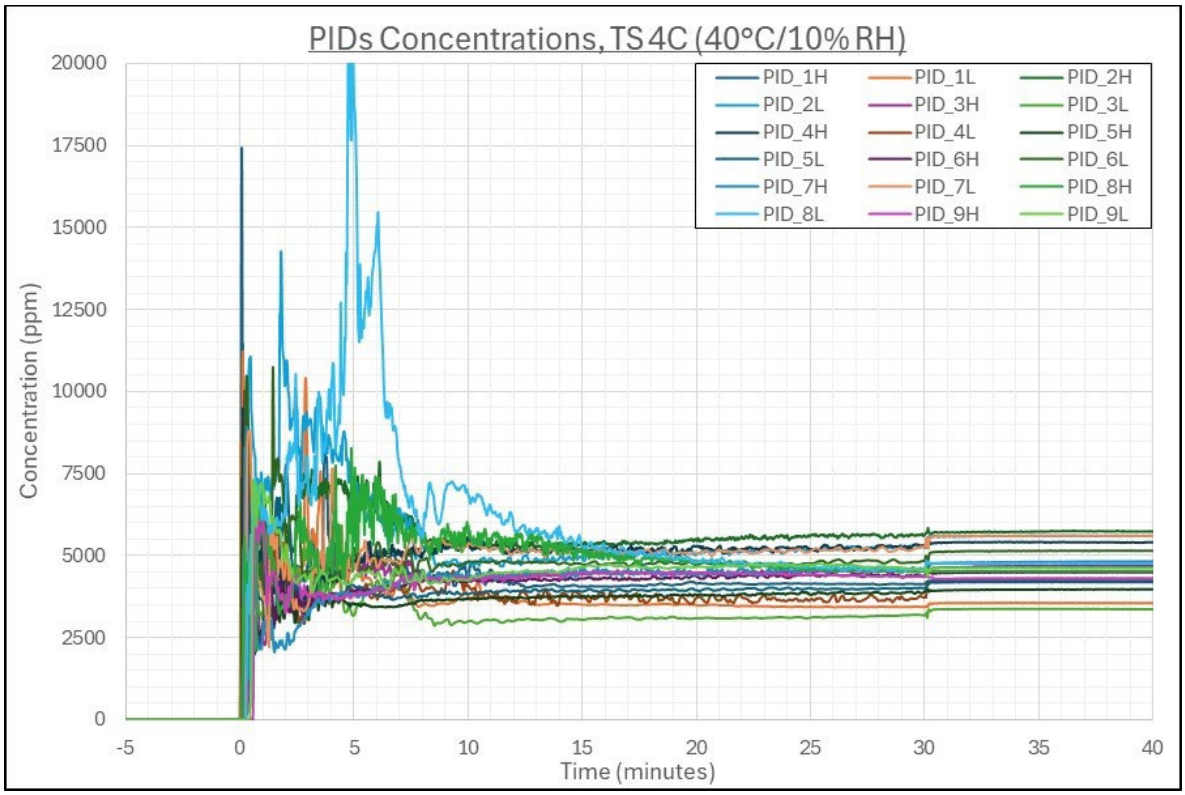

Figure D-17. Overlay of individual PID concentration time series, TS 4C.

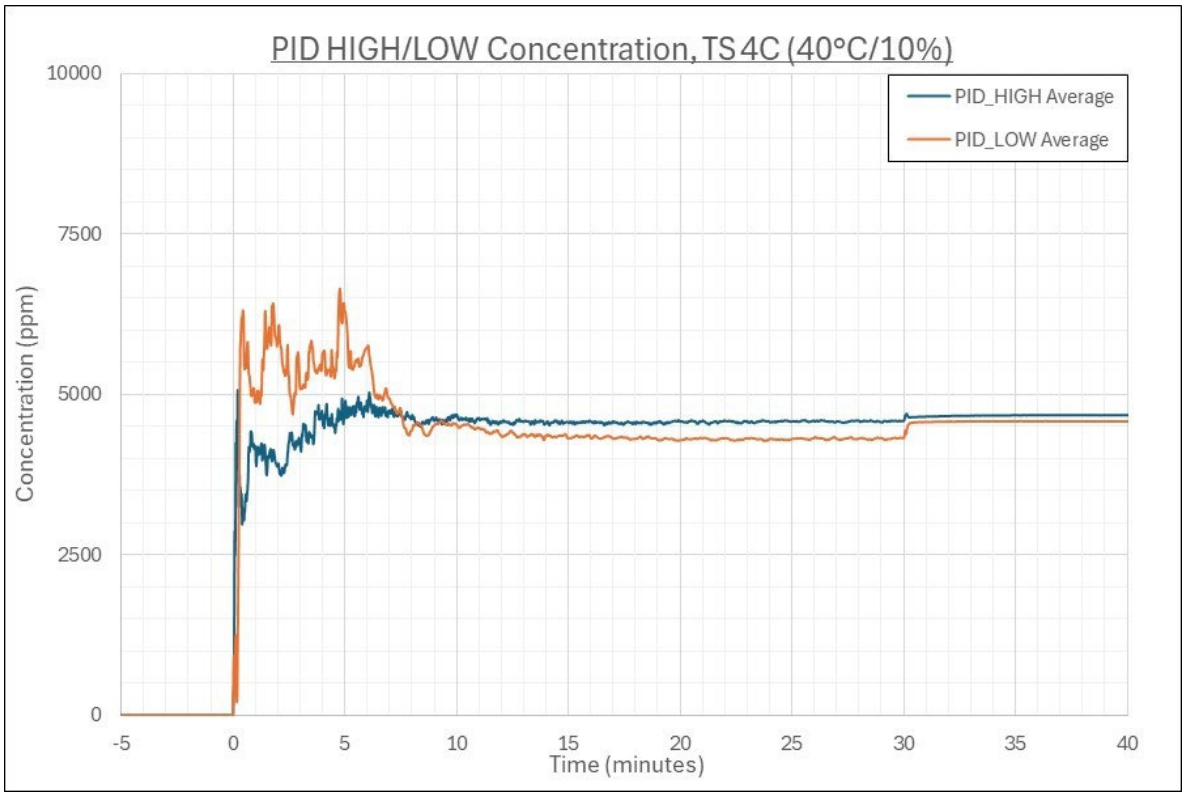

Figure D-18. Average concentration time series for HIGH PIDs and LOW PIDs, TS 4C.

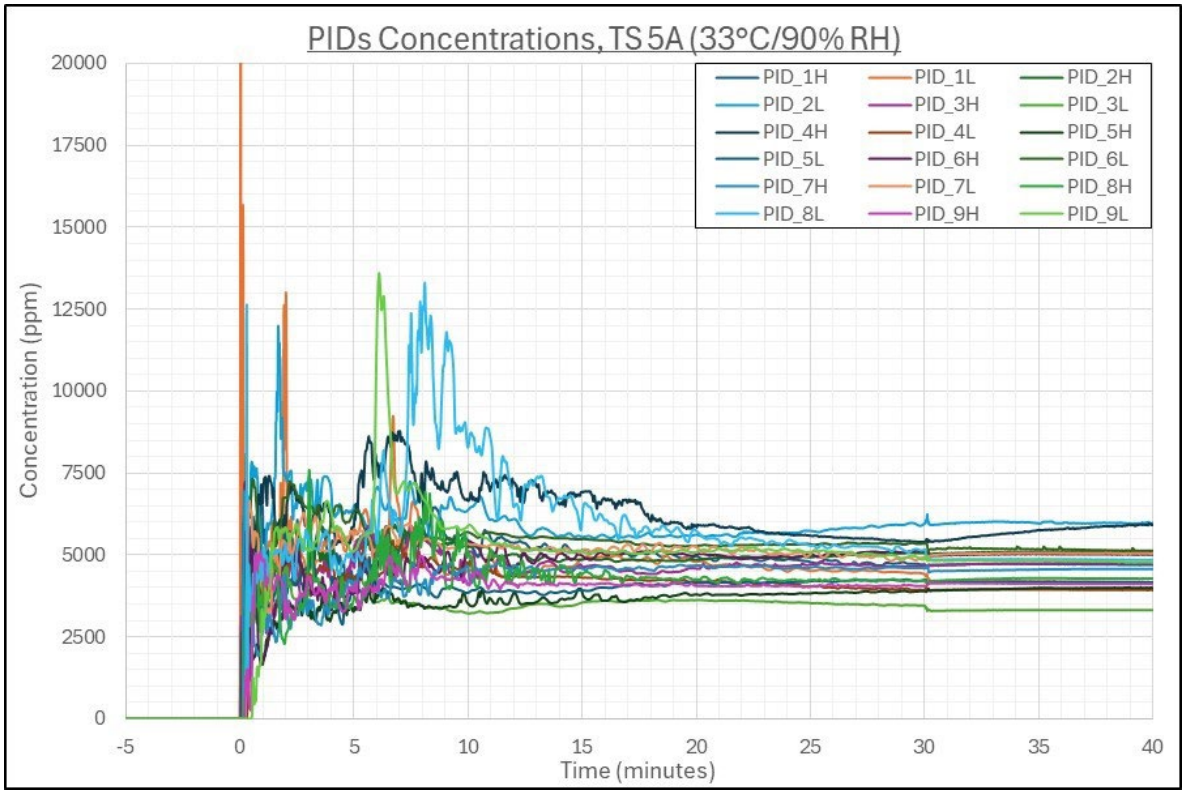

Figure D-19. Overlay of individual PID concentration time series, TS 5A.

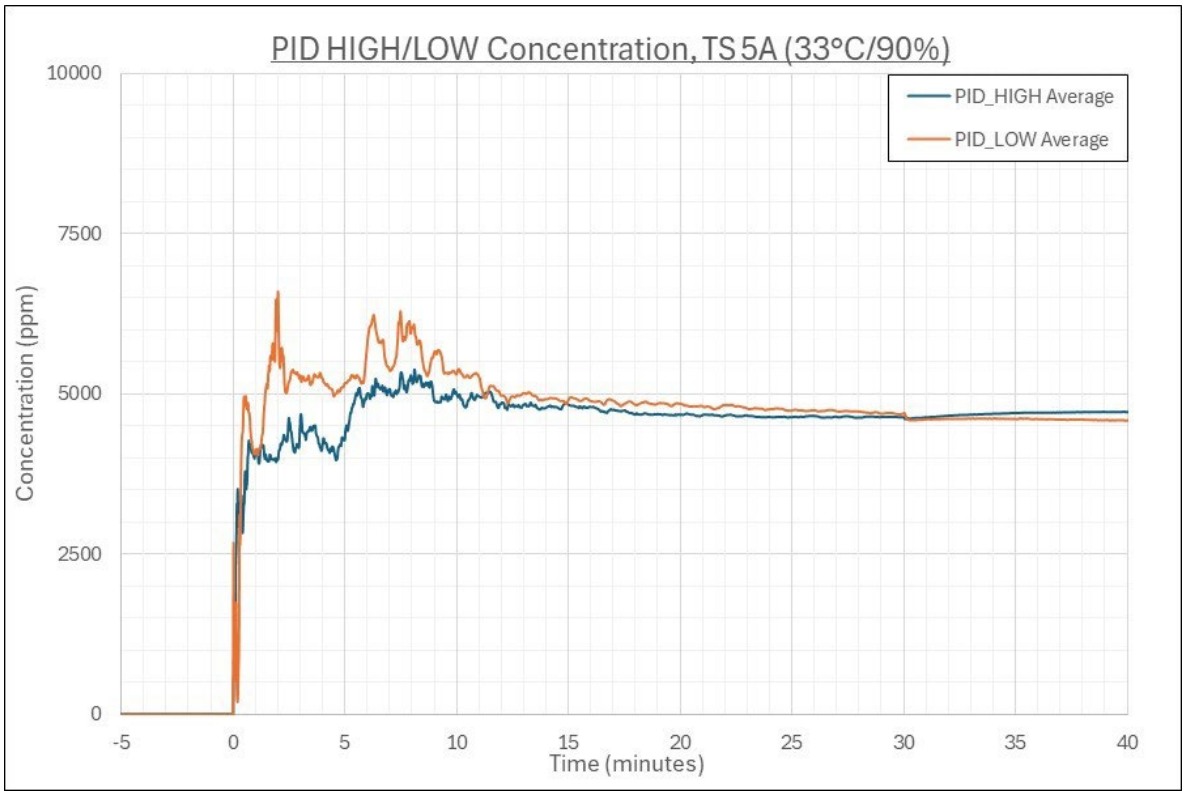

Figure D-20. Average concentration time series for HIGH PIDs and LOW PIDs, TS 5A.

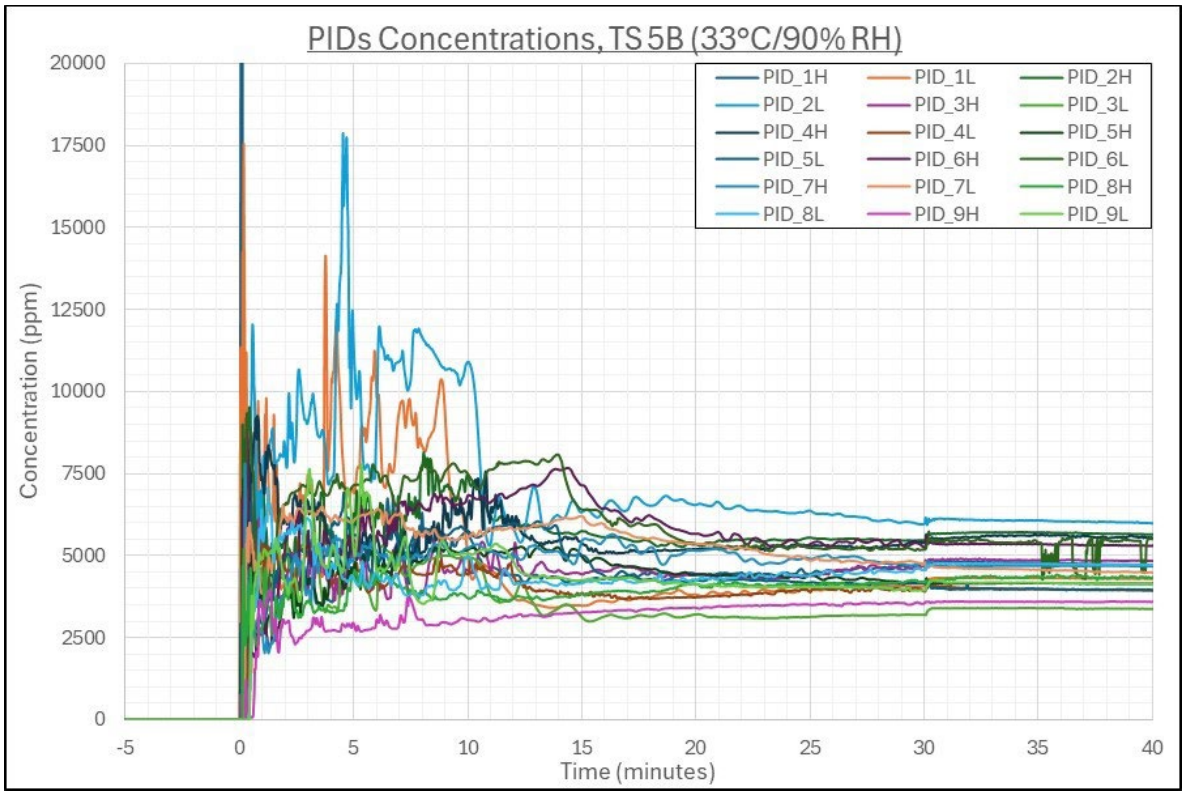

Figure D-21. Overlay of individual PID concentration time series, TS 5B.

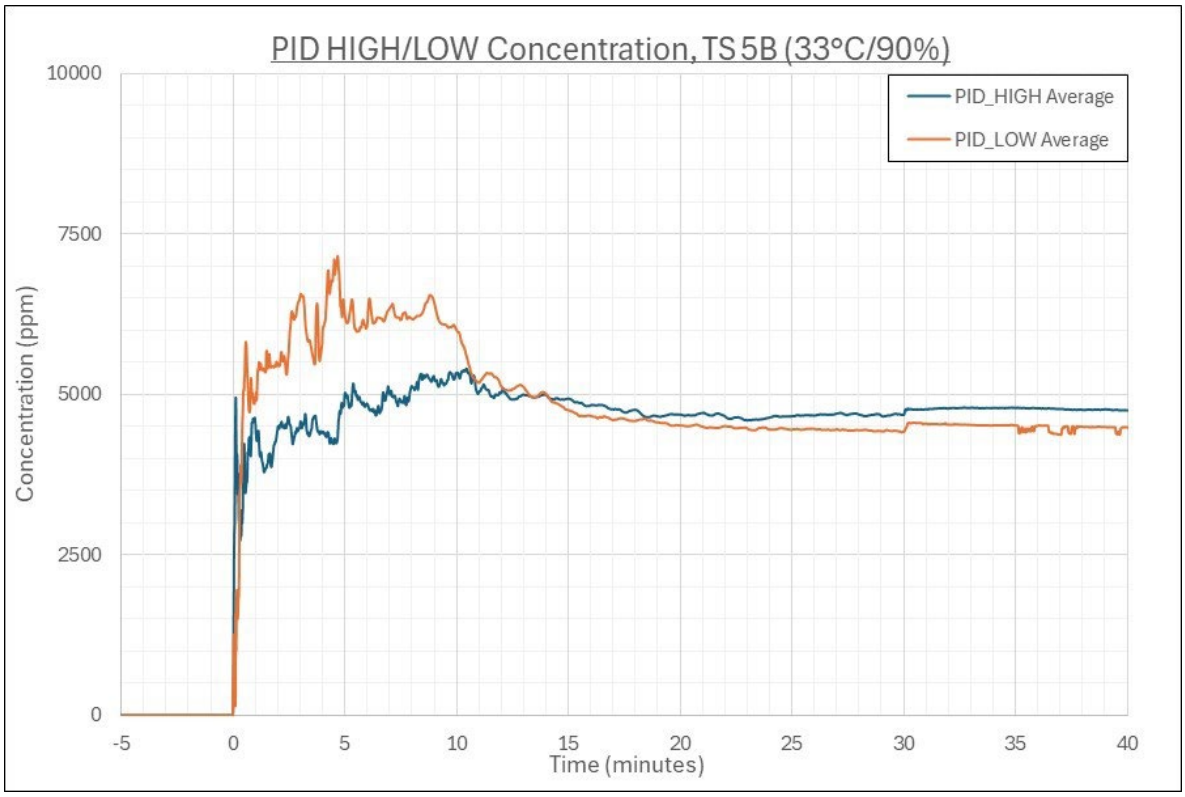

Figure D-22. Average concentration time series for HIGH PIDs and LOW PIDs, TS 5B.

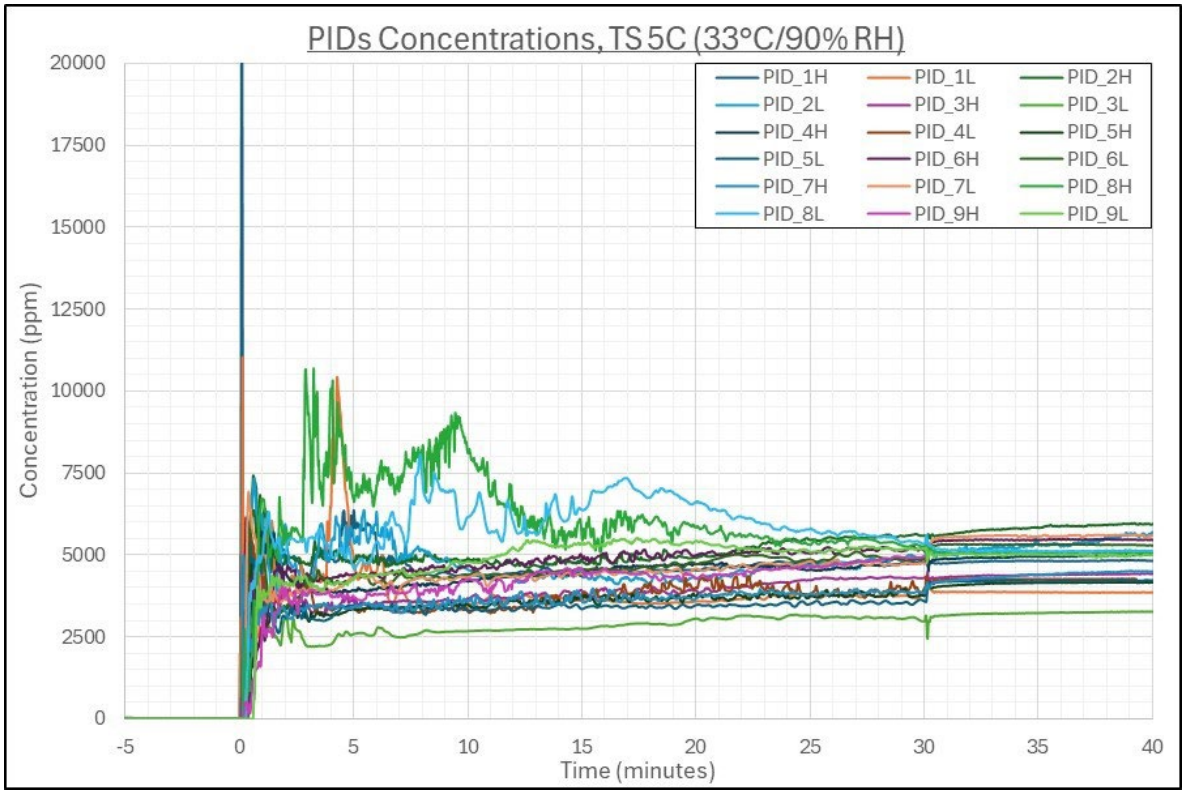

Figure D-23. Overlay of individual PID concentration time series, TS 5C.

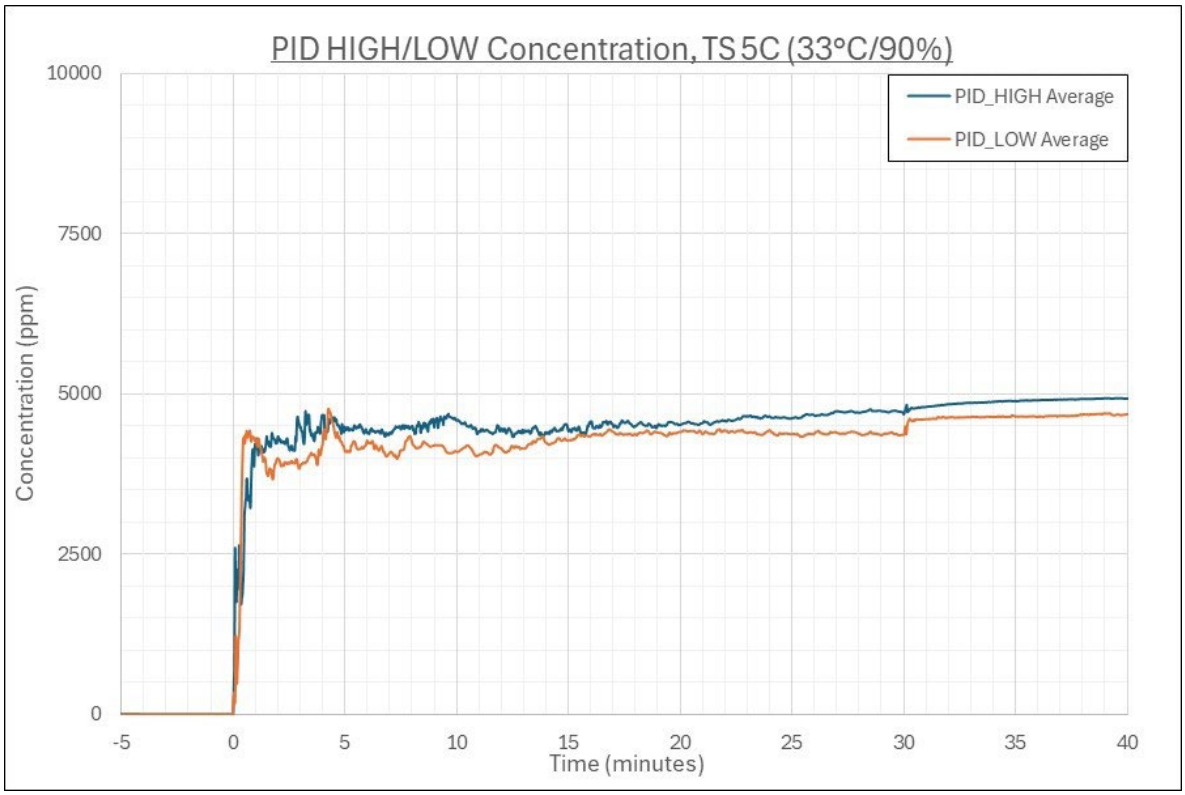

Figure D-24. Average concentration time series for HIGH PIDs and LOW PIDs, TS 5C.

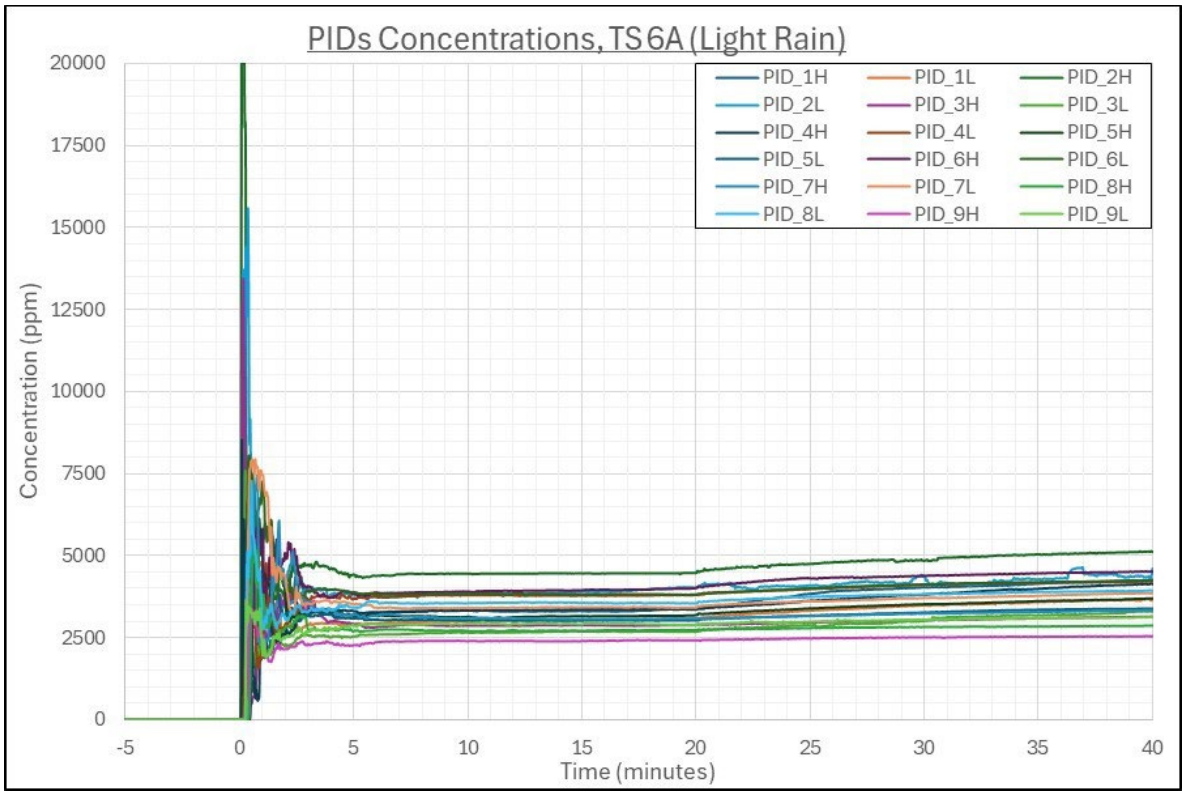

Figure D-25. Overlay of individual PID concentration time series, TS 6A.

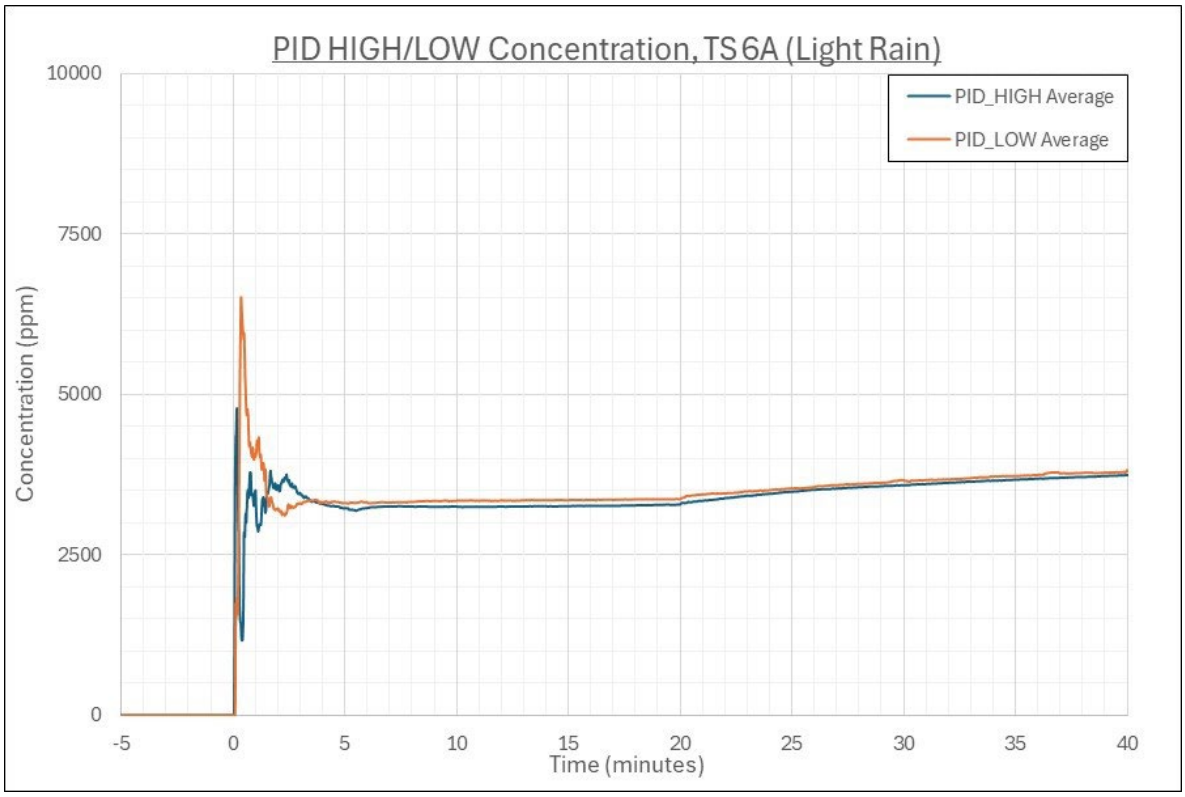

Figure D-26. Average concentration time series for HIGH PIDs and LOW PIDs, TS 6A.

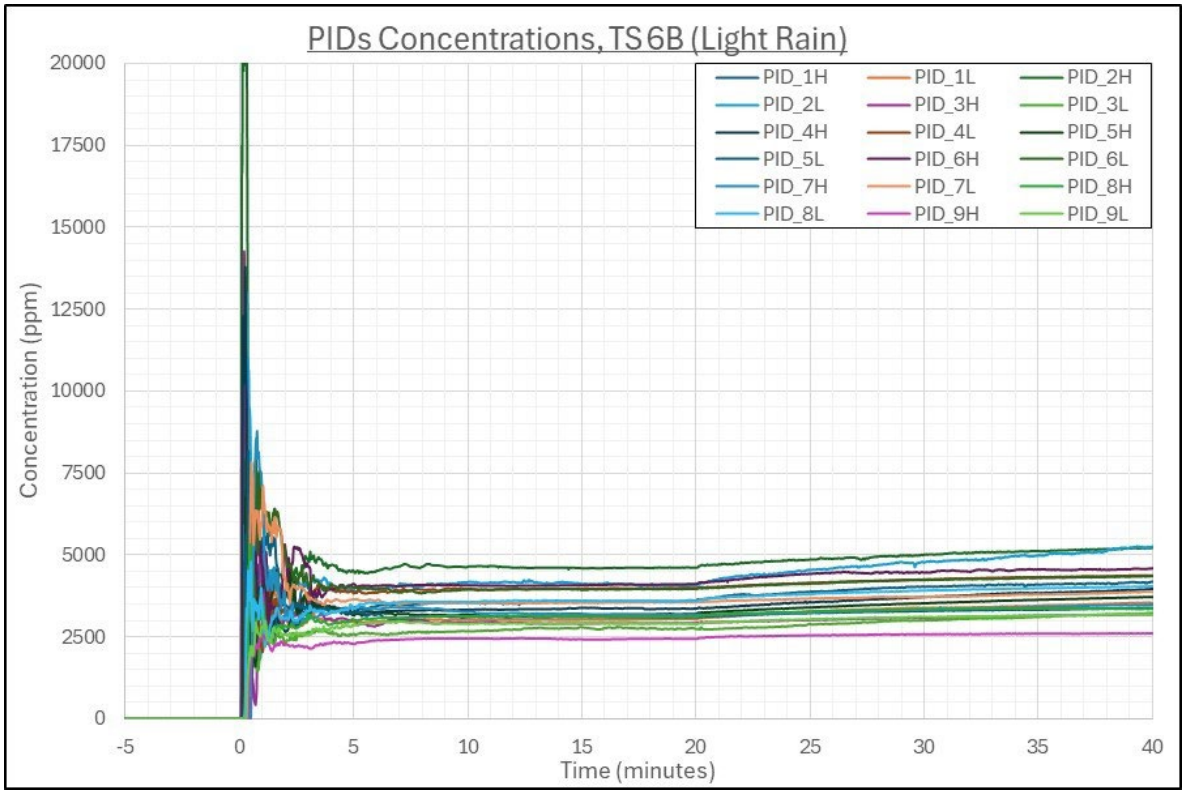

Figure D-27. Overlay of individual PID concentration time series, TS 6B.

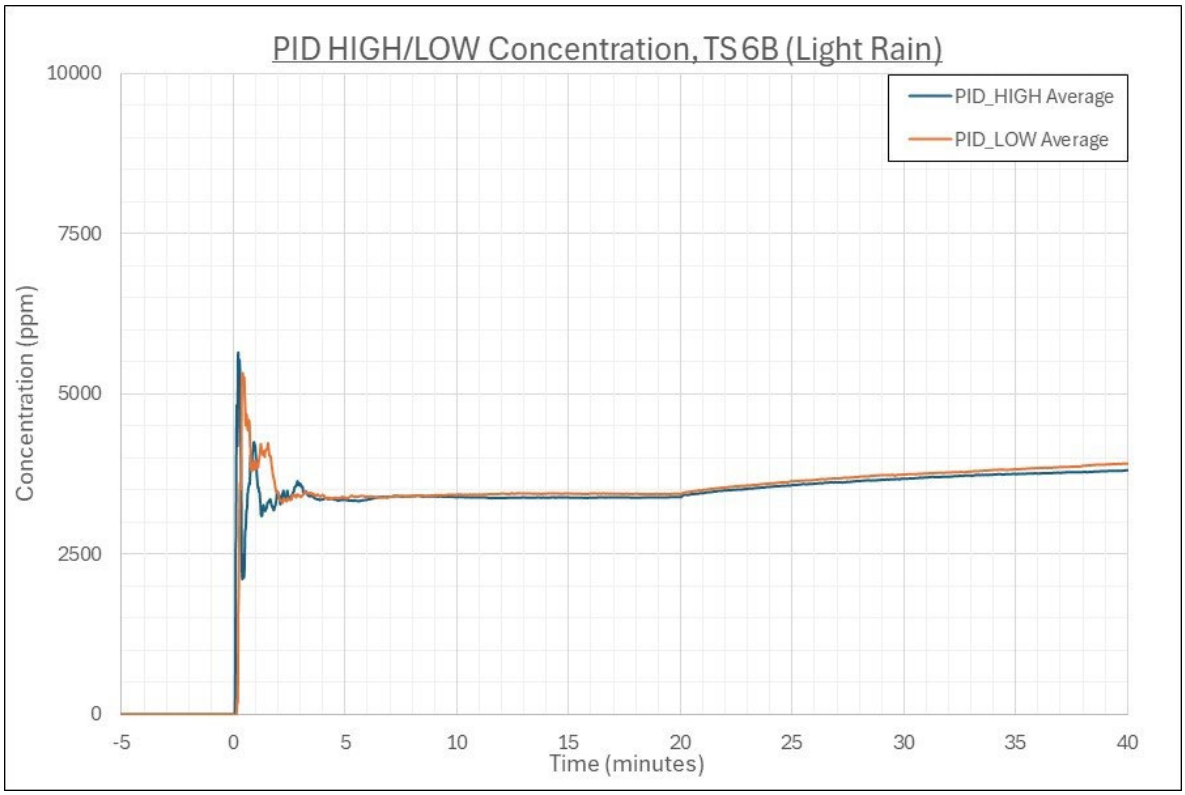

Figure D-28. Average concentration time series for HIGH PIDs and LOW PIDs, TS 6B.

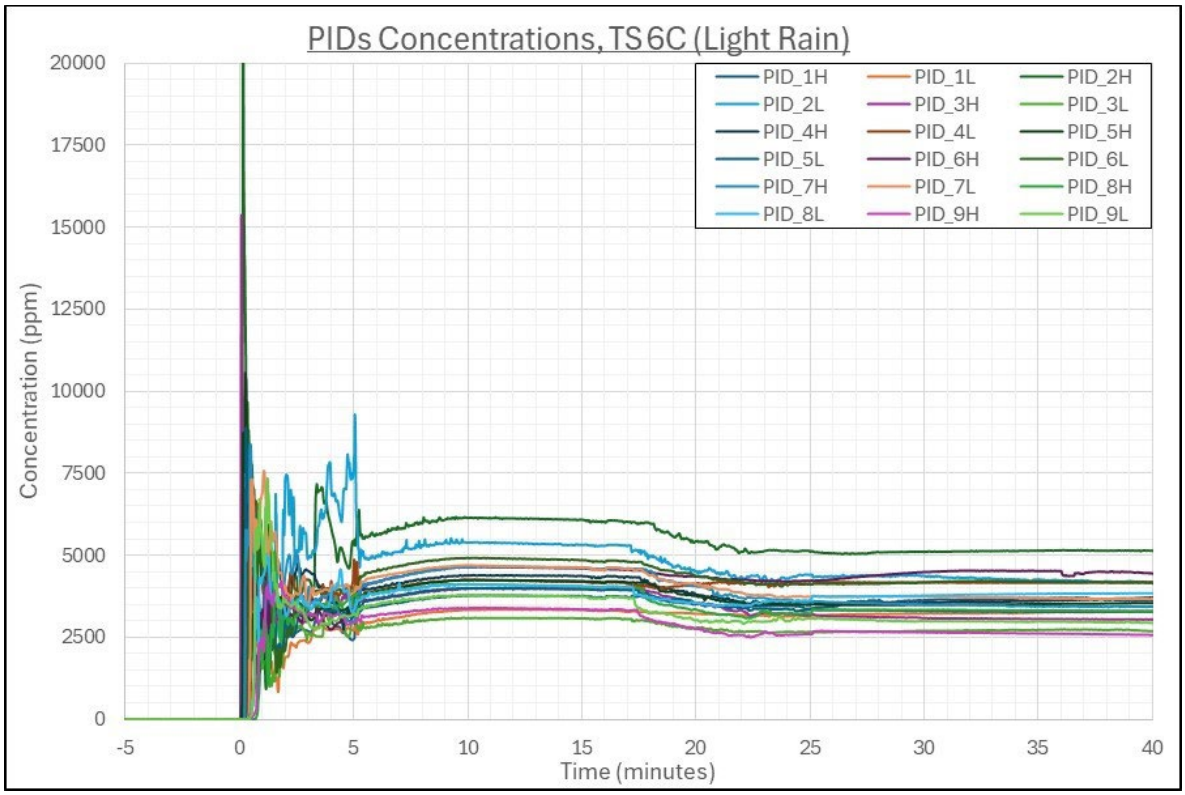

Figure D-29. Overlay of individual PID concentration time series, TS 6C.

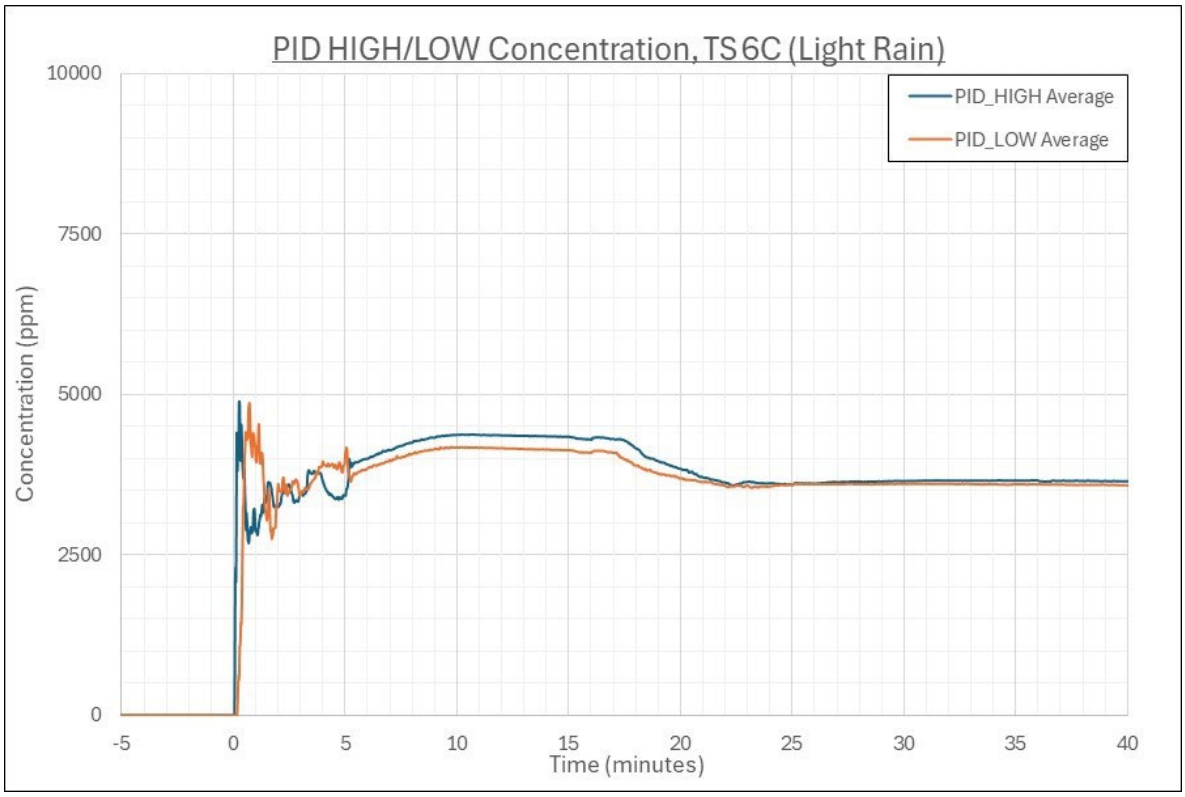

Figure D-30. Average concentration time series for HIGH PIDs and LOW PIDs, TS 6C.

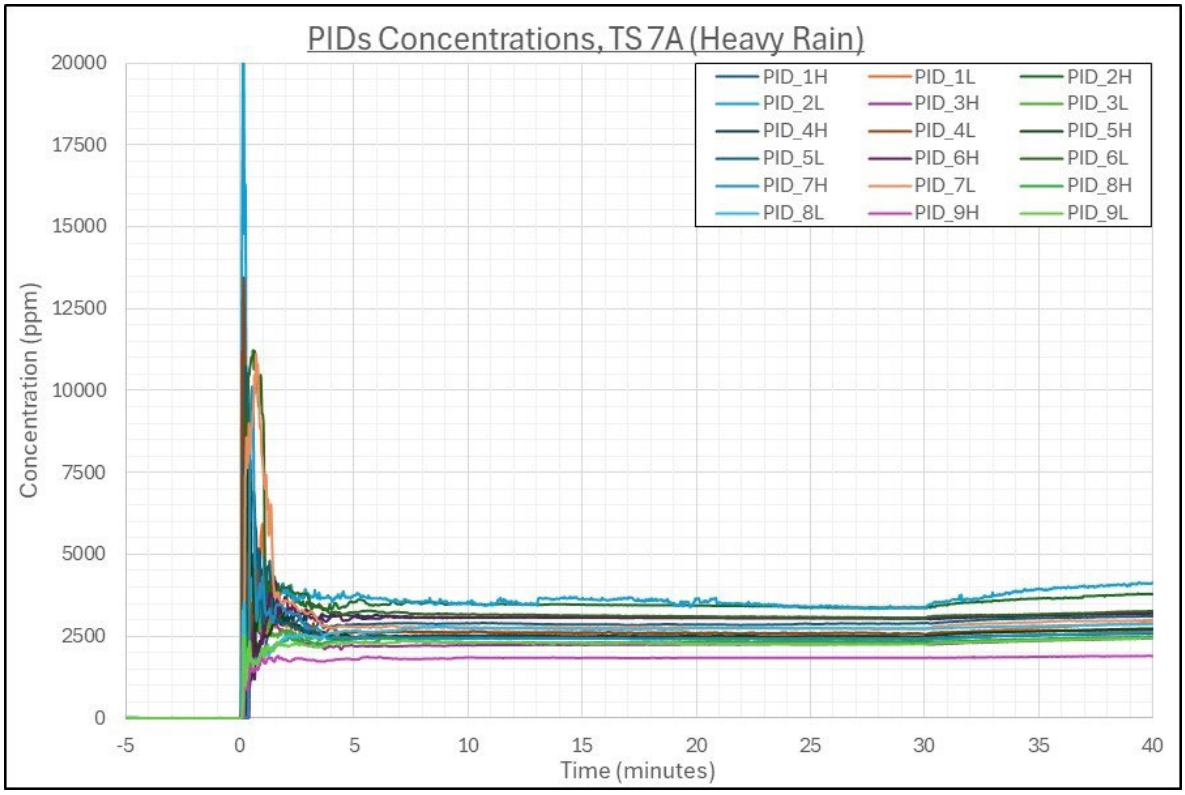

Figure D-31. Overlay of individual PID concentration time series, TS 7A.

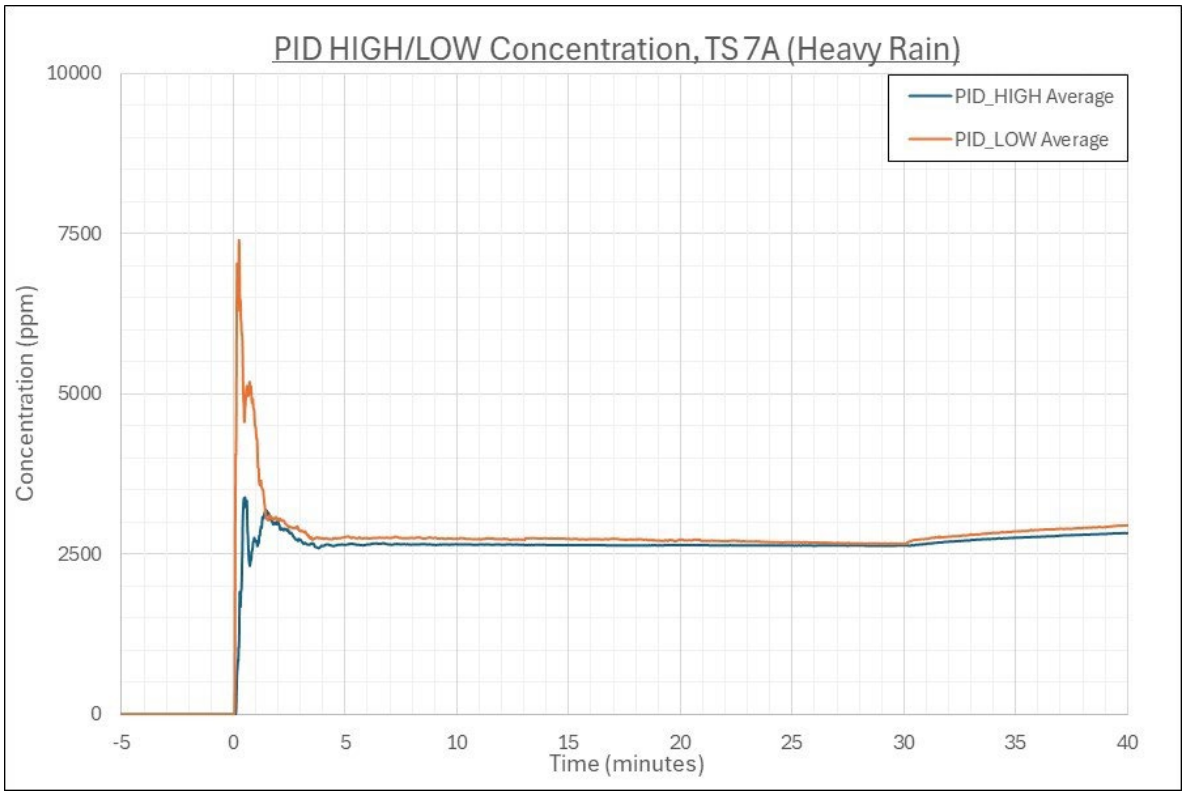

Figure D-32. Average concentration time series for HIGH PIDs and LOW PIDs, TS 7A.

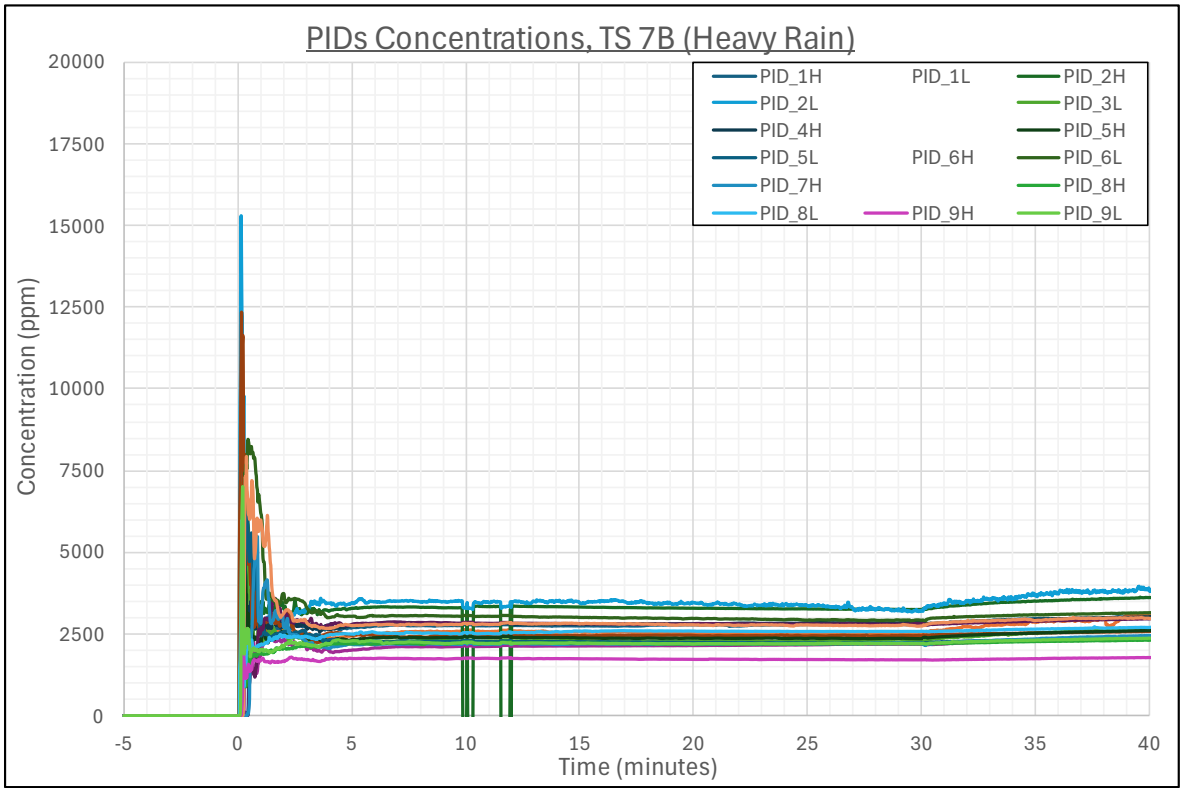

Figure D-33. Overlay of individual PID concentration time series, TS 7B.

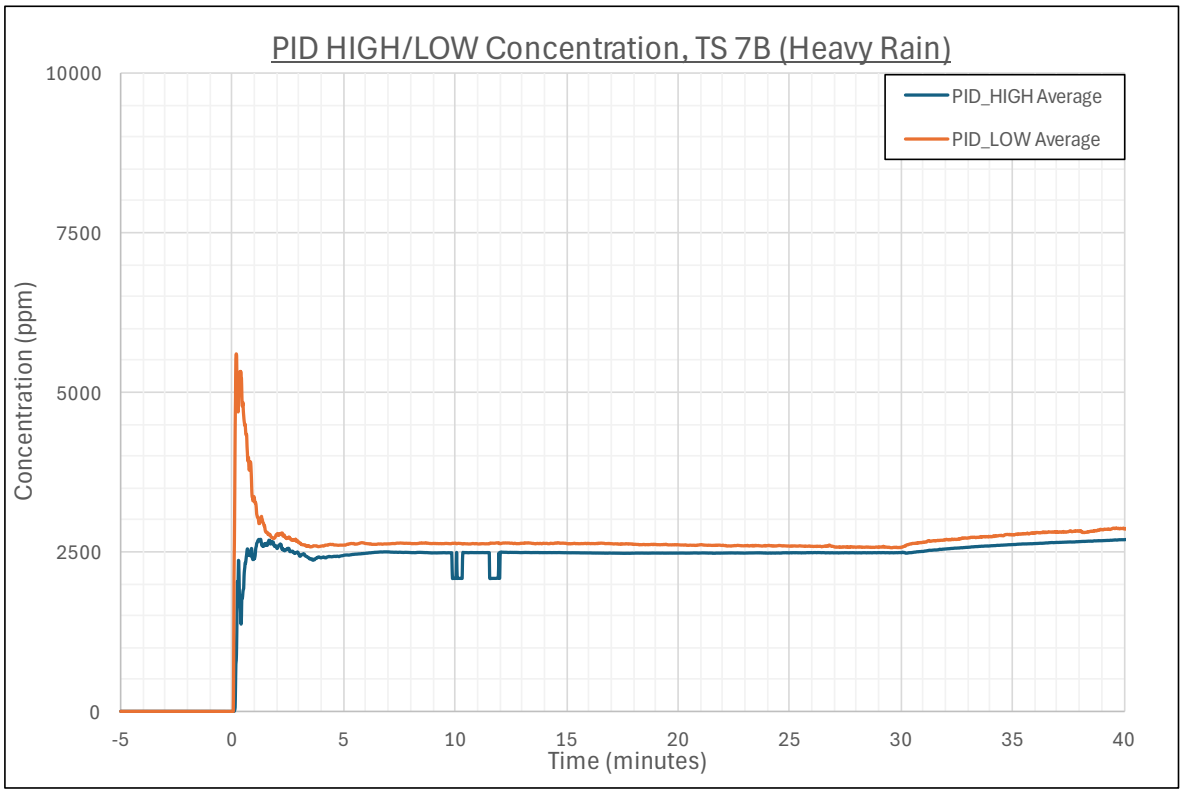

Figure D-34. Average concentration time series for HIGH PIDs and LOW PIDs, TS 7B.

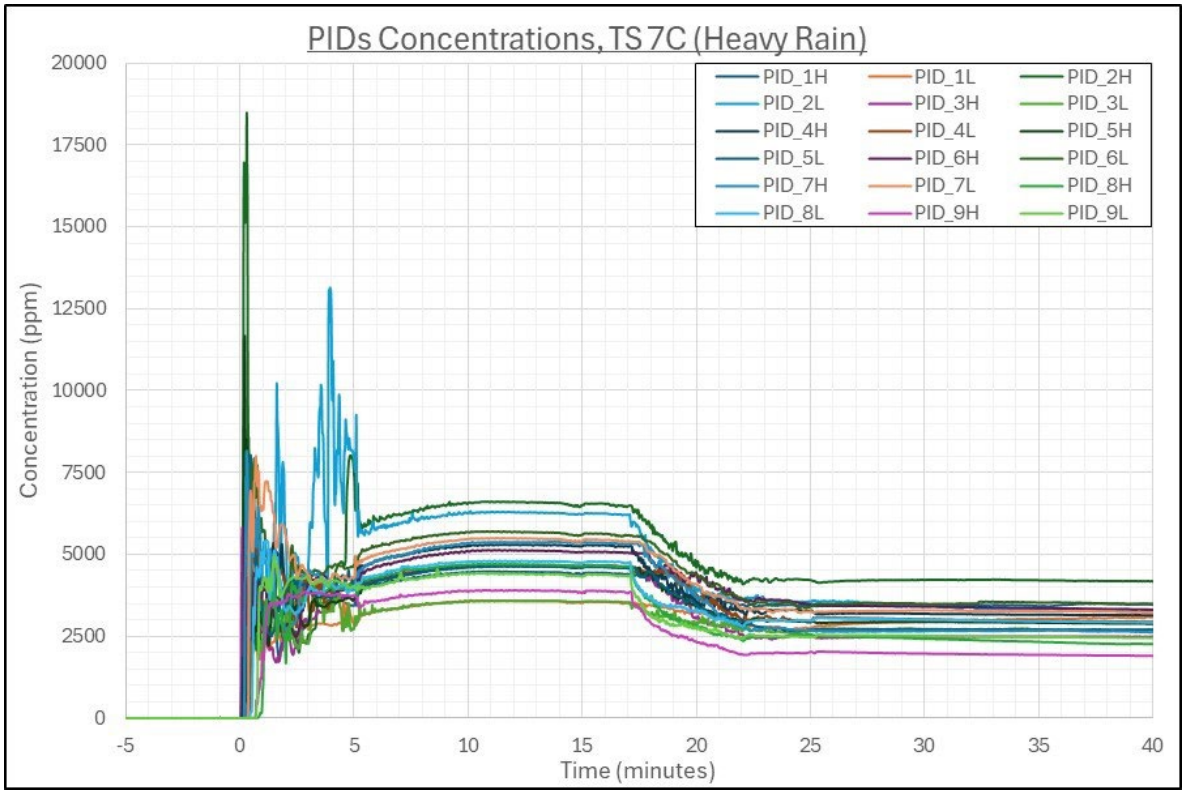

Figure D-35. Overlay of individual PID concentration time series, TS 7C.

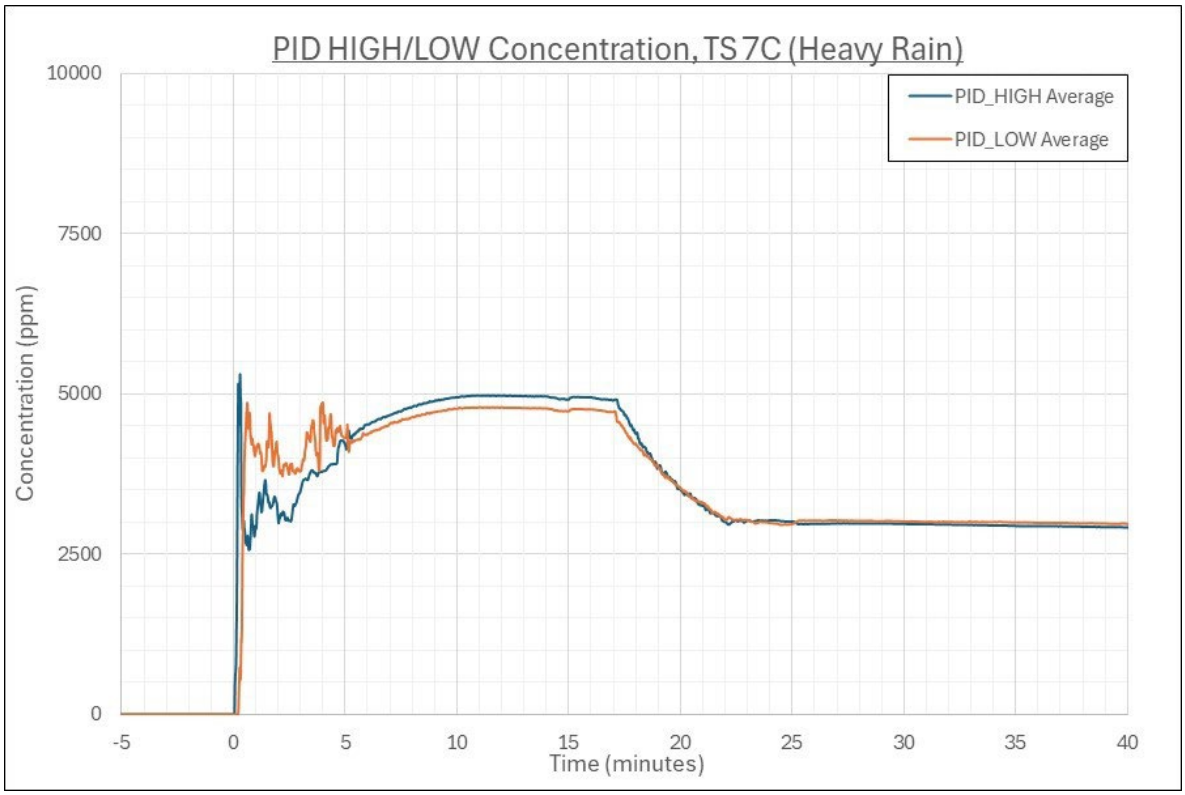

Figure D-36. Average concentration time series for HIGH PIDs and LOW PIDs, TS 7C.

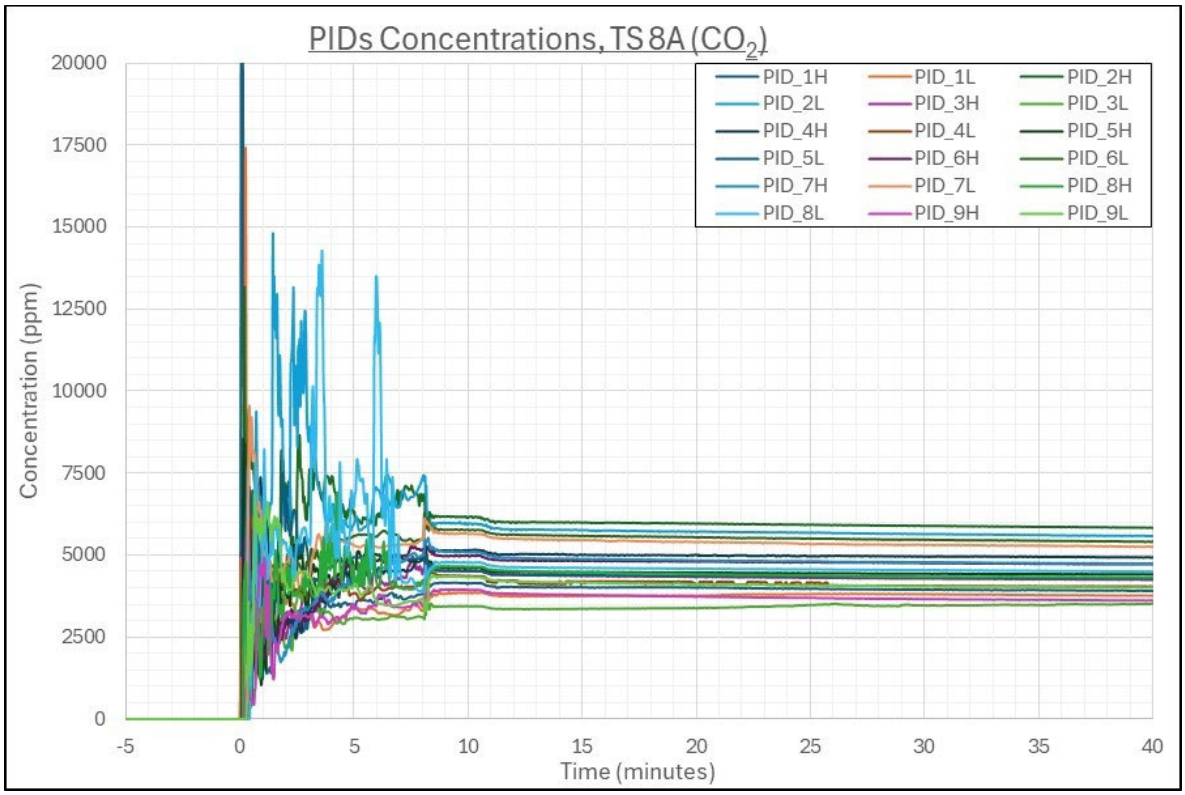

Figure D-37. Overlay of individual PID concentration time series, TS 8A.

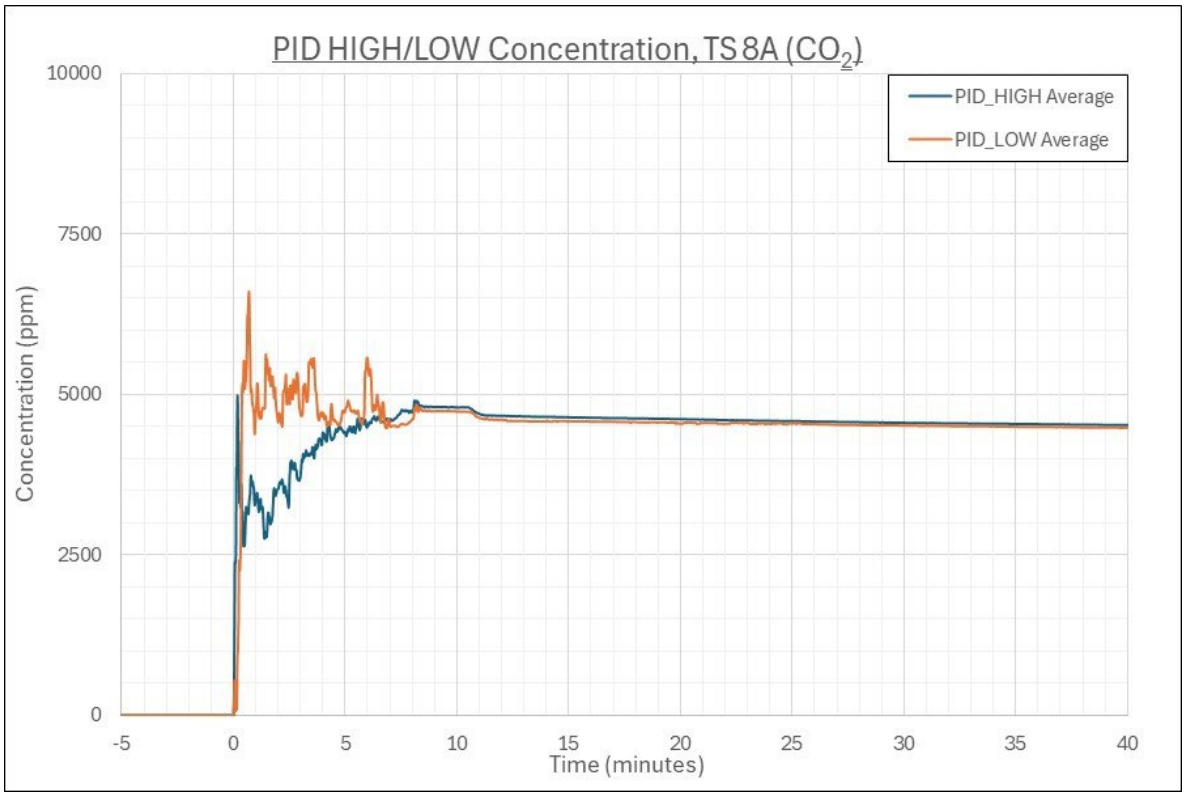

Figure D-38. Average concentration time series for HIGH PIDs and LOW PIDs, TS 8A.

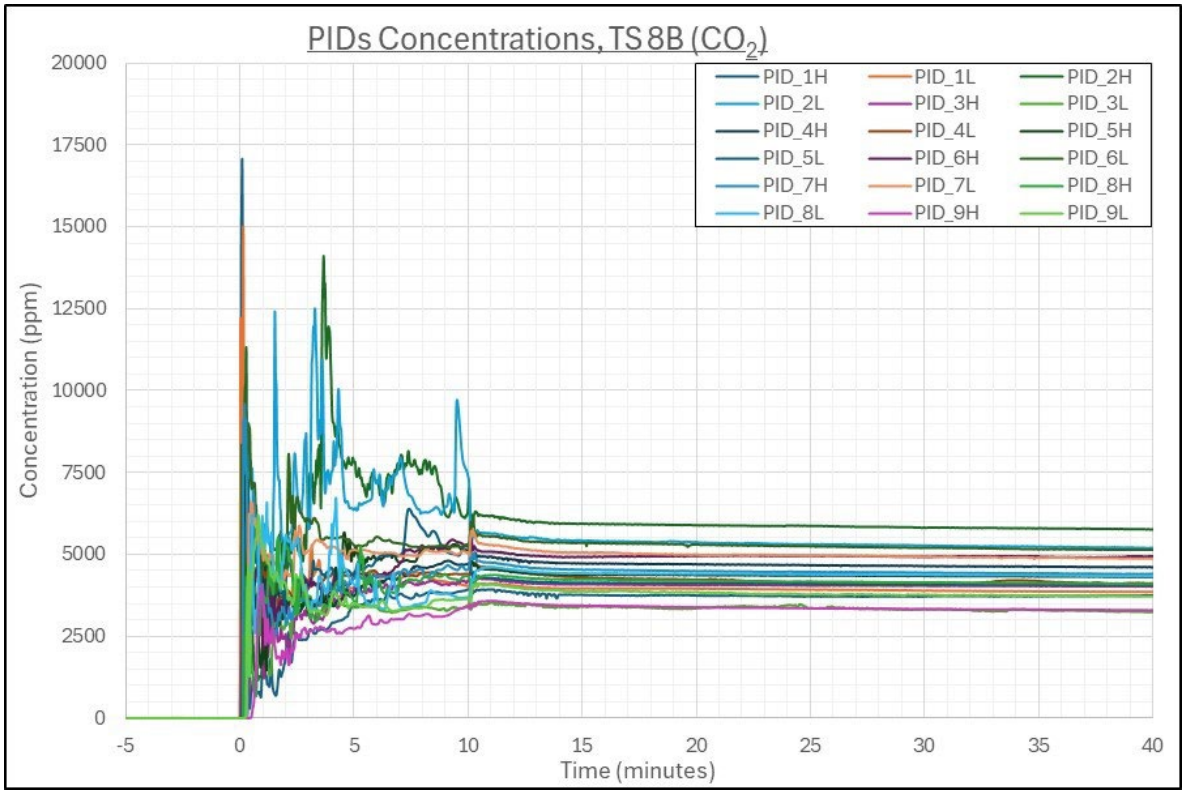

Figure D-39. Overlay of individual PID concentration time series, TS 8B.

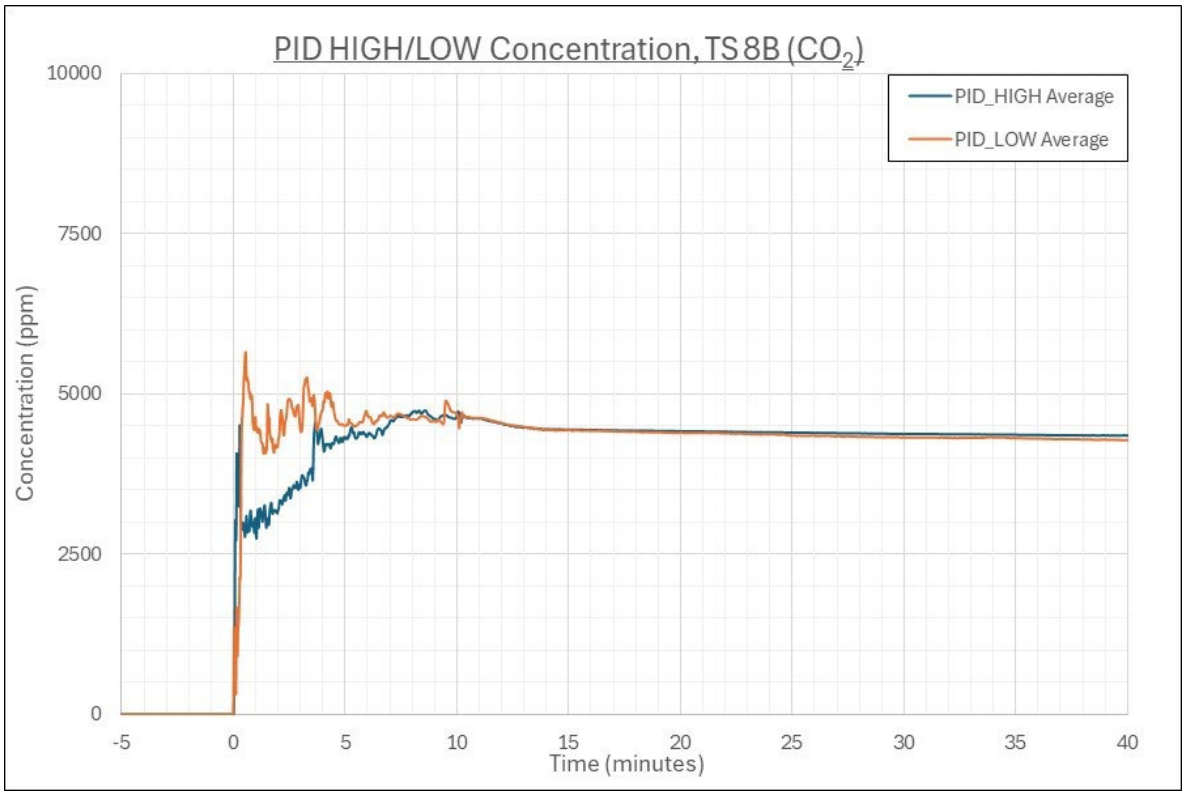

Figure D-40. Average concentration time series for HIGH PIDs and LOW PIDs, TS 8B.

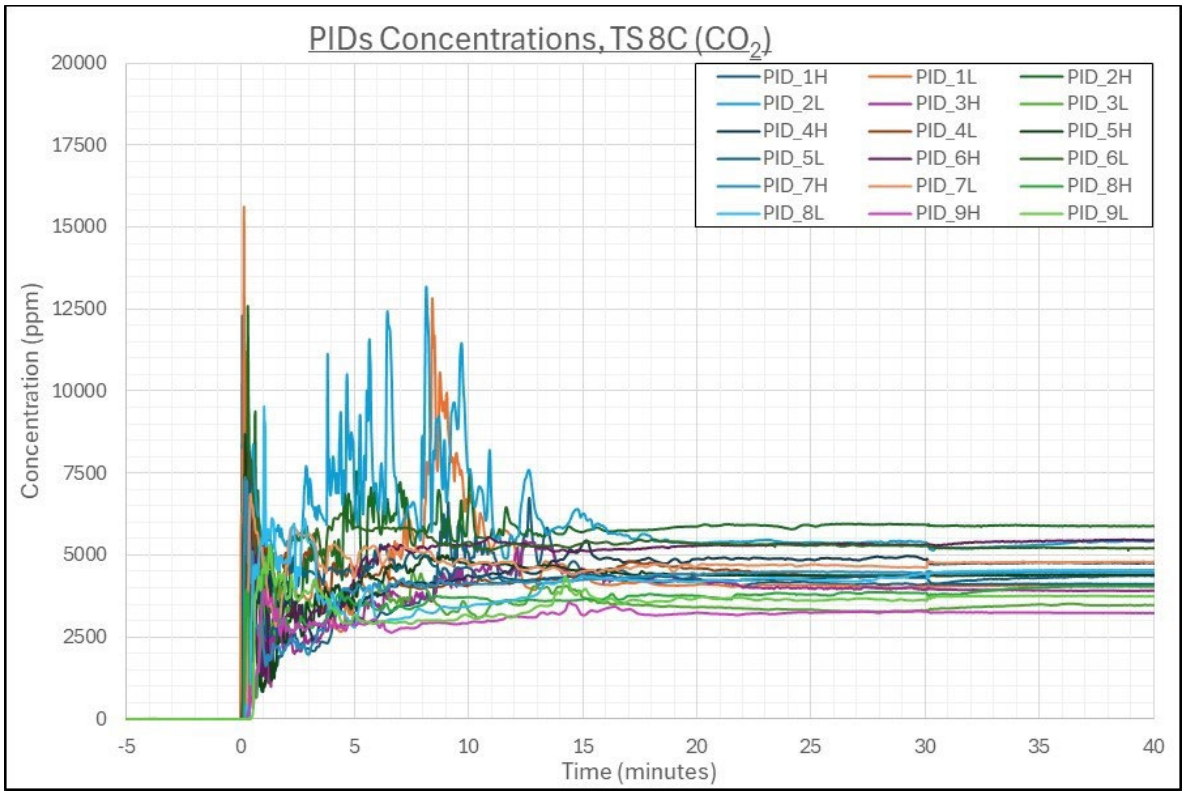

Figure D-41. Overlay of individual PID concentration time series, TS 8C.

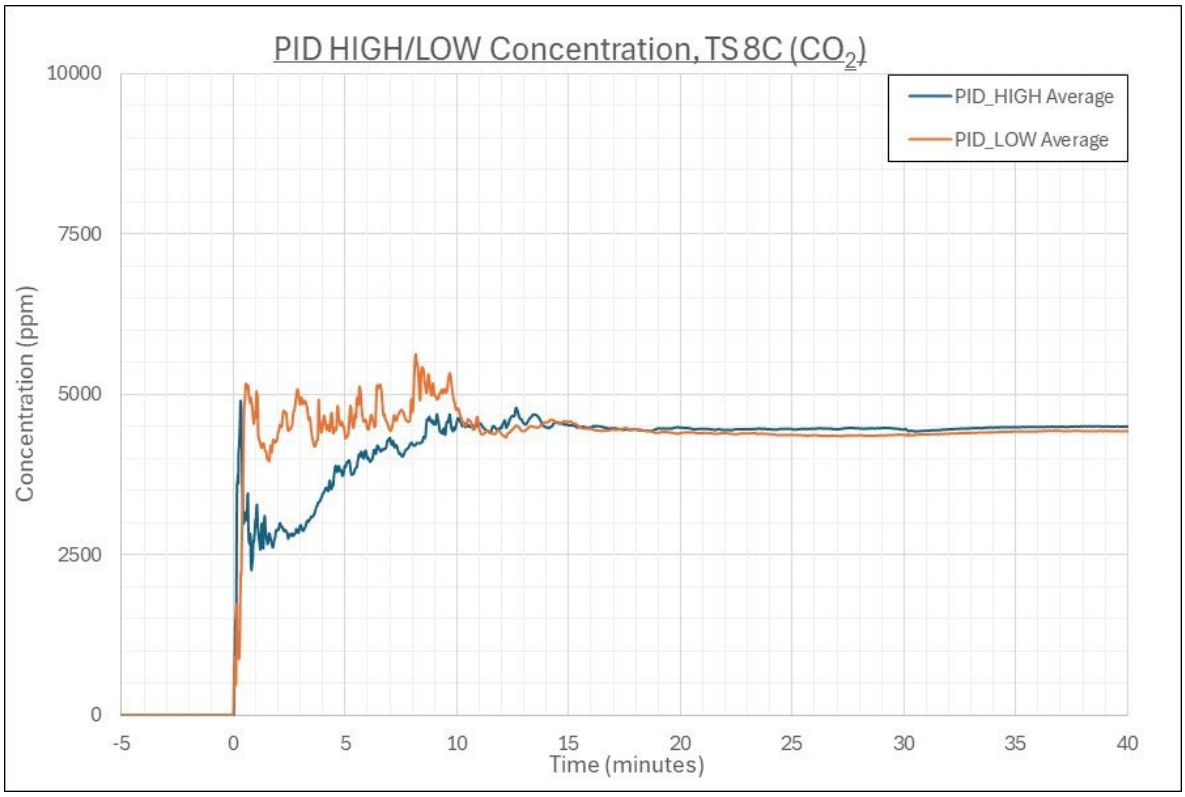

Figure D-42. Average concentration time series for HIGH PIDs and LOW PIDs, TS 8C.

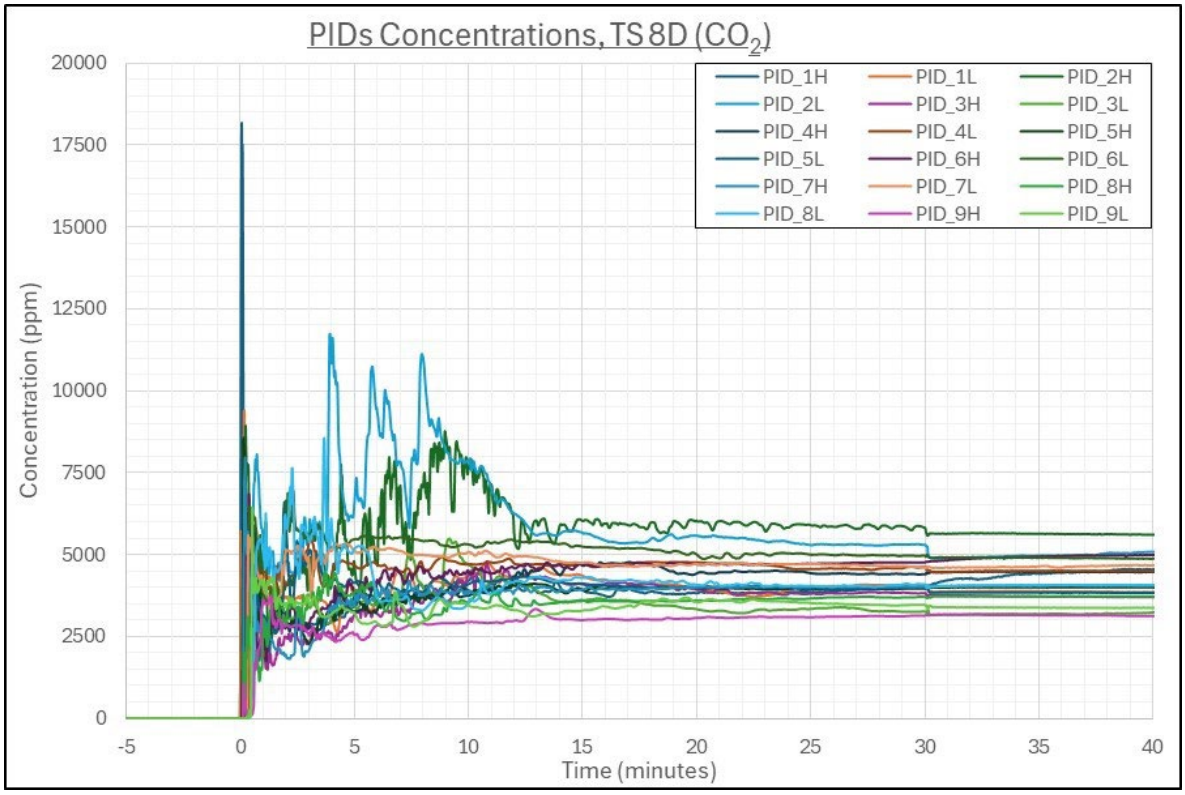

Figure D-43. Overlay of individual PID concentration time series, TS 8D.

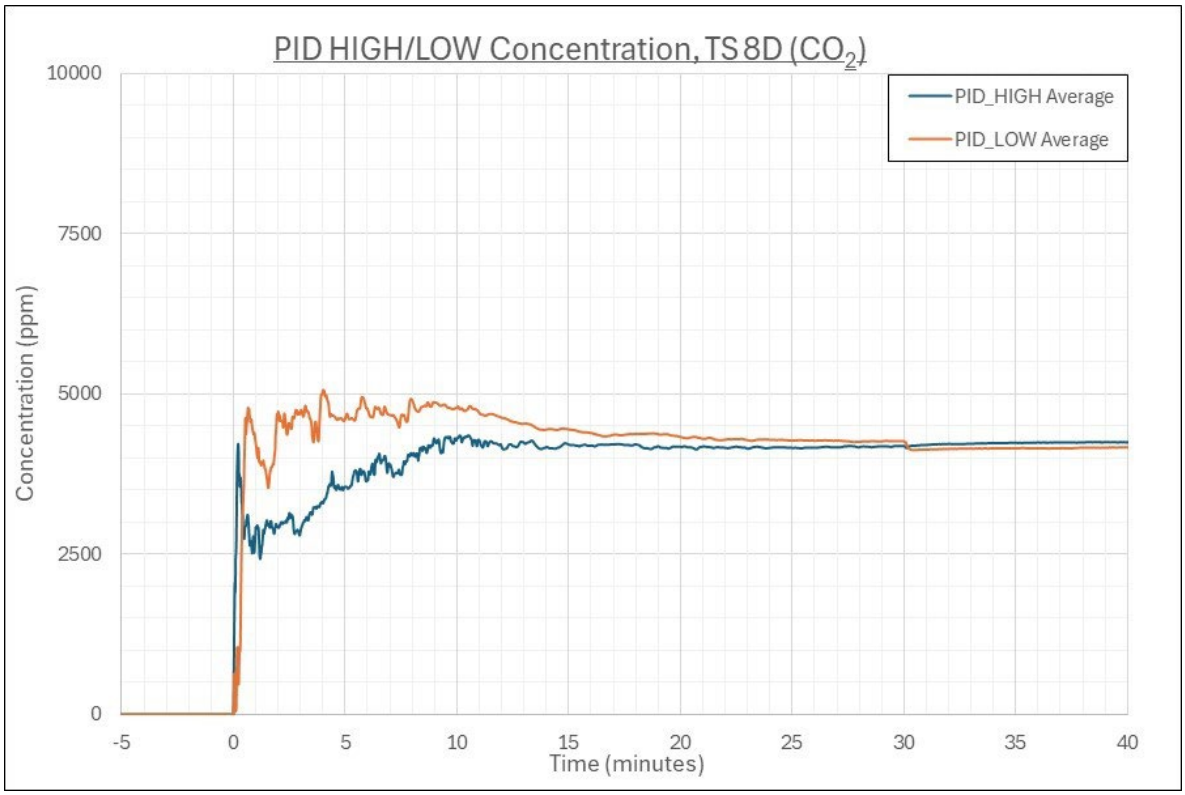

Figure D-44. Average concentration time series for HIGH PIDs and LOW PIDs, TS 8D.

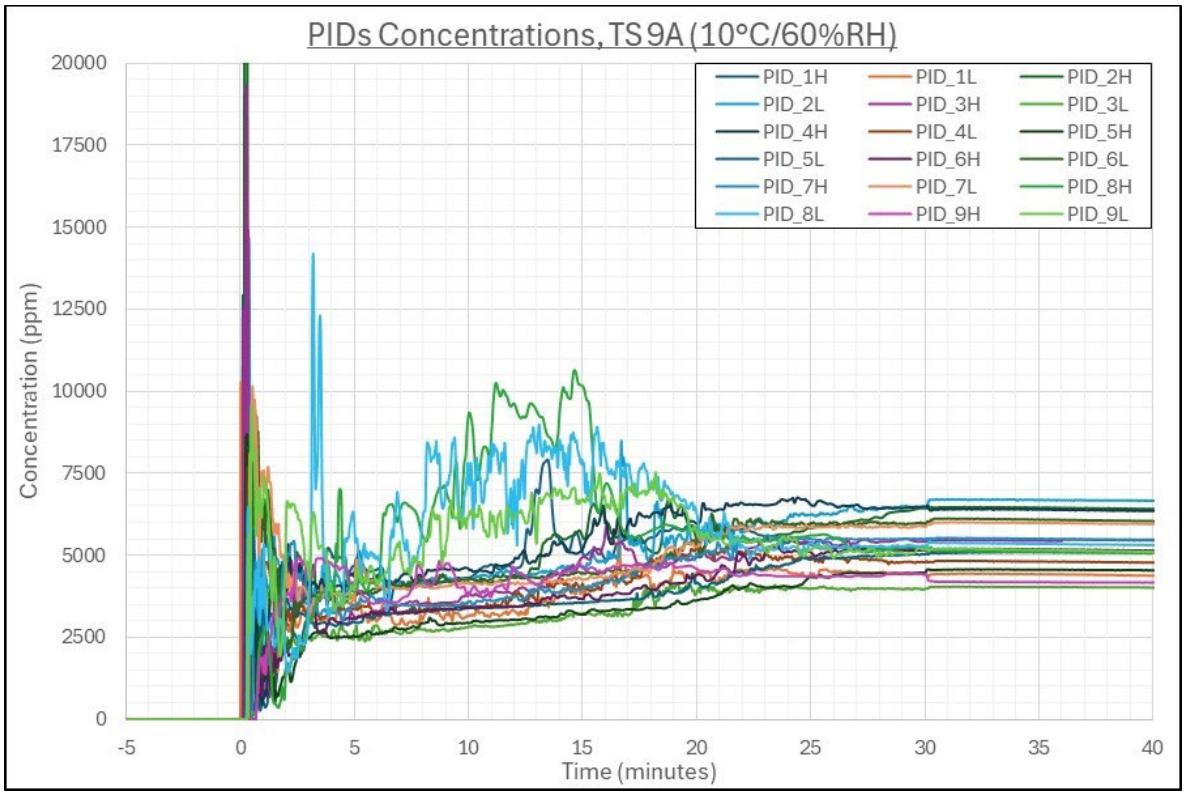

Figure D-45. Overlay of individual PID concentration time series, TS 9A.

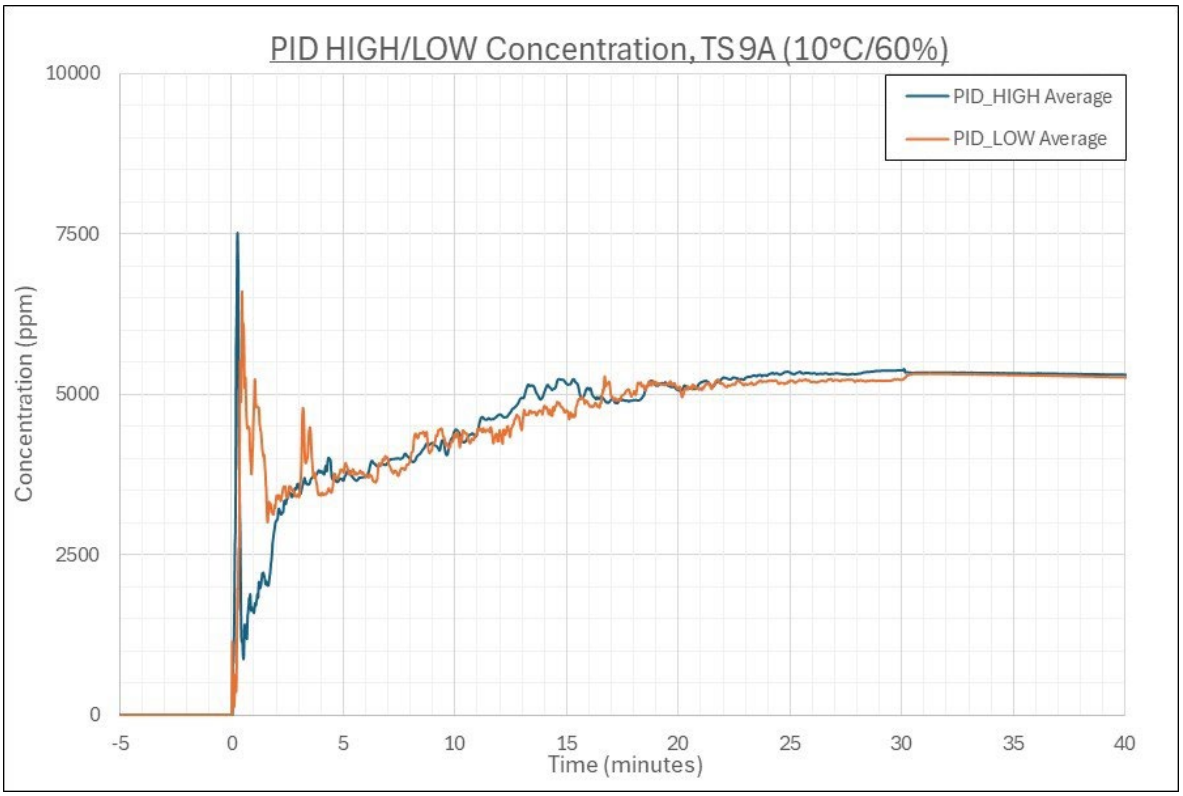

Figure D-46. Average concentration time series for HIGH PIDs and LOW PIDs, TS 9A.

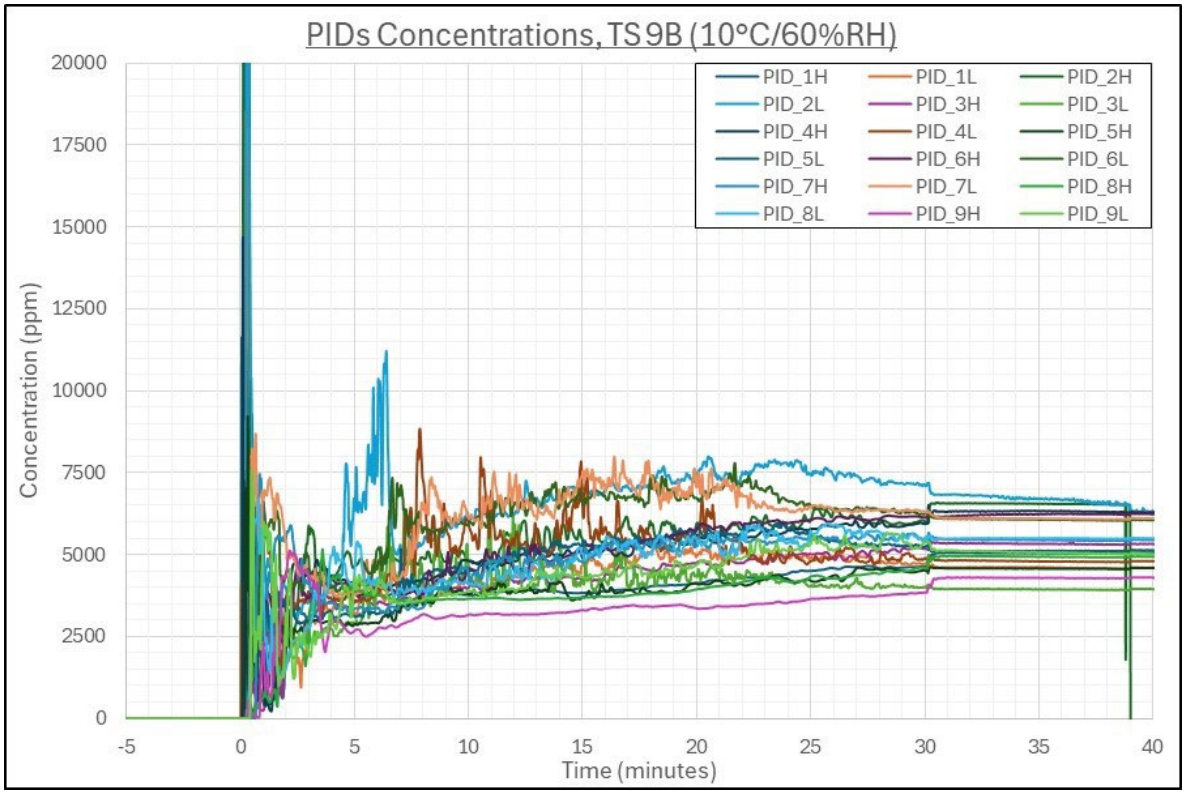

Figure D-47. Overlay of individual PID concentration time series, TS 9B.

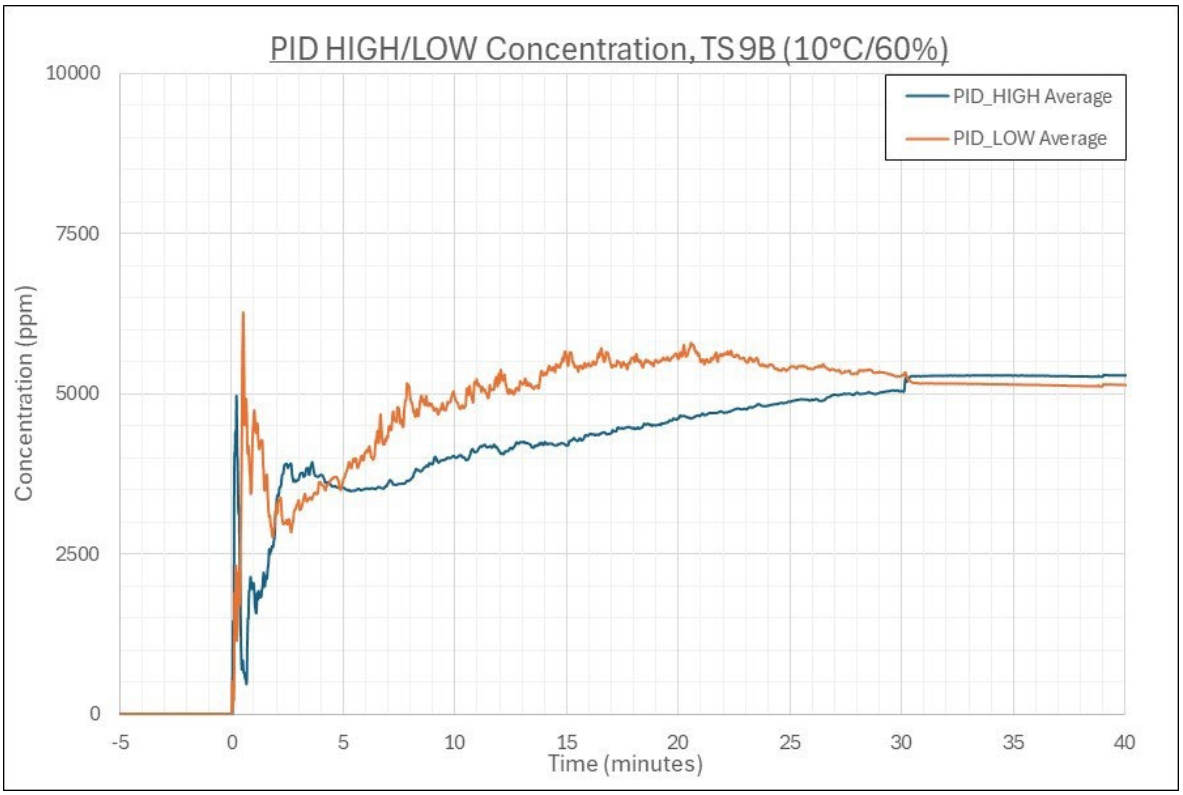

Figure D-48. Average concentration time series for HIGH PIDs and LOW PIDs, TS 9B.

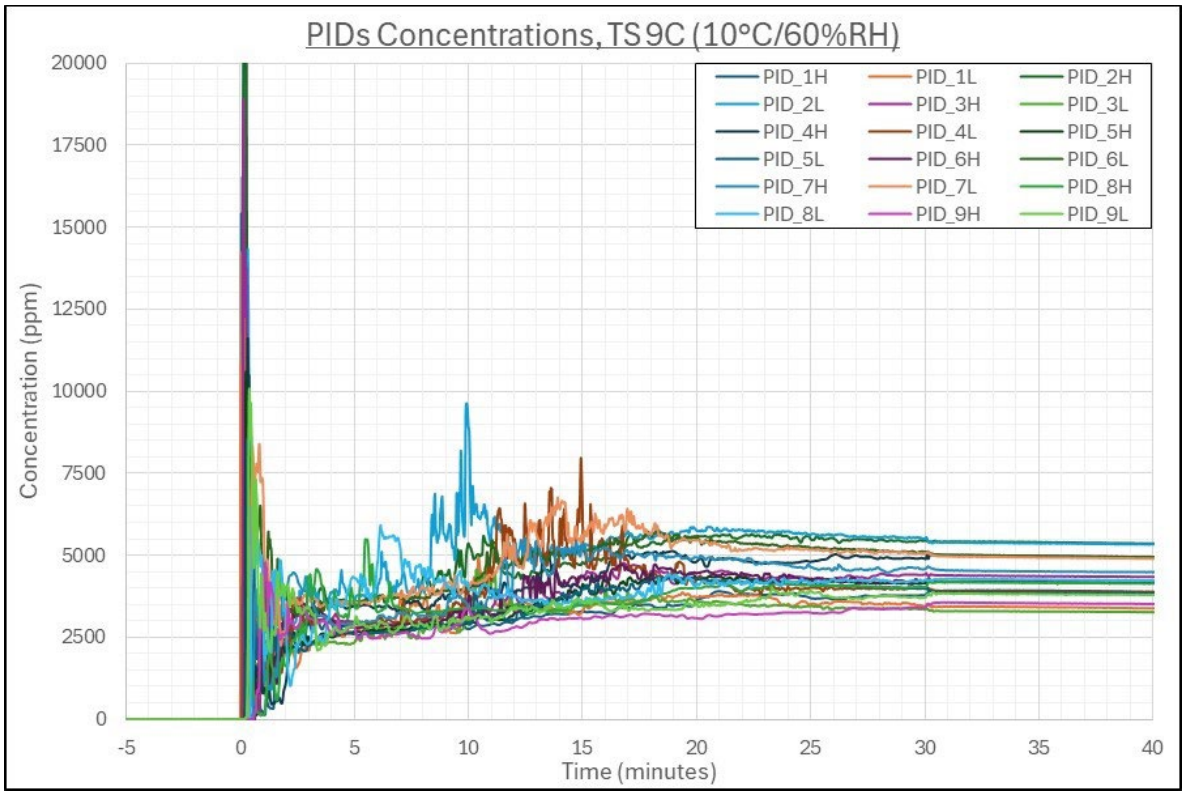

Figure D-49. Overlay of individual PID concentration time series, TS 9C.

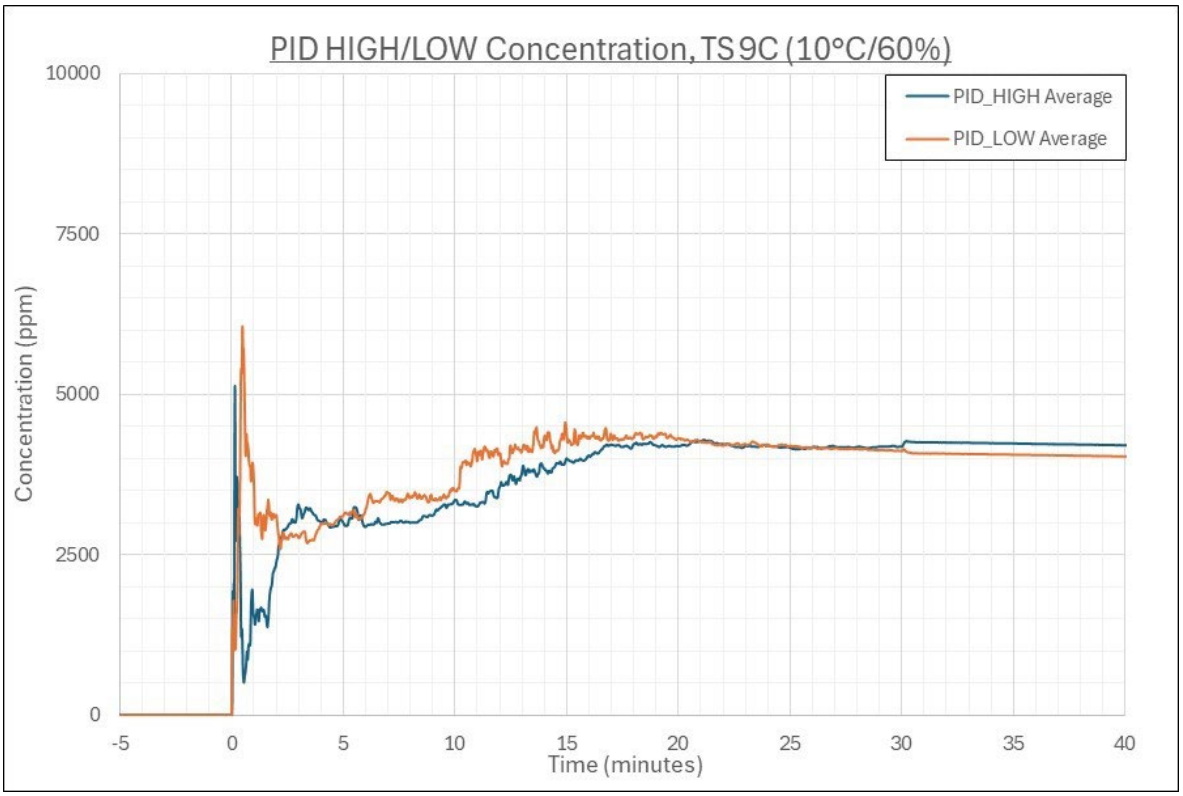

Figure D-50. Average concentration time series for HIGH PIDs and LOW PIDs, TS 9C.

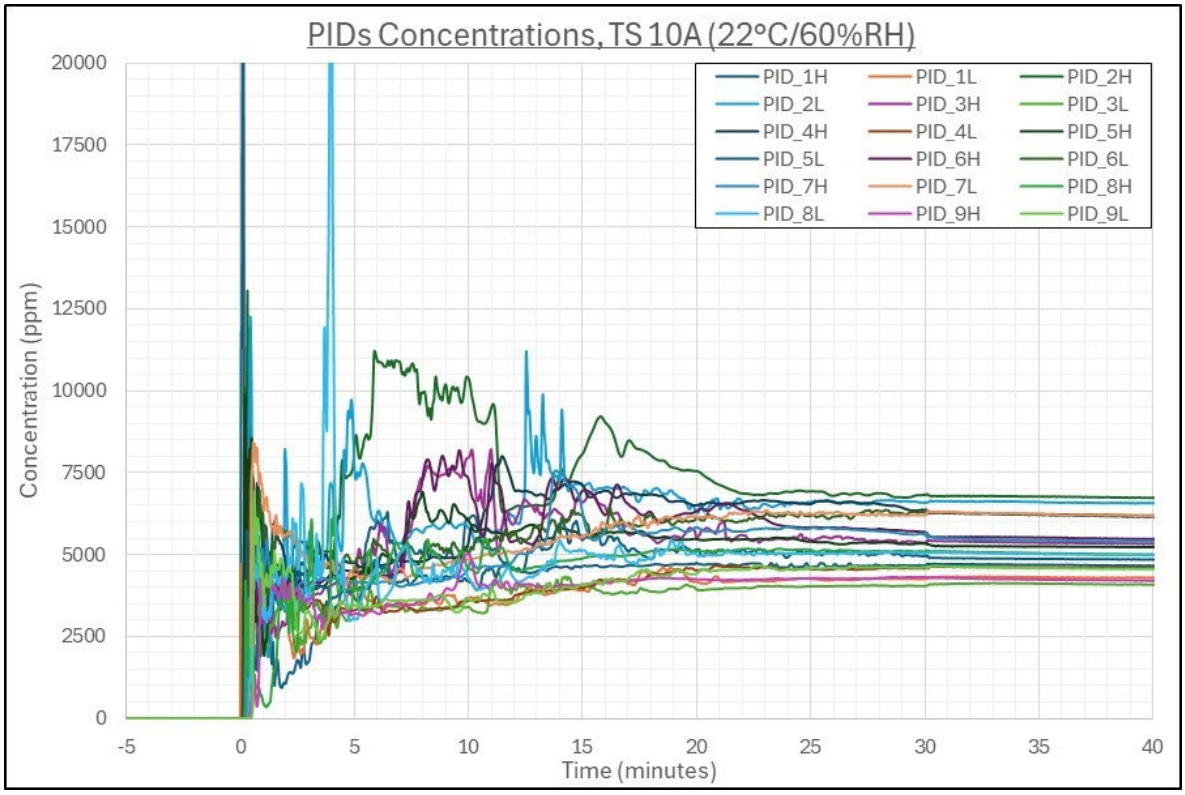

Figure D-51. Overlay of individual PID concentration time series, TS 10A.

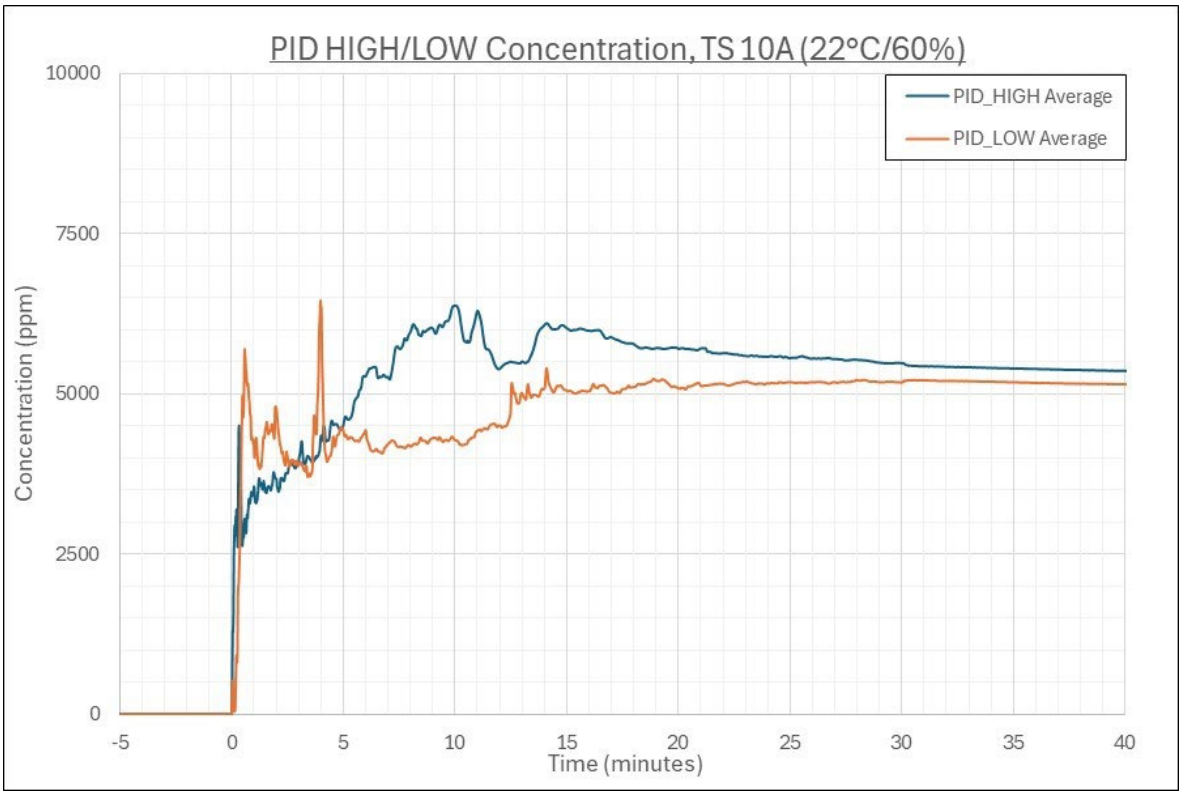

Figure D-52. Average concentration time series for HIGH PIDs and LOW PIDs, TS 10A.

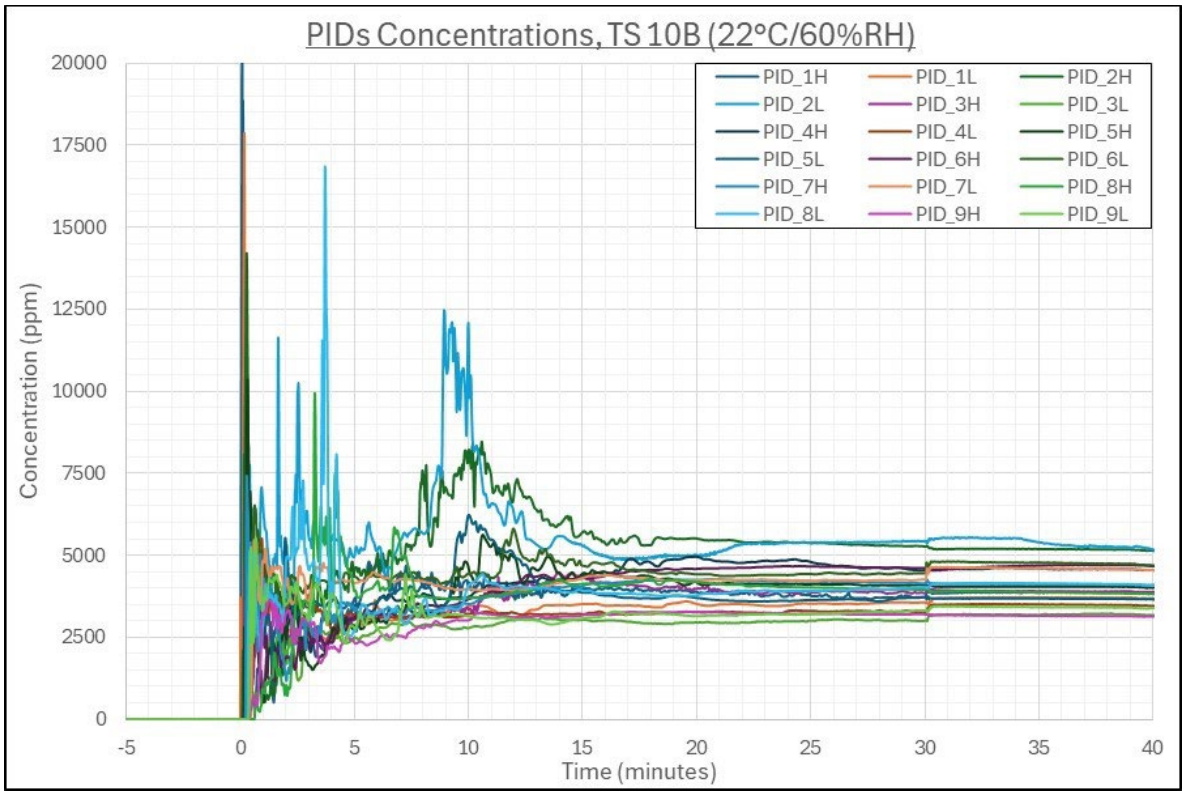

Figure D-53. Overlay of individual PID concentration time series, TS 10B.

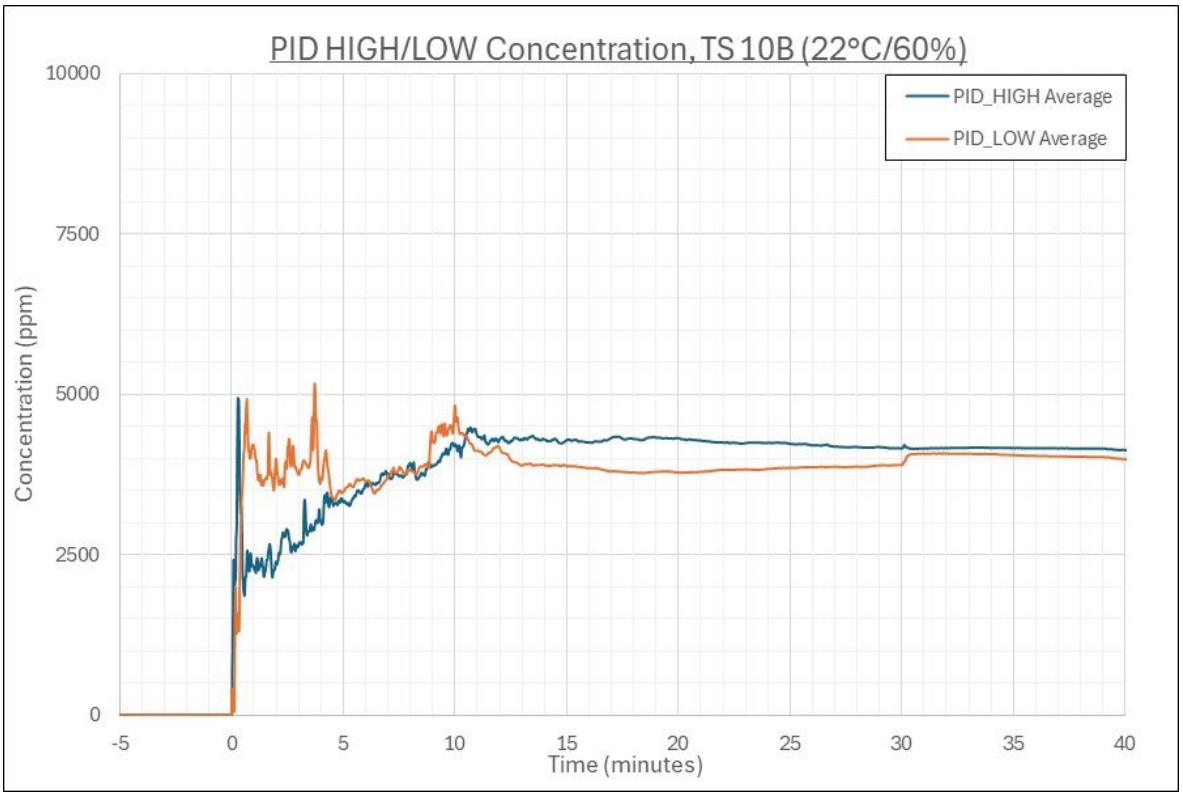

Figure D-54. Average concentration time series for HIGH PIDs and LOW PIDs, TS 10B.

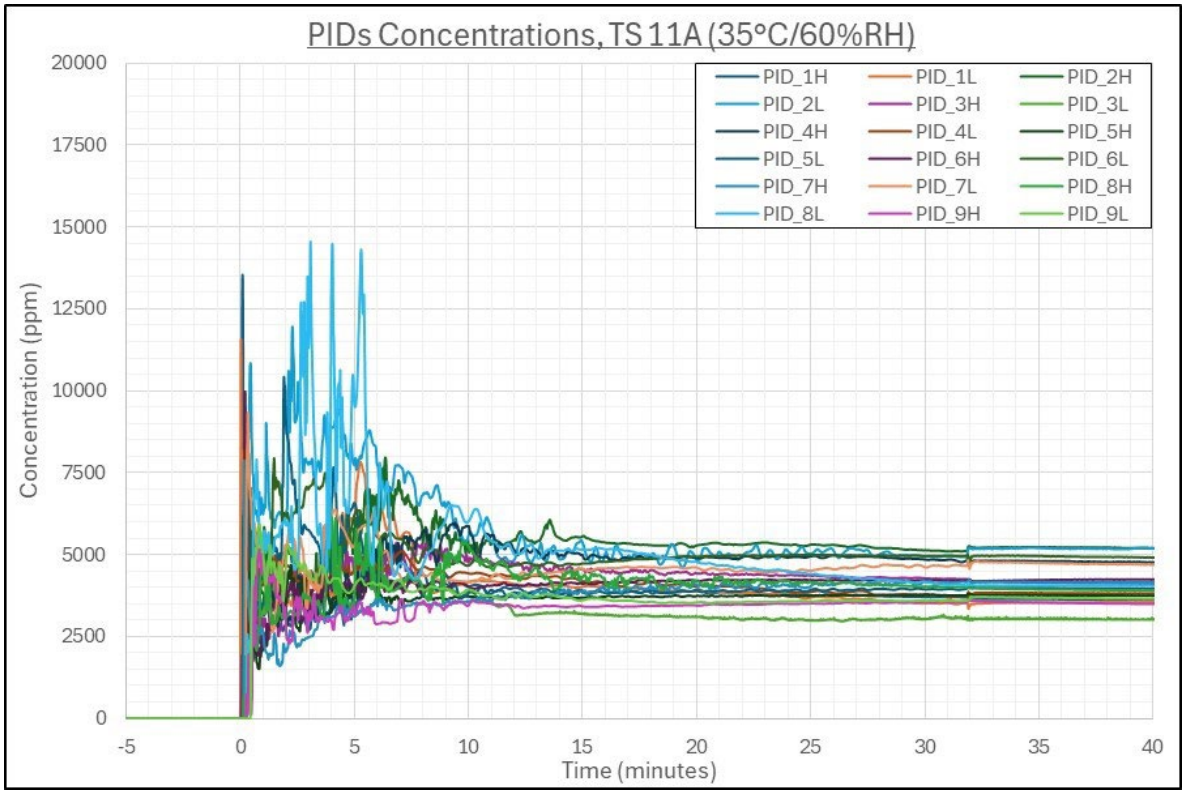

Figure D-55. Overlay of individual PID concentration time series, TS 11A.

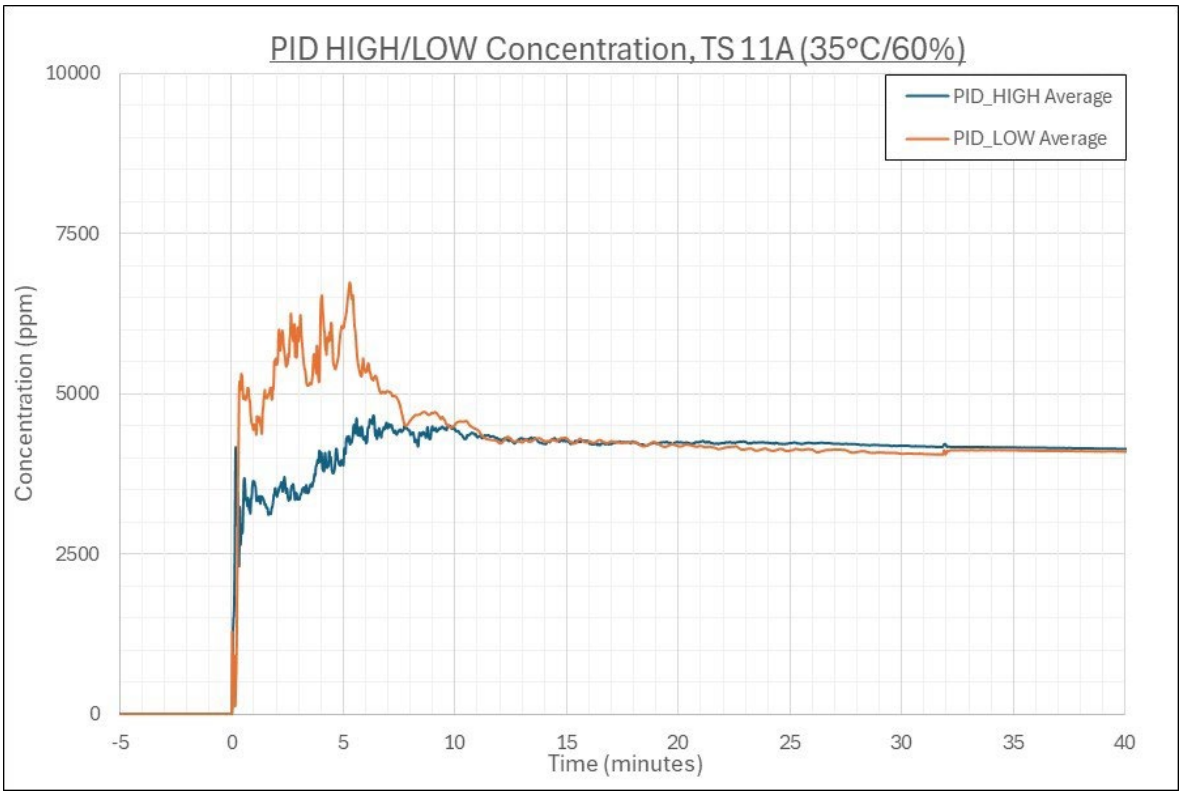

Figure D-56. Average concentration time series for HIGH PIDs and LOW PIDs, TS 11A.

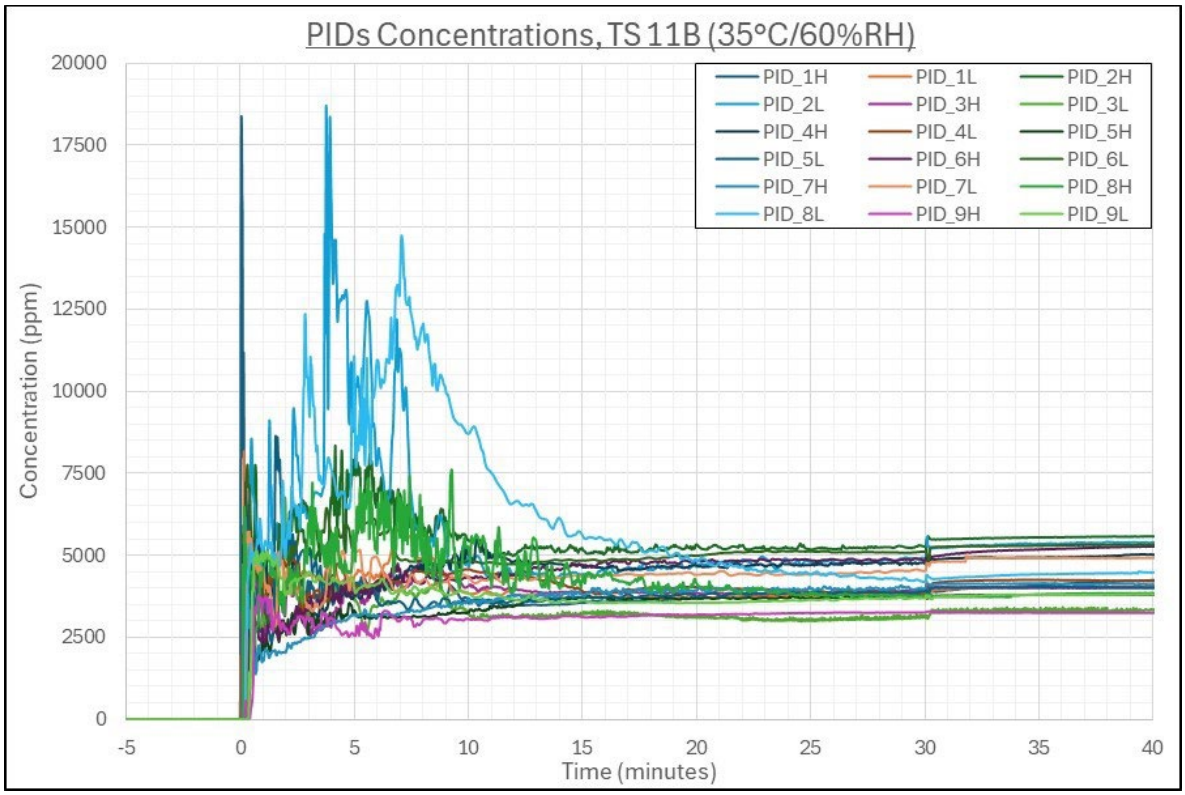

Figure D-57. Overlay of individual PID concentration time series, TS 11B.

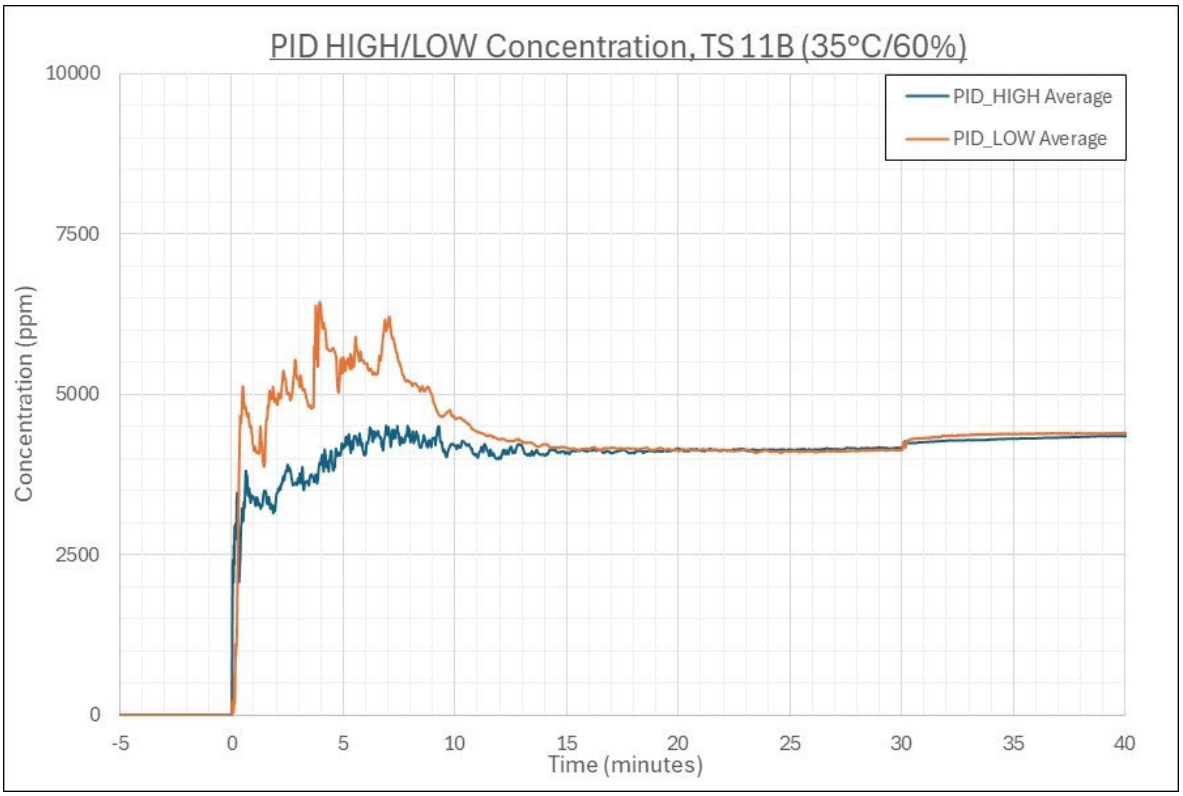

Figure D-58. Average concentration time series for HIGH PIDs and LOW PIDs, TS 11B.

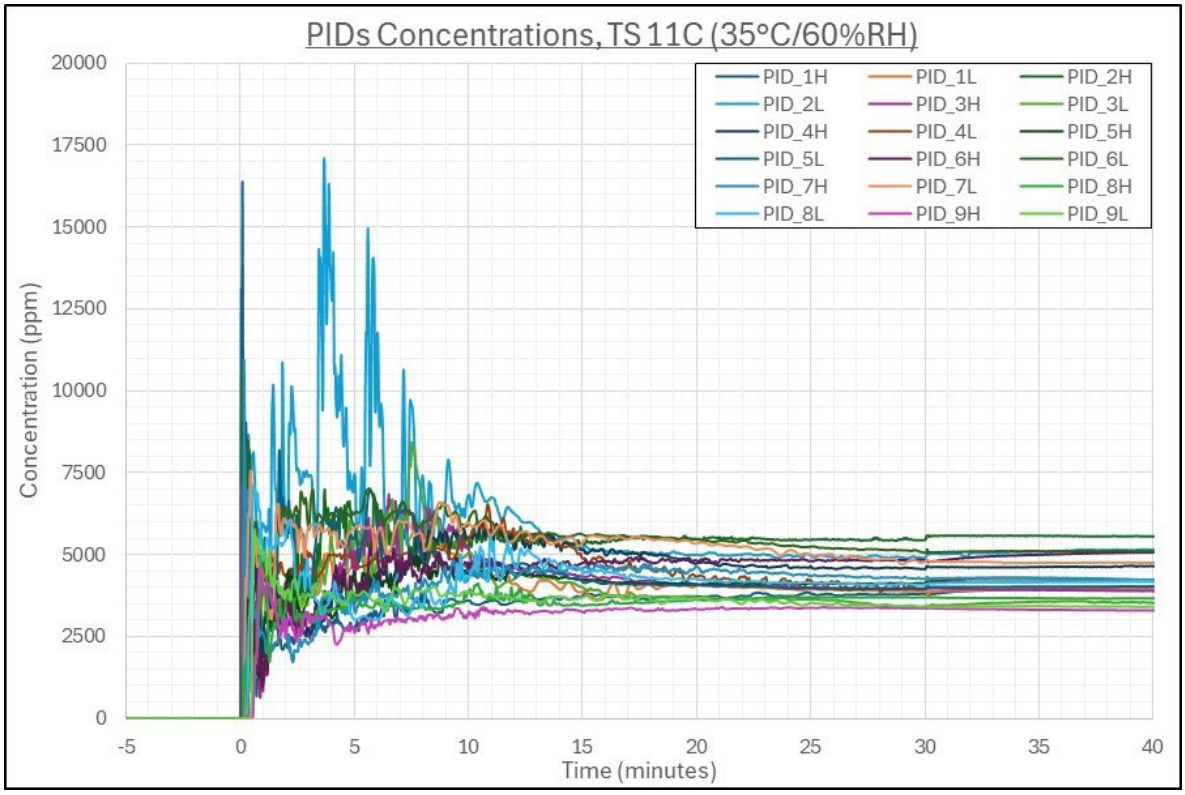

Figure D-59. Overlay of individual PID concentration time series, TS 11C.

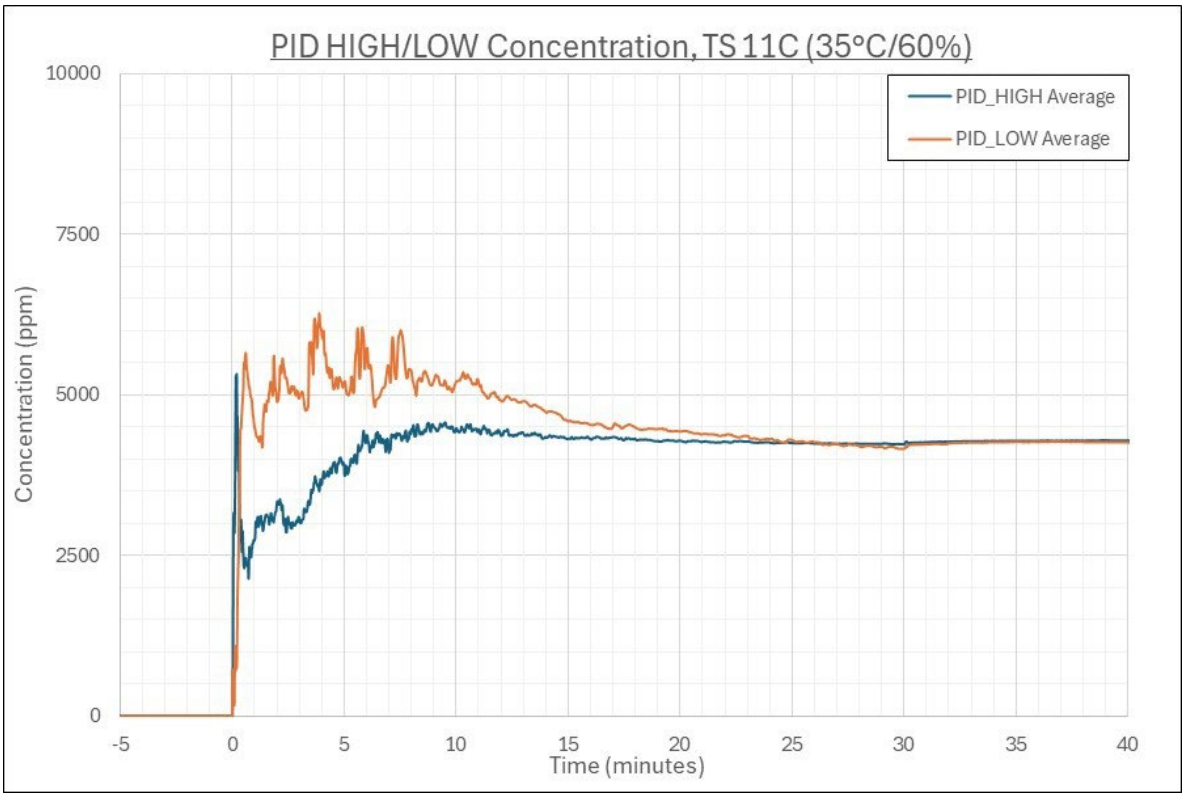

Figure D-60. Average concentration time series for HIGH PIDs and LOW PIDs, TS 11C.

This page intentionally left blank.

APPENDIX E: AIR DENSITY PLOTS

This page intentionally left blank.

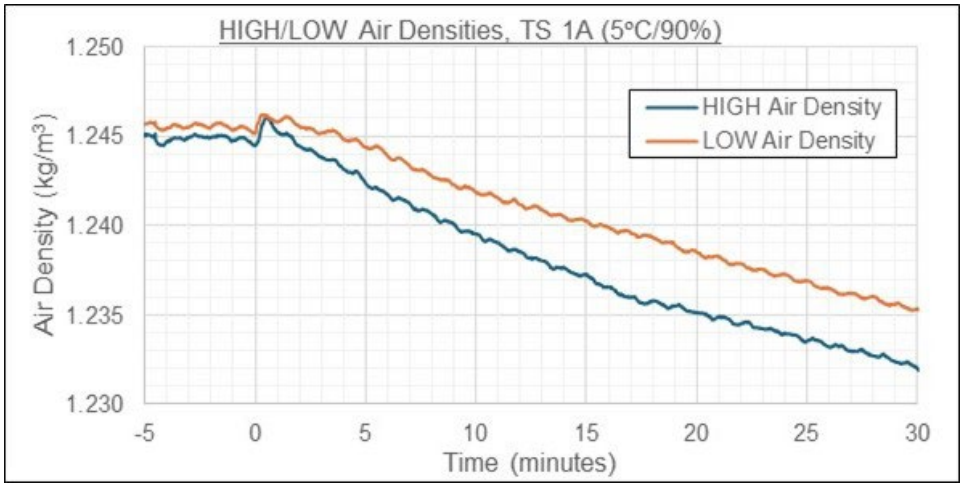

Figure E-1. HIGH and LOW air density time series, TS 1A.

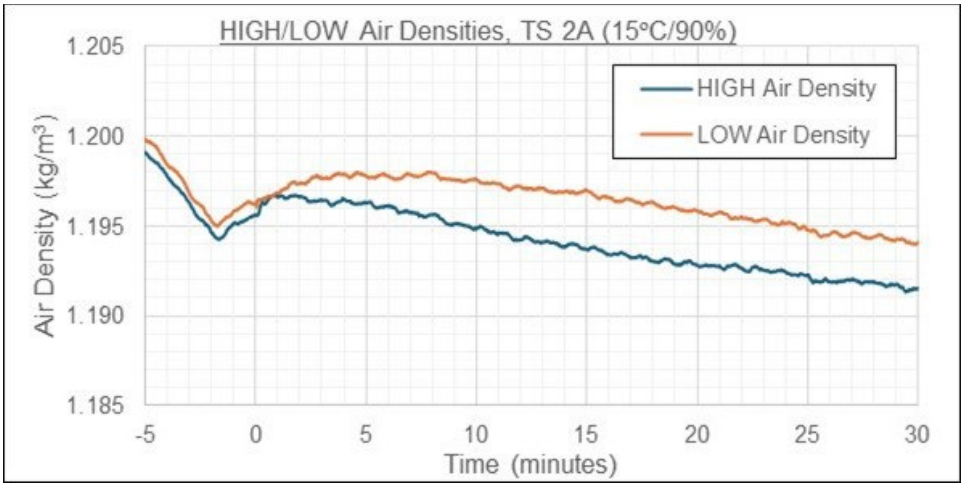

Figure E-2. HIGH and LOW air density time series, TS 2A.

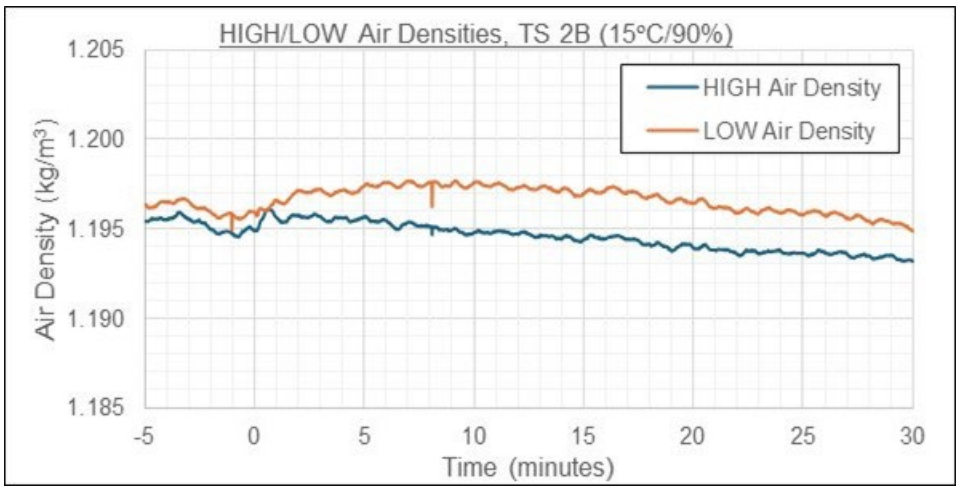

Figure E-3. HIGH and LOW air density time series, TS 2B.

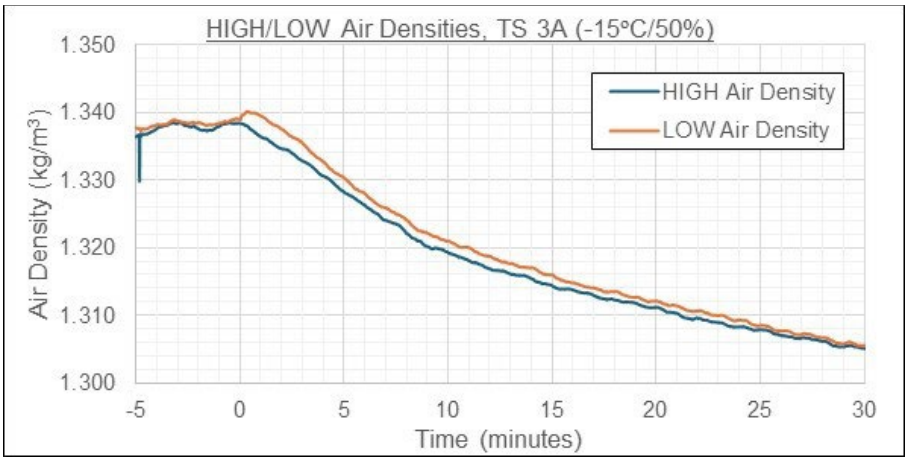

Figure E-4. HIGH and LOW air density time series, TS 3A.

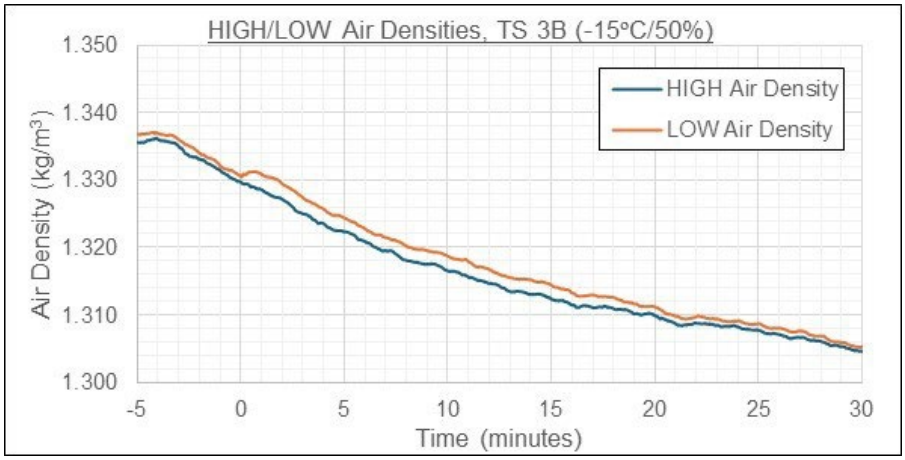

Figure E-5. HIGH and LOW air density time series, TS 3B.

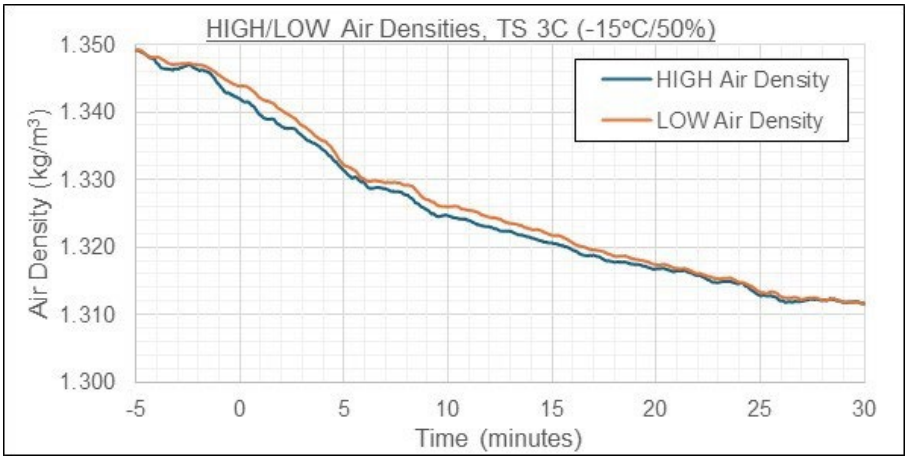

Figure E-6. HIGH and LOW air density time series, TS 3C.

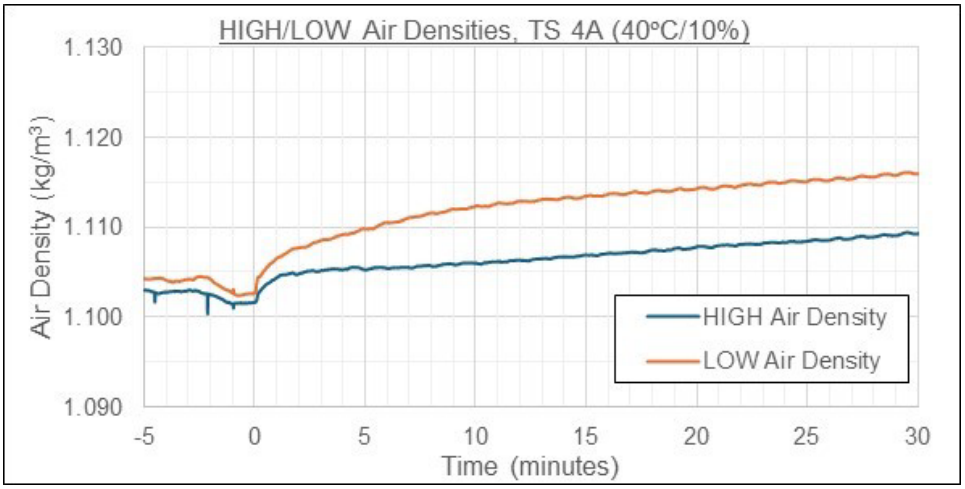

Figure E-7. HIGH and LOW air density time series, TS 4A.

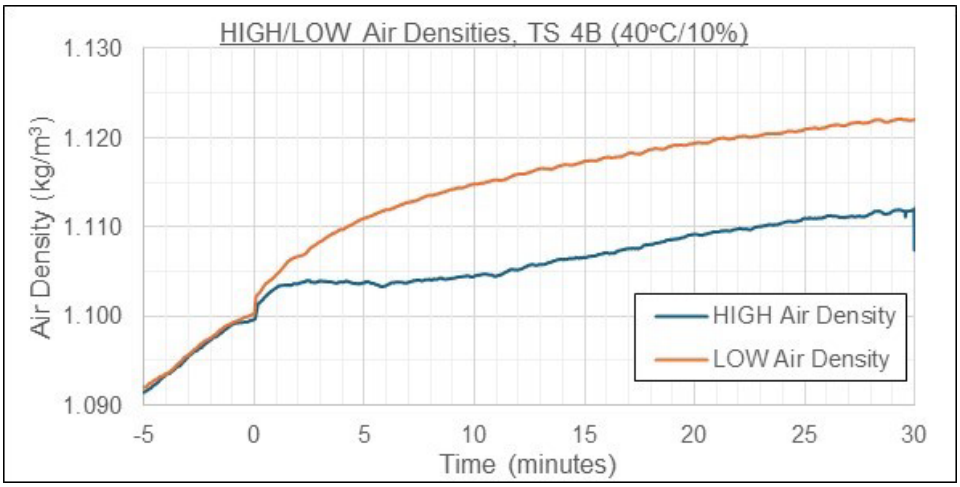

Figure E-8. HIGH and LOW air density time series, TS 4B.

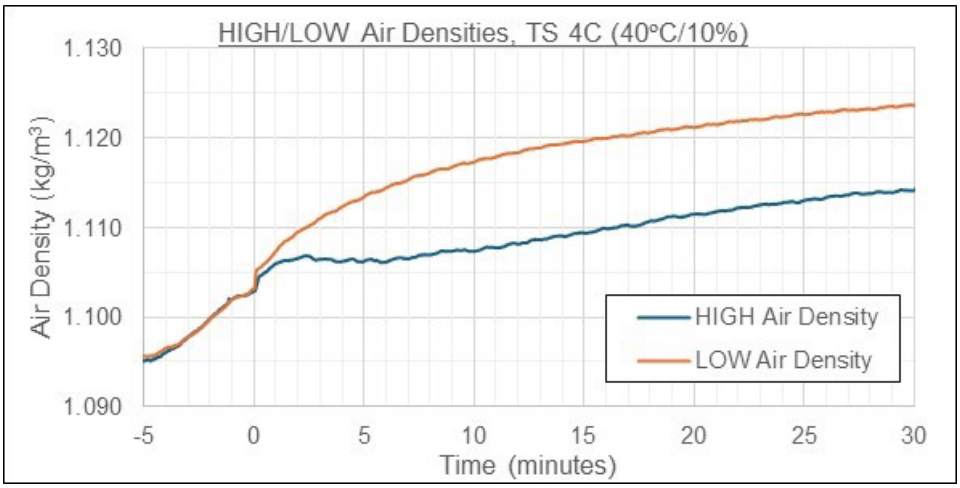

Figure E-9. HIGH and LOW air density time series, TS 4C.

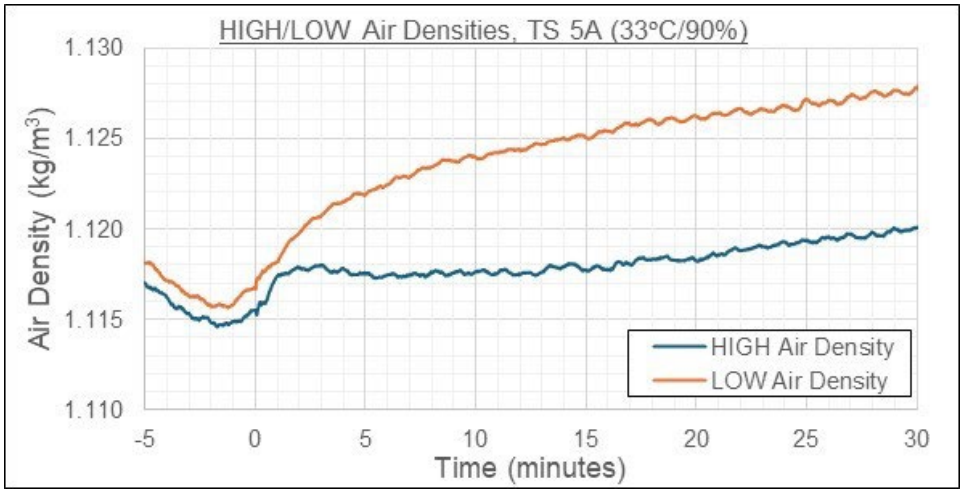

Figure E-10. HIGH and LOW air density time series, TS 5A.

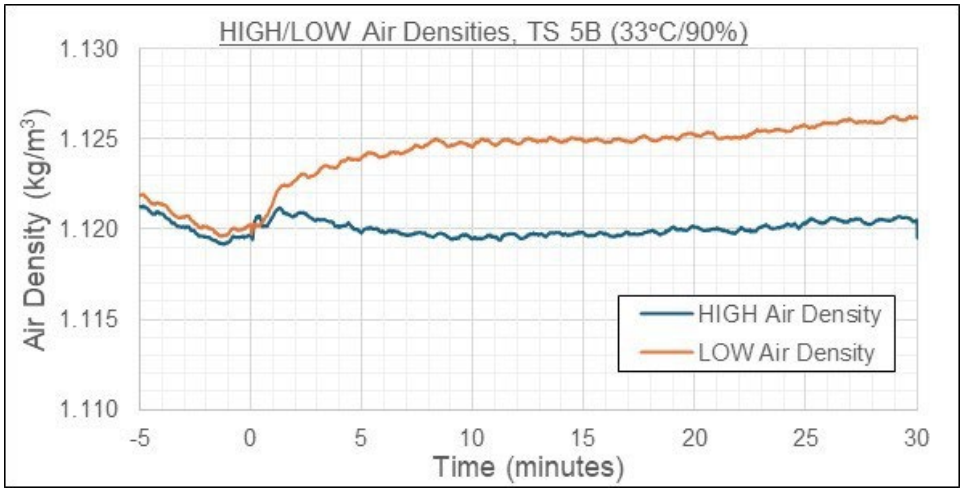

Figure E-11. HIGH and LOW air density time series, TS 5B.

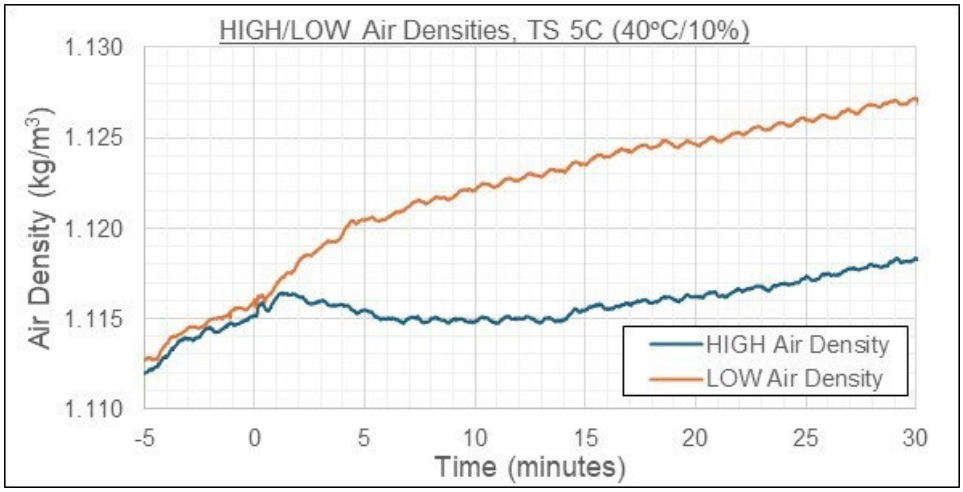

Figure E-12. HIGH and LOW air density time series, TS 5C.

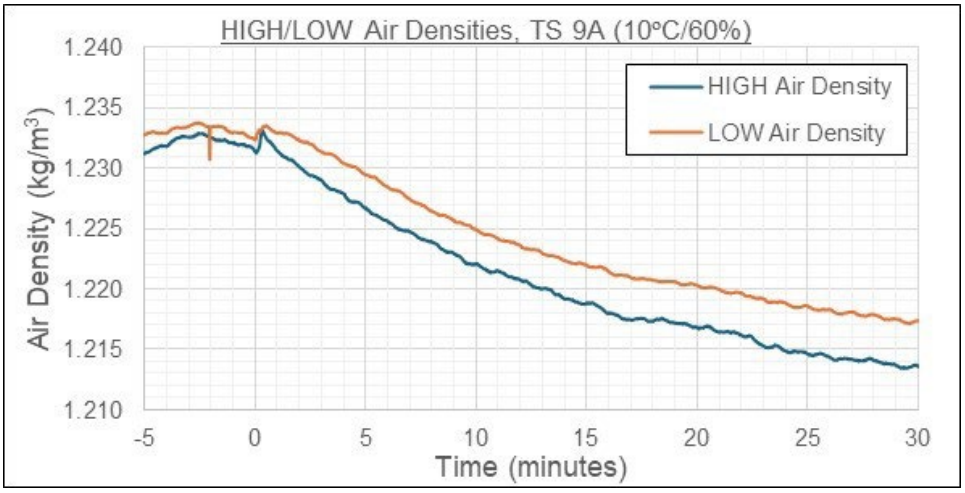

Figure E-13. HIGH and LOW air density time series, TS 9A.

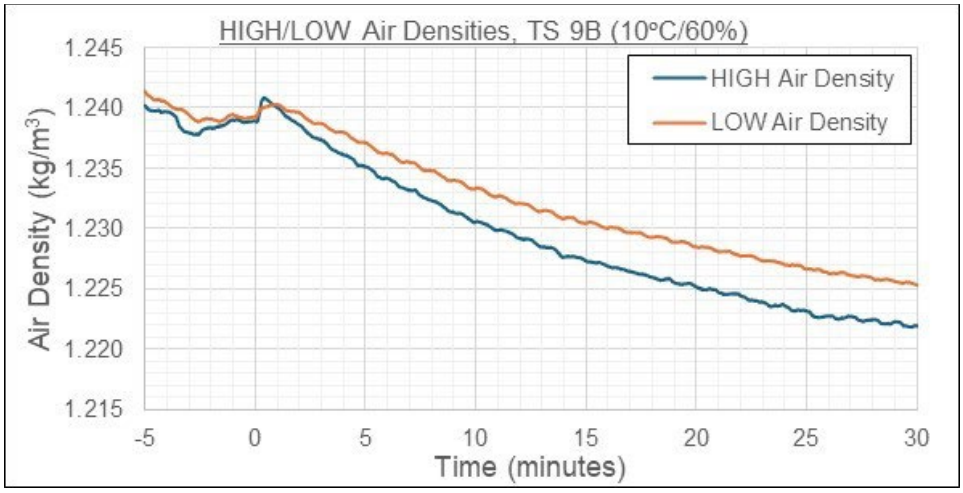

Figure E-14. HIGH and LOW air density time series, TS 9B.

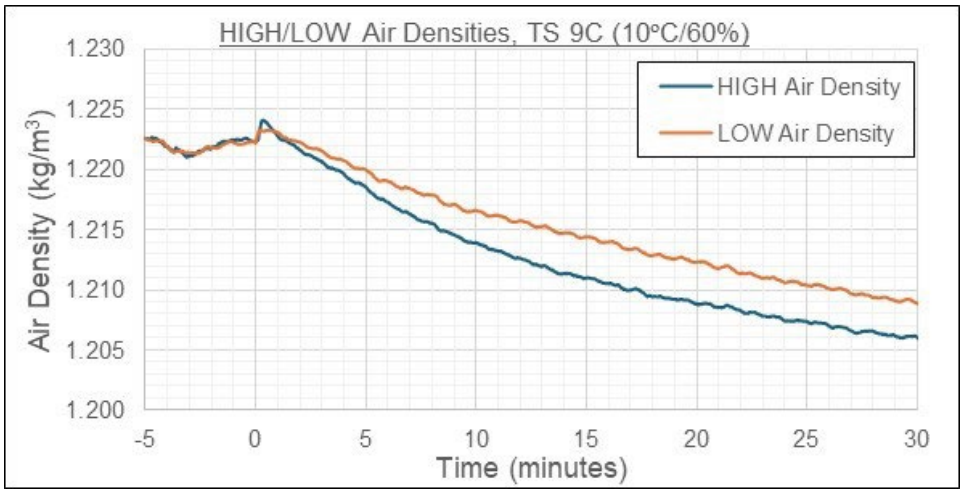

Figure E-15. HIGH and LOW air density time series, TS 9C.

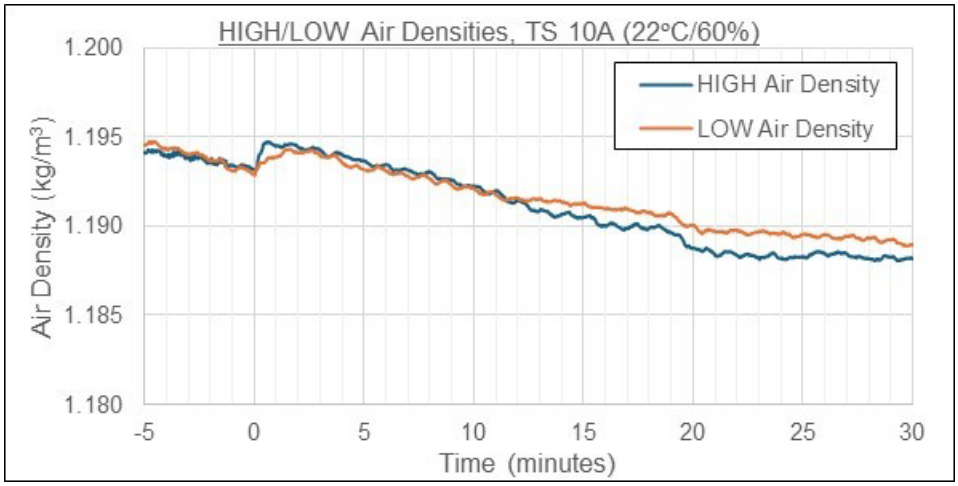

Figure E-16. HIGH and LOW air density time series, TS 10A.

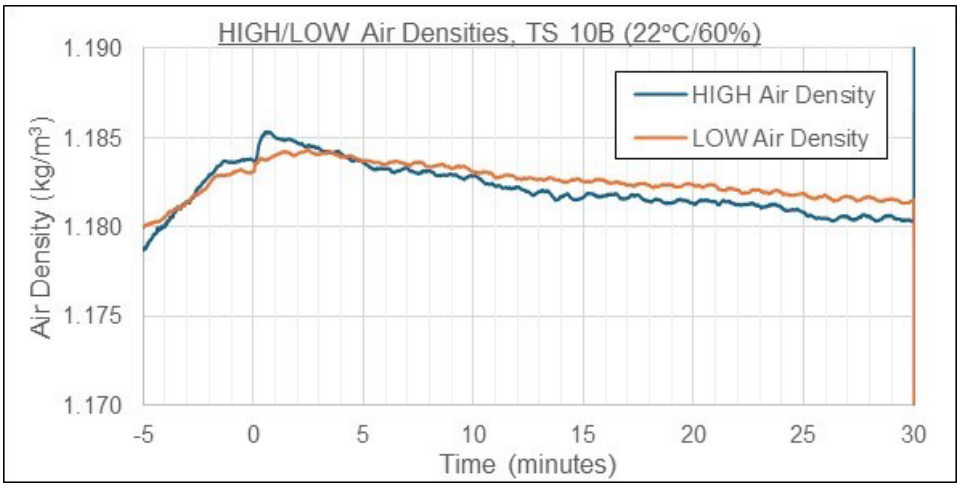

Figure E-17. HIGH and LOW air density time series, TS 10B.

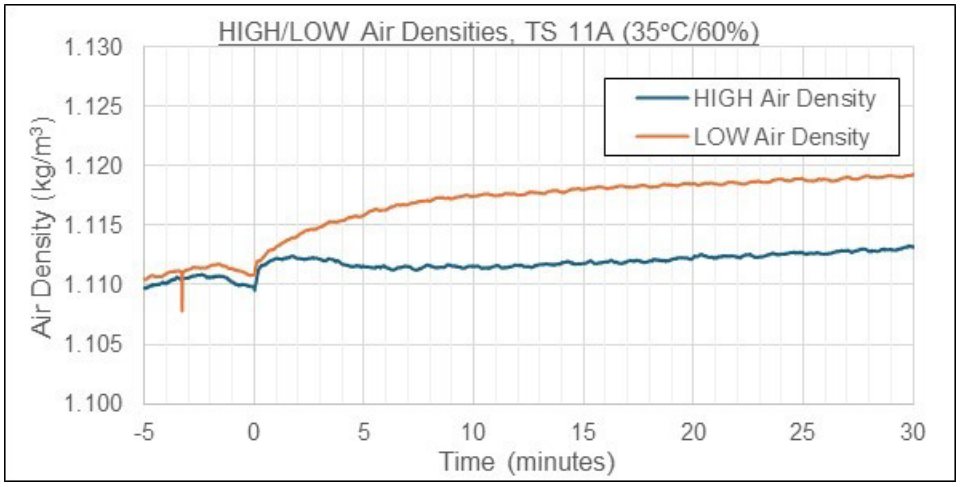

Figure E-18. HIGH and LOW air density time series, TS 11A.

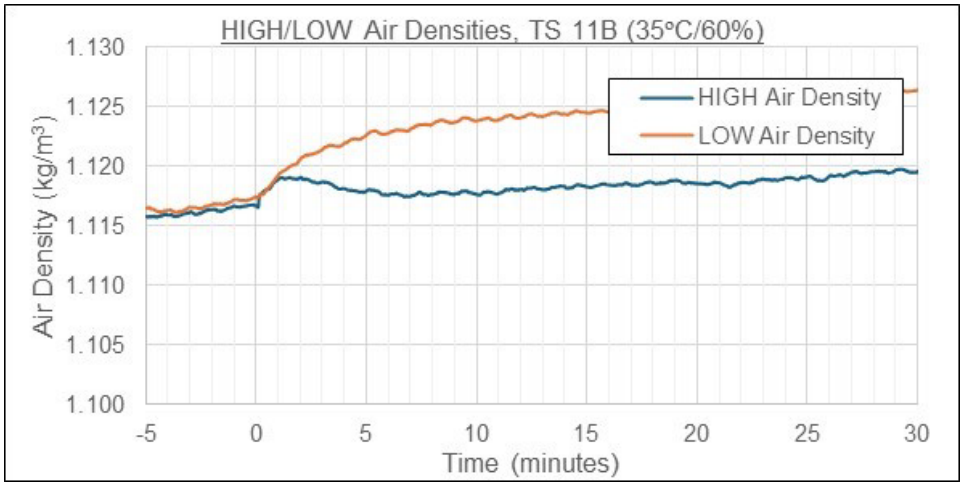

Figure E-19. HIGH and LOW air density time series, TS 11B.

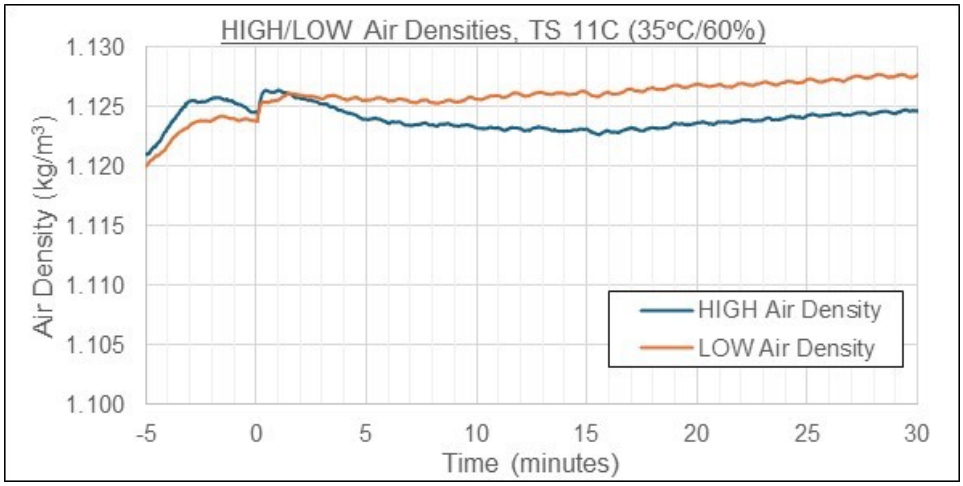

Figure E-20. HIGH and LOW air density time series, TS 11C.

This page intentionally left blank.

APPENDIX F: WATER SENSITIVE PAPER CARDS

This page intentionally left blank.

Water sensitive paper (WSP) cards were integrated into the test environment during TSs 9/10/11 to evaluate the formation of drops from water vapor condensation during the release event and ammonia plume dispersion. The WSP cards (3.00” (7.62 cm) W x 1.00” (2.54 cm) H) were bright yellow and turned permanent blue upon contact with water; they were placed in the test environment according to **Figure F-1**.

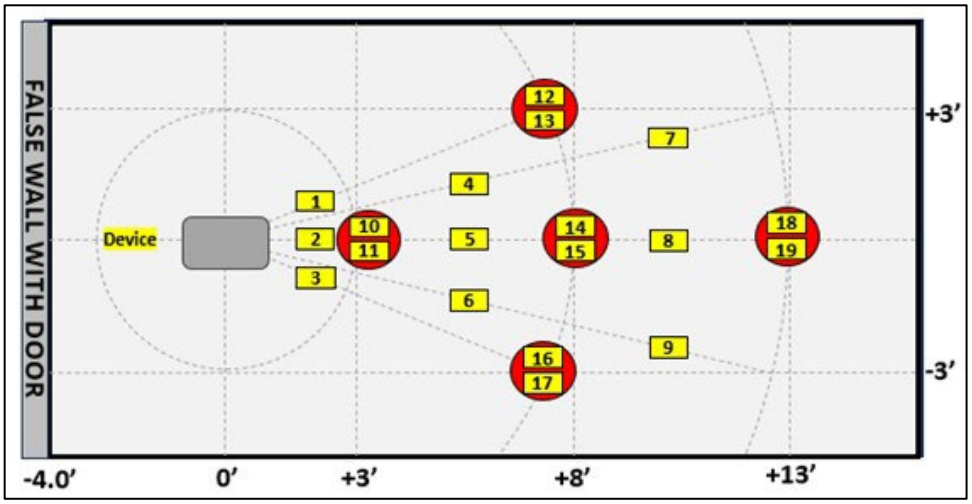

Figure F-1. WSP layout in test environment, TSs 9/10/11.

WSP cards 1–9 were placed on the test environment floor and cards 10–19 were placed on the sensor nodes at 2.0-foot (0.61 m) and 6.0-foot (1.83 m) high locations. The results were documented post-test and an example set from TS 11A is provided in **Figure F-2**. The left photograph is the WSP card set after test completion (top left: WSP 1–9 and bottom left: WSP 10–19). The right photograph is the same WSP card set 4 days later.

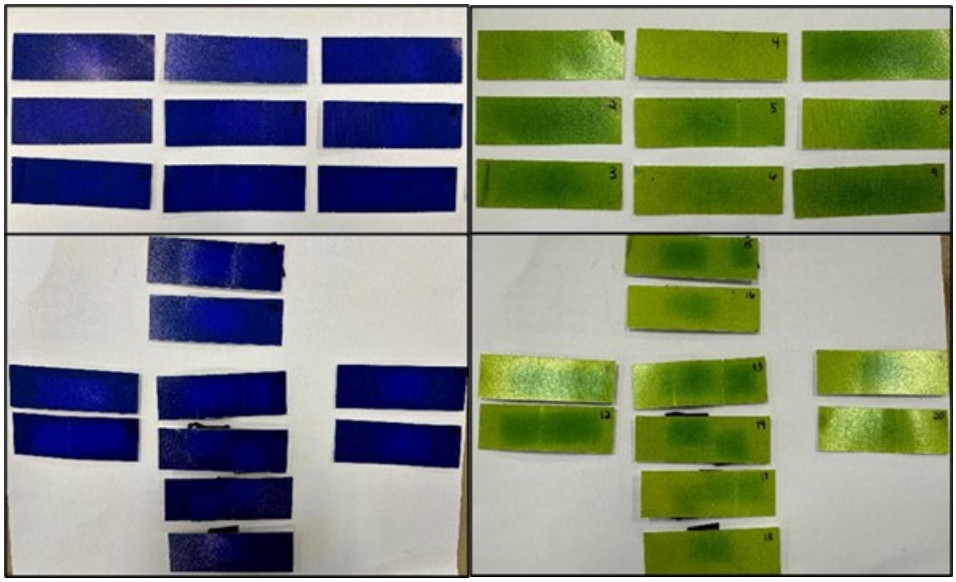

Figure F-2. WSP cards results, TS 11A, post-test (left) and 4 days later (right).

All WSP cards turned dark blue shortly after the release initiation. There were no observable water drops on the cards. It was assumed that if the blue color was formed by water vapor, then the WSP cards would permanently remain blue. The TS 11A post-test WSP cards were left at ambient conditions for 4 days and the dark blue faded back to a yellow tone. Therefore, it was believed that the ammonia caused the blue color response.

The WSP card results were validated with a side study with a post-test blue card and a pre-test yellow control card. Water drops were sprayed onto the cards to understand if the water drops could be distinguished after the cards turned blue from ammonia exposure. The results are provided in **Figure F-3**.

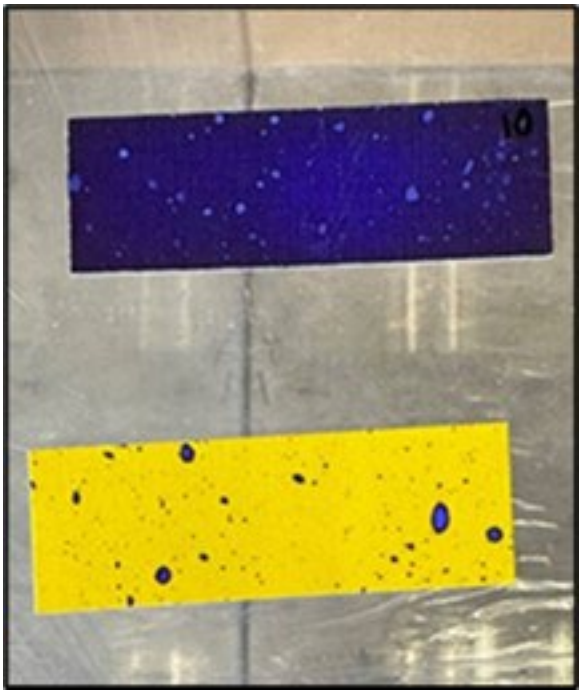

Figure F-3. WSP cards controls, post-test control (top) and pre-test control (bottom).

The water drops were clearly distinguished against the blue background and validated with the control card. Additional attempts were made to improve water drop detection. For example, Node 1 was completely lined with WSP cards, but there were no observable water drops on the cards after test completion. Thus, the WSP cards results were inconclusive due to the lack of observed water drops.

This page intentionally left blank.

APPENDIX G: AMMONIUM SALT SOLID ANALYSIS

This page intentionally left blank.

Project Memorandum

Date:	20 August 2024
To:	Matt Rowley, Jen Holdridge
From:	Aaron J. Frank
Subject:	FTIR, DSC, and TGA Analysis
Samples:	JR3 CO_2 Test Solid (TS 8C) JR3 Tray Solid (TS 8D)

Background

Two (2) unknown samples (JR3 CO_2 Test Solid and JR3 Tray Solid) were submitted for identification using infrared (IR) spectroscopy. The objective of analysis was to identify the chemical composition of the two unknown samples using the three known samples as reference.

Procedure

Fourier Transform Infrared (FTIR) Analysis: An Agilent Cary 670 FTIR spectrometer (Battelle ID: ZA0541) outfitted with a Harrick GladiATR attenuated total reflectance (ATR) accessory was used for all IR analyses. ATR-IR spectra were obtained using a diamond crystal and analyzed at 4 cm^{-1} wavenumber resolution for the range of 4,000 to 650 cm^{-1} wavenumbers. A total of 100 scans were collected for each sample. The ATR crystal was wiped clean with methylene chloride between each new analysis and the instrument was re-baselined, as necessary. The spectra were processed and searched against a spectral database using Wiley Science Solutions' "KnowItAll" software and digital IR libraries, which contains over unique 264,000 IR spectra.

Differential Scanning Calorimetry (DSC): DSC was performed on a TA Instruments DSC250 with an RCS 90 (Refrigerated Cooling System). Samples were run in both sealed and open aluminum pans. Testing was performed from -20°C to 200°C at 10°C per minute under nitrogen. Results were analyzed using TA Instruments' Trios software.

Thermalgravimetric Analysis (TGA): TGA was performed on a TA Instruments TGA550. Samples were evaluated in an open platinum pan from ambient (~25°C) to 200°C at 10°C per minute under nitrogen. Results were analyzed using TA Instruments' Trios software.

Reference Standards: Ammonium carbonate (Sigma-Aldrich, ≥30.0% NH_3), ammonium bicarbonate (Sigma-Aldrich, ≥99.0%), and ammonium carbamate (Oakwood Chemical, ≥95%) were used as received.

Results/Discussion

FTIR Analysis: The reference standard compounds were individually analyzed. The IR spectra of the ammonium carbonate, ammonium bicarbonate, and ammonium carbamate reference standards were consistent and congruent with library reference spectra (**Figures G-1** to **G-3**). The spectrum for ammonium carbonate collected in this study using the reference standard has a few features that are not aligned (intensity and wavenumber) with the reference spectrum (WSAAX #3900, ammonium carbonate, corrected) from Wiley. The ammonium carbonate spectra

were further compared to assignments from Khanna and Moore[1] and agreed with the ammonium carbonate spectra collected here. Both unknown samples, JR3 CO_2 Test Solid and JR3 Tray Solid, have spectra that are highly congruent with each other (**Figure G-4 [D-E]**). The spectra obtained for both unknown samples match ammonium bicarbonate and are highly congruent for peak position, intensity, and shape. The IR spectra suggests both JR3 CO_2 Test Solid and JR3 Tray Solid are predominantly ammonium bicarbonate.

Reference spectra for ammonium carbonate and ammonium carbamate are similar, but contain distinct spectral features that are not present in the ammonium bicarbonate or JR3 CO_2 Test Solid and JR3 Tray Solid spectra (**Figure G-4 [A-E]**), which includes prominent peaks at ~3,450 cm^{-1}, ~1,120 to 1,130 cm^{-1}, and ~570 cm^{-1}. Other subtle differences in spectral time series within the fingerprint region were also observed suggesting the unknown compounds are not ammonium carbonate or ammonium carbamate.

TGA and DSC Analysis: TGA analyses were performed on the ammonium carbonate, bicarbonate, and carbamate salts. All salts underwent thermal decomposition with less than 0.2% of the starting material present at 193°C. The onset temperature for the ammonium salts was established using the extrapolated onset temperature method. The onset temperature for decomposition by TGA was approximately 55°C, 78°C, and 124°C for ammonium carbamate, ammonium carbonate, and ammonium bicarbonate, respectively. The onset decomposition temperature for JR3 CO_2 Test Solid and JR3 Tray Solid were 83°C and 80°C, respectively.

DSC was also performed on the same set of samples. Endothermic time series were observed for all samples (**Figure G-5**). Peak temperature for ammonium carbamate, ammonium carbonate, and ammonium bicarbonate were ~74°C, 100°C, and 112°C, respectively. Peak temperatures for JR3 CO_2 Test solid Open Pan and JR3 Tray Solid Open Pan were 99°C and 94°C, respectively. Thermogram time series for the field samples were smooth and continuous. The time series for the stand materials were slightly irregular. Ammonium carbamate exhibits a steady and gradually increasing temperature profile, starting at approximately 0°C and moving into a step-like pattern around 95°C. Ammonium carbonate also has a long rising profile starting around 20°C with a discontinuity occurring around 75°C. The deflection from baseline for ammonium bicarbonate starts around 50°C and maximized around 112°C. An irregularly shaped foot and tail are observed on the ascending and descending slope of the thermogram for ammonium bicarbonate.

Summary

The IR spectra for the three ammonium salts were sufficiently distinct to permit differentiation by IR spectroscopy. Both unknown samples, JR3 CO_2 Test Solid and JR3 Tray Solid, produced spectra that strongly correlated with ammonium bicarbonate. The DSC analysis suggests a mixture of components especially in the ammonium carbamate and ammonium bicarbonate samples owing to the complex thermogram time series. The profile shape and maximum temperature for both field samples and ammonium carbonate are similar, suggesting an ammonium carbonate component that was not evident in the FTIR analysis. The lack of congruence between the FTIR and DSC analyses is not fully understood and additional research to resolve this discrepancy was not undertaken due to budget limitations. Based on this study, however, the field samples do not appear to be consistent with ammonium carbamate. The IR spectra and decomposition temperature are not congruent with the standard material or reference IR spectrum.

[1] Khanna, R. K.; Moore, M. H. "Carbamic acid: molecular structure and IR spectra" *Spectrochimica Acta Part A,* 1999, *55*, 961-967.

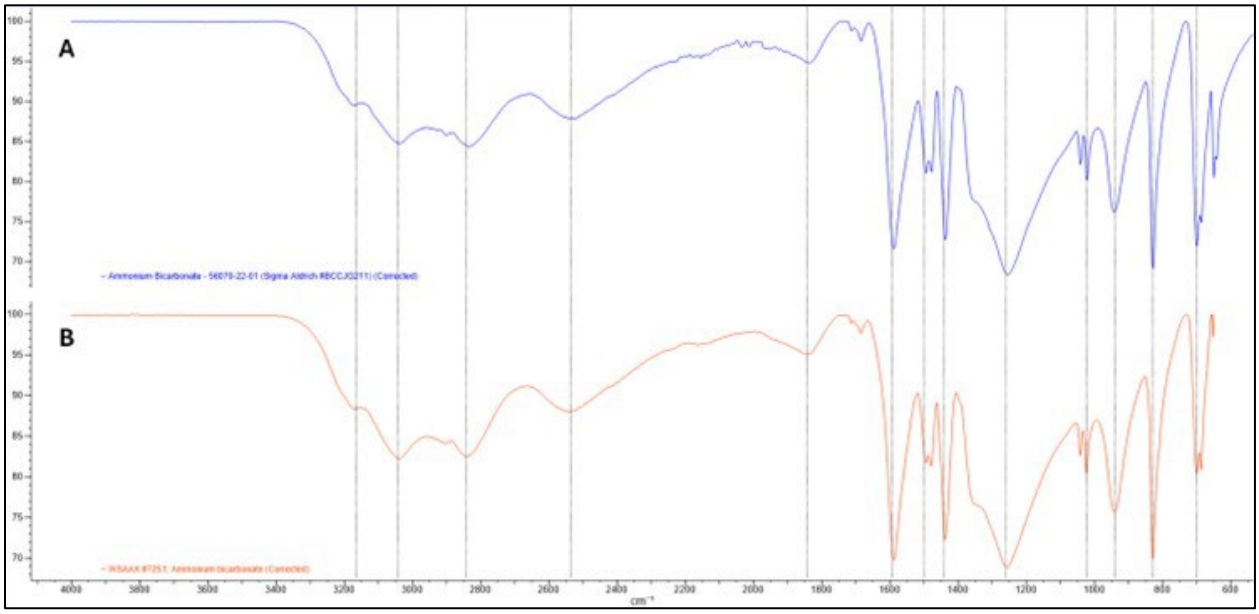

Figure G-1. A) Ammonium bicarbonate standard and B) library reference spectrum. Prominent spectral features highlighted with dashed line to demonstrate congruency.

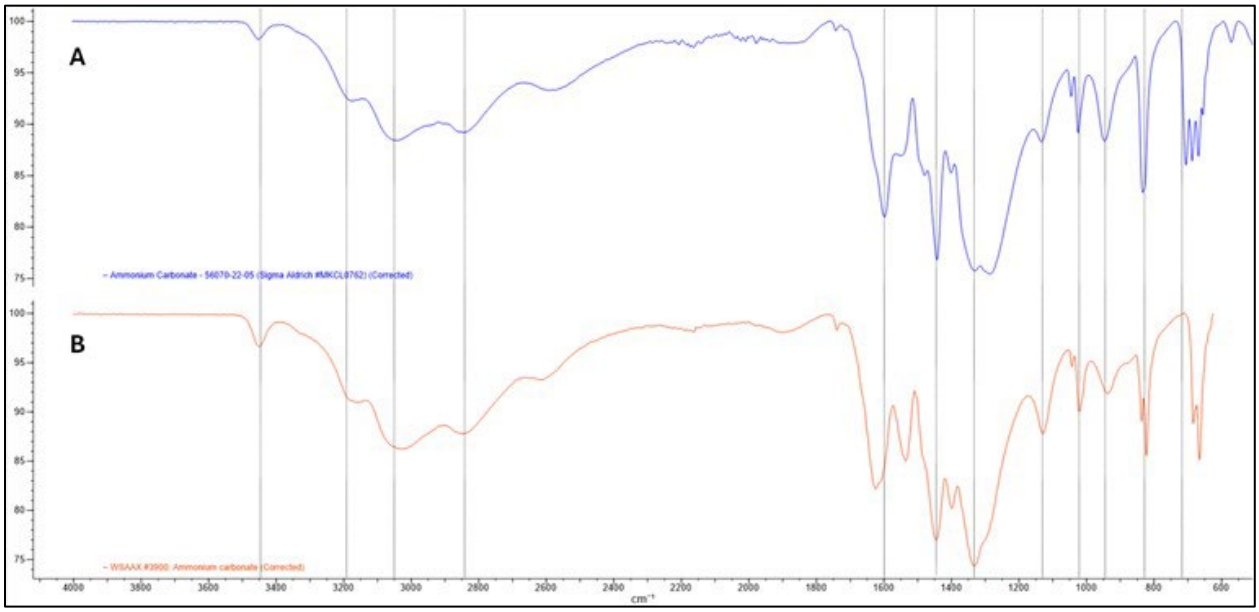

Figure G-2. A) Ammonium carbonate standard and B) reference library spectrum for ammonium carbonate. Prominent spectral features highlighted with dashed line to demonstrate congruency.

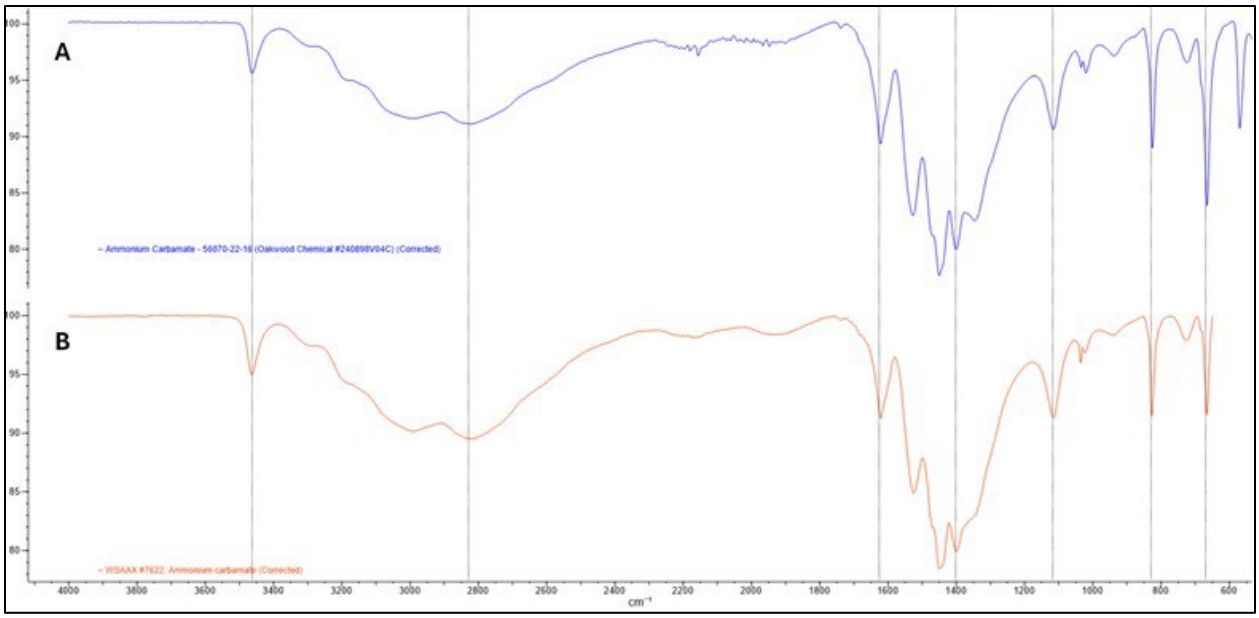

Figure G-3. A) Ammonium carbamate standard and B) reference library spectrum for ammonium carbamate. Prominent spectral features highlighted with dashed line to demonstrate congruency.

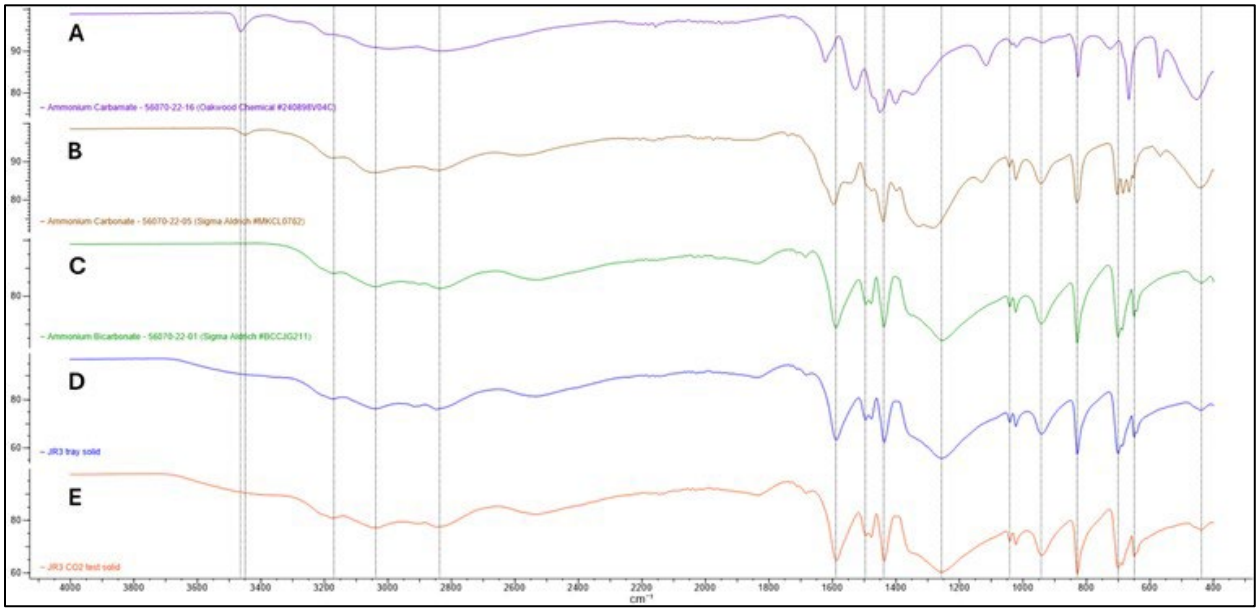

Figure G-4. A) Ammonium carbamate standard, B) ammonium carbonate standard, C) ammonium bicarbonate standard, D) JR3 tray solid, and E) JR3 CO_2 test solid.

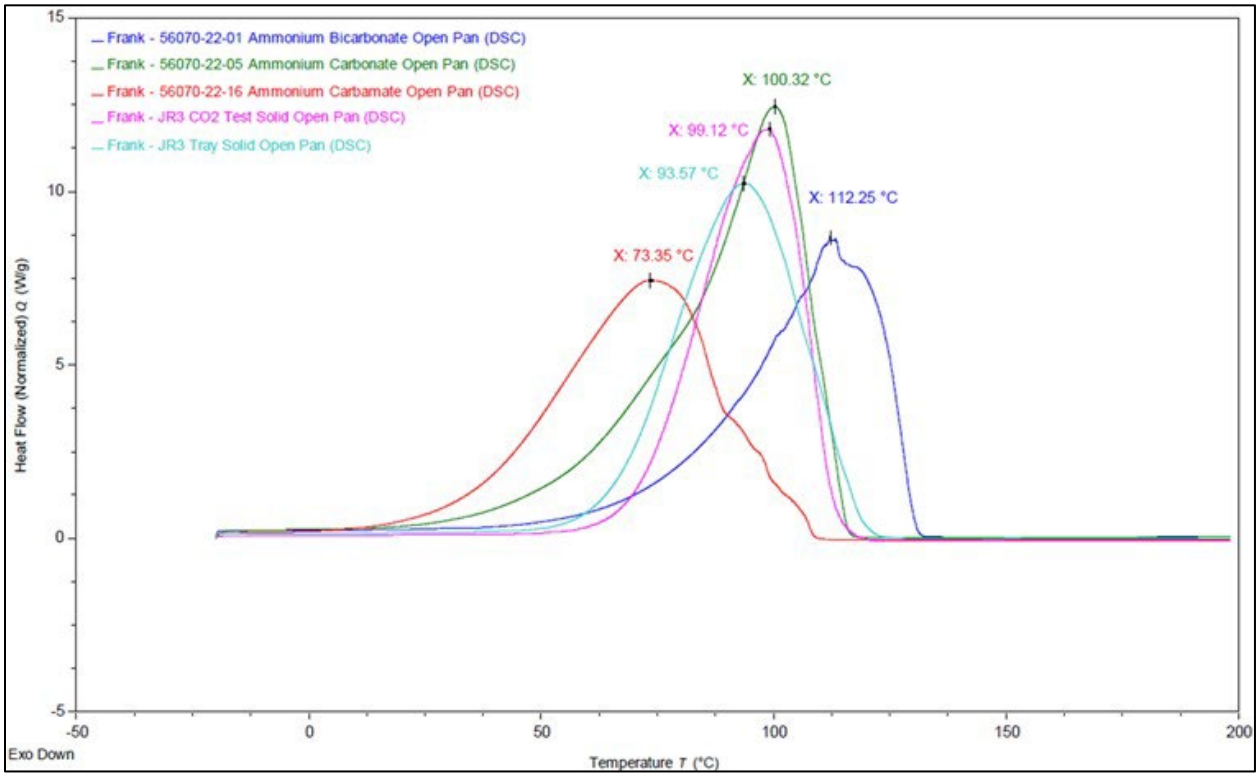

Figure G-5. DSC thermogram plots for ammonium salts and field samples.

Science & Technology